# TUNNEL CONVERGENCE IN STRESS-FRACTURED GROUND

by

Marta Ríos

A thesis submitted in partial fulfillment

of the requirements for the degree of

Master of Applied Science (M.A.Sc.) in Natural Resources Engineering

The Faculty of Graduate Studies

Laurentian University

Sudbury, Ontario, Canada

**THESIS DEFENCE COMMITTEE/COMITÉ DE SOUTENANCE DE THÈSE**
**Laurentian Université/Université Laurentienne**
Faculty of Graduate Studies/Faculté des études supérieures

Title of Thesis
Titre de la thèse TUNNELCONVERGENCE IN STRESS-FRACTURED GROUND

Name of Candidate
Nom du candidate Ríos, Marta

Degree
Diplôme Master of Applied Science

Department/Program
Département/Programme Natural Resources Engineering

Date of Defence September 14, 2017
Date de la soutenance

**APPROVED/APPROUVÉ**

Thesis Examiners/Examinateurs de thèse:

Dr. P.K. Kaiser
(Supervisor/Directeur de thèse)

Dr. Ming Cai
(Committee member/Membre du comité)

Dr. D. R. McCreath
(Committee member/Membre du comité)

Dr. M. S Diederichs, Queen's University
(External Examiner/Examinateur externé)

Approved for the Faculty of Graduate Studies
Approuvé pour la Faculté des études supérieures
Dr. David Lesbarrères
Monsieur David Lesbarrères
Acting Dean, Faculty of Graduate Studies
Doyen intérimaire, Faculté des études supérieures

**ACCESSIBILITY CLAUSE AND PERMISSION TO USE**

# Abstract

When tunnelling at great depth in hard brittle rock or when mining-induced stresses cause stress-fracturing of brittle rock, the resulting rock fragments cannot fill the original space. As during a rock blast, geometric bulking occurs when brittle rock is fractured, and the volume occupied by fractured rock is much larger. Near underground excavation, this volume increase causes convergences including floor heave because the fractured rock can only move into the excavation. Unfortunately, analytical tools such as the convergence confinement method (CCM) or the ground reaction curve (GRC) do not account for this rock mass bulking action. Similarly, numerical continuum model, while accounting for material dilation, do not account for the unidirectional expansion (bulking) of the fractured rock.

The purpose of this thesis is to combine semi-empirical relations of bulking, established based on field measurements and numerical discontinuum models, with the analytical GRC-method and with 2D numerical models (specifically Phase2$^{TM}$) to provide a means for estimating the impact of bulking on tunnel convergence. The outcome of this thesis therefore is to provide a means of bulking enhance convergence prediction by analytical and numerical solutions. This is presented for circular tunnels, to facilitate use of analytical solutions, in different rock mass types (plastic and brittle) and for various stress states (stress ratio k = 1 and 0.5) as well as for mining conditions with associated stress changes.

The examples presented in this thesis demonstrate that rock mass bulking in brittle rock often dominates tunnel convergence. It is also shown that bulking by extension failure primarily affects

the shallow radial displacement profile (near the excavation wall) whereas shear-related bulking, if not suppressed by sufficient confinement, causes deeper-seated radial displacements.

The practical implication of this work is that rock support experiences significantly more radial strain and deformation than predicted by conventional analytical and numerical solutions. These models therefore tend to underestimate the straining of installed rock support.

**Keywords**: tunnel convergence, Ground Reaction Curve (GRC), brittle failure, geometric bulking, Bulking Factor (BF), confinement distribution, strain, stress ratio, in-situ stress, mining-induced stress, Geological Strength Index (GSI), Damage Initiation Spalling Limit (DISL), Excavation Damage Zones (EDZ), elastic-plastic, elastic-brittle, depth of yield, tensile fracture, shear fracture, displacement.

# Acknowledgements

I would like to start by thanking my supervisor *Dr. Peter Kaiser* for his thoughtful guidance and expert advice. For the past years, he has not only assisted me with the technical aspects of this thesis, but he has also taught me the importance of having a strong work ethic in research. He has lead me by example and his considerate treatment of me will be always cherished.

I would also like to acknowledge my Committee members *Drs. Ming Cai and Dougal R. McCreath* and my external examiner *Dr. Mark S. Diederichs*. Their feedback has helped me improve my understanding of the subject and this thesis.

This research time could not have been possible without financial support from the Natural Sciences and Engineering Research Council of Canada (NSERC) and the Ontario Research Fund (SUMIT program) and MIRARCO. Dr. Shelly Watson of Laurentian University deserves special thanks for provide me with economical support trough Laurentian University.

On a more personal note, I would like to express my gratitude to my friends *Alberto, Javier, Kim Amina and David*. Some of the talks with them have given me the extra-encouragement that was sometimes so necessary to keep going.

My most sincere thanks go to my parents *Javier* and *Rosa*. I owe them all. This thesis is dedicated to them.

*Marta Ríos*

*September 2017*

# Table of Contents

# List of Figures

# List of Tables

# List of Symbols and Acronyms

| | |
|---|---|
| $\sigma_1$ | major principal stress (compressive stresses are taken as positive) |
| $\sigma_3$ | minor principal stress |
| $\sigma_3$ | normalized minor effective principal stress |
| $\sigma_c$ | unconfined rock strength |
| $\sigma_{ci}$ | unconfined rock strength by back projection from triaxial tests |
| ***UCS*** | unconfined compressive strength |
| $\sigma_d$ | defected rock strength |
| $\sigma_{max}$ | maximum induced stress around circular opening in elastic material |
| $\sigma_t$ | tensile strength |
| $\varepsilon$ | strain |
| $\rho$ | rock density in $kg/m^3$ or $t/m^3$ |
| $\gamma$ | unit weight, $N/m^3$ |
| $\mu$ | the coefficient of friction |
| ***BF*** | Bulking Factor, is the change in radial length with respect the initial length. |
| $\overline{BF}$ | Average or mean BF over the depth of failure is the change in the radial length over $d_f$ |
| ***c*** | cohesion |
| $d_f$ | depth of failure in an unsupported excavation |
| $d_y$ | depth of yield |
| $D_v$ | total number of discontinuities per cubic metre of rock mass |
| ***Fc*** | competence factor |
| $J_a$ | joint alteration number (of least favourable discontinuity or joint set) |
| $J_n$ | joint frequency or the joint set number |
| $J_v$ | number of joints/discontinuities per unit length |
| $J_w$ | joint water reduction factor |
| ***k*** | is the slope given by the ratio σ1 to σ3, $\sigma_1/\sigma_3$ |
| $k_o$ | is the ratio of horizontal stress to vertical, $\sigma_h/\sigma_v$ |
| ***AECL*** | atomic energy Canada limited |
| ***CANMET*** | Canada centre for mineral and energy technology |

| | |
|---|---|
| ***CI*** | crack initiation stress |
| ***CD*** | critical threshold damage |
| ***CDZ*** | construction damage zone |
| ***D&B*** | drilling and blasting |
| ***DISL*** | damage initiation spalling limit |
| ***DRMS*** | design rock mass strength |
| ***EDZ*** | excavation damage zone |
| ***EdZ*** | excavation disturbed zone |
| $EDZ_i$ | inner excavation damage zone |
| $EDZ_o$ | outer excavation damage zone |
| ***ESR*** | excavation support ratio |
| ***EIZ*** | excavation influence zone |
| ***GSI*** | geological strength index |
| ***HDZ*** | highly damaged zone |
| ***LDP*** | longitudinal displacement profile |
| ***Q*** | rock mass Quality index |
| $Q_o$ | Q-value based on $RQD_o$ instead of RQD in the original Q calculation |
| ***RMR*** | rock mass rating (rock mass classification) |
| ***RMS*** | rockmass strength (rock mass classification) |
| ***RQD*** | rock quality designation (rock mass classification) |
| ***RQDo*** | RQD-value oriented in the tunnelling direction |
| ***SL*** | stress level = $\sigma_{max}$/UCS or = $\sigma_{max}$/CI |
| $SL_{CI}$ | stress level normalized to the crack initiation |
| $SL_{UCS}$ | stress level normalized to the unconfined rock strength |
| ***TBM*** | tunnel boring machine |
| ***URL*** | underground research laboratories |

# Chapter 1

# 1 Introduction and Literature Review

## 1.1 Scope and Project Overview

### *1.1.1 Problem Definition*

In underground excavations, rock mass instability can be classified in two forms: (1) structurally controlled (gravity-driven) fall and (2) stress-driven (or yielding) failure. The dominant behaviour depends on the in-situ stress, the geological conditions (i.e., degree of jointing and fracturing in the rock mass) and the induced stress affecting the excavation.

This thesis focuses on the second type of instability, stress-driven failure mechanism of tunnels excavated in hard brittle rock. For the understanding of this damage process, it is of vital importance to estimate the strength of the rock correctly. Many authors (Martin et al., 1999; Kaiser 2000 and 2006; Diederichs 2007; Radoncic 2008 and others) have studied the design of tunnels in highly stressed brittle rock, and these investigations have helped to the understanding of how the instabilities of the rock mass are generated.

Stress-driven processes involve tensile fracturing where fractures form and propagate parallel to the boundary of the excavation or parallel to the major principal stress (Griffith, 1924). As Kaiser (2006) explained, when the stress level SL = $\sigma_{max}/\sigma_{ci} > 0.4$ massive rock starts to fracture and interacts with structures and at $\sigma_{max}/\sigma_{ci} > 0.8$ stress-driven processes dominates over structurally-controlled processes. $\sigma_{max}$ is the maximum tangential stress at the boundary of a circular opening in elastic ground ($\sigma_{max} = 3\sigma_1 - \sigma_3$) and $\sigma_{ci}$ is the uniaxial compressive strength of the intact rock

obtained from results of triaxial tests. Due to the nature of stress-driven fracturing, it cannot be prevented by typical support pressures (<0.5 MPa). The depth of failure is thus essentially independent of the support pressure. At higher stresses ($\sigma_{max}/\sigma_{ci} > 1.15$), the rock becomes heavily fractured to greater distances from the tunnel wall and tends to fail in a combination of extension and shear failure. Geometric bulking starts as soon as stress-fracturing is observed and increases in magnitude as the depth of stress-fracturing increases and in some cases, as it will be demonstrated in Chapter 3, can dominate the behaviour of the tunnel.

A complete analysis of underground openings requires knowledge of three variables: (1) the in-situ stress condition; (2) the rock mass strength; and (3) the geometry of the excavation. In mining, stress-induced changes resulting from excavation sequencing also need to be considered.

The scope of this thesis includes a discussion of the fundamental processes of brittle failure in hard rock that are relevant when assessing excavation stability for ground control and rock support in brittle failing rock.

### *1.1.2 Focus and Scope of Study*

The rock mass strength and in situ stresses can be highly variable and thus generate many different instability scenarios along a tunnel or shaft. In this thesis, the findings from studies of underground excavations, particularly small circular tunnels, experiencing stress-driven failure modes leading to brittle failure mechanisms are summarized.

The stability analyses have been conducted by using the finite element program Phase$^2$ (RocScience 2002, v.8.0) and by analytical solutions providing Ground Reaction Curves (GRC). Both methods provide estimates of displacements produced by tunnel excavation. Since these

models do not account for geometric bulking of stress fractured ground, this thesis expands these methods to account for brittle failure scenarios where bulking ground around the walls, roof and floor of the excavation causes additional strain and displacements.

The tunnel has been subjected to different stress conditions, conditions typically encountered in mining. Loading and unloading conditions (causing relaxation) are investigated. The quantification of stresses and deformations that a tunnel experiences and the analysis of how it performs under those stresses is vital to establish correctly the support system requirements. If bulking is ignored, the displacements loading the support will be underestimated and the resulting support systems may be ineffective.

### *1.1.3 Overview of Stability Assessment Approaches*

Underground excavations can experience various instability modes as illustrated in Figure 1-1. This matrix indicates that starting from the top, at low stress, structurally-controlled failure is the predominating behaviour mode. When proceeding down the chart, stress-driven failure or fracturing mechanisms get involved and a combination of structural and stress-fracturing cause instabilities.

At the extreme (right bottom of the chart) with high stress and poor rock mass quality, shearing leads to squeezing conditions. This thesis focuses on matrix elements that are highlighted (green) in the tunnel behaviour matrix in Figure 1-1 (brittle failure mechanism) when stress-driven failure mechanism dominate the excavation behaviour, i.e., when the overburden stress is greater than 15% of the unconfined strength of the rock or when the tangential stress around the circular excavation is greater than 40% of unconfined strength (shown by the stress level *S*L on the right side of the matrix). This stress level *S*L was introduced by Kaiser et al. (2000) as a measure to help

anticipate brittle, spalling-type failure processes. The SL is more meaningful than the principal stress to strength ratio because it takes deviatoric stress and thus the stress ratio *k* into account, which is relevant in mining and in conditions like those observed in Canada where k > 1. Without consideration of the *k* effect, the impact of brittle failure in the design of the tunnel may be underestimated.

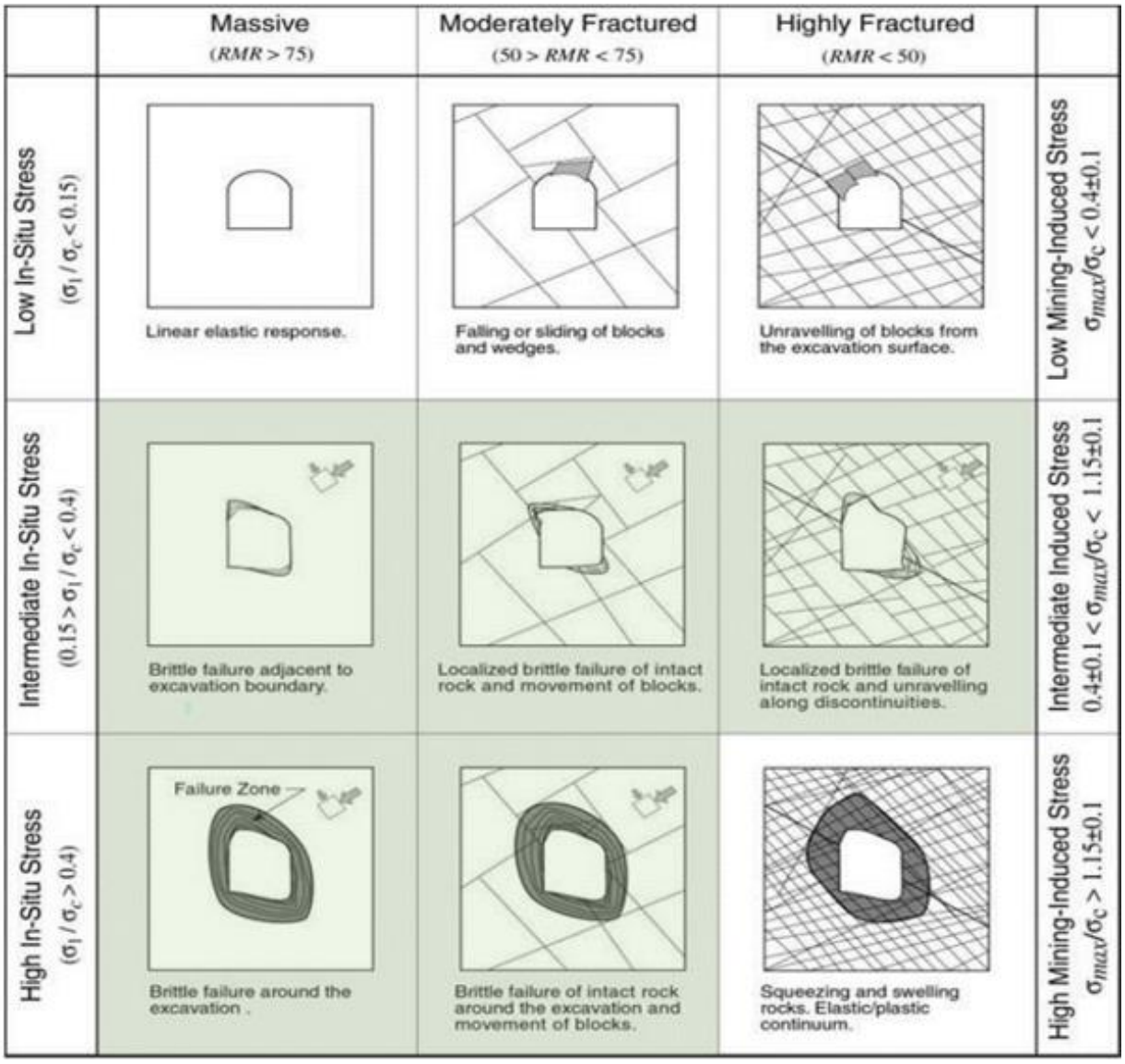


*Figure 1-1 Rock mass behaviour matrix (Kaiser et al., 2000 based on Hoek et al., 1995).*

Because this thesis focuses on stress-driven failure mechanisms, it is essential to understand and quantify the depth of failure $d_f$ that brittle rock mass failing will create. Between the wall of an excavation and the depth of failure, stress-fracturing will generate bulking ground caused by the disintegration of the rock mass. Because the failed ground, due to geometric incompatibilities, is not going to fit together, the volume of the rock mass will increase. This increased volume of rock mass has to be taken into consideration when designing a tunnel support system.

This thesis is not dealing with conditions described by the 9th element in the matrix (Figure 1-1) which corresponds to swelling and squeezing rock. It also does not cover the low in situ-stress conditions (first three elements of the matrix).

One of the key parameters characterizing brittle failure in hard rocks is the stress magnitude required to initiate and propagate stress-induced fractures through massive to tightly interlocked, non-persistent jointed rock. Initially, at intermediate depths, these stress-induced fractured regions are localized near the tunnel perimeter but at great depth the fracturing involves the entire boundary of the excavation.

### *1.1.4 Definition of Factor of Safety*

For engineering design purposes, the Factor of Safety FS is used to define the proximity to failure. The Factor of Safety relates the Demand, coming from the rock mass, to the Capacity, typically provided by the support.

$$\mathrm{FS}_{\mathrm{Load}} = \frac{\text{Support Load Capacity}}{\text{Load Demand}} \qquad \text{Equation 1-1}$$

The Load Demand is influenced mainly by the geometry (volume) of the rock failing and it is typically assumed that both capacity and load are independent of deformation or strain. However,

if the rock is failing by stress-fracturing, bulking may impose extra deformation on the support and equilibrium can only be established after some permanent deformations have been accommodated. It is therefore often necessary to define a displacement-based factor (Kaiser, 2014) of safety $FS_{Displacement}$ (Equation 1-2) to assess the safety margin during static or dynamic failure processes.

$$FS_{Displacement} = \frac{Support\ Displacement\ Capacity}{Displacement\ Demand} \qquad \text{Equation 1-2}$$

The deformation demand stems from elastic, plastic and bulking deformations and the deformation capacity comes from the yielding bolts or support systems. In other words, in bulking ground, it is important to establish sufficient margin against displacements (deformations).

Based on contributions by Hoek and Corkum (2002) and Corkum et al. (2011, 2012), Table 1-1 provided guidance for four typical tunnelling conditions.

*Table 1-1 Tunnel conditions, typical problems, critical parameters to consider, analysis methods and design criteria (Corkum et al., 2011).*

| TUNNEL CONDITION | | TYPICAL PROBLEMS | CRITICAL PARAMETERS | ANALYSIS METHODS | ACCEPTABILITY CRITERIA |
|---|---|---|---|---|---|
| SQUEEZING | 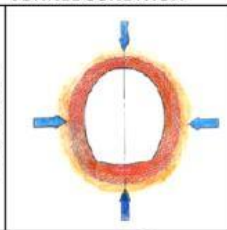 | Rock Failure where induced stresses exceed strength.<br><br>Swelling, squeezing or excessive closure if support is inadequate | • Strength of rock mass and of individual structural features.<br>• Swelling potential, particularly with clay-rich rocks.<br>• In situ stresses<br>• Excavation method and sequence<br>• Capacity and installation sequence of support systems | Stress analysis using numerical methods to determine extent of failure zones and probable displacements in the rock mass. Rock support interaction analysis using closed-form, empirical or numerical methods to determine capacity and installation sequence for support and to estimate displacement in the rock mass. Tunnel strain evaluation using statistical-based charts. | Capacity of installed support should be sufficient to stabilize the rock mass and to limit closure to an acceptable level. Tunnelling machines and internal structures must be designed for closure of the tunnel as a result of swelling or time-dependent deformation. Monitoring of deformation is an important aspect of construction control. |
| STRUCTURALLY CONTROLLED | 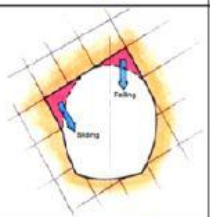 | Gravity driven falling or sliding wedges or blocks defined by intersecting structural features.<br><br>High stresses may confine wedges or blocks contributing to overall stability.<br><br>Otherwise, unravelling of inadequately supported surface material. | • Orientation, inclination and shear strength of structural features.<br>• Shape and orientation of tunnel.<br>• Quality of excavation drilling and blasting.<br>• In situ stresses in the rock mass<br>• Water<br>• Capacity and installation sequence of support systems | Stereonet or analytical methods are used for the determination and visualization of all potential wedges in the rock mass surrounding the tunnel. Parametric analysis of critical wedges using limit equilibrium (LE) or direct analysis using distinct element method (DEM) on the mode of failure, factor of safety and support requirements | Factor of safety, including the effects of reinforcement, should exceed 1.5 for sliding and 2.0 for falling wedges and blocks.<br>Support installation sequence is critical, and wedges or blocks should be identified and supported before they are fully exposed by excavation. Displacement monitoring is of little value. |
| BRITTLE | 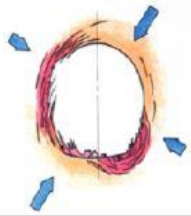 | Stress driven instability leading to spalling or slabbing of the rock surrounding the excavation leading to eventual tunnel collapse if rock support is inadequate.<br><br>Rock bursting potential. | • In situ stress (magnitude and orientation) in the rock surrounding the excavations.<br>• Orientation, inclination, and shear strength of structural features.<br>• Rock mass spalling strength<br>• Shape and orientation of the tunnel<br>• Capacity and installation sequence of support systems | Empirical design or stress analysis using numerical methods, to determine the depth of failure and probable displacements. | Support must be capable of stabilizing fractured rock and accommodate imposed loads and displacements |
| TRANSITIONAL | 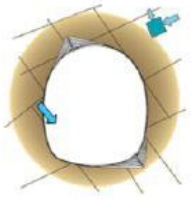 | Brittle failure of intact rock and movement of blocks or shear failure of rock mass and movement of blocks.<br><br>Large deformations and significant yielding possible where support is inadequate | • Orientation, inclination, and shear strength of structural features.<br>• Excavation method and sequence<br>• Quality of excavation drilling and blasting<br>• Shape and orientation of the tunnel<br>• Rock mass compressive strengths<br>• Capacity and installation sequence of support systems | Complex interaction of tunnel instability modes requires numerical analysis to predict depth of failure and displacements | All the above |

Specifically, Table 1-1 provides guidance for squeezing ground (matrix 3,3 in Figure 1-1), structurally controlled failure (matrix 1,1 to 1,3), brittle failing tunnels (matrix 2,1 and 3,1), as well as transitional failure modes (matrix 2,2; 2,3; 3,2). It also lists typical problems, critical design parameters, applicable analytical methods, and acceptability criteria. In the case of brittle failure rock, these relate to estimates of the maximum displacement that a tunnel can experience and a support can tolerate to retain stability (developed in detail in Chapter 3).

### *1.1.5 Rock Mass Properties*

Accurate estimations of the strength and deformation of the brittle rock mass are required when

analyzing underground excavations. Hoek and Brown (1980) proposed a method to obtain the strength of jointed rock masses. It was developed based on Dr. Hoek's experiences in weak rock tunnelling and it expanded to brittle rock by considering Griffith's crack theory (1920, 1924) to define a relation between shear and normal stress at fracture initiation. By associating fracture initiation with fracture propagation and rock failure, Hoek and Brown (1980) fit, by trial and error, several curved failures envelop to triaxial test data to establish their criterion.

This failure criterion presents several advantages, as for example, it is non-linear which agrees with experimental data over a range of confining stresses. Another positive point is that it was developed through an extensive evaluation of laboratory test data covering a wide range of rock types. It provides a reliable empirical means to estimate the rock strength when combined with the GSI (Geological Strength Index).

In order to use the Hoek-Brown criteria for estimating the strength and deformability of jointed rock masses, three rock mass properties have to be estimated:

- Uniaxial compressive strength $\sigma_{ci}$ of the intact rock;
- Hoek-Brown constant $m_i$ for these intact rock; and
- Geological Strength Index *GSI* for the rock mass (discussed in detail in section 1.3.3.4).

The Hoek-Brown failure criterion has been updated several times in response to experience gained with its use and to address practical limitations (Hoek and Brown 1997; Hoek et al., 1992, 1995 and 2002). The generalized form of the criterion was defined by Hoek et al. (1995) as:

$$\sigma_1 = \sigma_3 + \sigma_{ci} \left( m_b \frac{\sigma_3}{\sigma_{ci}} + s \right)^a \qquad \text{Equation 1-3}$$

where, $\sigma_1$ and $\sigma_3$ are the maximum and minimum effective stresses at failure, $m_b$ is the value of the

Hoek-Brown constant *m* for broken rock. The $m_i$ value had been reassessed and found to depend upon the mineralogy, composition and grain size of the intact rock (Hoek et al., 1992). The exponent *a* was added to address the system's bias towards hard rock and to better account for poorer quality rock masses by enabling the curvature of the failure envelope to be adjusted, particularly under very low normal stresses (Hoek et al., 1992). The Geological Strength Index (GSI) was subsequently introduced to obtain $m_b$, *s* and *a* for different structure of the rock mass (or blockyness) and surface conditions of the discontinuities (Hoek et al., 1995).

For the intact rock, Equation 1-3 defines the intact strength:

$$\sigma_1 = \sigma_3 + \sigma_{ci} \left( m_i \frac{\sigma_3}{\sigma_{ci}} + s \right)^a \qquad \text{Equation 1-4}$$

The relation between the principal stresses $\sigma_1$ and $\sigma_3$ at failure for a given rock is conditioned by two constants (*s* and *a*), the uniaxial compressive strength, $\sigma_{ci,}$ and the material constant for the intact rock, $m_{i.}$ The values of these rock mass properties should be determined by analysis of the results of a set of triaxial tests on core samples carefully prepared.

Considerable progress has been made in applying the Hoek-Brown criterion to the assessment and prediction of brittle fracture damage. Martin et al. (1999) provided an empirical depth of spalling failure relation using the Hoek-Brown criterion, setting m = 0 and s = 0.11. The fundamental assumption made it was that the stress-controlled failure process around the tunnel is dominated by cohesion loss. For instance, the $m_b$ parameter, which describes the frictional strength component, is set to zero. This m=0-approach differs from elasto-plastic yielding failure processes where the frictional strength is mobilized and thus dominates the behaviour of the rock mass. The findings and the empirical relations suggested by Martin et al. (1999) have since then, been confirmed in other studies of tunnel stability in highly stressed and fractured rock by Kaiser et al.

(2000), Diederichs et al. (2004) and many others.

### *1.1.6 Site Characterization*

A site characterization program for a deep tunnel begins by compiling the geological and geotechnical information for a proposed route and as the design moves forward, detailed information is acquired of the individual rock units, discontinuities, groundwater, etc.

As mentioned previously, brittle failure is clearly dominated by stress-induced fracturing of intact rock. The strength and deformation characteristics of the intact rock, as well as the in-situ stress magnitudes therefore are essential for the design of underground excavations in hard rock.

Rock characterization has to provide reliable properties for engineering design by geological data collection, laboratory testing and rock mass mapping. The process of rock characterization is a continuous improvement process where one starts with some assumptions, e.g., what is known from other comparable sites or what is known from similar rock conditions, and then gradually replaces every assumption by facts and data coming from boreholes and eventually from monitoring and back-analyses.

The resulting design parameters are then incorporated into numerical models. These parameters ideally could be obtained from in situ testing but, because the access to deep underground excavations (2000 m and more) is quite limited in practice, it is necessary to apply rock mass characterization systems and then through back analysis verify the rock mass properties. The excavation stability assessment process is summarized in Figure 1-2.

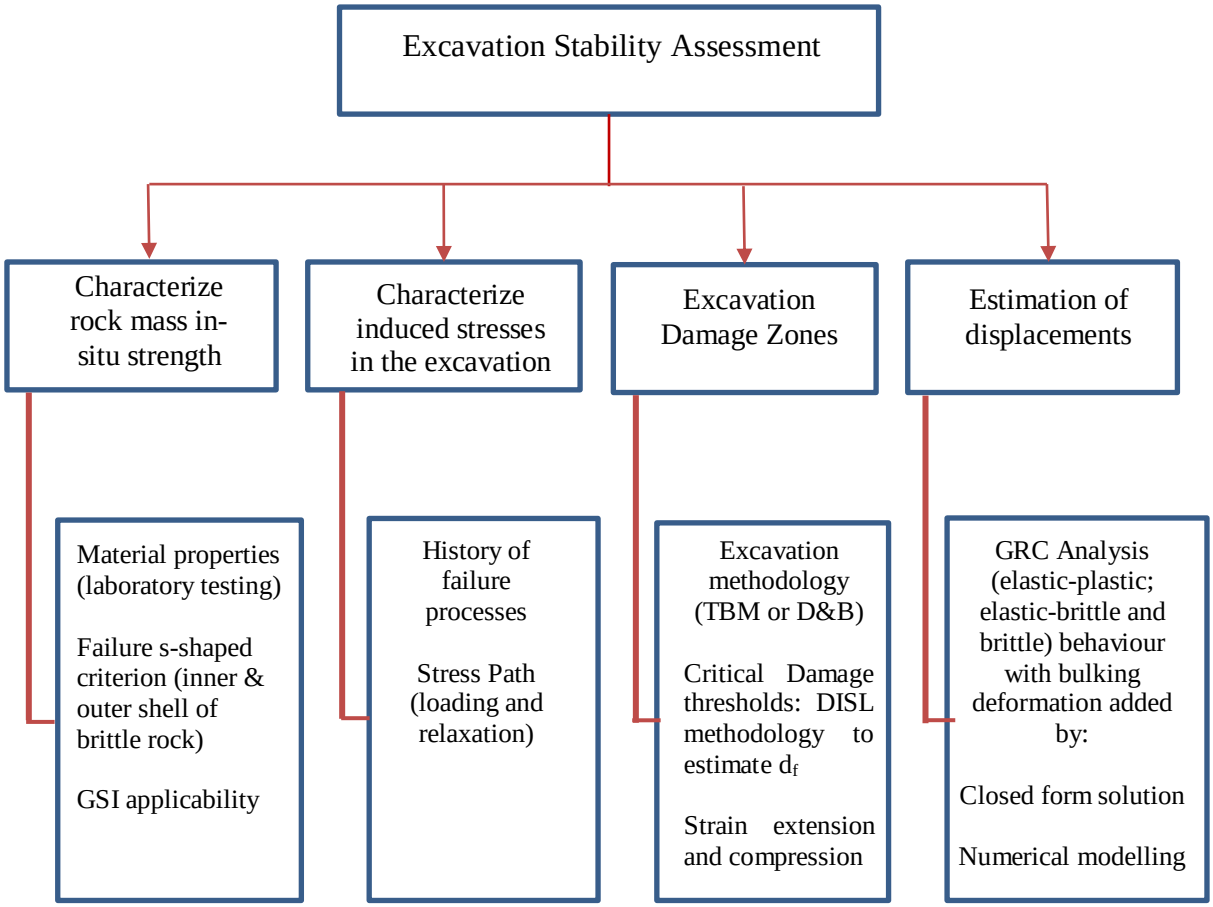


*Figure 1-2 Excavation stability assessment process.*

Empirical methods to classify the rock mass, particularly Q, RQD, MRMR, and the GSI system will be described in section 1.3.3.

When characterizing a site, it is also necessary to correctly establish the in-situ stresses because they are magnified near excavations and start the failure process. The mining-induced stress concentration factor or stress level SL = $\sigma_{max}/\sigma_{ci}$, or damaged index $D_i$ (Martin et al. 1999) is an appropriate indicator to gauge stress-driven excavation behaviour. Using this indicator, the relative in situ stress range shown in the matrix in Figure 1-1 (on the left) can be replaced by the mining-

induced stress concentration or SL on the right.

This thesis focuses on both the intermediate mining-induced stress level, corresponding to a range of $0.4 \pm 0.1 < \sigma_{max}/\sigma_c < 1.15 \pm 0.1$ and the high mining-induced stress with values $\sigma_{max}/\sigma_c > 1.15 \pm 0.1$.

The predominant behaviour mode for each stress domain also depends on rock type, jointing degree and the level of heterogeneity in the rock mass.

### *1.1.7 Rock Support Interaction for Tunnel Design*

#### 1.1.7.1 Introduction

When rock is excavated during tunnel advance elastic and plastic deformations occur. A simple plot illustrating this phenomenon is presented in Figure 1-3.

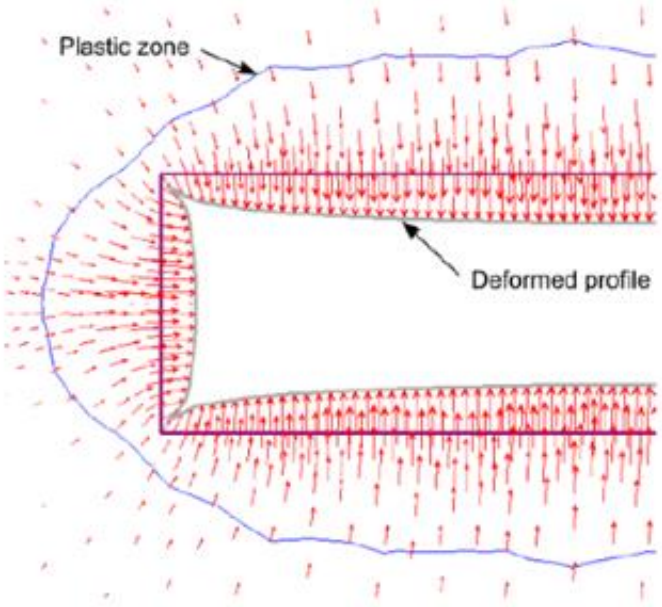


*Figure 1-3 Deformation pattern in rock mass surrounding the face of an advancing circular tunnel; displacement vectors and deformed tunnel profile (Hoek, 2008).*

The theoretical analysis of tunnel behaviour can be described as follows. For this it is assumed that

a circular tunnel of radius $r_o$ is subjected to a hydrostatic stresses $p_o$ and a uniform internal support pressure $p_i$ *(or* $p_s$ for support pressure*)* as illustrated in Figure 1-4.

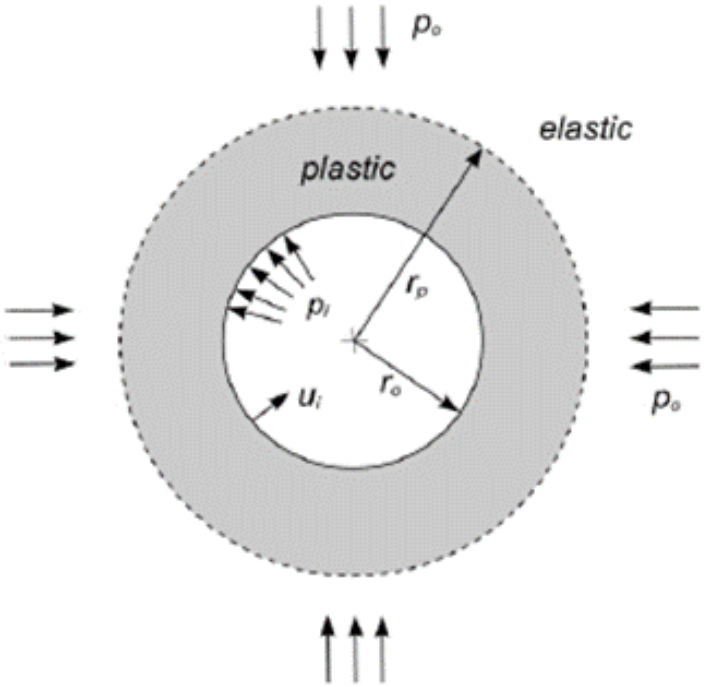


*Figure 1-4 Plastic zone surrounding a circular tunnel (Hoek, 2010).*

Failure of the rock mass surrounding the tunnel will occur when the internal pressure $p_i$ is less than a critical support pressure $p_{cr}$ defined by:

$$p_{cr} = (2p_o - \sigma_{cm})/(1 - k) \qquad \text{Equation 1-5}$$

where, $\sigma_{cm}$ (or UCS) is the uniaxial compressive strength of the rockmass:

$$\sigma_{cm} = (2c'cos\phi')/(1 - sin\ \phi') \qquad \text{Equation 1-6}$$

c' is the cohesion and k is the stress ratio or slope in the principal stress diagram ($\sigma_1$ versus $\sigma_3$), and is defined as a function of the effective friction angle ϕ':

$$k = (1 + sin\phi')/(1 - sin\phi') \qquad \text{Equation 1-7}$$

If the internal support pressure $p_i$ is greater than the critical support pressure, $p_{cr}$, the rock behaves elastic and no failure occurs. The tunnel then experiences an elastic displacement ($u_{ie}$ inward radial elastic displacement). When the internal pressure $p_i < p_{cr}$, failure occurs and a plastic zone is created causing a plastic displacement ($u_{ip}$ inward radial displacement) as shown in Figure 1-4.

#### 1.1.7.2 Ground Reaction Curve Concept

The plot of displacement of the wall of the tunnel $u_i$ (mm) versus the internal support pressure $p_i$ is known as Ground Reaction Curve (GRC). This plot or curve is based on the assumption that the rock at the tunnel face initially provides a support pressure equal to the in-situ stress $p_o$.

As the tunnel face advances and the face moves away from the section under consideration, the fictitious support pressure gradually decreases until it reaches zero at some distance behind the face.

In other words, the Ground Reaction Curve or Pacher-Fenner (1964) curve named after its original developers) describes the interaction of ground deformation (convergence or inward displacement) during tunnel advance and the support deformation. Although tunnelling is a 3D process, the GRC represents the equivalent relation between the decrease of internal support pressure and the wall displacements in 2D.

In order to accurately simulate the loading of support or the effects of sequential excavation, the two-dimensional model must capture the pre-face conditions (response in front-of the tunnel), the state of displacement and plasticity at the face and the subsequent development of deformation and yielding.

The basic premise of 2D tunnel modelling is that the internal outward radial pressure applied to

the tunnel boundary to replace in situ conditions reduces monotonically until the full excavation is represented (Cantieni and Anagnostou, 2009). In cases where in situ stress ratio k = 1, the tunnel boundary moves inward as the tunnel face passes the modeled section.

This inward displacement of the tunnel boundary can be simulated by replacing the rock inside the tunnel by an outward pressure $p_i$ (from the initially value of the in-situ pressure $p_o$) and reducing it to zero. The blue dashed line in Figure 1-5 corresponds to GRC.

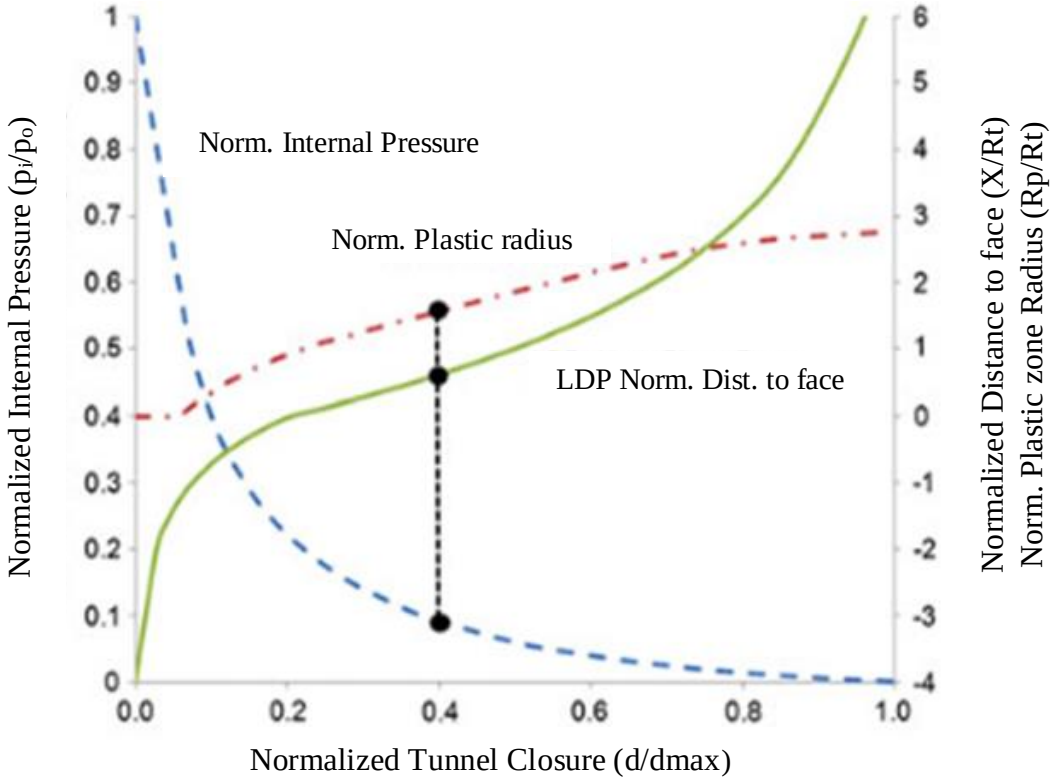


*Figure 1-5 Relation between internal pressure, plastic radius, tunnel closure and position. (Vlachopoulous and Diederichs, 2014).*

This reduction of the internal support pressure results in a redistribution of stress within the model

and can lead to yielding of the rock mass around the tunnel. The plastic zones may initiate in front of the tunnel or after the passage of the tunnel face and grows to a maximum, coincident with the maximum tunnel closure. The internal pressure and plastic zone radius are linked to tunnel closure (radial displacement) as displayed in Figure 1-5.

Vlachopoulous and Diederichs (2009, 2014) made improvements to the calculation of the Longitudinal Displacement Profile (LDP) for tunnels with extensive plastic zone developments. This approach adjusts the longitudinal displacement profile for unsupported tunnels in order to account for plastic yield in front of the advancing tunnel. This technique can now be extrapolated to staged excavations sequences and supported tunnels.

The interaction of the GRC, LDP and the characteristic support response curve is showed in Figure 1-6.

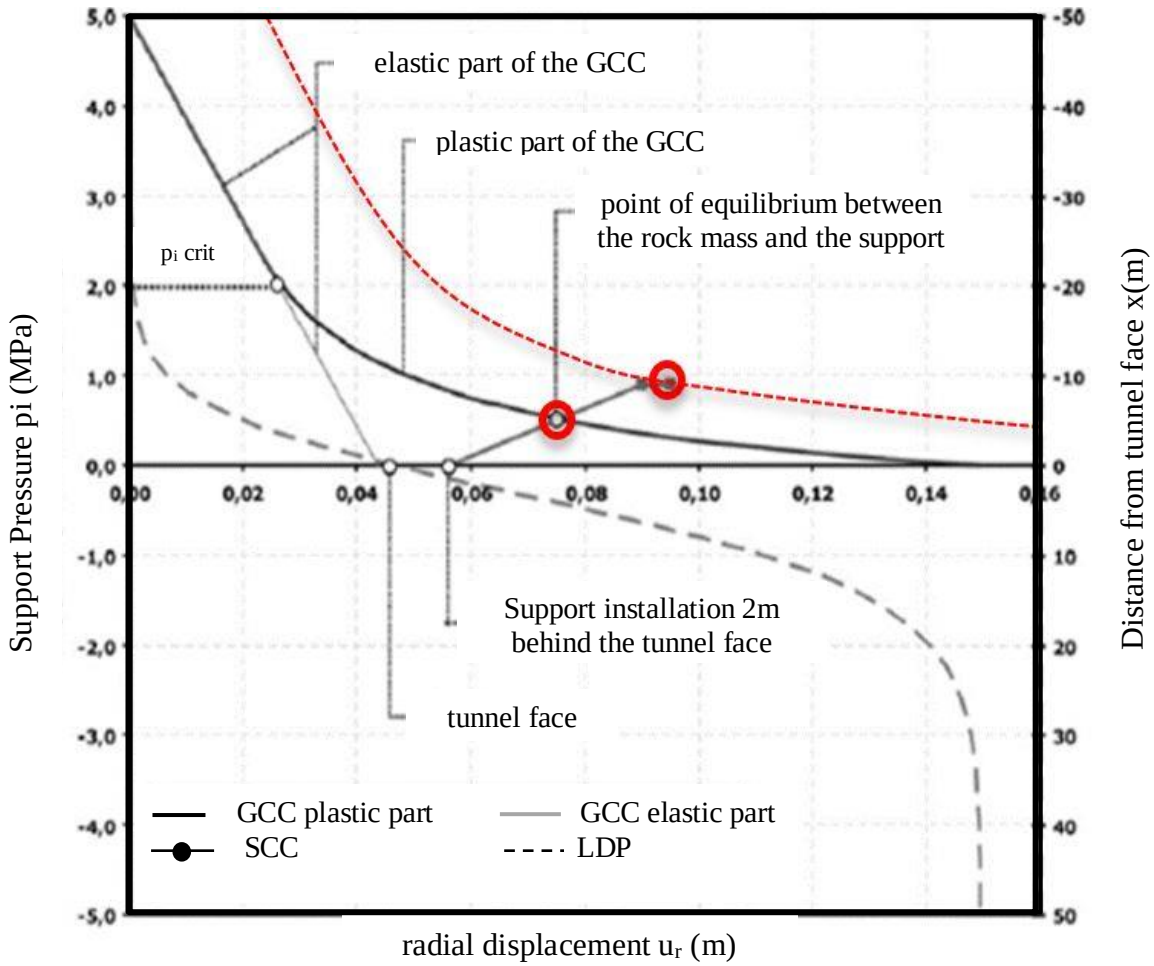


*Figure 1-6 Schematic representation of tunnel advance (modified after Gschwandtner, 2011).*

The GRC, showing tunnel wall displacement as a function of fictitious internal support pressure intersects the support curve at the location highlighted by the red circle. The rock-support interaction analysis is therefore useful for understanding the process of rock mass deformation around the advancing tunnel and the response of support installed inside. It will be expanded in this thesis, to ground that is bulking inside the "plastic" or stress-fractured zone.

The situation represented by the conventional GRC (Figure 1-6) is valid before mining changes

the stress state. When mining activities induce a stress change, the rock containing a tunnel and the tunnel itself experiences additional deformations causing an upward shift of the GRC and a translation to the right (red dashed curve in Figure 1-6).

If support was installed near the face while tunnelling, mining will impose an additional deformation and the support installed in the development tunnel stage is experiencing the entire excavation and mining-induced deformation. Therefore, the point of equilibrium as illustrated in Figure 1-6 is moved as indicated by the second red circle (at higher deformation).

A review of the impact of mining-induced stress change and a description of how the behaviour of an excavation is modified is presented in the following section.

## 1.2 In situ and Mining-Induced Stress

### *1.2.1 Introduction*

In order to establish the dominant mode of failure in the excavation (as indicated in matrix of Figure 1-1) it is necessary to estimate the in-situ stress level. The stress flow around a tunnel magnifies the in-situ stress (concentration or localization of stresses) and the associated stress redistribution during rock mass failure is a complex phenomenon that depends on such factors as the characteristics of the rock mass (heterogeneities, discontinuities, geological structures etc.) and the loading history of the site itself (tectonic activity, or in the case of a mine the loading-unloading cycles consequence of the production activities). The contribution each of these factors makes on the tunnel behaviour has to be well understood when designing an excavation.

Martin et al. (1990) summarized all the techniques that were used at AECL, to determine the in-situ stress (Table 1-2). As Amadei and Stephansson (1997) stated, in-situ stresses can at best be

determined with an error of $\pm 10 - 20\%$ . Factors and conditions influencing the in-situ stresses in the Canadian Shield region, an igneous rock area (result from volcanic history) that stretches north from the Great Lakes area to the Arctic Ocean, are briefly discussed in this section. The updated database (Maloney 2005, Kaiser 2016) provides best-fit equations that can be used to estimate stresses as a function of depth (ranging from 0 to 2550 m).

The works conducted at the URL indicated that when *SL* is high the results obtained by different stress measurement devices are extremely difficult to interpret. In the Canadian Shield this typically occurs at depths of approximately 1000 to 1500 m. In 1990, Kaiser and Wiles showed how under-excavation technique can be used to overcome the limitations of conventional stress measurement techniques.

*Table 1-2 Stress measurements techniques used in AECL's URL (Martin et al., 1990).*

| In situ stress Method | Device used | Technique |
|---|---|---|
| ***Indirect*** | *Triaxial Strain Cells* | *Modified CSIR*<br>*CSIRO*<br>*Swedish State Power Board*<br>*Sherbrooke Cuis Cell*<br>*Borre probe* |
| | *Biaxial Strain Cells* | *CSIR door Stopper*<br>*USBM gauge*<br>*Block Slotter* |
| | *Hydraulic Fracturing* | *Maximum Stress* |
| ***Direct*** | *Hydraulic Fracturing* | *Minimum stress* |
| ***Large Scale Back-analysis*** | *Convergence*<br>*Under-excavation*<br>*Mine-by-experiment*<br>*Depth of failure*<br>*Radial displacements* | *Martin et al (1996)*<br>*Kaiser and Wiles (1990)*<br><br><br>*Read (1994)* |

At the URL, the in situ-stress state was not determined by using a single method and the majority

of the indirect methods failed below 300 m of depth, giving some erroneous results (Martin 1990). Only by combining all the results from the various techniques was it possible to arrive at a valid stress tensor below 300 m depth. One of the findings of this combination of methods was that the large-scale methods using back-analysis techniques gave the most consistent results when compared to the small-scale traditional methods. They provided the most reliable results of stress measurements for deep excavations. Kaiser and Wiles (1990) showed that even for very good rockmass conditions, like those encountered in URL, ten over core tests were needed to provide statistically significant results and that with less than ten measurements the results were erratic.

Some other findings from in-situ stress characterizations can be summarized as follows:

Traditional methods are suitable for shallow depths (where the ratio of the far-field major principal-stress $\sigma_1/\sigma_c < 0.15$; if this ratio is > 0.15, the rock mass response near the borehole or excavation wall will be non-linear and this may negatively affect the results. Maloney and Kaiser (2005) demonstrated for the Canadian Shield that three stress domains are to be expected: *Domain I* (0 – 300 m depth) is stress relaxed mainly due to the movement along local flat-lying geological structures; *Domain II*, for intermediate depths of 300 to 600 m, is less disturbed when compared to the upper zones but may still be locally relaxed (it is a transition zone to *Domain III*); and *Domain III* (below 600 m) is undisturbed and the stress is defined by regional geological structures and its tectonic strain history. It was shown that the stress gradients at depth are much steeper than those obtained from gravitational gradients.

- Where the horizontal stress is the maximum stress, hydraulic fracturing produces sub-horizontal fractures, and these are difficult to interpret for horizontal stress magnitudes. Because hydraulic fracturing only provides the minimum stress, hydraulic fracturing

results tend to reflect some component of the vertical stress and the minimum horizontal stress. In addition, the pressure required for fracturing the rock at depths greater than 1000 m are beyond the capabilities of standard hydraulic fracturing equipment. This may limit the applicability of hydro-fracturing for in situ stress determinations.

- Large-scale observations and back-analysis of the failures, using depth and extent of failure can reduce the variability and provide consistent stress orientations and magnitudes when combined with accurate convergence measurements.

- A study of the results of in situ stress measurements from around the world suggests that the horizontal stress is often greater than the vertical stress particularly at less than 1000 m depth (Brown and Hoek, 1978; Sheorey, 1994). The vertical stress is normally assumed to be equal to the product of the unit weight of the rock mass and the depth below surface (so called overburden pressure) and measured in situ stresses are usually in agreement with this assumption. The ratio of average horizontal stress to vertical stress, k, can be as high as 3 and values of 1.5 or 2 are frequently assumed for prefeasibility studies.

- It is always recommended to measure the in-situ stress as early in the project as possible. Also, it is advisable, to use stress information that has been accumulated on previous projects to estimate the regional stress state.

- Many countries have compiled stress databases that are publicly accessible. For example, databases, including results from both over coring and hydro-fracturing have been established for both the Scandinavian and Canadian Shield. The world stress map project provides indicators for many parts of the world.

This thesis focuses particularly in the in-situ stresses found in the Canadian Shield and its consequences for excavation stability.

### *1.2.2 Stress Field in the Canadian Shield*

As part of Ontario Power Generation`s Deep Geologic Repository Technology Program, a review of stress measurements data available for the Canadian Shield was conducted with the goal of establishing average, representative, in-situ stress conditions appropriate for sub-regional modelling activities. The aim was to get a good understanding of the stress regime in the Canadian Shield. The results of these investigations were published by Maloney et al. (2006) and were revised in a supplemental report in 2016. Kaiser et al. (2016) elaborates on the impact of tectonic and thermal strains on the variability of stresses in heterogeneous ground.

The conceptual model by Maloney et al. (2006) consisted of the three stress domains introduced earlier in section 1.2.1 and described the stress state in the upper 1500 m of the Canadian Shield. Whereas specific measurements of ground stress magnitudes and directions will be required to refine site-specific repository design and reduce uncertainty in the simulations of excavations response, pre-feasibility studies can be based on this existing knowledge. The Canadian Shield is composed of metamorphic and igneous Precambrian rocks that can be divided in seven geological provinces (Figure 1-7).

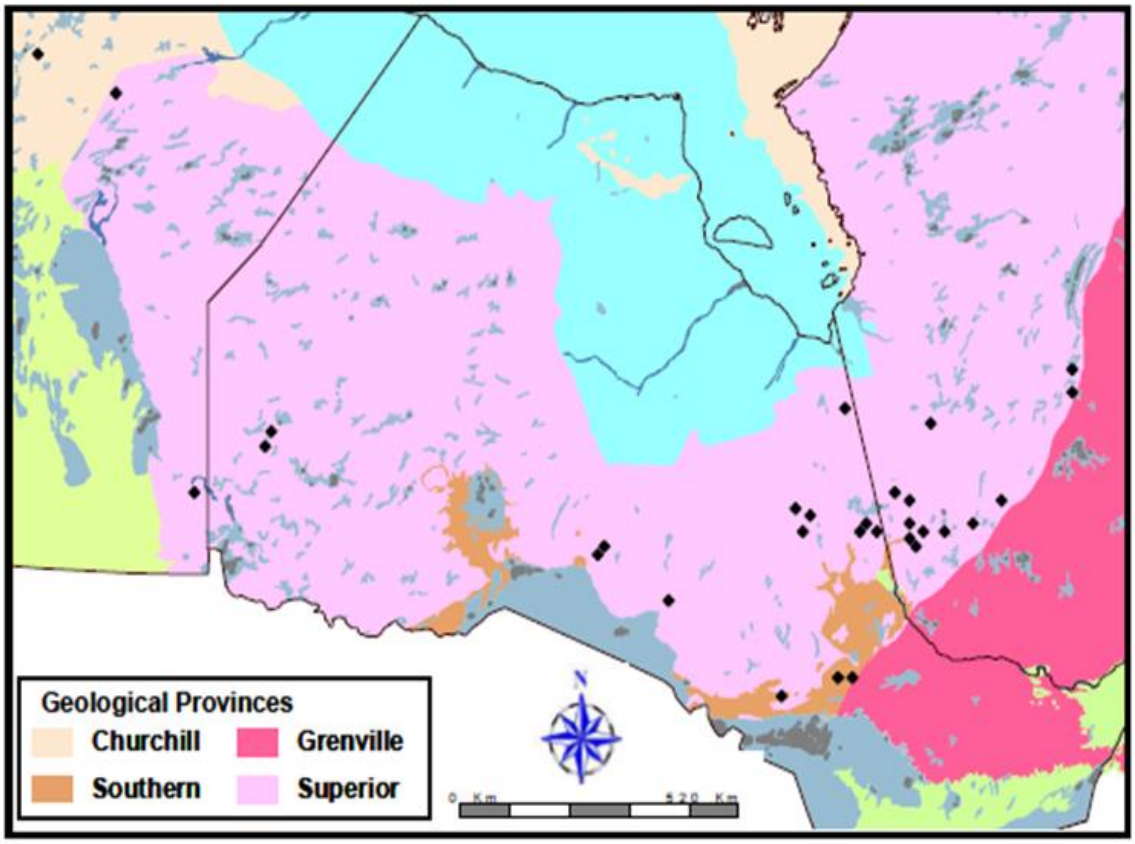


*Figure 1-7 Approximate location of stress measurements sites (black diamonds) in the Canadian Shield (Maloney et al. 2006).*

These seven provinces are distinguished by age, tectonic setting and metamorphism. Three of them are located in the Province of Ontario.

An extensive database on ground stresses in Canada has been compiled and maintained by CANMET (Canada Centre for Mineral and Energy Technology). With the exception of the stress measurement data obtained at AECL`s URL, most of the published stress measurement data from the Canadian Shield have been obtained from mining locations in Ontario, Manitoba and Quebec, using almost exclusively the borehole strain-relief technique.

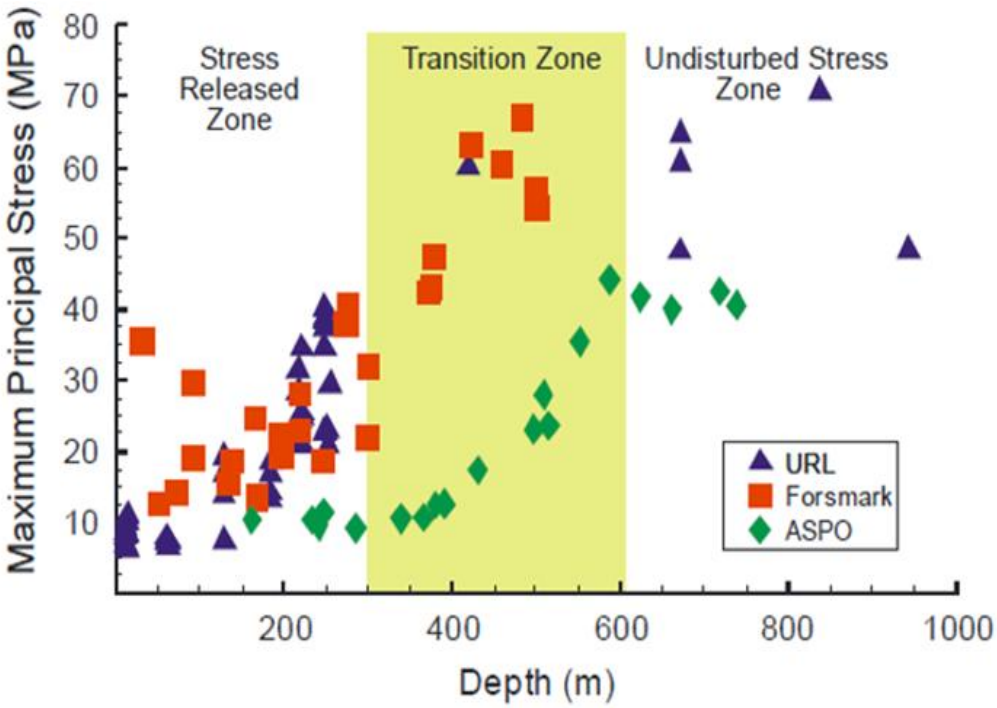


*Figure 1-8 Data from the URL and from two sites in the Scandinavian Shield (Martin et al., 2003, modified by Maloney et al., 2006).*

As indicated earlier, there are generally three Domains as shown in Figure 1-8. In *Domain I* (<300 m) the stress is disturbed or relaxed, due to yielding of the rock mass because of low confinement. This was more evident in areas close to flat geological structures (faults) near the surface. In *Domain III (> 600 m)*, the rock mass does not yield under the stresses from thermal and tectonic straining and therefore, in this Domain, the stress remains undisturbed. *Domain II* is referred as the transition zone from the disturbed to the undisturbed domain. In very strong rock masses, where there is absence of mechanisms for stress relaxation, *Domain III* may extend to the ground surface.

These stress domains typically exist in the upper crust and are the result of various loading and unloading processes.

There is always a degree of uncertainty when establishing the stress tensor based on field

measurements due to experimental errors (instrumental issues, installation or procedural mistakes) or analysis errors (misinterpretation of material properties, wrong assumptions associated with each technique etc.). Also, part of the difficulty in determining unique stress tensors in a rock mass stems from the fact that the in-situ stresses in rock are rarely uniform (Kaiser *et al.*, 2016). Their distribution depends on factors related to the rock mass heterogeneity in strength and deformation modulus, and on the loading history to which the rock mass has been subjected, for example, erosion, glaciation or tectonic activity, or thermal straining , as suggested by Sheorey (1994). The result of these influence factors is that the local stresses are clearly related to geology, material properties and loading history may look similar to the general stress state. Consequently, the contribution of these various factors must be understood when anticipating the local stress conditions and its variability.

For deep mining, it is most important to define the stress state in *Domain III* as this stress state provides the far-field boundary condition for numerical modelling. For the Canadian Shield, Martin et al. (2003) suggested that stress magnitude with depth it is best matched by an asymptotic function that provides an overall better fit. Arjang (2004) has reaffirmed a linear expression. The recommended equations given in Table 1-3 are linear and clearly non-consistent with the above discussed domaining.

*Table 1-3 Expressions for the principal stresses in the Canadian Shield, where z is given in meters to obtain stress in MPa (Martin, 2003; Arjang, 2004).*

| | ***Martin et al. (2003)*** | ***Arjang (2004)*** |
|---|---|---|
| $\sigma_1$ | $117\text{-}111e^{-0.00052z}$ | *13+0.0345z* |
| $\sigma_2$ | $61\text{-}59.9\ e^{-0.00077z}$ | *7+0.0232z* |
| $\sigma_3$ | *0.025z to 0.030z* | *3+0.0180z* |

These relations do not represent optimum expressions for *Domain III*, Maloney et al. (2006) based on the review of the Shield data, has recommended the following relations for *Domain III* (Table 1-4).

*Table 1-4 Expressions for the principal stresses in the Canadian Shield, Domain3(reviewed Maloney et al., 2006 and updated 2016).*

| | ***Reviewed 2016*** |
|---|---|
| $\sigma_1$ | *(11±4) +(0.038±0.004) z* |
| $\sigma_2$ | *(8±3) +(0.024±0.003) z* |
| $\sigma_3$ | *(0.7±0.8) +(0.021±0.001) z* |

| | ***Recommended 2006*** |
|---|---|
| $\sigma_1$ | $(23 \pm 11)$*+(0.026 ±0.012) z* |
| $\sigma_2$ | *(17±10) +(0.016±0.010) z* |
| $\sigma_3$ | *(1±8) +(0.020±0.008) z* |

Kaiser et al. (2016) presented a series of conclusions to consider for the design of underground excavations, related to stress variability:

- Stress data should be grouped by stress domain for shallow and deep domains; only data from Domain III should be used to extrapolate to great depth (>600 m).

- Stress variability can be attributed to rock mass heterogeneities that become dominant in conditions where the crust is thermally or tectonically strained. Near surface, strength heterogeneity tends to dominate the in-situ stress variability.

- At shallow depth, the stress variability tends to dominate excavation stability, causing relaxation or generating rapid changes in the depth of failure. At depth, it is the variability in rock strength what dominates the depth of failure although stress variability stills contribute to a gradual increase in the depth of failure.

### *1.2.3 Stress Path and Mining- induced Stresses*

For mining applications, it is important to know the history of loading and unloading of an

excavation. The stresses to which an excavation is exposed (loading and relaxation) changes as the extraction ratio changes or other mining-induced influences are experienced; e.g., during the advance of an undercut or during the propagation of a cave. As Martin (1997) stated, in practice the stress may not monotonically increase as in the laboratory; the in-situ loading path is much more complex. In reality, the loading path involving stress increase, decrease, and also stress rotations close to the boundary of excavations (e.g., near the face of excavation). Because the rock mass behaves different when in tension (much weaker) that when in compression it is most relevant to understand the impact of stress-path and the mining-induced stresses.

The stress path experienced by the rock mass in the roof and walls of the tunnel, can be estimated by using three-dimensional linear elastic or elastic-plastic stress analyses and plotting the results in the $\sigma_1$-$\sigma_3$ space. However, to properly simulate the effect of the brittle failure process, it is necessary to select numerical models that accurately quantify the stress redistribution around the tunnel when yielding by stress-fracturing. Mining activities induce a significant perturbation to the original stress state ($k_o$) modifying the stress ratio to k.

When a large excavation, a stope or other mining underground construction, is excavated in the vicinity of an existing tunnel the stress magnitudes near the tunnel wall are altered. Understanding the effects of induced stresses on the excavation behaviour is of vital importance. Such stress changes were monitored by Kaiser et al. (2000) at the Winston Lake Mine (Canadian Shield). In the relaxation zone (the hanging wall) and in the compression zone (in the back) during the excavation of a panel-shaped stope excavated in high-horizontal stresses as shown the stress paths presented in Figure 1-9.

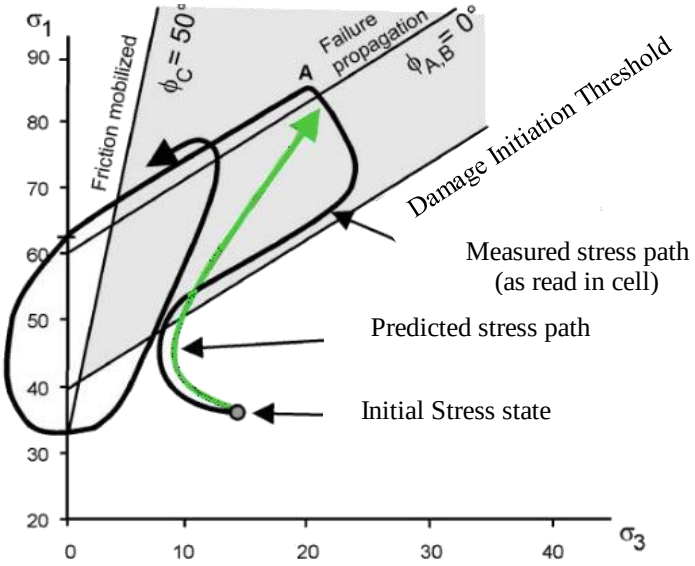


(a)

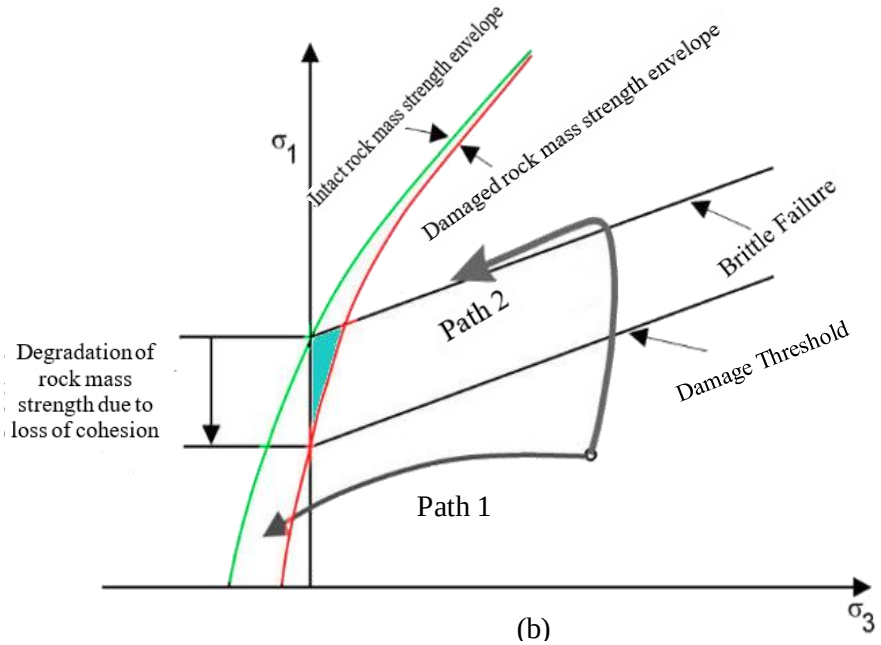


(b)

*Figure 1-9 (a) Measured and predicted stress paths; and, (b) schematic representation of Path 1 (relaxation) and Path 2 with stress-driven failure (Kaiser, 2001).*

This case study has been chosen because it exemplifies, what is analyzed in this thesis, i.e., how

the stress caused by mining activities can influence the tunnel stability. The importance that the stress redistribution, have on the final stability is explained with this case example and will be further commented when describing one of the tunnels models.

It is the induced stress near an excavation what determines what type of failure will occur by affecting and dominating the effect that the stress concentration has in the wall of the tunnel nearby.

Stress cells and extensometers were installed at Winston Lake mine, as a mean to establish the complete stress history of the rock mass and to study the stress path. There were monitored stress rotations by the cells installed (CSIRO type). It was found out that these large stress rotations can disturb pre-existing discontinuities (under shear in this case), causing fracture propagation, opening pre-existent joints and in general originating a great degradation of the rock mass (Figure 1-9b).

Particularly in laminated chert, where weak foliation planes exist, does stress rotation generate a loss in the tensile strength of the hanging wall. Path 1 in Figure 1-9b corresponds to a stress relaxation at stress levels below the damage initiation threshold, but it eventually produces failure in tension. Along stress path 2, which causes a stress driven wedge type failure, the predicted and measured stress paths were very different. It was observed how the redistribution of stress confinement, (specifically the loss of confinement or, situations where $\sigma_3 \rightarrow 0$) happened before the failure envelop (conventional failure criterion, curve in green in Figure 1-9a) could be reached. This loss in confinement generated a stress path higher than the conventional predicted (Figure 1-9b, red curve).

Figure 1-10a and b show a schematic stress change $\Delta\sigma$ that an excavation may experience. Virgin stress field, is represented by the black dot where ($\sigma_3/\sigma_c$ = 0.2 and $\sigma_1/\sigma_c$ = 0.25 in Figure 1-10a), measured at the wall, the minimum stress level is 0.3 and the maximum 0.5. If the tunnel experiences an increase in stress, in the major principal stress from the previous 0.25 to the indicated 0.4, the correspondent increase of minimum principal stress $\sigma_3$ changes from 0.2 to 1 (much bigger increase) as seen by Point A in Figure 1-10b.

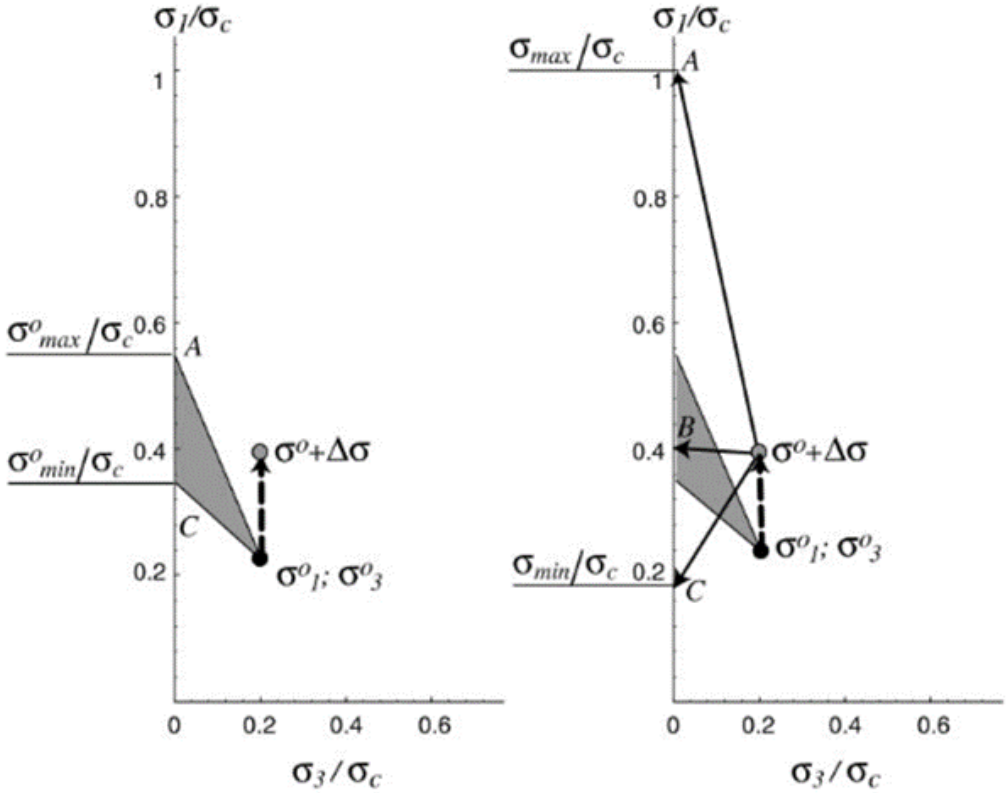


*Figure 1-10 Schematic stress path representation: (a) initial stress path, (b) final stress path after a stress increment $\Delta\sigma_1$ leading to relaxation to C and loading to A.*

Typically, the minor principal stress decreases near large excavations while the major principal stress may increase or decrease as illustrated by Figure 1-10 .

Mining-induced stress changes, in general aggravate the stress level. This change in stress leads to a drastic increase in the *SL* (Point A in Figure 1-10a) leading to spalling, and a corresponding decrease in the minimum *SL* (Point B in Figure 1-10b) causing relaxation. Hard rock, particularly brittle rock, is highly sensitive to stress increases and decreases as both paths can cause excavation damage.

If the minimum stress level change from an initially confined state to a relaxed state, occurs in the roof of an excavation, structurally controlled failure modes will be triggered. Consequently, mining-induced stress path often dominates the behaviour mode of excavations.

In summary, these induced stress changes can lead to stress fracturing or relaxation causing collapse of otherwise stable rock masses. It is necessary to recognize the potential for these mechanisms in order to improve mine sequencing and support design to minimize these types of failures. This is an issue of special importance in mining, because complex mining geometries, driven by operational constraints and ore body geometries may cause stress concentrations or reduce confinement and induce stress-driven or structural instabilities.

## 1.3 Rock Mass Strength for Stability Assessment of Deep Excavations in Mining

### *1.3.1 Introduction*

Rock mass characterization for strength estimation for excavations at great depth presents several challenges. This thesis focuses on the analysis of confinement dependent failure modes of brittle rock. The stability assessment strongly depends on a reliable determination of the rock strength and this will be covered in detail in Section 1.3.3. Here a discussion of mechanical conditions that

are encountered when excavating in depth is presented.

One of the challenges of excavations at great depth is that it is difficult to engineer a stable reinforced rock arch of broken rock that surrounds the excavation (at very little confinement). The behaviour of rock mass when is at deep depth differs with the variation of the confinement pressure, resulting in brittle fracturing at lower confinement and ductile behaviour when highly confined. In deep mines where high temperatures and high confinement pressures are typically found, the rock mass may deform in a brittle-ductile manner and rock mass failure is accompanied by large "plastic" deformations.

Since first experimental tests on granite by Von Karman (1911), many experimental studies have contributed to a better understanding of the effect that confining pressure has on the behaviour of brittle rocks. Patterson (1958) demonstrated using marble samples that the brittle-ductile transition increases with confining pressure. Observations from Mogi (1965, 1966) also demonstrated the existence of a rock behaviour transition related to the rock strength. It was then concluded, that rock fails in different manner under the action of different confining pressure. In this manner, it was differentiated that brittle failure was associated with relatively small plastic deformation, whereas large plastic deformations are associated with ductile behaviour. Heard (1960) and Singh et al, (1989), for example, defined the strain value of rock as an indicator to differentiate brittle from ductile behaviour.

Another characteristic of the ultra-deep environments is the time-dependent behaviour of deep excavations in hard rock (behaviour of the wall rock). As Muirwood (1972) indicated, the problems when designing tunnels are directly related to the competence of the ground. Thus, he explained that in soft ground the main problem is in the need of immediate support, whereas in

more competent ground the need of immediate support will depend on the stress-strain characteristics of the ground. He introduced a bearing factor ratio, $F_c$ that relates the unconfined compressive strength of the ground under uniaxial load to the pressure of the overburden. This ratio has been modified since, and updates for the tunnel stability classification presented as a matrix of Figure 1-1. Time dependent behaviour of wall rock, in high confining pressure, is also evidenced in ultra-deep gold mines in South Africa (Malan, 1999 and 2002).

Another point to consider, as noticed by many researchers, is the complex stress field that is created in the vicinity of excavations. From a mechanical point of view, there are three different zones surrounding the wall of a tunnel: elastic, plastic, and relaxation zones. It is often difficult to estimate or anticipate the extent (length or depth of failure; treated in Chapter 2. As exposed by He (2006), the problems associated with deep mining can be summarized as the following: determination of strength criterion and modelling of stability controls. The first refers to the complex, heterogeneous stresses composed of tension and compression, generated by the high variability in strength and stresses around an excavation. Loading and unloading are simultaneously produced in the radial and tangential direction, respectively, meaning that it will not be possible to estimate the rock mass strength only by tests, being necessary the use of a strength criterion that differentiates compression and tension (s-shape failure criteria introduced by Kaiser in 2008, treated in Chapter 2). Stability control model refers to the necessity of possibly using multiple support systems to endure stability. In other words, the importance of correct estimation of rock strength is key to avoid safety issues and to ensure effective tunnel advance.

Next aspect to discussed on how to obtain the rock mass strength. The aim of this section is to review the current methodology of rockmass quality and strength estimation. The following

Chapter 2 will then emphasize the analysis of rock strength and excavation behaviour in hard brittle rock.

### *1.3.2 Laboratory Testing to Estimate Rock Strength*

Laboratory testing should provide the strength and deformation properties that are necessary to characterize the rock. Due to the defected nature of brittle hard rocks, it is necessary to introduce some adjustments. Thus, the intact rock strength (UCS or $\sigma_{ci}$) and the defected rock strength ($\sigma_d$) that accounts for the strength of heterogeneous blocks of rock, containing defects, has to be determined by laboratory testing.

Bewick (2015) published an article describing how to properly obtain UCS parameter. Critical factors that impact that parameter are reviewed. He found out that the variability of UCS is around 25% in homogeneous and up to 35% in heterogeneous rock being the failure mode variation the main reason that causes this difference.

For deep mining is critical the understanding of the intact peak strength as obtained from three main laboratory tests: 1) tensile strength tests, 2) uniaxial compressive strength (UCS) tests and 3) confined triaxial tests. With the entire spectrum of strength from tension to high confinement defined, is then possible to anticipate the expected depth and also the shape of the failure of the excavation damaged zones around a tunnel.

In 2008, Kaiser and Kim provided guidance for design parameter selection for brittle intact rock. They explained how indiscriminate data processing programs can lead to highly misleading parameters. They suggested that design parameters, especially for brittle failing rocks have to be carefully selected. In the case of defected rock types, the intact rock strength is not representative

of the block strength required for the estimation of the rockmass. The orientation of defects affects the tests results and the mean value. For defected rock, the block strength is lower than the strength measured in the intact part of the rock. For brittle rock, is better to use back-projections of the Hoek-Brown criteria (non-linear) to obtain the intact strength of the low confinement range (or at zero confinement $\sigma_{ci}$). They indicated that filtering by mechanism of failure is essential to prevent strength underestimation. It is essential that groups of failure categories be combined like: rocks with failure through intact rock, failure involving intact rock and defected rock combined, and failure along defects.

They also discussed the issues of the triaxial testing. This type of testing is usually conducted as single-stage tests at one confinement stress magnitude. This type of single-stage strength test, is aimed to obtain the peak strength, so it can be load controlled or strain controlled. Some laboratories offer multi-stage tests sequencing the confinement in increments ranges. The testing procedures for multi-stage triaxial tests on brittle rock do require special equipment and the results are complex to interpret. The first difficulty is related to the determination of reliable imminent failure points for brittle rock specimens. Therefore, the results from multi-stage tests are often misleading.

Test results from lab test should be grouped in terms of their characteristics (specimen characteristics such as alteration, type and frequency of defects) and failure mode. Only the strength results obtained for intact rock specimens should be considered to establish the failure criterion.

Eventually, the failure data for intact and defected rock can be plotted in the principal stress space and the failure envelopes for intact and defected rock can then be obtained by fitting these data

sets.

### *1.3.3 Empirical Methods to Classify Rock Masses and to Estimate the Rock Mass Strength*

When describing the properties of the rock mass, rock mechanics engineers tend to differentiate between two terms: classify and characterize. In reality, the difference is not that noticeable. Rock mass classification is a means to differentiate features and to combined them into a group or class that follow specific principles or systems. Classification of the rock is an indirect method, it does not provide a direct measure of mechanical properties. The result is a subjective quantification of bad, to good to exceptional rock quality. Descriptive terms constitute the main difference between characterization and classification systems (Palmström, 1995).

Rock mass classification/characterization systems are used in the early stages of a project when little information is available and not detailed yet. There are several rock mass classification systems developed for various purposes. Those applicable to mining and tunnelling projects are briefly summarized here.

The main limitation of these systems, as mentioned by Riedmüller et al. (1999), is that a single number cannot describe a rock mass, its anisotropy, its variability, its time dependent behaviour, etc. Most classifications do not consider the failure mechanisms and thus may not be applicable to brittle failing ground.

The following systems summarized in Table 1-5 are discussed in some detail in this section

*Table 1-5 Rock classification/characterization according to Palmström, (1995) (Table based on Edelbro, 2003)*

| Name of Classification | Author and First Version | Application | Form and Type | Remarks |
|---|---|---|---|---|
| ***RQD*** | *Deere et al. 1966* | *Core logging, Tunnelling* | *Numerical F* General T*** | *Sensitive to orientation effects* |
| ***Q-system*** | *Barton et al. 1974* | *Tunnels, Large chambers* | *Numerical F. Functional T**** | |
| ***Mining RMR*** | *Laubscher 1977* | *Mining* | *Numerical F* Functional T* | |
| ***Geological Strength Index (GSI)*** | *Hoek et al. 1995* | *Mines and Tunnels* | *Numerical F. Functional T* | |

**Numerical F stands for Numerical Form: the input parameters are given numerical ratings according to their character; ** General T stands for General Type: the system is to serve as a general characterization; and ** Functional T stands for Functional Type: the system is structured for a special application (for example for rock support).*

Since different classification/characterization systems emphasize different parameters, it is often recommended to use at least two methods when classifying a rock mass (Hoek, 2001).

The most commonly used parameters are the intact rock strength, $\sigma_{ci}$, the joint strength, and joint spacing and ground water conditions. When analyzing a rock mass, scale is key parameter to consider as well, both small-scale and the large-scale joint characteristics must be taken into account.

#### 1.3.3.1 Rock Quality Designation (RQD)

Deere established in 1966 an index to assess quantitatively rock quality. It is the percentage of

core recovery that is based on the number of fractures observed in the drill core. Only intact pieces with a length greater than 100 mm are taken into account. They are summed and then divided by the total length of the core according to the following formula:

$$RQD = \frac{\Sigma \text{ Length of core pieces} > 10\ cm}{Total\ core\ length}\ x\ 100\ (\%) \qquad \text{Equation 1-9}$$

The greatest advantage is its simplicity. Core break produced by drilling should be discounted. Priest and Hudson (1976) found that, if no cores are available, RQD can be obtained from joint spacing (λ [joints/meter]) measurements by using the following equation:

$$\text{RQD} = 100\ e^{-0.1\lambda}\ (0.1\ \lambda + 1) \qquad \text{Equation 1-10}$$

RQD can also be determined from the number of joints/discontinuities per unit volume $J_v$, on the rock surface. $J_v$ is known as volumetric joint count and is the sum of the number of joints per unit length for all joint sets. Palmström, in 1982 developed a relation for a clay-free rock mass:

$$\text{RQD} = 115 - 3.3\ J_V \qquad \text{Equation 1-11}$$

The RQD system presents some disadvantages. According to Merritt (1972) the RQD presents some limitations in zones where joints are filled with clays because the joint friction is reduced in those areas leading to an overestimation of the RQD. The RQD is not scale independent. For excavations with large spans, it offers questionable values. Similarly, RQD is a good system in the case of rock masses with joints distances near 100 mm. RQD is relatively insensitive to changes in block size (Milne et al., 1991).

#### 1.3.3.2 The Rock Mass Quality (Q)-system

Barton et al. (1974) introduced the rock tunnelling quality index Q. This classification method was based on the analysis of 212 case records, mostly from tunnelling projects in Sweden and Norway.

It was developed to provided support recommendations. A large majority of the case records (180 of 212) were supported excavations. The excavations depths ranged from 5 to 2500 m. Several updates of the Q-system have been incorporated but the original parameters have remained. In 2002, some Q-value correlations were presented by Barton. The original Q-rating is defined by the following equation:

$$Q = \left(\frac{RQD}{Jn}\right)\left(\frac{Jv}{Ja}\right)\left(\frac{Jw}{SRF}\right) \qquad \text{Equation 1-12}$$

where, $J_n$ is the joint set number, $J_r$ is the joint roughness number (of least favourable discontinuity or joint set), $J_a$, is a joint alteration number, $J_w$, accounts for the joint water and pressure reduction factor, and SRF is the stress reduction factor.

According to Barton, the fundamental geotechnical parameters are, block size, minimum inter-block shear strength and active stress. The value of the minimum inter-block shear should be collected for the critical joint set, meaning the joint set which is most unfavourable for stability of a key block rock. Joint orientation is not included in this system.

The Q-system is specially recommended for tunnels and cavern with arched roofs. It encompasses the whole spectrum of rock mass qualities from heavy squeezing ground to massive rock. Q values range from 0.001 (extremely poor rock quality) to 1000 (exceptionally good).

To relate the tunnelling quality index Q to the behaviour and support requirements of an underground excavation, a term called the equivalent dimension, was introduced, $D_e$. It is the ratio of span to ESR which is a factor that depends on the utilization of the excavation (with or without entry of personnel and live of excavation):

$$D_e = \frac{Excavation\ span,\ \ diameter\ or\ height\ (m)}{Excavation\ support\ ratio} \qquad \text{Equation 1-13}$$

The following relation was established:

$$SPAN = 2Q^{0.66} = 2(ESR)Q^{0.4} \quad \text{Equation 1-14}$$

Q-system has been modified due to changes in the stress reduction factor (Grimstad and Barton, 1993) and also due to de advances in supporting methods, such as the introduction of steel fibre reinforced shotcrete with systematic bolting. The new correlations introduced by Barton in 2002, are focused on the applicability of the Q-system in site characterization and tunnel design. Since 2002, this system can also be used to estimate the uniaxial compressive strength of rock mass:

$$\sigma_{cm} = 5\rho \, {Q_C}^{1/3} \quad \text{Equation 1-15}$$

where, ρ is the density of the rock (t/m$^3$). This equation has not been widely tested and can lead to unreasonable values for massive to moderately jointed rock.

#### 1.3.3.3 Mining Rock Mass Rating (MRMR)

MRMR was developed for mining applications by Laubscher in 1975. This system builds on the basic RMR developed by Bieniawski (1973). It is determined by the rating of intact rock strength, RQD, joint spacing, joint condition and joint orientation. The RMR and MRMR values range from 0 to 100, covering all jointed rock mass qualities from very poor to very good. In 1984, Laubscher introduced a relation between MRMR and the in-situ rock mass strength by means of the following equation:

$$\sigma_{cm} = \sigma_c \, \frac{(MRMR - rating \; for \; \sigma c)}{100} \quad \text{Equation 1-16}$$

The MRMR classification includes adjustments for rock mass veining, the effect of blasting and weathering.

#### 1.3.3.4 Geological Strength Index (GSI)

Hoek et al. in 1995, developed this index from experience with slopes stability and tunnel projects. It is the only system that was specifically developed for rock mass strength determination by linking the generalized Hoek-Brown rock failure criteria parameters $s$, $a$ and $m_b$ to GSI. GSI estimates the reduction in intact strength to obtain the rock mass strength for different geological conditions. It is applicable to rock masses that consist of blocks that are formed by three sets of open joints.

GSI estimates the peak strength of a jointed rock mass as a function of the strength of the intact rock considering the rotation of the blocks. Cai et al., (2004) presented a quantitative approach including joint spacing and a description of the condition of the joint (joint condition factor adjustment) to overcome some of the deficiencies of the system. Cai et al. (2007) conducted several back analyses of large excavations, developing tools to estimate the residual strength or post-peak strength of the rock mass based on the GSI system (Figure 1-11).

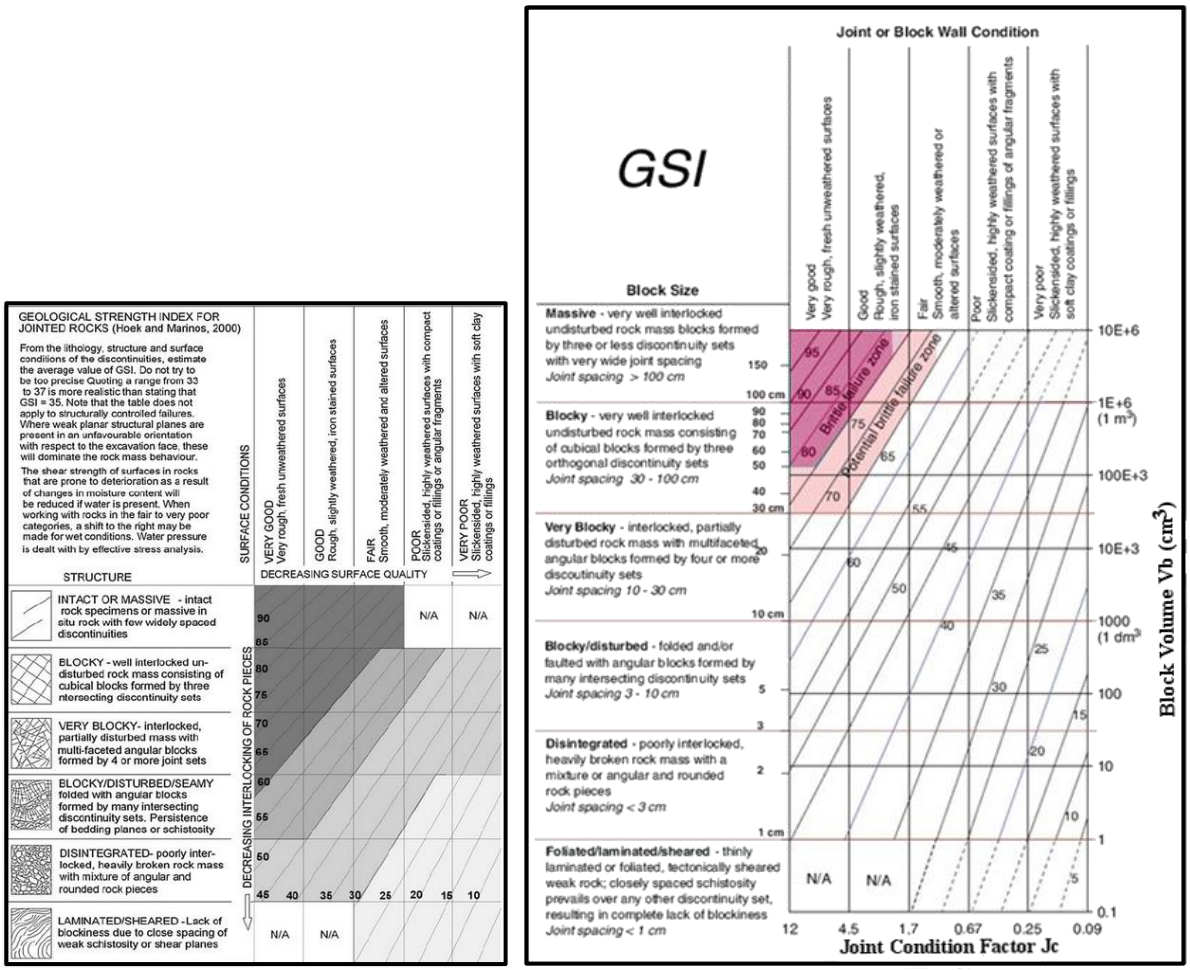


(a) (b)

*Figure 1-11 (a) Original GSI chart (after Hoek and Brown, 1997), (b) modified GSI chart (after Cai et al., 2004).*

GSI has been correlated with RMR and Q but it is best to establish the GSI value directly. Recently, it has been commented by Kaiser in 2016 in the 13th ISRM online lecture how those relations introduce errors, because RMR and Q-system considers factors that the GSI does not and therefore tend to mislead. In general, these relations results in an underestimation of the GSI by as much as 20 points, which translates into an underestimation by one rock class.

After the 13th online lecture conducted by Kaiser in March 2016, new limits of applicability of the

GSI system have been defined, as well as some guidelines to correctly estimate the rock mass strength when GSI is not applicable were developed. Following his lecture, this thesis reproduces and summarizes the concepts and ideas introduced in the lecture.

The GSI, when is applicable, constitutes a tool that has been field tested and is suitable for the estimation of the rock mass strength, especially when using a curved failure criteria and stress-driven failure conditions. Acceptability conditions consist of conditions where blocks are formed by open joints and can rotate and deform.

It is necessary to estimate the intact strength of the rock, $\sigma_{ci}$, when using the GSI system. When dealing with defected rock or blocks of defected rock, the rock mas is a heterogeneous with a lower strength. The GSI may then be misleading without appropriate adjustments.

GSI is also scale dependent, and as a general rule, it can be assumed that if the excavation size is at least 10 times the size of the blocks, the GSI will properly capture the failure mechanisms forming the basis for the GSI development. Translating this into the GSI chart, where excavation span is represented on the horizontal axis and blockiness is represented on the vertical one, the area where GSI is applicable can be defined as illustrated in Figure 1-12.

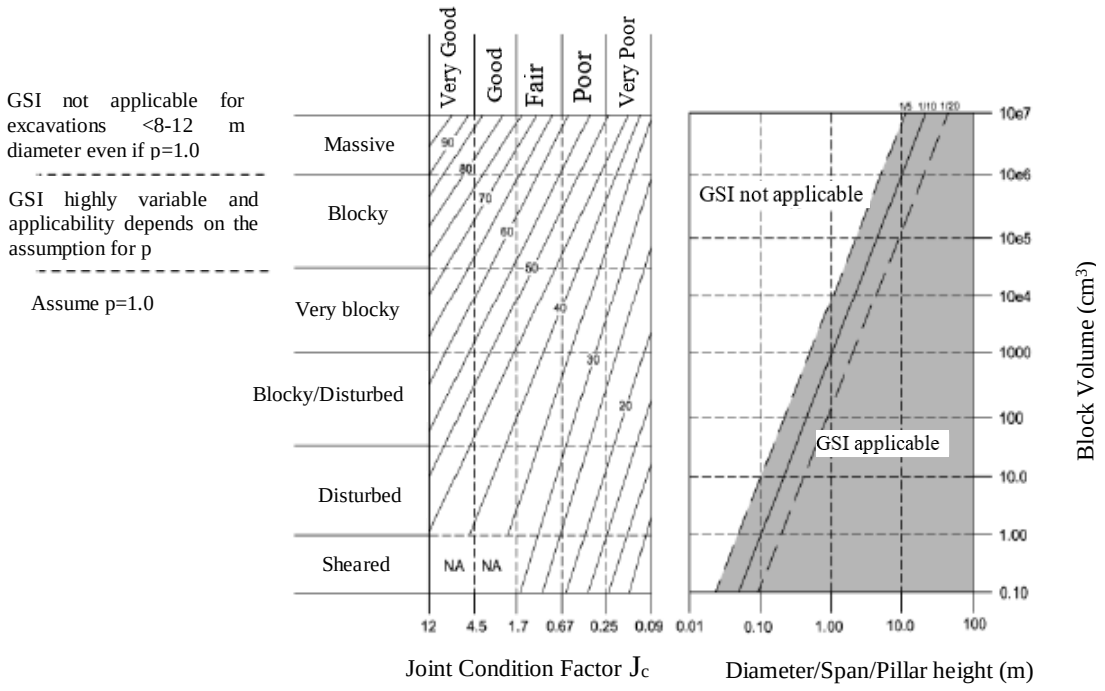


*Figure 1-12 Limits of applicability of GSI system (Kaiser, 2016)*

GSI is only applicable for excavations where open joints are forming the blocks. For instance, it must be checked very carefully if set blocks can be formed. As well, GSI is only valid if the excavation is formed by three joint sets and all of them are opened.

When GSI is applicable the following equations can be used to obtain the Hoek and Brown parameters s, $m_b$ and a:

$$\sigma_1' = \sigma_3' + \sigma_c \left(m_b \frac{\sigma_3'}{\sigma_c}\right)^{0.5} \quad \text{Equation 1-17}$$

$$s = exp\left(\frac{GSI-100}{9}\right) \quad \text{Equation 1-18}$$

$$\frac{m_b}{m_i} = exp\left(\frac{GSI-100}{28}\right) \quad \text{Equation 1-19}$$

According to Hoek and Brown papers, the strength of the intact rock needs to be determined by

considering intact rock; therefore, if during laboratory tests combined failures or defects are found they have to be eliminated. Hoek and Brown clearly specified that the data should come from triaxial test data. However, common and erroneous practices often utilize mean unconfined compressive strength values, and as a consequence, tend to underestimate in the input for the GSI system. In cases when only unconfined strength data is available, is absolutely essential to filter the data and only utilize values form truly intact samples, and not those affected by defects or flaws.

Therefore, when dealing with defected rock, there are several challenges to be overcome. Particularly there are three issues that deserve special consideration. Sometimes joints from core drilling are just defects due to mechanical processes during drilling itself or due to transportation of the sample to the lab. These are no natural joints and if by mistake they are accounted for in the GSI, the GSI is underestimated.

Another important aspect to take into account when dealing with defected rock, is the fact that when the peak strength is compared with the slope of the defected rock, it is noticed that the slope in the principal stress space of the defected rock is much steeper in defected conditions, because, the breakage leads to dilation of the joint. In this case, GSI is not taking into account the high degree of interlock and therefore is underestimating the m-value.

In other words, there are several factors that lead to incorrect estimates of the rock mass strength at depth. Quite often, in defected rock, users of GSI violate principles of applicability. When laboratory test data including unconfined strength data if is not adequately filtered, errors are introduced. In defected rock, when the defects are treated like open joints, but they are not, severe strengths underestimations are obtained.

GSI was developed where inner shell conditions dominate rock behaviour (this inner shell behaviour is further explained in Chapter 2). The GSI was therefore developed for conditions that constitute the framework of this thesis. It is important to notice that when rock is confined there are other factors that increases the strength of the rock mass, and they are related to interlock. These situations, where GSI is not valid are outside the scope of this thesis. However, it is explained here in an attempt to provide a fully understanding of the applicability of this system.

The first factor is over-closure. Barton in 1974 and 2007 published the findings of his study on joints, showing that when they are preloaded, they have a much higher strength. Over-closure increases the angle of friction and the apparent cohesion. It means that if for example two identical rock masses are compared, and one is highly confined, the block boundaries are much stronger than the rock mass coming from a high confinement zone. This is one of the reasons that explain why the GSI index underestimates rock mass strength in high confinement environments.

Another factor is the interlock. GSI indicates that there is a decreasing interlock from the top to the bottom of the GSI chart, in terms of blockyness (Figure 1-12). But this decrease, does not deal with the interlock caused by stress fracture rock where the blocks are fitting together. For instance, when GSI is not applicable, it is critical to take into account the tight interlock that is created in hard rock conditions, where the confinement prevents block rotation. It is important to differentiate between massive and defected conditions, but in both situations, the standard equations, (Equations 1-17, 1-18 and 1-19) will not be not be applicable. Because the apparent cohesion is high, the parameters of the Hoek and Brown criteria, values of $a$, $m_b$ and $s$ will be much higher than assumed for non-interlocking ground, and therefore are no longer valid.

In situations of non-applicability, it is necessary to establish the spalling strength of the rock mass

as well as the strength when the rock is confined but blocked (further commented in Chapter 2).

In the low confinement and for homogeneous rock, it is necessary to get the modified strength of the intact rock as $\sigma'_{ci} = 0.8\ \sigma_{ci}$ (Equation 1-20), and for the spalling strength of the rock, it can be used the method established by Martin in 1995 (Chapter 2).

In high confinement situation, and for homogeneous rock, the principles of Hoek and Brown are valid, but GSI is not. Therefore, the block strength is used instead, $\sigma'_{ci}$, and s and $m_i$ of the Hoek Brown criteria (as established in 1997). With this correction, the resulting strengths are now much higher than those obtained if the original GSI was used (because of GSI underestimation in this scenario).

The procedure for the low confinement situation and when the rock is defected, is to first establish the block strength, $\sigma_{bl}$, and then obtain the spalling strength by the same principles that Martin introduced in 1995. In this case, the block strength is used, instead of the intact strength.

In high confinement, and again, for defected rock, the block strength is applied as well, $\sigma_{bl}$, and an adjustment in the Hoek and Brown criteria is introduced, using $m_{bl}$, instead of $m_i$, being $m_{bl} >> m_i$.

The block strength can be determined by using the MRMR system as defined by Laubscher and Jakubec (2000) because it provides reliable instructions on how to establish the block strength.

Another important recommendation is to realize that when the rock is fractured, the blocks cannot rotate near to the excavation, which leads to shear rupture, and eventually when confined, leads to the tri-linear failure criteria.

As consequence, it is necessary to differentiate between inner shell and outer shell behaviour and

rock properties either have to be established separated for each shell or a solution to match the two behaviour zones has to be adopted.

The approach adopted in this thesis, for excavation stability assessment is to consider the spalling strength and account for the transition, which cannot be made by a linear failure criterion, therefore an s-shaped is applied. For inner shell behaviour, this is reflected in the DISL approach introduced by Diederichs et al. (2003, 2007)) (see Chapters 2 and 3).

In summary, and according to the 13$^{th}$ ISRM, given by Kaiser in March 2016, the following steps are summarized as a methodology or guideline to obtain reliable rock mass strength parameters:

1. Establish GSI independently by assessing all the relevant factors and applicability criteria.

2. Obtain correct intact rock strength, $\sigma_{ci}$ ; do not use defected rock strength; filter the data properly.

3. Check when GSI is applicable and do not use it when not applicable (scale, interlock, trace length, etc.).

4. Use the methodology explained before to obtain the block strength, $\sigma_{bl,}$ and place it in the GSI equations; replace intact rock strength, $\sigma_{ci}$, by block strength $\sigma_{bl}$.

5. When GSI is not applicable, distinguish between low confinement and high confinement conditions and obtain separately the rock mass strength parameters and get the anchor points for the tri-linear failure criteria envelope.

6. Once the failure envelope is established fit it, depending on the adopted numerical model

capability, with representative linear or curved peak failure envelops.

7. Establish the post-peak strength separately.

### *1.3.4 Conclusions*

Rock mass characterizations systems tend to underestimate the confined strength because the stress induced failure mechanisms are not properly accounted. Among all the empirical methods, the GSI approach gives the most reliable strength properties if it is applicable (used in its limits of viability) and if the data from field is processed properly.

RMR and Q-system methods are most useful for direct support selection in situations where mining-induced stress changes and stress-fracturing is not involved.

For conditions of GSI>65, the GSI is generally not applicable and it is necessary to account differently for the inner and the outer shell characteristics.

The methods described here provide a basis for design and it is necessary to implement them correctly and verify them with field observations, monitoring as well as use of back analyses to ensure that the characterization is the appropriate for the conditions encountered.

# Chapter 2

# 2 Brittle Failure Processes

## 2.1 Introduction

Brittle failure is caused by localized extension strain or tensile stress caused by compressive loading (tangential strain) that occurs near the boundary of an excavation at low confinement conditions. Hence, it is necessary to understand the mechanisms of the formation or initiation and evolution or propagation of crack damage.

Brittle rocks, when unconfined or lightly confined (near excavation boundary) fail by extensional crack damage leading to spalling near excavations in the" inner shear" with low confinement. Failure by shear at high confinement is also facilitated by crack damage mechanisms, but with short crack lengths due the restricting confinement. This means that brittle rocks experience two different modes of failure; extension or tensile fracture and shear failure or shear rupture (Griggs and Handin, 1960). Shear failure is the dominant failure mode observed in triaxial compression tests at high confining

Before going further in the characterization of brittle failure, the theory of rock fracture and mechanics producing this failure is briefly reviewed.

## 2.2 Fundamental Mechanics of Brittle Failure

Griffith (1921) proposed that tensile failure in brittle materials is caused and controlled by the presence of small cracks, which he represented by flat elliptical openings. His initial work dealt with fracture in a material subjected to tensile stress, but later he extended the concept to include

biaxial compression loading (Griffith, 1924). He developed parabolic failure envelopes based on crack propagation with shear at the cracks. In the 1960's, Griffith's two-dimensional theory was eventually extended to three dimensions by various authors.

As Hoek and Martin (2014) indicated, Griffith theory is only truly valid when referring to the initiation of tensile failure in compression. However, under certain conditions when tensile stresses exceed the tensile strength, tensile failure initiation can lead to crack propagation. In these cases, the tensile cracks propagate in the direction of the major principal stress ($\sigma_1$). The original theory of Griffith was developed from analyses of crack initiation at the tip of an open elliptical crack. In the case of rocks, most of the defects from which tensile cracks originate are weakly "cemented" grain boundaries.

McClintock ad Walsh (1962), proposed that tensile failure from closed Griffith cracks can be predicted on the basis of the Mohr-Coulomb equation, where $\phi$ is the angle of friction and $\tau_o$ is the shear strength at zero normal stress (the cohesion).

$$\tau = \tau_0 + \sigma \, tan\phi \qquad \text{Equation 2-1}$$

Hoek (1965) discussed the transition from the Griffith theory for open cracks, which applies for confining stresses $\sigma_3 < 0$, and the modified theory for closed cracks that applies for compressive confining stresses. A graphical representation of the brittle fracture initiation criteria is represented in Figure 2-1.

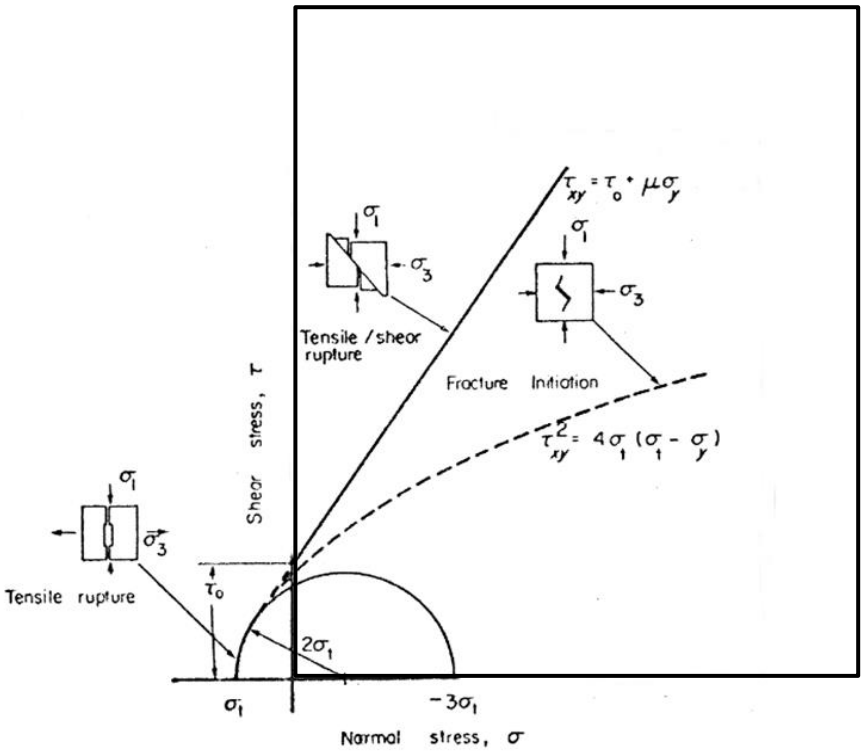


*Figure 2-1 A rupture criterion for brittle rock (figure from Hoek, 1968)*

Zuo et al. (2008) examined the growth of micro cracks in brittle rocks and assumed a sliding-crack model to generate new cracks when the frictional strength of the sliding surfaces is overcome and found that the failure initiation criterion can be expressed as follows:

$$\sigma_1 = \sigma_3 + \sqrt{\frac{\mu}{k}\frac{\sigma_c}{|\sigma_t|}\sigma_c\sigma_3 + \sigma_c^2} \qquad \text{Equation 2-2}$$

where, $\mu$ is the coefficient of friction, the coefficient k is based on a maximum stress criterion, $\sigma_c$, is the uniaxial compressive strength, and $\sigma_t$ is tensile strength.

### *2.2.1 Fracture Initiation and Propagation*

Griffith theory of brittle fracture initiation and its several modifications have been discussed by many authors. His theory offers an important background for an understanding of the mechanics of brittle failure initiation. However, it also brings controversies and limitations of applicability because observed realities sometimes seem to contradict this theory. Griffith suggested that the

failure occurs when the most unfavourable oriented crack (most vulnerable) begins to extend under the applied stress. This seems to be contradicted in reality when fractures originating and propagating from grain boundaries occur. Most important, it is not that common that the crack will follow the path suggested by Griffith. Instead, tensile crack paths will follow paths dictated by grain boundaries with only some cracks running across stronger, intact grains.

The initiation of tensile cracks near the tip of a Griffith crack, whether this crack is open or closed, depends upon the orientation of the Griffith crack in relation to the applied stresses. This process of initiation, is extremely sensitive to the magnitude of confinement and the extent of failure (induced crack length) reduces quickly as the minor principal stress ($\sigma_3$) increases. For a certain level of confinement, in the range of $\sigma_3 / \sigma_1 = 0.2$, tensile failure is prevented as the predominant failure mechanism and the peak strength is controlled by shear failure.

For applications to confined brittle rocks, the modified Griffith crack model (Equation 2-1 and Equation 2-2) is more appropriate. The shear strength of the confined defects (grain boundaries) is a key parameter in the initiation and propagation of the tensile failure. The ratio of uniaxial compressive strength to tensile strength ($\sigma_c/\sigma_t$) is important in understanding the failure of brittle rock.

This thesis focuses on the analysis of the behaviour of brittle rocks in the low confinement spectrum where extensional failure processes dominate, and spalling occurs. In heterogeneous rock masses, this extensional failure process is typically combined with some shear failure on weakness planes such as joints or veins. In this thesis, the term spalling is used to describe this combined failure process and not just extensional failure.

### *2.2.2 Spalling at the Tunnel Scale*

Spalling is the failure mechanism seen in the walls of excavations promoted by extensional fractures under a compressive field stress, i.e., failure is seen in the walls of excavations in rocks with a low ratio of tensile to compressive strength (brittle rocks). As indicated before, some shear slip is often part of the spalling process.

There are two practical issues associated with spalling:

- identifying the conditions that will initiate spalling; and
- defining the extent and depth of spalling failure.

The transition between pure shear and extension-type failure is represented in Figure 2-2 by the spalling limit defined by a constant stress ratio $\sigma_1/\sigma_3$; typically, between 10 and 20 for intact rock.

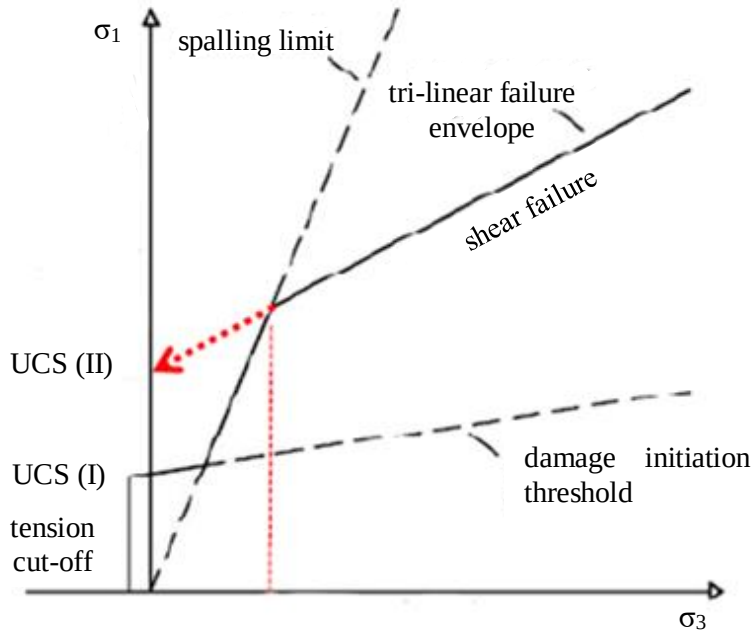


*Figure 2-2 Tri-linear failure envelope accounting for the dominating damage initiation and extensional fracture propagation processes (Kaiser and Kim, 2008); UCS(I) is the actual UCS as measured in laboratory tests; UCS(II) is the back-projected, apparent UCS.*

According to Kaiser and Kim (2008), the Mohr-Coulomb shear failure criterion does not account for the strength reduction due to extensional damage initiation and propagation, and therefore, is only applicable to the right of the spalling limit. To the right of the spalling limit, standard shear failure criteria tend to under-predict the in-situ rock mass strength and to the left of the spalling limit (low confinement zone), they tend to overestimate the in situ rockmass strength by not taking into account the reduction of in-situ strength due to the loss of cohesion as a consequence of the tensile crack damage.

With respect to the post-peak strength of brittle materials, the fundamental shear strength equation with strain-independent parameters is not valid:

$$\tau = c + \sigma' \tan\varphi \qquad \text{Equation 2-3}$$

Martin (1997) showed that the cohesional and frictional strength components need to be mobilized by strain and do not mobilize together in brittle rocks. The strength components depend on the cumulative damage or plastic strain. To reflect this Kaiser and Kim (2008) introduced Equation 2-4 which is a reformulation of Equation 2-3 with strain-dependent terms:

$$\tau = c\,(\varepsilon, \sigma_3) + \sigma'\,(\varepsilon, \sigma_3) \tan\,(\varphi + i(\sigma_3)) \qquad \text{Equation 2-4}$$

It is important to note that spalling associated with hard rock excavations, while brittle in nature can be violent or non-violent. This process dominates rock damage and failure processes in crystalline rocks near excavation boundaries under high stress. In unsupported conditions and under an anisotropic in situ stress field, the process of spalling leads to commonly observed notch geometries. If violent, it leads to strainbursts.

### *2.2.3 Brittle Failure Strength Envelope or Spalling Limit*

As discussed above, brittle rocks experience two different modes of failure, extension or tensile

fracture and shear failure. As confinement is decreased and the ductile transition is approached from the high confinement zone with shear failure, damage and deformation becomes characterized by extensional fracturing instead of shear fracture. Various studies (Kaiser et al., 1996; Martin et al., 1999; Kaiser et al., 2000; Diederichs, 2003 and many others) revealed that brittle failure processes often dominate the rock mass behaviour near excavations (e.g., Martin and Christiansson, 2003,2009) and Kaiser and Kim (2008) demonstrated for massive to moderately jointed brittle rock masses that the strength envelope is best represented by a tri-linear or s-shaped failure envelope (Figure 2-2).

Kaiser and Kim (2008) also showed that the tri-linear or s-shaped envelope is applicable for many rock types. By extrapolation the equivalent strength envelope can be established for massive to moderately jointed, brittle rock masses as shown in Figure 2-3.

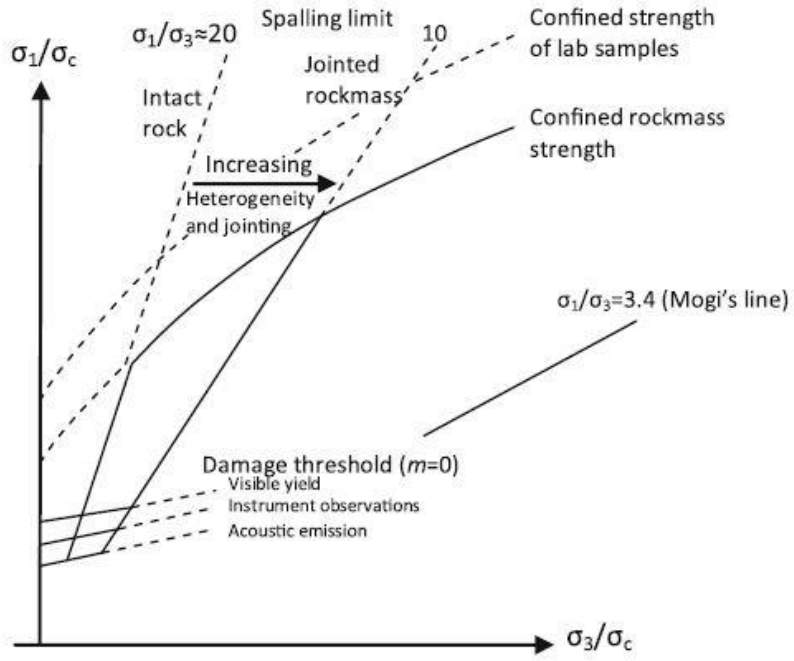


*Figure 2-3 Schematic s-shaped failure envelope with spalling limit cut-offs for brittle rock and rock masses (Kaiser et al., 2000, Diederichs, 1999,2003)*

The first portion of the brittle strength envelope in Figure 2-3, i.e., the damage threshold, is modeled using the brittle strength parameters (m = 0, s = 0.11). This damage threshold depends on the degree of damage and the heterogeneity.

Above this threshold, the confined strength envelope, is cut-off by the spalling limit at $\sigma_1/\sigma_3$ = 10 to 20 for intact rock and lower for rock masses. It depends on factors such as the rock heterogeneity and joint frequency and persistence. These two components of the failure envelope are captured by the DISL approach (see later in Section 2.4.1). The shear strength to the right of the spalling limit is of little relevance for tunnel design as failure can rarely be caused at related very high confining pressures.

Knowing that spalling can occur in brittle rocks, the next step is to establish the severity of the failure in terms of the failed rock volume or the depth of failure.

## 2.3 Depth of Brittle Failure Estimation

The depth of failure $d_f$ covers the area where the rock is stress-fractured and prone to ravelling if unsupported. It is important to differentiate this depth of failure $d_f$ from the depth of yield, $d_y$, which defines the limit ti where the rock is permanently deformed or plastically strained ($d_y$ is obtained by numerical models; $d_f$ is obtained from observations of notch formation in tunnels). Therefore, $d_y > d_f$ because yielded rock is damaged but still is cohesive and does not unravel.

The depth of failure, $d_f$, can be estimated by semi-empirical numerical modelling (Martin et al., 1999) or by empirical charts (see Section 2.3.1). This depth of failure depends on the stress level, SL, defined as the ratio of the maximum tangential induced stress $\sigma_{max}$ at a circular excavation in elastic ground to the unconfined rock strength, $\sigma_c$ *or UCS*. It is also influenced by rock mass

structures and the geometry of the opening. Kaiser (2016) clarified that the data used for the empirical equations was from locations of extreme instability and thus termed it as the "extreme" depth of failure, $d_f^e$. The depth of failure is also dependent on the stress path that an excavation experiences because of the sensitivity of brittle hard rock to stress changes.

Detournay and St John (1988) categorized possible yield failure modes around a circular unsupported tunnel as shown in Figure 2-4.

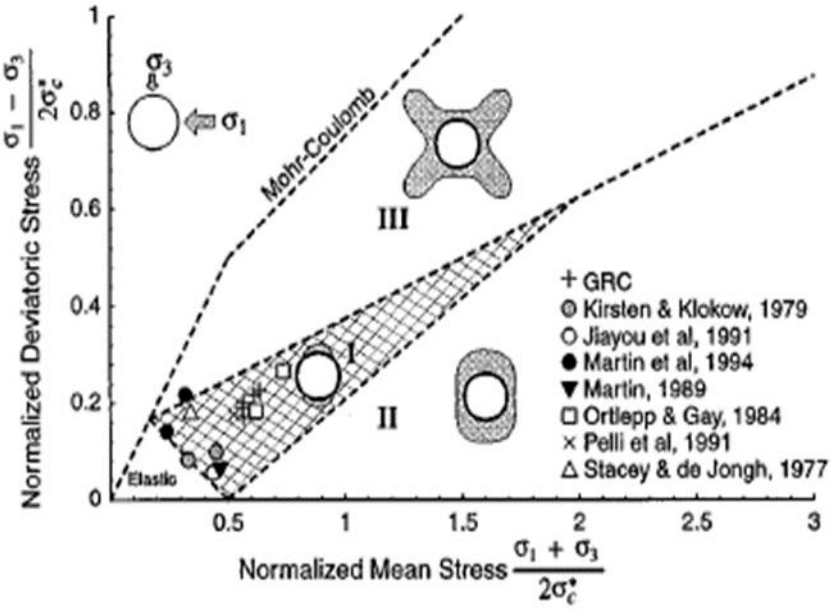


*Figure 2-4 Relationship between failure modes and far-field stress state for unsupported circular opening (Detournay and St John, 1988)*

In this graph, the normalized uniaxial compressive field strength $\sigma^*_c$ is assumed to be $0.5\sigma_c$. In region I the extent of the predicted failure zone is localized. The data from Martin et al. (1999) all fall into this region. Only for high normalized stress values does the failure shape become continuous around the excavation.

Martin and Chandler (1994) showed in damage-controlled laboratory tests that the accumulation of extension cracks reduces the cohesion of the intact rock. Their results showed that cohesions experienced a reduction by 70% when friction is fully mobilized. During the brittle failure process peak cohesion and friction are not mobilized together. After performing experiments in the Mine-by-test tunnel, they demonstrated that damage initiation and the depth of failure could be obtained from contours of constant deviatoric stress and established the following equation in terms of Hoek-Brown parameters (s, $\sigma_c$).

$$\sigma_1 - \sigma_3 = \sqrt{s\sigma_c^2} \qquad \text{Equation 2-5}$$

This equation should only be applied when considering stress-induced brittle failure. It cannot be used to define regions of tensile failure because it overestimates the tensile rock strength.

At low confinement levels, the accumulation of significant rock damage, equivalent to loss cohesion, occurs when the principal stress difference ( $\sigma_1$- $\sigma_3$) = $^1/_3$ to ½ $\sigma_c$ is reached or exceed. This is equivalent to a bi-linear failure envelope cut-off starting at m = 0 (Hoek and Brown) as discussed by Kaiser (1994).

The shape of the region defined by Equation 2-1 is controlled by the stress ratio ($k_o$) of the major to the minor principal stress ($\sigma_1/\sigma_3$) in the plane of the tunnel as illustrated by Figure 2-5.

For $k_0$ =1, the stress is identical around the circumference and excavation damage should be uniform around the tunnel as seen in Figure 2-5 (left model), that correspond to a tunnel under a uniform field stress equal to 54 MPa. On the right of Figure 2-5 it, is represented this concept for $k_0$=2, which corresponds to a tunnel modeled in Phase 2, where the horizontal stress is 54 MPa, and vertical stress is 27 MPa.

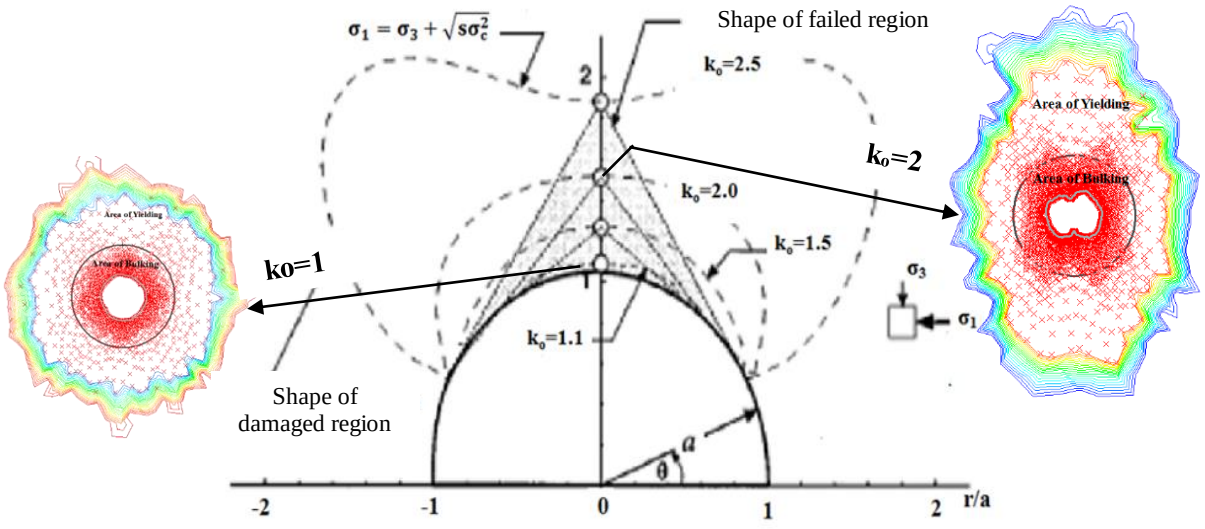


*Figure 2-5 Extent of yield or damage around a circular opening defined by Equation4-1 for various $k_o$ ratios (modified from Martin et al., 1997)*

The stress gradually increases as a tunnel advances and stress driven progresses and notches start to propagate from the point of maximum tangential stress (located in the roof at $\Theta$=90°) towards the damage initiation limit, described by Equation 2-1, until it reaches the deepest point of damage in the direction of the minor principal stress. For $k_o$ = 2, it is seen how the damage around the excavation is localized (in this specific model it propagates in the roof location because of how the stress are applied.

In reality, there is however always a weak point around an excavation and practical experience indicates that due to heterogeneities, failure is not symmetric and often localized on one side.

### *2.3.1 Empirical Approaches for Estimation of Depth Failure*

By analyzing case studies of observed extreme depths of failure from excavations damaged by rock bursts (Kaiser et al., 1996) and tunnels from around the world failing in non-violent manner

(Martin et al., 1999), an empirical relationship between the depth of failure (recently clarified by Kaiser (2016) as the extreme depth $d_f^e$ ) and the stress level *SL* was established for brittle rock. The formula introduced in Equation 2-6, shows that the depth of failure normalized to the tunnel radius *a* is linearly increasing with the stress level $SL = \sigma_{max}/\sigma_c$.

$$\frac{df}{a} = 1.25\,\frac{\sigma_{max}}{\sigma_c} - 0.51 \pm 0.1 \qquad \text{Equation 2-6}$$

where, $\sigma_{max}$ is calculated as the ratio of maximum tangential stress at the wall of a circular opening in elastic ground and $\sigma_c$ is the uniaxial compressive strength. This ratio is referred as $SL_{UCS}$.

Martin et al., (1999) demonstrated that the empirical relationship established by Equation 2-6 could also be predicted using Hoek-Brown brittle parameters (m = 0, and s = 0.11) in elastic numerical modelling. Figure 2-6a illustrates that this equation defines the extreme depth of failure (failure at locations where the maximum failure was recorded).

Recently, Perras and Diederichs (2016) demonstrated that this "extreme" depth of failure is usually an overestimation or a very conservative measure of the damage. From their observations and new data, they established lower values of the average or typically encountered depths of failure (Figure 2-6b). Kaiser (2016) based on this new evidence, labelled this as the mean depth of failure $d_f^m$ and provided the following approximate relation to the extreme depth of failure.

$$d_f^m = \frac{d_f^e}{3.5\ to\ 4.5} \qquad \text{Equation 2-7}$$

The difference between these two depths of failure becomes relevant for specific applications. For example, the extreme depth of failure (Equation 2-6) is useful to determine the length of the bolt to be installed, whereas the mean depth of failure gives an idea of the average over break that should be expected from stress fractured ground.

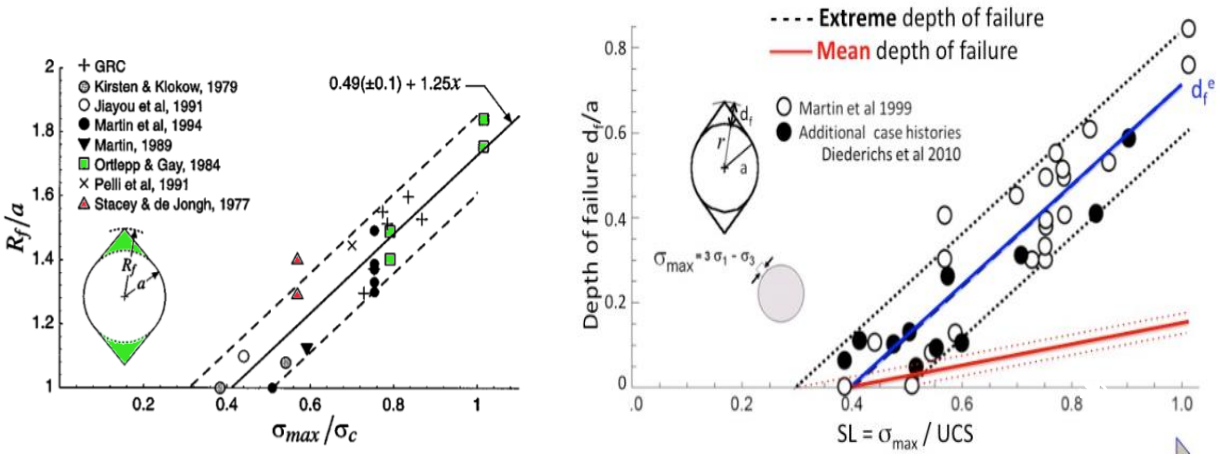


*(a)* *(b)*

*Figure 2-6 a) Empirical prediction of depth of stress-induced failure using the Hoek-Brown brittle parameters (Martin et al., 1999), b) chart by Perras and Diederichs (2016) modified by Kaiser (2016).*

Perras and Diederichs (2016) have shown that the trend lines flatten at high SL. Hence, the limits of applicability of this empirical chart is $\sigma_{max}/\sigma_c = 1$. As was mentioned in the problem definition in Chapter 1, this thesis deals with excavations that present a high mining induced stress with $\sigma_{max}/\sigma_c > 0.8$ and intermediate level of stress with $\sigma_{max}/\sigma_c < 0.8$). This means that this semi-empirical approach will tend to overestimate the depth of failure for excavations in high stress environments but is applicable in tunnels under intermediate stress level.

Another empirical approach to estimate the extent of failure consists in using brittle parameters ($\phi = 0$ and a rock mass strength equal to $q = \sigma_c \sqrt{s}$), and then match it with what is predicted in the closed-form solutions illustrated in Figure 2-4 by Detournay and St John (1988).

Combining the empirical relationships to estimate the depth of failure with mining-induced stress level calculations is possible to estimate the impact of stress and stress change on the stability of the tunnel in highly stress fractured rock.

In summary, to estimate the extreme depth of brittle failure around tunnels in intermediate stress environments, the empirical criterion by Martin et al. (1999) is applicable. The stress-induced failure process begins at stress levels of about 40% of the rock's unconfined compressive strength.

When this condition occurs, the depth of stress-induced brittle failure around a tunnel in massive to moderately fractured rock can be estimated by using elastic stress analysis and Hoek-Brown failure criterion with the associated parameter (m = 0 and s = 0.11). There is a fundamental assumption considered here, that the stress-controlled failure process around the tunnel is dominated by cohesion loss. For instance, the $m_b$ parameter, which can be equated to frictional strength, is set to zero. It should be clarified that this approach (m = 0) differs from what would be used for an elasto-plastic yielding failure mechanism, where the frictional strength component mobilizes and dominates the behaviour of the rock mass, requiring the m value to be set to a typical value for the rock type in question. The m= 0 approach is to be used with elastic models and only to obtain the depth of extreme failure (not the lateral extent).

These findings and the empirical relationship have been repeated and confirmed in other studies of tunnel stability in highly stress-fractured ground. For example, Diederichs et al. (2010) plotted the maximum tangential stress normalized to the crack initiation (CI), as a way to introduce an alternative to the stress level $SL_{CI.}$ Their results confirmed that Martin (1999) approach was correct.

The latest findings performed by Perras and Diederichs (2016) however suggests that the empirical depth of failure limit described by Diederichs (2007, 2010) and by Martin (1999) should be used cautiously at higher maximum tangential stress to strength ratios ($SL_{UCS}$). Their numerical results indicate the existence of a non-linear relationship with the depth of failure. They indicate that linear trend used up to now may overestimate the $d_f$ when SL >1. Their approach is further

developed later in Section 4.4.

### *2.3.2 Modelling Approach to Estimate the Depth of Stress-Induced Failure*

As mentioned above it has been widely established that shear-based failure criterion like Hoek-Brown or Mohr-Coulomb yield criteria over-estimate the in-situ strength of brittle rock in the low confinement zone (left to spalling limit).

A different methodology for predicting the extreme depth of spalling overbreak for deep tunnels is provided by Diederichs (2003, 2007). This methodology has been further developed by Kaiser and Kim (2008) Kaiser (2010) and Cai and Kaiser (2014) as the s-shape failure criteria mentioned before. The procedure introduces a bi-linear failure criterion that accounts for the different stress thresholds under which brittle fractures initiates and propagate during spalling. The criterion captures the dependence of fracture propagation on confinement for materials that are prone to spalling, and can be incorporated into a non-elastic numerical model using modified Hoek-Brown parameters. The consideration of the confining stress dependency for the spalling process is key, since this failure mechanism will stabilize at certain distance behind the rock mass boundary (wall) due to the increase in confinement.

For brittle rock, the strength envelope can also be represented by a bi-linear failure envelope cut-off as illustrated in Figure 2-7.

In this envelope, there is an upper bound that correspond to the limit of the yielding of the brittle rock, instead of the peak envelope obtained from laboratory testing. As Diederichs (2003) explained the yielding limit is the starting point of crack coalescence and propagation. This limit is refereed as Critical Damage threshold (CD).

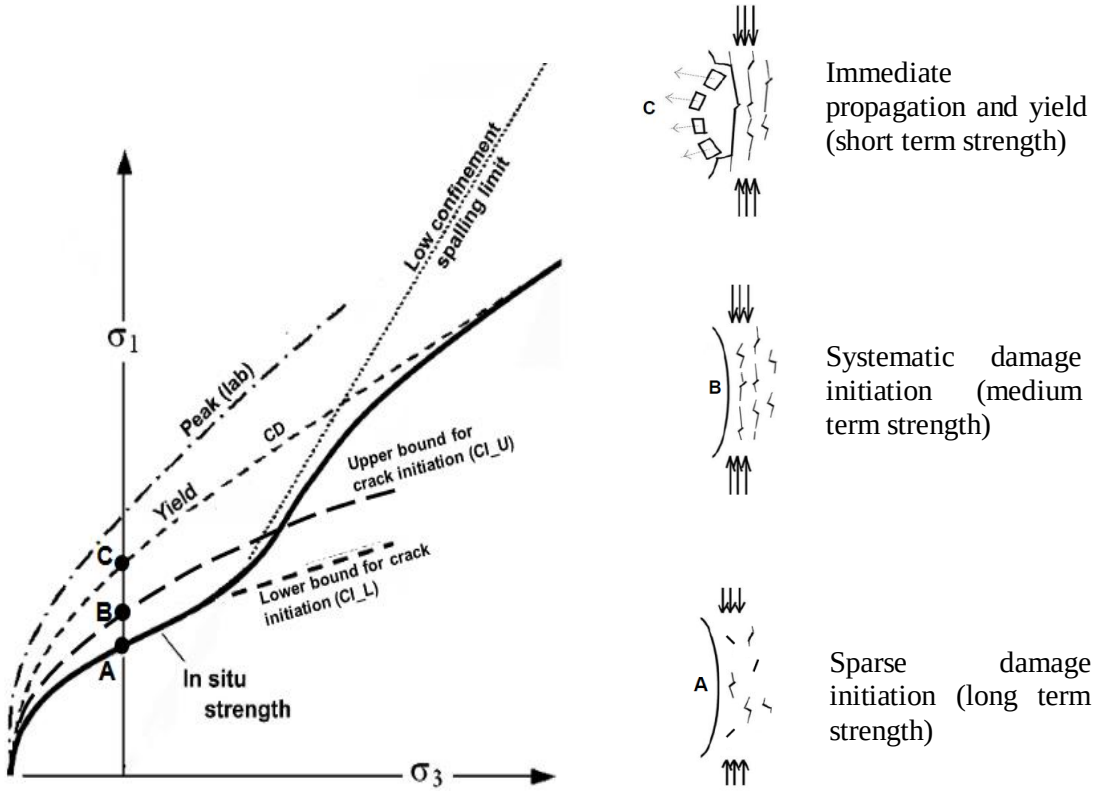


*Figure 2-7 Damage initiation and damage thresholds (Ghazvinian 2012, modified after Diederichs 2007)*

Below a damage threshold (m = 0), the rock is not damaged and remains undisturbed. When this threshold is exceeded, seismicity is observed, and damage accumulates, leading to macro-scale failure if the confinement level is sufficiently high preventing unstable crack or fracture coalescence.

Research carried out over the last decades, and summarized by Murrel (1963), Martin (1997, 2010), Kaiser et al. (2000) and by Diederichs (2003, 2007, 2010), has demonstrated that brittle rocks present a maximum tunnel wall strength of no more than half of the unconfined compressive strength (UCS) measured in laboratory test. This lower bound strength threshold is relatively insensitive to confining stress such that the limit for major principal stress is approximately:

$\sigma_{1max} = CI + (1 \text{ to } 2)\ \sigma_3$ Equation 2-8

where, CI is the Crack Initiation threshold, with values in the ranges of 30-50% of UCS as Latjai (1996) and Pestman (1996) obtained through laboratory testing. It depends on heterogeneities, density and the nature of flaws. Back analysis of observed tunnel breakout (Martin 1997; Carter et al.2008, Hajiabdolmajid et al. 2002) indicated that this threshold only is applicable when failure occurs at low confinement. At higher confinement, the strength envelope makes a transition up to the envelope defined by the Crack Damage threshold, *CD*.

As seen in Figure 2-7, below the lower field strength envelope (CI), also referred to as the lower-bound in situ strength by Gazhvinian (2012), no damage occurs within the rock although stress changes occur. Above this envelope, micro-cracks initiate at the grain scale. Above CI but at high confinement, these initiating micro-cracks quickly stabilize as they propagate away from the boundary of the excavation. The upper bound strength (CD envelope) is controlled by shear fractures formed by micro-crack coalescence.

At low confinement near excavation walls, rock that is stressed above CI will experience spalling damage as new extension cracks and old cracks propagate in an unstable manner. In situ strength in this spalling zone is less than the predicted by lab testing.

The true strength limit will decrease from the CD upper bound to CI lower bound in that low confinement area. It could be an immediate strength reduction or may occur over time (CI corresponds to long term strength at low confinement). Significant fracturing occurs at stress levels defined by the in-situ strength envelopes.

As Diederichs and Martin (2010) stated, before applying this model or rock strength and

behaviour, it is necessary to establish several stress limits: the conventional strength index UCS (unconfined compressive strength), CD (critical crack damage or shear yield strength) and CI (crack initiation).

The use of Crack Damage strength, CD is recommended for the estimation of an upper bound for field strength. The rock mass undergoes a transition between load-parallel elastic response and non-linear behaviour. In the past, this yield strength has not been used in rock mechanics. However, this threshold, marks the last true rock strength threshold. Failure beyond this stress level in uniaxial loading is controlled by the sample scale, loading rate and configuration of the machine. Martin (1997) defined this threshold as $\sigma_{cd}$. The new ISRM Commission on Rock Spall Prediction has established CD as the new acronym.

The other threshold used for predicting the failure of excavation is the Crack Initiation (CI). It represents the stress level at which grain scale cracks begin to nucleate in the sample. Prior to reach this point, there is no new damage induced and the long-term strength of the rock remains unchanged. After new cracks begin to nucleate, they can propagate under low confinement conditions. Eventually, rock stresses above this threshold at low confining pressures will progress to spalling damage. The ISRM Commission on Rock Spall Prediction has established CI as the new standard.

Once CI has been determined, it is possible to establish a criterion, relating to the first empirical approach, showed previously in Figure 2-3. In this manner limits of depth of failure can be established, as illustrated in Figure 2-8. This figure is a normalization of the crack initiation stress.

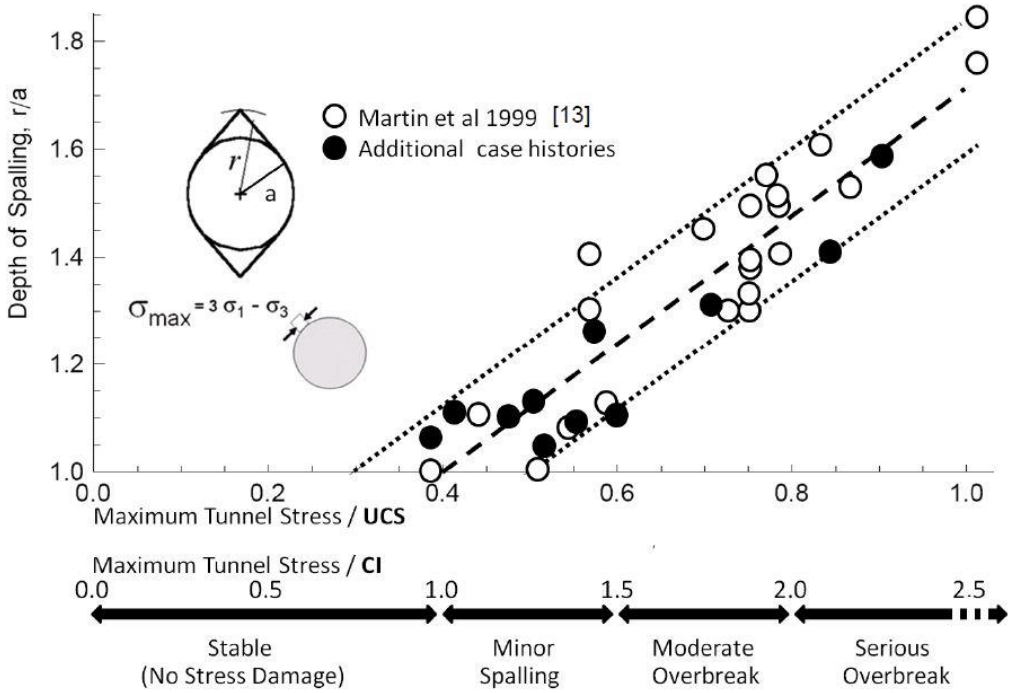


*Figure 2-8 Empirical spall prediction related to depth of over break for extreme conditions (Diederichs, 2010).*

This empirical approach, suggested by Diederichs (2007), is compatible with the fracture based criterion of Griffith (1924) and the associated work on fracture described by Hoek (1968) can be summarized in the following methodology:

- For the lower bound threshold for spalling initiation, determine UCS*CI. Although this value is best established using acoustic emission data from laboratory testing according to Eberhardt et al. (1998), a value of 0.4 UCS is generally suitable for crystalline rock and coincides with the ratio for spalling initiation on the tunnel boundary.

- For systematic damage, determine the crack damage strength, UCS*CD. Again, in the absence of acoustic emission and laboratory testing data, previous experiences, suggests a value of 0.6 UCS (Diederichs et al., 2004).

- Set the Hoek-Brown exponent a CI=0.2 to determine the maximum depth of damage (worst

possible case), and a CD= 0.25 to provide a more realistic prediction of actual visible spalling (worst probable case).

– Obtain a reliable measurement (or estimate) of tensile strength, T = $\sigma_t$.

This methodology lead to the development of the DISL approach (see Section 2.4.1).

For damage initiation and systematic damage, calculate the modified *s* and *m* values from:

$$S_{CI} = \left(\frac{UCS^*}{UCS}\right)^{1/A_{CI}} \quad \text{Equation 2-9}$$

$$S_{CD} = \left(\frac{UCS^*}{UCS}\right)^{1/A_{CD}} \quad \text{Equation 2-10}$$

$$m_{CI} = s_{CI}\left(\frac{ucs}{T}\right) \quad \text{Equation 2-11}$$

$$m_{CD} = s_{CD}\left(\frac{ucs}{T}\right) \quad \text{Equation 2-12}$$

## 2.4 Damaged Zones Around Excavations

The excavation process involves several sources of damage: disturbance originated when creating the opening (blasting and drilling (B&D or TBM) and damage induced by stress, stress changes and stress rotations.

For tunnel design purposes, it is necessary to establish the extent of the damage. The terminology to describe the different zones of damage has evolved over the years because of the improvement in knowledge about various damage processes (e.g., from Dinis da Gama and Torres (2002) to Siren et al (2015) to Perras and Diederichs (2016). For an excavation performed by blasting and drilling technique, Dinis da Gama and Torres (2002) classified the zones as: 1) zone of crushing, 2) zone of radial cracking, 3) zone of expansion and extension of fractures, and 4) elastic zone or

zone without cracks.

In this thesis, the nomenclature as established by Perras and Diederichs (2016) is followed. The following four zones (moving from far-field toward the excavation boundary) are:

- Undamaged, elastic ground.
- Excavation Influence Zone (EIZ): This stress-strain zone contains only elastic deformation. In the past, it was referred to as excavation disturbed zone (EdZ). This damage is reversible and changes in the deformation properties of the rock are minor.
- Excavation Damage Zone (EDZ): In this zone, the damage is in the form of grain scale fractures. There are two divisions: the inner zone ($EDZ_i$) and the outer zone ($EDZ_o$). Both contain irreversible micro-damaged rock. In the inner area, the rock presents significant dilation, and in the outer zone, little or not dilation is observed.
- Highly Damaged Zone (HDZ): This inevitable type of damage is a result of the geometry, structure an induced stress changes. It consists on interconnected macro-scale fracturing of stress-induced spalling. This zone experiences a considerable change of properties and becomes unstable if not supported. Rock mass bulking is observed due to geometric non-fit of fractured rock.
- Construction Damage Zone (CDZ): Is the zone that is damaged by the excavation process. This damage can be minimized by protective excavation methods.

The depth of failure of an unsupported excavation typically is composed of the CDZ, HDZ and part or all of the EDZi.

### *2.4.1 Conceptual Damage Initiation and Spalling Limit (DISL) Approach*

Perras and Diederichs (2016) conducted many in-situ observations and measurements of the extent of the various EDZs. The resulting depth of damage was normalized to the tunnel radius (circular

excavations) and plotted against the SL or ratio maximum tangential stress/ unconfined compressive strength. The resulting depth of failure line, normalized by Diederichs (2007) to the normalized crack initiation (CI), and supplemented by additional case studies has been established as a successful approach to predict the extreme depth of brittle spalling around tunnels. They found that this approximation of the empirical depth of failure, when compared to the depth of EDZs, represents the division between EDZi and EDZo. It is important to notice that this division is intuitive since it represents the transition between connected and isolated damage in the rockmass surrounding the excavation.

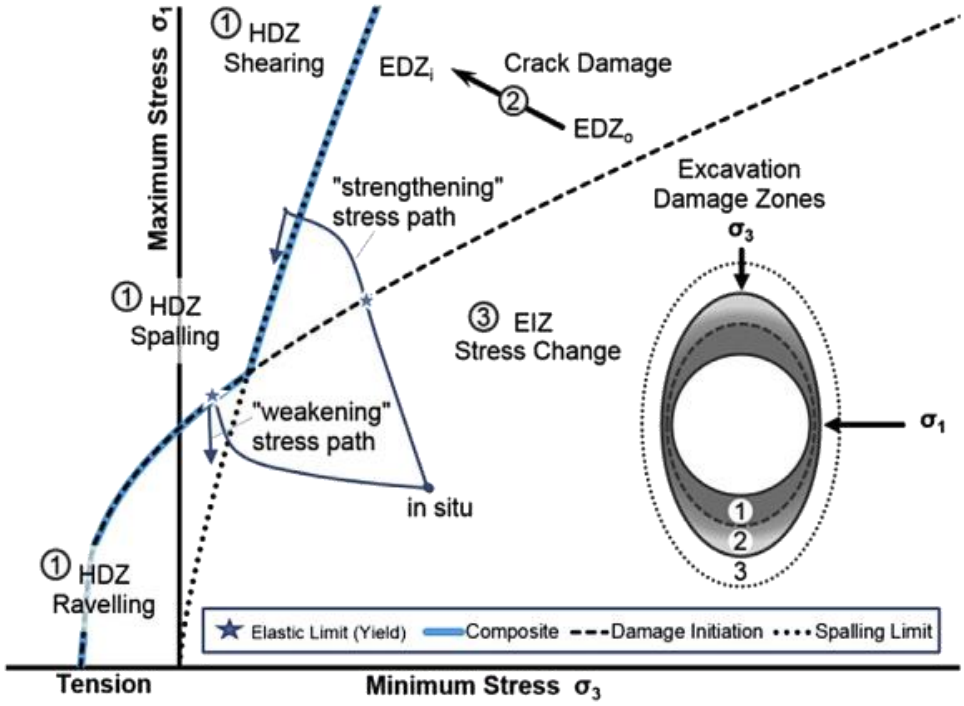


*Figure 2-9 EDZs matched with the conceptual DISL approach (after Diederichs 2003) by Perras and Diederichs (2016)*

The brittle damage and yield around excavations delimited in Figure 2-9, are based on the conceptual model of brittle spalling represented by cohesion loss and friction mobilization

(combined weakening-hardening approach) research by Martin (1997), Kaiser et al. (2000) Diederichs (2001, 2003, 2004) and Hajaibdolmajid et al. (2002). The base of this approach was the work by Schmertmann and Osterberg (1960) on stiff cemented soils and it was later adapted by Martin and Chandler (1994) to granite rocks. The "strengthening" and "weakening" stress paths indicated in Figure 2-9, represents the cohesion loss and friction mobilization, respectively. The strain hardening path corresponds to a confined damage accumulation path and the strain weakening path represents the brittle failure propagation path. This approach applies to massive and moderately jointed rock masses where jointing does not dominate the stress-driven failure process.

The DISL method requires the CI and UCS thresholds and the tensile strength as input properties. The resulting equations established by Diederichs (2007) are used later (in Chapter 3) to calculate the parameters *a*, *s* and *m* for peak and residual strength (Table 2-1).

*Table 2-1 Equations to determine the DISL model input parameters (after Diederichs, 2007)*

| **Peak** | | **Residual** | |
|---|---|---|---|
| **Input Parameter** | **Equation** | **Input Parameter** | **Equation** |
| $\mathbf{a_p}$ | 0.25 | $\mathbf{a_r}$ | 0.75 |
| $\mathbf{s_p}$ | $\left(\frac{CI}{UCS}\right)^{\frac{1}{a_p}}$ | $\mathbf{s_r}$ | $0.02\left(\frac{CI}{UCS}\right)^{\left(\frac{1}{a_r}\right)}$ |
| $\mathbf{m_p}$ | $s_p\left(\frac{UCS}{\lvert T\rvert}\right)$ | $\mathbf{m_r}$ | 6 to 12 |

The parameter *a*, which controls the curvature of the failure envelope, have been reported by Diederichs (2007) as 0.25 for the damage initiation ($a_p$) and 0.75 for spalling limit envelope ($a_r$).

The intersection between the initial and final strength limits, is defined as $\sigma_{3crt}$. Strain-softening occurs below this threshold. Lower values of $m_r$ are to be used for heterogeneous rocks. T is the tensile strength, and it can be determined in different ways, including from the Hoek and Brown failure criteria by applying the GSI method:

$$\sigma_t = -\frac{s\,UCS}{m_b} \qquad \text{Equation 2-13}$$

It can also be determined using the material constant $m_i$:

$$T_{HB} = -\frac{UCS}{m_i} \qquad \text{Equation 2-14}$$

If reliable tensile data is not available, the tensile strength can be estimated using Griffith's theory (1924). As Diederichs (1999) indicates, the Griffith's theory is consistent with the initiation of damage threshold and in tension, the damage initiation and peak strength are coincident. Therefore, the following equation can be applied to estimate the tensile strength:

$$T_{grif} = \frac{CI}{\beta} \qquad \text{Equation 2-15}$$

where β ranges from 8 to 12.

The Damage Initiation Spalling Limit (DISL) approach developed by Diederichs (2007) can be simulated in Phase2 to capture the confinement dependency of the brittle spalling process. The cohesion loss is obtained by a drop-in parameter s of Hoek-Brown criteria and friction is mobilized at elevated confinement (to the right of the spalling limit). In Phase2 or RS2, this is done by assigning peak parameters to the damage initiation and residual values for the spalling limit. It must be pointed out that the latter is only a brittle residual strength to the left of the intersection of the intersection of the two failure envelopes. To the right it is a strain-hardening failure envelope.

With the for the DISL approach established, is necessary to determine which methodology is to be

followed when modelling the EDZs. The selection is between the DISL equations and the Hoek-Brown non-linear failure criteria with GSI approach. Diederichs (2007) provided guidance in the form of

Table 2-2 which summarizes the applicability criteria.

*Table 2-2 Selection of methods to apply based on strength ratio (after Diederichs, 2007)*

| **Strength Ratio** | **GSI <55** | **55<GSI<65** | **65<GSI<80** | **GSI>80** |
|---|---|---|---|---|
| *UCS/T < 9* | *GSI* | *GSI* | *GSI* | *GSI* |
| *9 < UCS/T < 15* | *GSI* | *GSI* | *GSI* | *GSI /DISL* |
| *15 < UCS/T < 20* | *GSI* | *GSI / DISL* | *DISL/GSI* | *DISL* |
| *UCS/T > 20* | *GSI* | *GSI / DISL* | *DISL* | *DISL* |

Given that GSI values considered in this thesis range from <65 to 75 both approaches, GSI and DISL, may be applicable and are both therefore considered in Chapter 3.

### *2.4.2 Estimation of the Depth of Failure by Numerical Modelling*

Delineation of each EDZs is one of the most important factors when designing excavations, allowing the designer engineer to optimize the excavation geometry and select the most effective support. Indicators used for estimating the dimensions of the EDZs are the changes in stress concentrations and strain around the excavation. Following the work by Perras (2010, 2012, 2014) and later updates by Perras and Diederichs (2016), the following models were created for the excavations analyzed in the thesis. In all excavations, the delineation was calculated as follows:

- The HDZ-EDZi transition was taken at the first point where constant minimum principal stress ($\sigma 3$) increases from the value at the excavated surface and either maximum or rapidly decreasing tensile or shear strain moves from the excavation boundary (as near zero as

possible).

- The EDZi-EDZ$_O$ transition was taken at the start of tensile volumetric strain.
- The EDZo-EIZ transition was taken as the plastic yielding starting point.

In order to represent these damaged zones, the yielded element percentage and the volumetric strain and the maximum shear strain are plotted. These are the parameters that best represent where the damage is located around the excavation. The point where the volumetric strain goes from expansion (+ values) to contraction (- values) is defined as the transition zone between EDZi and EDZo. Where the yielded percentage drops to 0%, is defined as the zone where the EIZ begins.

Figure 2-10 presents and example of a tunnel of 3m radius, excavated at 2000m depth. The initial stress state with ko = 1 was subsequently changed to k = 0.6 (by adding a uniform load) for this example. Because of the ultimate non-uniform stress distribution, the tunnel behaviour is analyzed at two locations, wall and roof. Specifically, Figure 2-10a presents the delineation of the EDZs for the wall and Figure 2-10b for the roof.

From the analysis of the EDZs conducted at the wall (Figure 2-10a), it is seen that the highly damaged zone around the tunnel, extends over half a meter behind the wall, while the zone where the dilation occurs (EDZi) extends over 2.1 m from the boundary. Beyond that depth, the yielding plasticity dominates the damage behaviour, up to 5.5 m. At a greater distance from the wall the rock behaves in an elastic manner.

Figure 2-10b represents the delineation of zones for the roof of the excavation. The zone of high damage coincides with what was observed in the wall (0.5 m). However, the zone where dilation is observed (EDZi) is deeper reaching to approximately 3.5 m. The plasticity extends to more than

5.5. m in the roof.

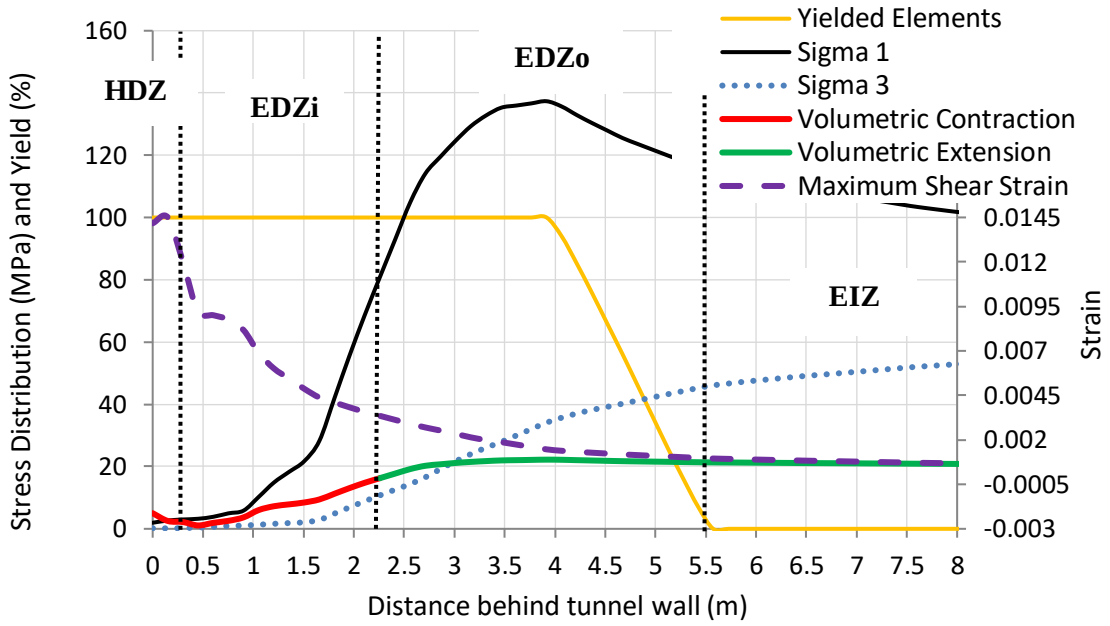


*(a)*

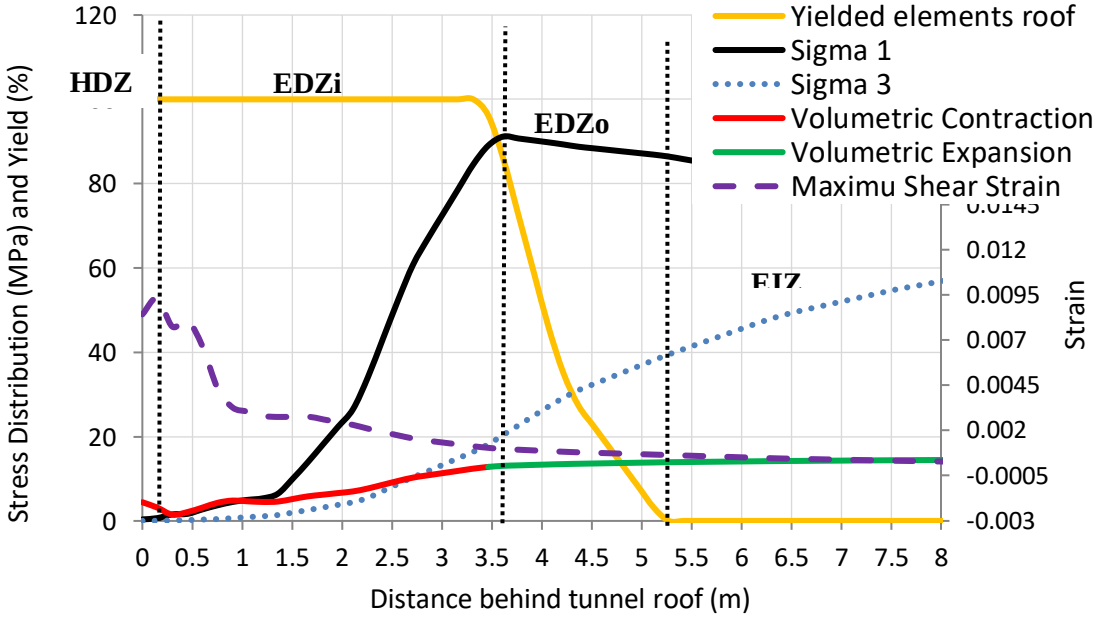


*(b)*

*Figure 2-10 Numerical delineation of the EDZs for a brittle tunnel excavated at 2000 m depth, with mining induced stresses: a) EDZs at wall location; and b) EDZs at roof location.*

It is noticed that these delineations of damage are an approximation of reality and give a general

idea of how the damage around the excavation is distributed. In reality, several other factors will affect the damage distribution.

## 2.5 Bulking of Stress-Fractured Ground

When stress-fractured rock is deformed, its volume increase. This process is called bulking, more specifically, geometric bulking because the rock fragments after fracturing do no longer fit together. Bulking is therefore defined as an increase in the volume of broken rock.

### *2.5.1 Confinement Dependence of Bulking*

Because rock can only deform into the excavation and because rock support is generally installed in a radial direction, it is meaningful to define bulking by a linear rather than volumetric bulking factor BF. Kaiser et al. (1996) defined the bulking factor in the CRBSHB as the percentage change in radial length $l_o$:

$$BF\ (\%) = {}^{\Delta l}/_{l_o} \qquad \text{Equation 2-16}$$

Measurements in South Africa mines by Ortlepp (1992) suggested that the bulking factor (BF) was logarithmically related to the the support pressure ($p_s$) as:

$$BF = a - b * \log(p_s) \qquad \text{Equation 2-17}$$

where, $p_s$ is the confinement at the tunnel wall or the support pressure. The parameters a and b were obtained by Kaiser et al (1996) based on Ortlepp's data (1984) in an empirical manner (from measurements in the African mines).

Cai (2006, unpublished report) used the ELFEN code to simulate the stress fracturing process and confirmed the logarithmic relation of BF as a function of the confining pressure p.

Then Equation 2-17 was rewritten as

BF= a- b *log (p) Equation 2-18

Figure 2-11 summarizes the result of this model and compares it to the range obtained from Ortlepp's data. This figure shows that the logaritmic relation holds but the paramters a and b may vary.

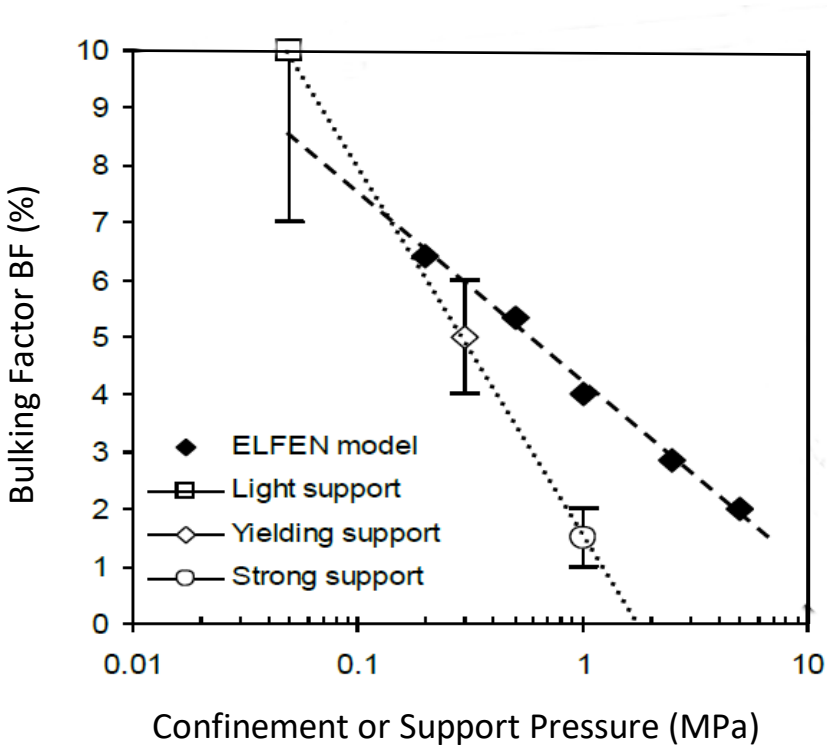


*Figure 2-11: Bulking factor dependence on confinement or support pressure.*

## *2.5.2 Strain Dependence of Bulking*

Intuitively, it must be expected that bulking should depend on the level of rock straining during the stress-fracturing process. Initially crack open and little bulking occurs. Eventually at large strains, fragments do no longer fit and much geometric bulking must occur. Recent work performed by the Rio Tinto Centre for Underground Mine construction at CEMI (Centre for Excellence in Mining

Innovation) introduced the dependence of bulking on axial strain (or tangential strain on excavation wall). Kaiser (2016) published the findings of that work. By use of Voronoi models with elastic blocks he demonstrated conceptually how the tangential and radial displacement or strain is related (Figure 2-12).

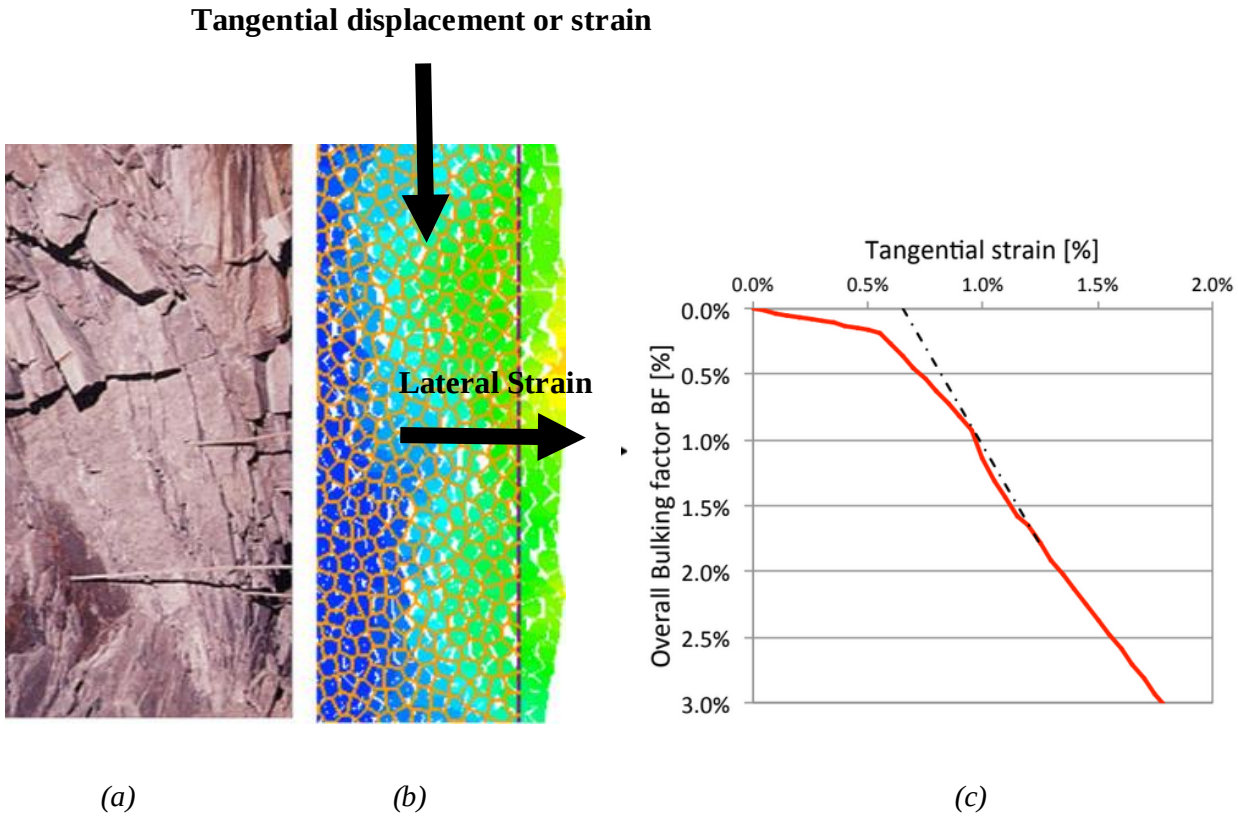


*Figure 2-12: Bulking tangential-strain dependent of a stress-fractured rock: a) massive to moderately jointed stress-fractured rock b) Voronoi model to simulate "geometric" bulking, c) relation between tangential and lateral strain (Kaiser, 2016).*

The results of the numerical Voronoi model presented in Figure 2-12c show that, in this particular case, the tangential to lateral strain ratio is about 1:3. This means for example that if the roof of excavation is deformed by 10 mm, the wall will experience a deformation of 30 mm. In the first part

of the curve, the deformation is elastic and only the Poisson's effect is registered. Then, as the sample or the excavation is further loaded (strained), and the blocks of the Voronoi model start to move relative to each other the rate of bulking and thus the bulk factor increases more rapidly.

This work demonstrated that "geometric bulking" (Kaiser 2016) and thus the bulking factor depend on the tangential strain.

In summary, geometric bulking depends on many factors, such as the geology, excavation geometry, the mining method and sequence (strain $\varepsilon_o$) and the confining pressure provided by the support or the rock ($p_s$ or $\sigma_{rr}$). In the thesis, the focus is on the analysis of this geometric bulking as a function of the strain and the confining pressure.

Bulking must be differentiated from dilation, which can be considered as bulking in all directions. Geometric bulking only causes displacements in one direction, into the excavation. Whereas dilation is accounted for in continuum numerical models, geometric bulking is not. Therefore, bulking has to be addressed separately and added to the continuum behaviour. In this thesis, a semi-empirical methodology is proposed (explained in Chapter 3) to estimate the deformation that this bulking imposes on the support near an excavation. Figure 2-13 illustrates in a schematic manner what geometric bulking is.

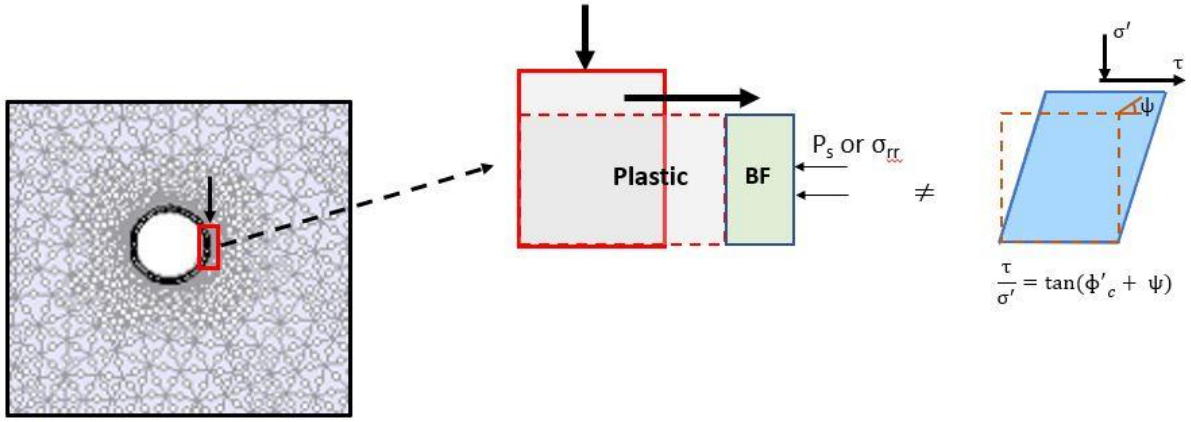


*Figure 2-13: schematic representation of geometric Bulking. Differentiation of Geometric Bulking and Dilation*

Geometric bulking produces additional deformation that needs to be added to the elastic and plastic deformation, as represented in Figure 2-13. Plastic deformation is obtained by the numerical model, but the geometric bulking is not. The bulking deformation can be controlled or at least diminished by increasing the support pressure in the excavation and by the reinforcement of the broken rock mass.

Also, there is a fundamental difference between bulking an dilation. According to the strength equation, shown in the above image (Figure 2-13), dilation models assume that the more the rock dilates the stronger it becomes. Bulking rock however, does not gain strength unless it is confined.

### *2.5.3 Empirical Bulking Charts*

Kaiser (2016) published an empirical bulking chart that accounts for the dependence of bulking on confinement (support pressure) and imposed strain (tangential loading of an excavation). The chart presented in Figure 2-14 forms the basis for the calculation of bulking in this thesis (Chapter 3)

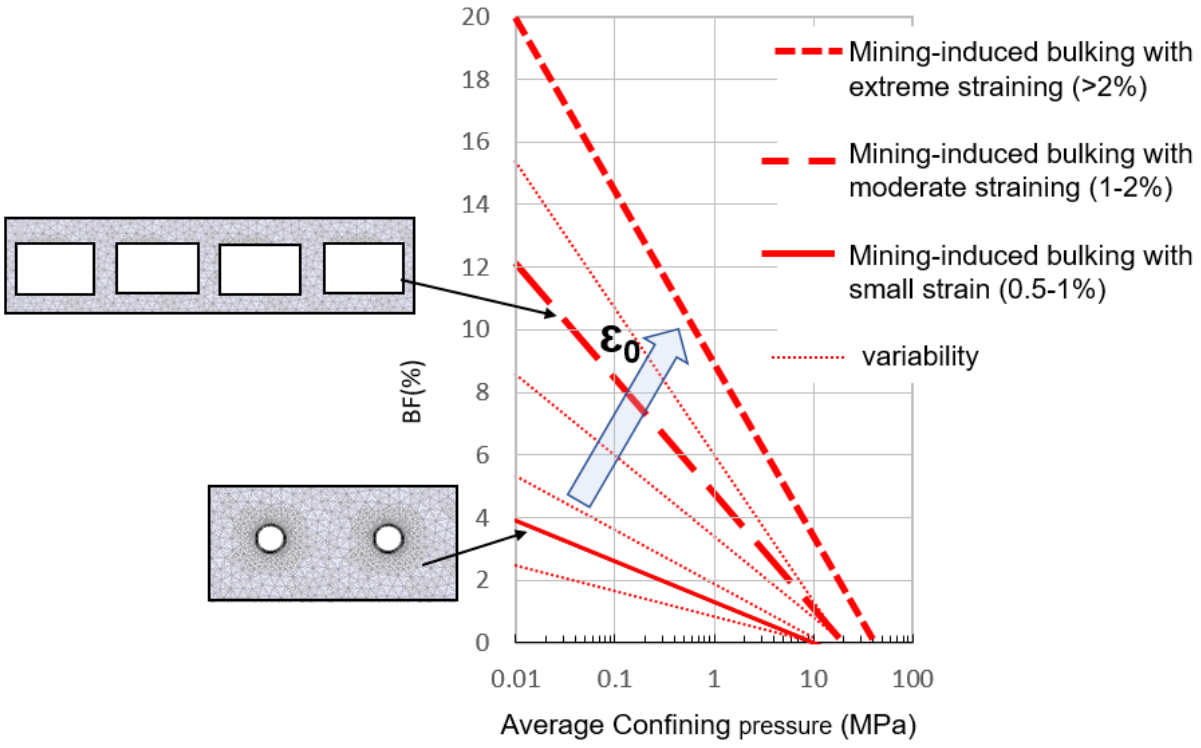


*Figure 2-14: Semi-empirical bulking factor chart (Kaiser 2016)*

In this chart, it is presented the bulking factor BF (%) (and respective ranges) as a logarithmic function of the confinement pressure for three different levels of strain. For small strain levels, typical of situations where one or two tunnels are advanced, the BF (%) at low or zero support is limited to 4% (±1.5%). Bulking is suppressed at 10 MPa. In later stage mining, when mining-induced strains are high, the bulking factors at low or zero confinement can reach 12% (±3%) and bulking is suppressed at about 20 MPa (i.e. several pillars situation). For extreme mining conditions, i.e., when excavations are near collapse, BF may reach values up to 20% and pressures greater than 20 MPa may be required to prevent bulking.

## 2.6 Base Assumptions for Analyses Presented in this Thesis

When rock fails in a brittle manner, the ground behaves different closer to the excavation than far from it, i.e., it fails by spalling rather than shear. The brittle rock failure is a progressive process, it starts by crack initiation and propagates by the coalescence of the fractures and eventually reaches the peak or spalling strength. Once it exceeds the crack initiation stage, it may fail in a brittle manner and drop to the residual strength. During this process, the rock mass dilates but most importantly also bulks in a unidirectional direction (i.e., into the excavation). The latter (bulking) is not simulated by the continuum model (Phase2 or RS2) and thus needs to be estimated separately. This will be covered in following Chapter 3.

For this thesis the analyses focus on tunnels in the lower strain environment typical encountered when single tunnels are advanced, and therefore, the relation between bulking and pressure support will be limited at the tunnel wall to about BF = 4% (see calculations in Chapter 3) and bulking is suppressed at 10 MPa (for confinement above this threshold there will only be elastic and plastic deformations). Hence, the bulking parameters a and b are set to a = b =1.3. The bulking relation shown in Figure 2-15 is assumed and applied to all analyses presented in this thesis.

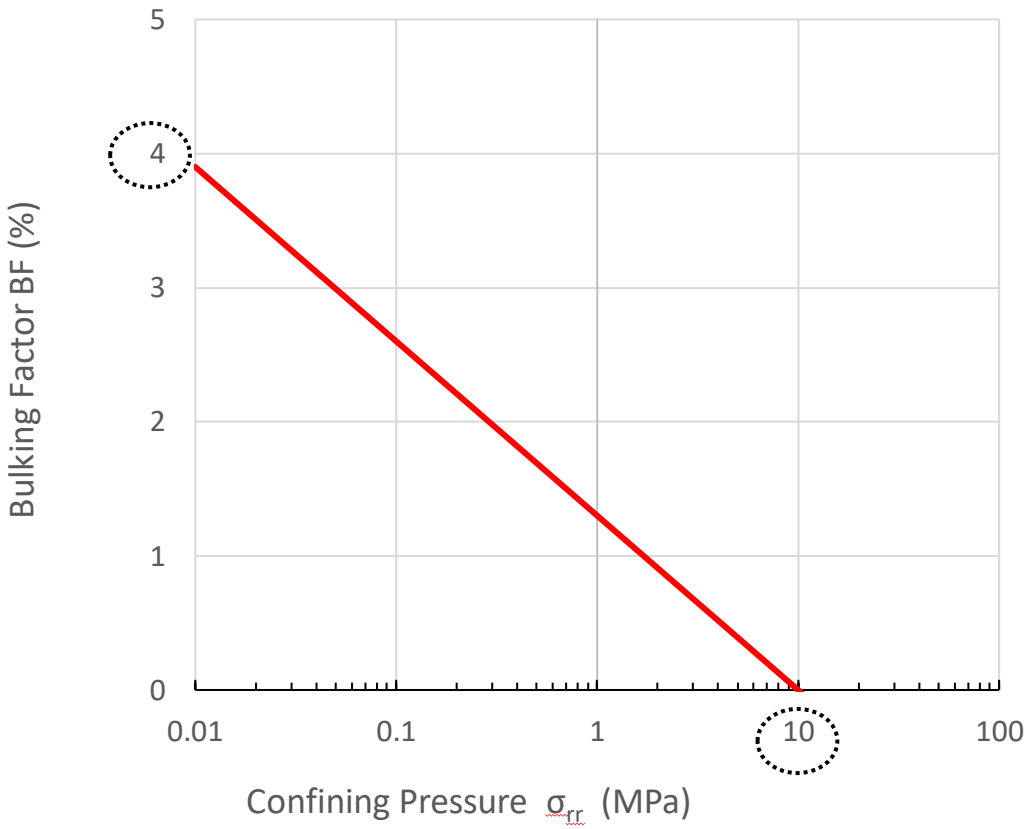


*Figure 2-15: Relation between BF (%) and support/confining pressure used for calculations in this thesis.*

In next Chapter 3, when tunnel displacement calculations are presented, two assumptions will be made: (1) that only rock that fails in extension (is in a state of stress with near zero confinement) bulks, and (2) that entire zone of yield (consisting of extension and shear failure) bulks. This will be analyzed by using both the rock mass parameters based on the GSI approach and the DISL methodology developed by Diederichs (2007)

# Chapter 3

# 3 Estimation of Tunnel Wall Displacement in Bulking Ground using the GRC Concept

## 3.1 Ground Reaction Curve (GRC) Concept

Ground Reaction Curve (GRC) is a graphical representation of a closed form solution where the internal support pressure in a tunnel is plotted against the wall displacement. It accounts for elastic and plastic displacements. In this research, these elastic and plastic displacements are obtained from numerical models using the RocScience code in Phase2. The wall displacements are obtained by sequentially lowering the internal pressure, usually referred as the 'distributed load method'. However, the GRC obtained in this manner lacks the displacements produced by the bulking (signalled by the arrow in Figure 3-1). These bulking displacements are added using the semi-empirical relations presented in Chapter 2.

Figure 3-1 presents the GRC of a tunnel with elastic and plastic displacements obtained in this manner by use of the numerical code Phase2. Two bulking scenarios are superimposed: (1) for tensile failure zone bulking only (green dashed) and (2) for tensile and shear bulking (red).

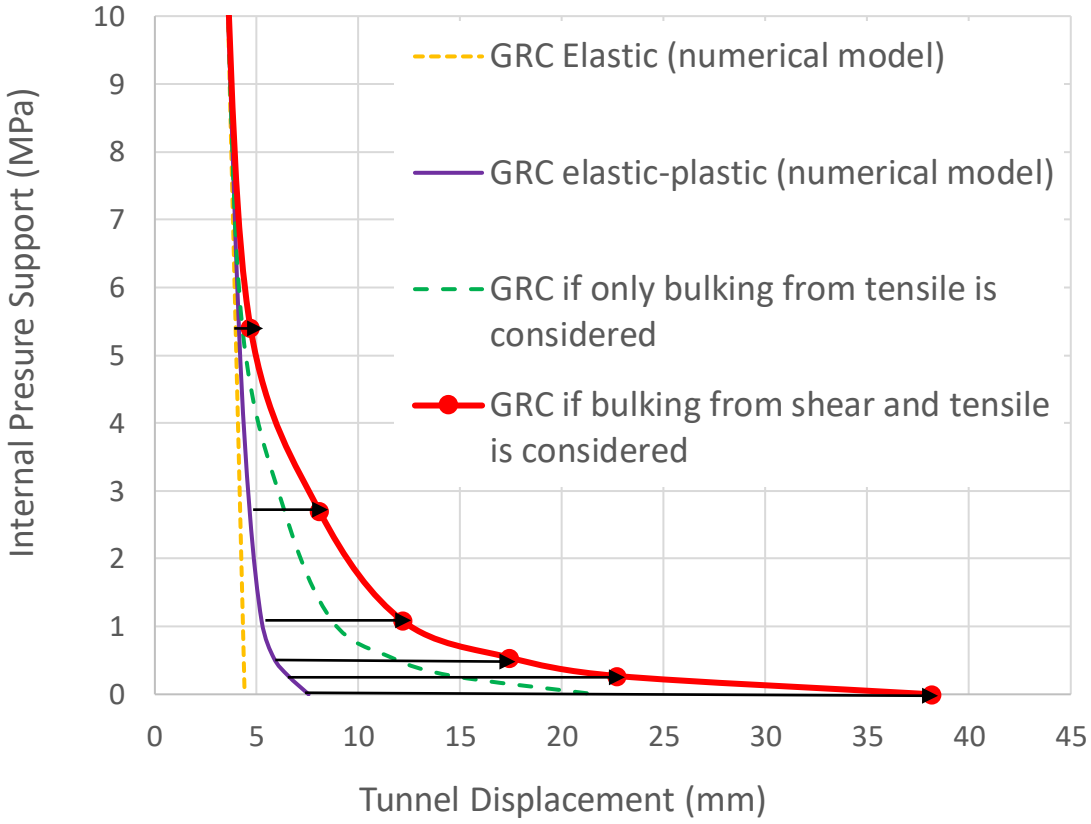


*Figure 3-1: GRCs of a tunnel with different types of displacement sources.*

The following sections explain how the displacement from bulking is calculated.

## 3.2 Excavation Simulation

The excavations were modeled using sequenced excavation stages and a graded 6 nodes triangle type of mesh (Figure 3-2). This type of mesh was chosen among all possibilities that Phase2 offers, including the possibility of customizing different advanced mesh regions around the tunnel, because it was observed for this type of tunnels of simple geometry, was sufficient to provide reliable stress distributions.

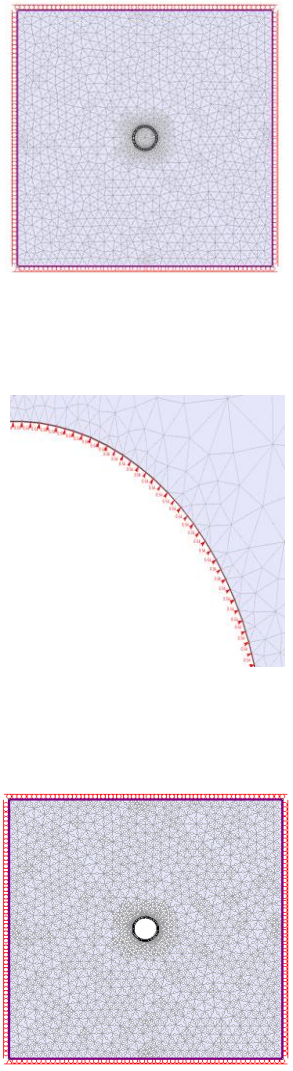

| Stage Number | SFR | pi (MPa) |
|---|---|---|
| *Stage 1: Virgin Field (Non-excavated)* | *0* | ------- |
| *Stage 2* | *1* | *27* |
| *Stage 3* | *0.8* | *21.6* |
| *Stage 4* | *0.6* | *16.2* |
| *Stage 5* | *0.4* | *10.8* |
| *Stage 6* | *0.3* | *8.1* |
| *Stage 7* | *0.2* | *5.4* |
| *Stage 8* | *0.1* | *2.7* |
| *Stage 9* | *0.05* | *1.35* |
| *Stage 10* | *0.02* | *0.54* |
| *Stage 11* | *0.01* | *0.27* |
| *Stage12: Tunnel fully excavated* | *0* | *0* |

*Figure 3-2:Schematic representation of initial and final stage of the excavation and detail of an intermediate stage, showing how pi distributes at the boundary condition.*

From the two widely accepted techniques available to simulate the three-dimensional excavation process with a two-dimensional numerical model, material softening (Young's modulus $E_i$ reduction) or load-splitting (Internal support pressure $p_i$ reduction), the second methodology was chosen. As demonstrated by Vlachopoulos and Diederichs (2014) in simple tunnel geometries (circular tunnels analyzed here), the estimation of GRC is insensitive to the choice of the adopted methodology, as long as the stage size is well controlled. This is done in Phase 2 by setting smaller

split factors, in the later stages of the excavation, which correspond to the states with plastic yield. As Figure 3-2 shows for the excavation of a tunnel in a hydrostatic stress field of 27 MPa, among the 12 stages, the last four steps are reduced in smaller increments to capture the plastic deformation that occurs in the unsupported tunnel.

## 3.3 Methodology to Estimate Bulking

Because bulking depends on the confining pressure, it is necessary to obtain the confinement profile for the excavated tunnel. Figure 3-3 presents an example of radial confining pressure profiles for various internal support pressures (the support pressure is provided in the legend).

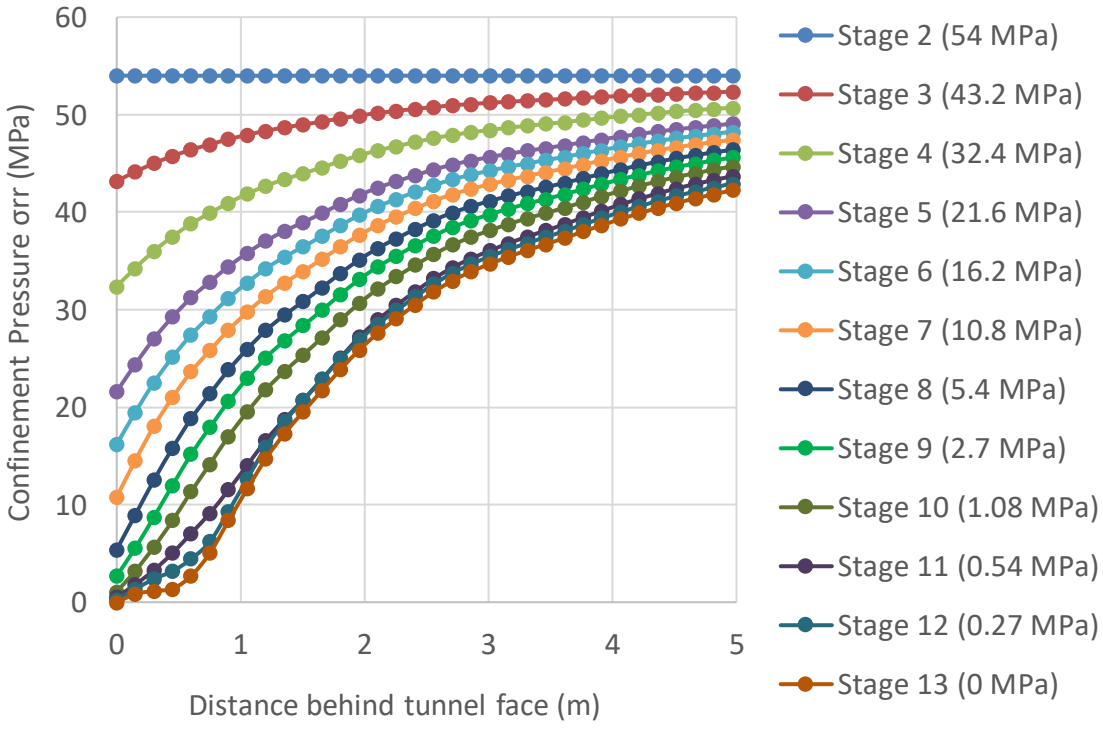


*Figure 3-3: Confinement Profile distribution of the excavation of tunnel*

As noted in Chapter 2, the level of confinement to suppress bulking is assumed to be 10 MPa. This means, that the stages below this threshold are the only ones contributing to bulking displacements. In the calculation part of this chapter, section 3.5, they are referred to as the yielding stages or stages where plastic behaviour occurs, as can be seen in Figure 3-4.

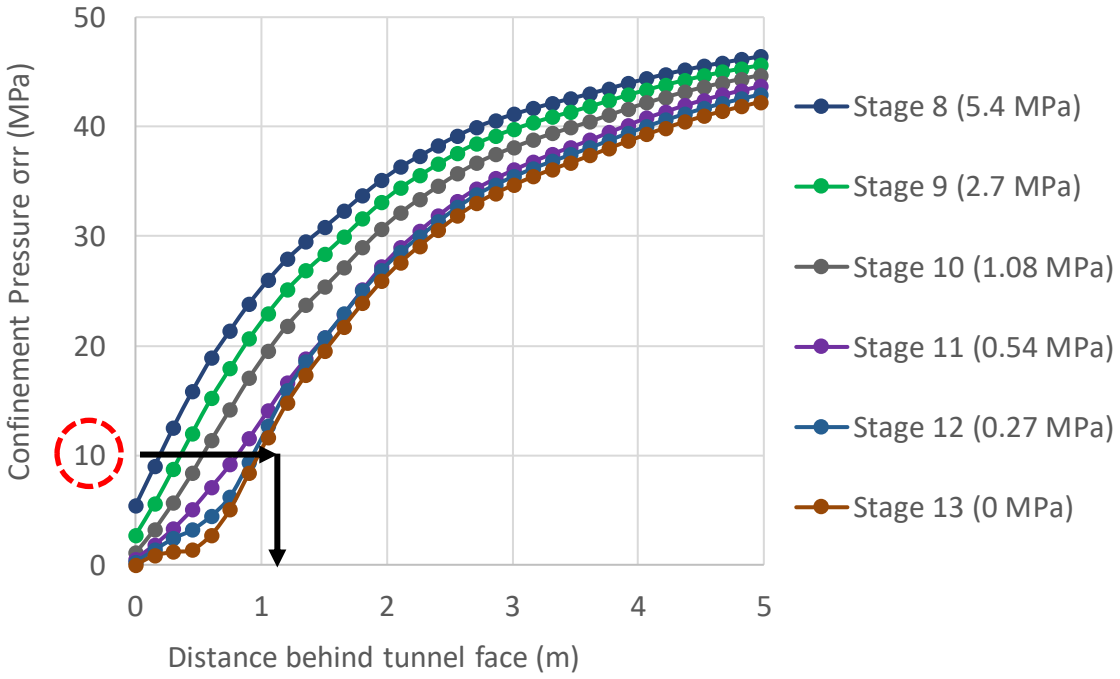


*Figure 3-4: Confinement distribution of stages involving yielding ground.*

Although the confinement distribution it is plotted in this Figure 3-4 up to 5 m behind the tunnel wall, only the first metre will contribute to bulking. Beyond this narrow shell near the excavation the confinement is higher than 10 MPa (highlighted by red dashed circle and arrows). Deeper in the rock there may still be yielding but the confinement is high enough to prevent bulking.

The second step is to calculate the bulking for each support pressure stage. The bulking percentage is estimated by using Equation 2-16 (introduced in Chapter 2) where BF = a - b * log $p_i$. Because this

thesis deals with single tunnels, the chosen parameters for a and b are set equal to 1.3 producing a maximum bulking factor of 4% at the wall.

The bulking profile is calculated (using the logarithmic relation) for each support pressure level and presented in charts such as Figure 3-5. At the final excavation stage (no support), the bulking reaches 4% at the wall (black curve for stage 13). This evolution of bulking distribution allows one to obtain the displacement profiles at each level of support pressure $p_s$ (Figure 3-6). Most importantly, it provides the wall displacements to generate the GRCs with bulking. The different amounts of bulking are obtained for each yielding stage, according to the respective support pressure level $p_s$ are presented in Figure 3-5.

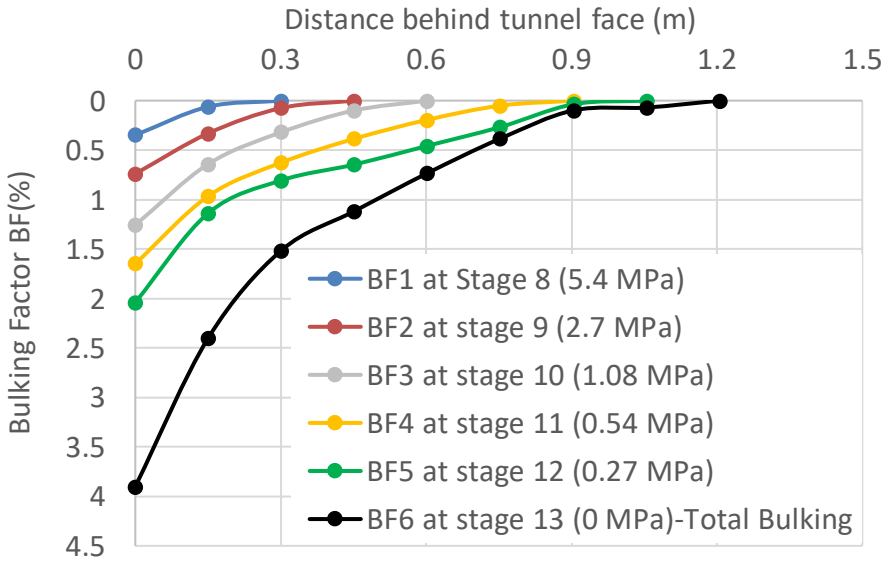


*Figure 3-5: Distribution of BF (%) for each level of internal pressure support (ps)*

The bulking displacements are obtained by summing the incremental bulking displacements from the deepest point (where bulking is suppressed at 10 MPa; in this thesis, increments of bulking length were set at 0.15 m). The total length, x (m) behind wall, where bulking is occurring is given by the

numerical solution (Figure 3-6). For this case, for example, the total length where bulking occurs is estimated at 1.2 m.

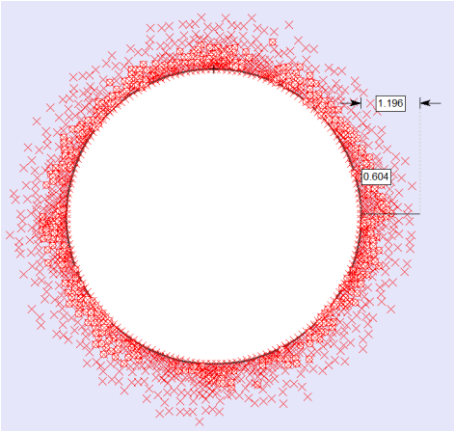


*Figure 3-6: distribution of the yielding zone at wall of the excavation*

Figure 3-7 presents the resulting displacement profiles for all excavation stages causing bulking in the tensile and shear zone.

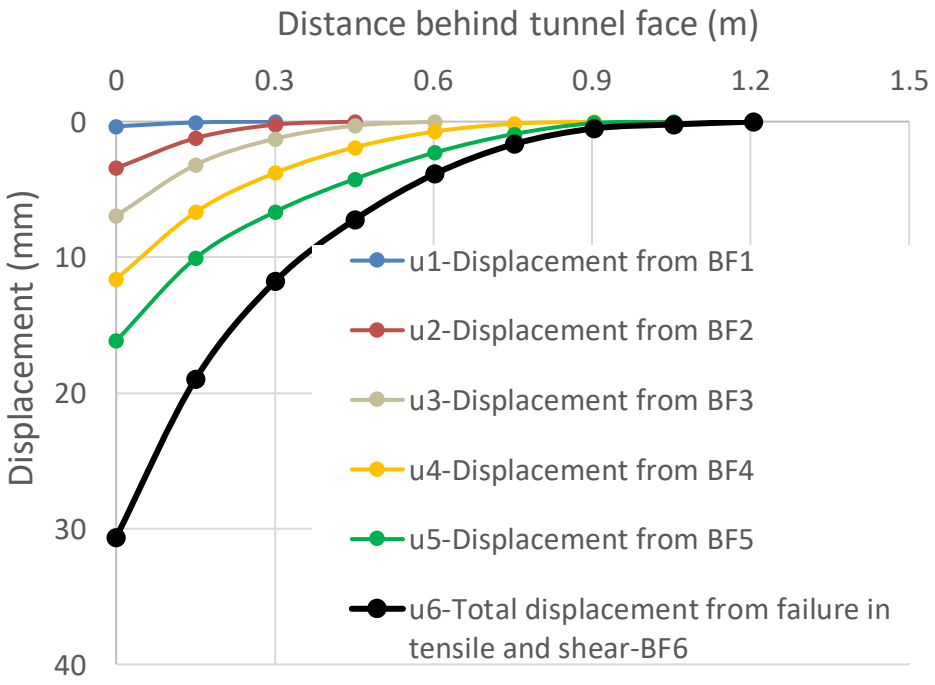


*Figure 3-7: Displacement from the bulking at each level of internal pressure support for failure in tension and shear.*

For this specific case, the respective displacements at the wall increase slowly from 0.34 to 3.5 to 7mm for the first three stages and then more rapidly from 11.6 to 16 to eventually 30 mm for the last three stages. These bulking displacements are then incrementally added to the displacements obtained from the numerical model shown in Figure 3-8 for the last stage of a tunnel (at 0MPa).

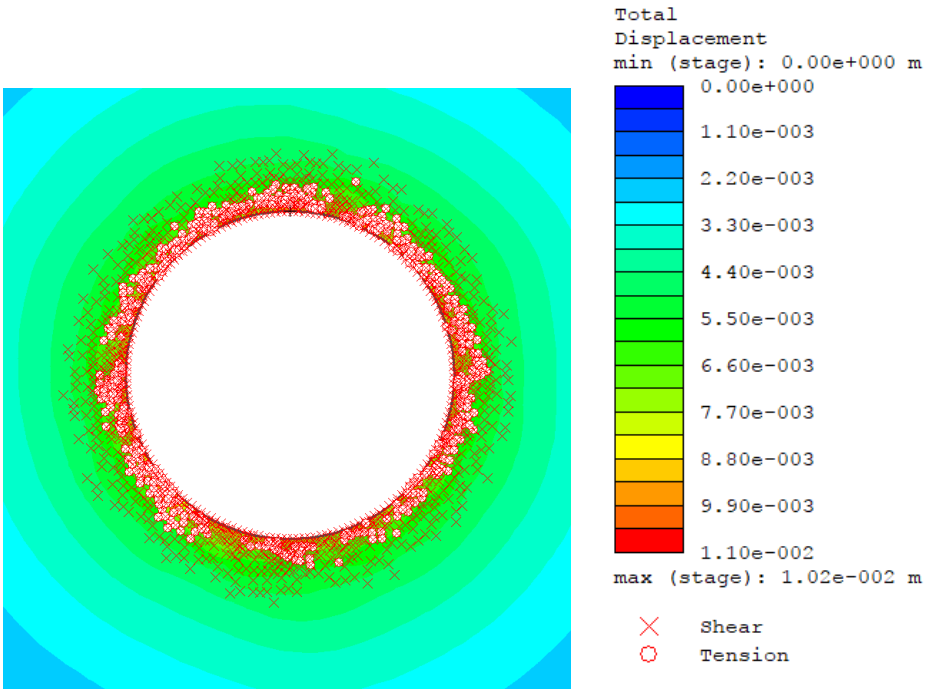


*Figure 3-8: Detail of displacement from the numerical solution for the last stage of excavation*

Table 3-1 presents the component and cumulative displacements for Stages 8 to 13.

*Table 3-1: Displacements corresponding to each internal pressure support level from numerical and semi-empirical methodology*

| **Excavation Stage** | **Internal Pressure Support $p_s$ (MPa)** | **Displacement from numerical model (mm)** | **Displacement from the bulking (mm)** | **GRC Input (mm)** |
|---|---|---|---|---|
| Stage 8 | 5.4 | 4.1 | 0.3 | 4.5 |
| Stage 9 | 2.7 | 4.7 | 3.5 | 8.1 |
| Stage 10 | 1.1 | 5.2 | 7.0 | 12.2 |
| Stage 11 | 0.5 | 5.8 | 11.6 | 17.4 |
| Stage 12 | 0.3 | 6.6 | 16.0 | 22.6 |
| Stage 13 | 0 | 8.0 | 30.0 | 38.0 |

Summing the numerical and the semi-empirically displacements for each level of internal pressure support provides total displacement that for the GRC with bulking as presented in Figure 3-1.

The displacements are calculated for the entire depth of yield of the tunnel which comprises shear and tensile failure as well as for the tensile failure zone alone. The reason for this separation is that although the entire depth of tensile fractures creates bulking, it is uncertain to what extent shear fractures contribute to bulking. The two solutions bound the practical range from minimal tensile bulking to maximum combined tensile and shear bulking. Figure 3-9 illustrates this concept.

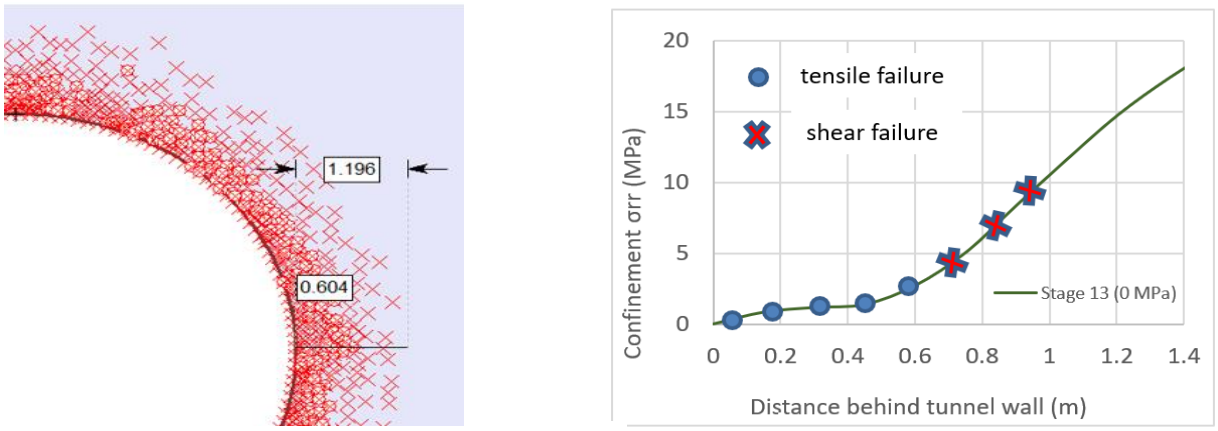


(a)

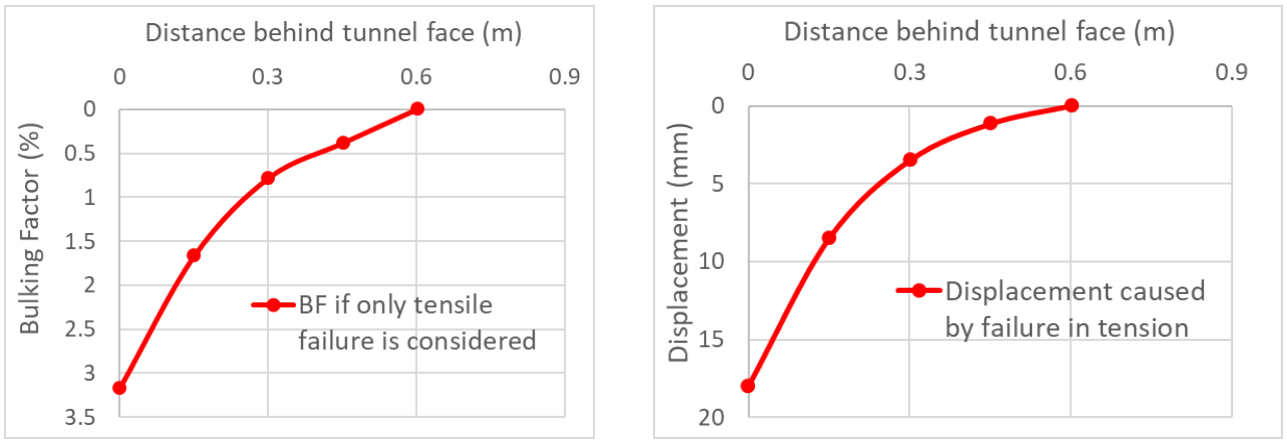


(b)

*Figure 3-9:a) Detailed distribution of the tensile and shear failure around tunnel boundary; b) Bulking Factor and displacement profiles from bulking if only tensile failure is considered.*

Profiles for tensile bulking only and for tensile and shear bulking are presented to bound the possible range of bulking.

Finally, the calculated displacements for the various stages are incorporated in the GRCs and factors affecting the GRCs with bulking are explored for three material types and three stress paths.

## 3.4 Bulking Estimation for Different Rock Types

### *3.4.1 Introduction*

Three material types are investigated: elastic-perfectly-plastic, elastic-brittle-plastic, and brittle.

Figure 3-9a, b and c illustrates the respective stress-strain curves for each type. The elastic-perfectly-plastic and elastic-brittle-plastic material analysis will be performed by modelling the tunnel in a rock that follows the curved Hoek-Brown failure criteria with different GSI values. For the former, the peak is equal to the residual strength and for the latter the strength is defined by a peak and a residual failure envelope. The brittle material is modeled following the DISL approach introduced by Diederichs et al. (2003, 2007). It uses the bi-modal failure criterion introduced in Chapter 2. The aim is to investigate a range ground conditions and stress states to gain a better understanding of how bulking influences the tunnel convergence response.

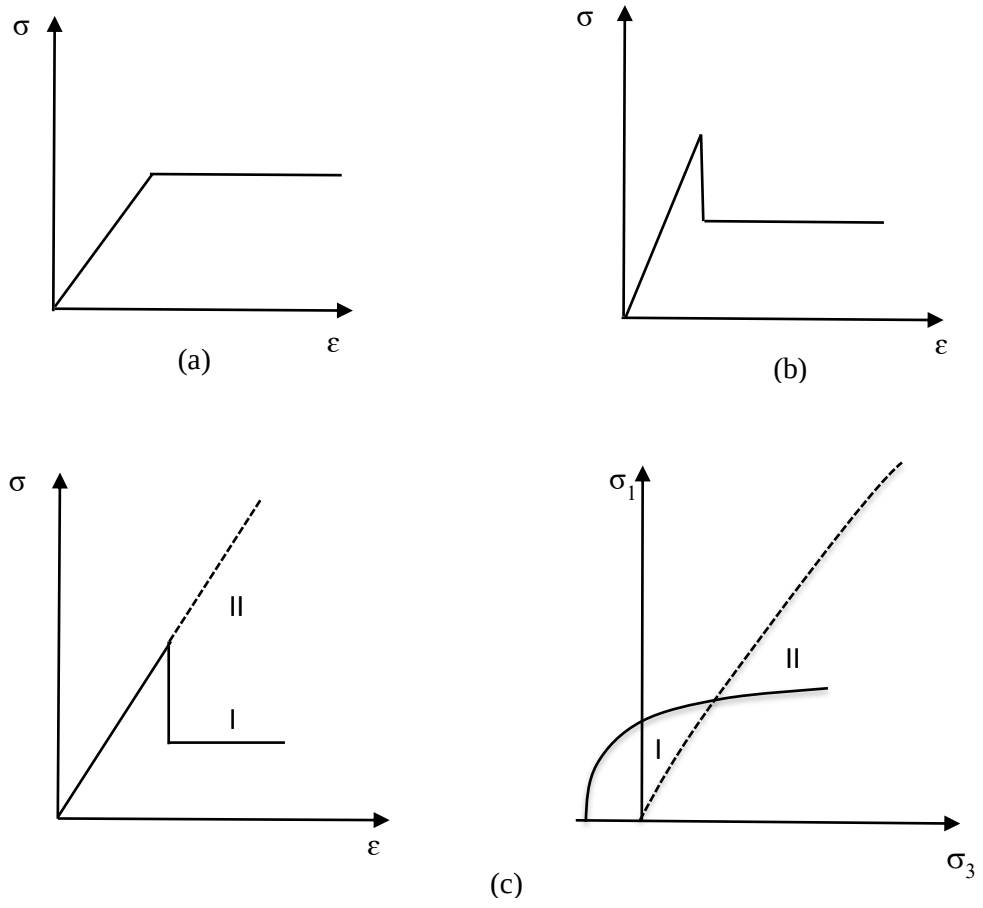


*Figure 3-10: Stress-strain relations for the tunnel excavated in (a) an elastic-perfectly-plastic material(b) an elastic-brittle-plastic material; and (c) DISL material where brittle (I) failure occurs to the left and strain-hardening (II) to the right of the spalling limit (dashed line in principal stress graph).*

### *3.4.2 Selection of Methodology to Model Brittle Failure in the Excavations*

Cai et al. (2004) indicates in the GSI chart of Figure 3-11 that brittle rock behaviour should be expected for GSI values greater than70 or 75. Recent work by Kaiser (2016) presented in the 13th ISRM lecture, suggest that the brittle threshold should be set at GSI = 65 (both limits highlighted in the image in blue and green respectively).

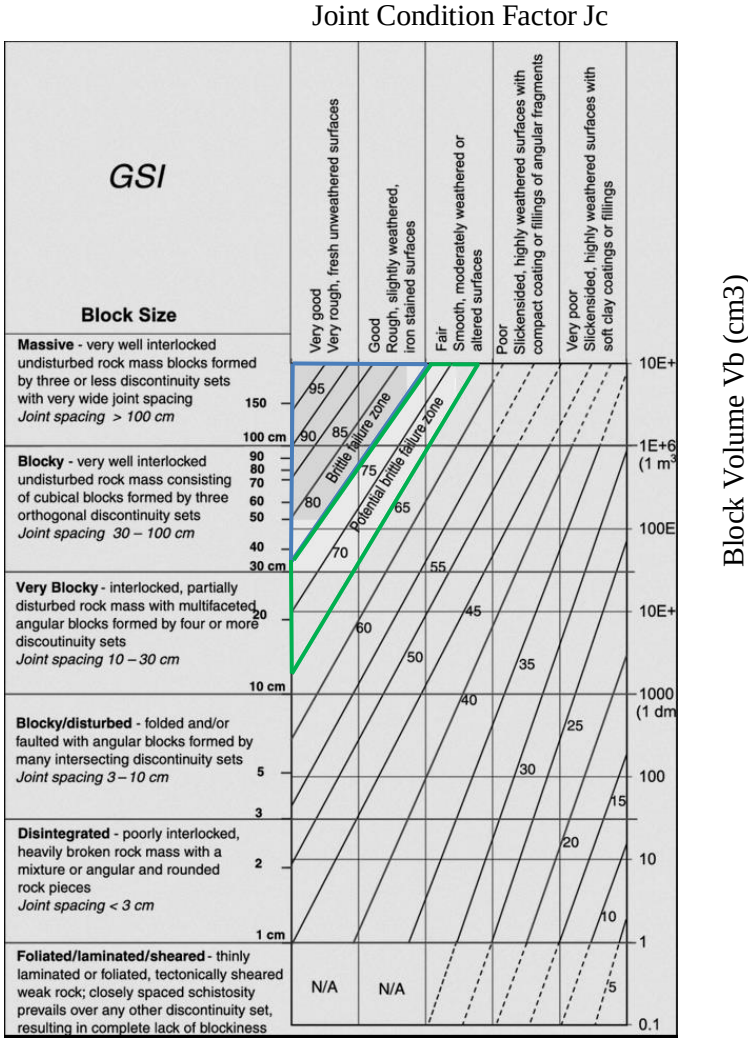


*Figure 3-11: GSI Chart establishing where brittle failure starts (after Cai et al., 2004)*

Diederichs (2007) discussed the applicability of the GSI approach for brittle rock, introducing

tensile strength ratio criteria as summarized in Table 3-2.

*Table 3-2:Selection of methods to model brittle failure according to strength criterion (Diederichs, 2007)*

| Strength Ratio | GSI <55 | 55<GSI<65 | 65<GSI<80 | GSI>80 |
|---|---|---|---|---|
| UCS/T < 9 | GSI | GSI | GSI | GSI |
| 9 < UCS/T < 15 | GSI | GSI | GSI | GSI /DISL |
| 15 < UCS/T < 20 | GSI | GSI / DISL | DISL / GSI | DISL |
| UCS/T > 20 | GSI | GSI / DISL | DISL | DISL |

This thesis focuses on the yellow shaded conditions and GSI values between 55 and 75 are used. Representative material parameters used for model the tunnel in each type of rock are summarized in Table 3-3.

*Table 3-3: Peak and residual material properties used to model each type of rock*

| Material modelled Approach | Elastic perfectly plastic GSIp=GSIr=65 | Elastic-Brittle $GSI_p$=65 $GSI_r$=55 | Brittle DISL |
|---|---|---|---|
| $m_p$ | 5.73 | 5.73 | 1 |
| $s_p$ | 0.02 | 0.02 | 0.0033 |
| $a_p$ | 0.501 | 0.501 | 0.25 |
| $m_r$ | 5.73 | 4.009 | 7 |
| $s_r$ | 0.02 | 0.067 | 0.000001 |
| $a_r$ | 0.501 | 0.504 | 0.75 |

The peak values of the material properties are represented as $m_p$, $s_p$ and $a_p$ and the residual values are represented as $m_r$, $s_r$ and $a_r$.

The excavation in elastic-perfectly plastic material, was modeled by setting the peak equal to the residual material properties. The generalized Hoek-Brown failure criterion with GSI = 65 was used to be representative of brittle rock types. As was commented previously in Chapter 1, rock masses with GSI = 65 are at the margin of brittle behaviour. This case analyzes excavations that are at the limit between non-brittle and brittle behaviour. By assuming elastic-perfectly plastic behaviour, it is implied that this material is not losing strength within the applied levels of rock mass strain. This is representative for small strain situations where little or no strength is lost post peak.

The second material studied is elastic-brittle. The generalized Hoek-Brown failure criterion is also adopted but it is assumed that some strength is lost after peak is reached. For the 'residual' strength properties GSI is set equal to 55. The reason that residual is placed in hyphens is because this is not the true residual strength of the brittle rock. Because the post-peak strength is not lost instantaneously (as simulated in Phase2), the mobilized post-peak strength (Kaiser 2016) depends on the applied loading strain. Hence, relatively high GSI-values have to be assumed when modelling in Phase2 for tunnels experiencing small to moderate loading strains. Lower GSI values should be considered for large strain problems with large mining-induced strains.

The third material presented is brittle following the DISL approach which is modeled using a bi-modal failure criterion. In Phase2, the strength is instantaneously lost to the left of the spalling limit ((I) in Figure 3-10c) and pre-peak strengthening is simulated to the right of the spalling limit ((II) in Figure 3-10c).

The three adopted failure criteria are not identical (although elastic-plastic peak material curve matches with elastic-brittle material peak curvature). They are presented in Figure 3-12 for comparison purposes.

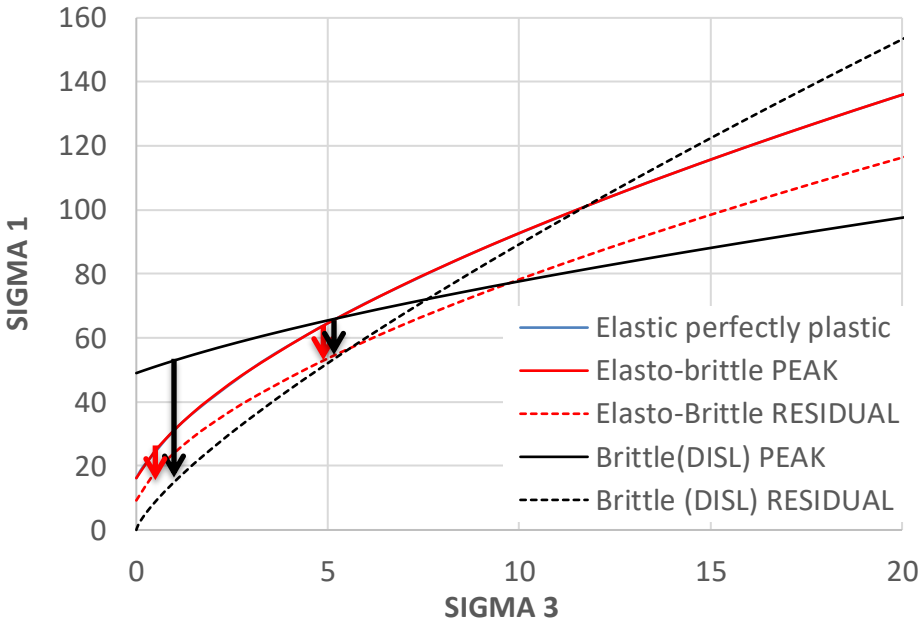


(a)

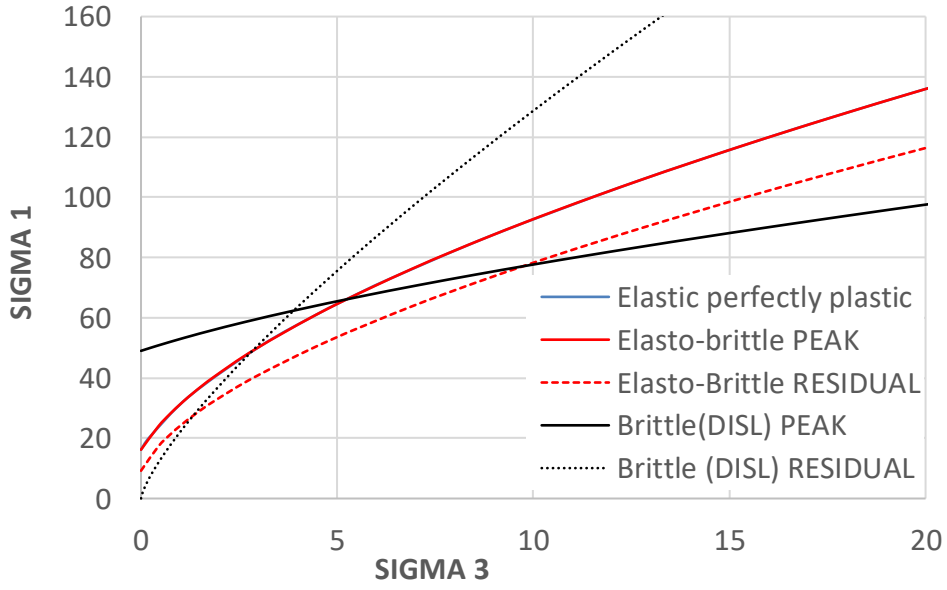


(b)

*Figure 3-12: Failure criteria for three materials: (a) DISL with $m_r$ = 7 and (b) for $m_r$ = 12.*

For the DISL model, the m value is the controlling parameter for the depth of yield. Figure 3-12a shows the DISL model with $m_r$ = 7 and Figure 3-12b for $m_r$=12. It can be seen that the spalling limit shifts to the left under these conditions. The brittle transition (where the spalling limit

intersects the peak envelop) shifts from about $\sigma$ = 7 to 4 MPa. As will be shown later, this controls the extent of failure in the DISL model. As indicated by the two arrows in Figure 3-12a, the DISL model with the adopted parameters is much more brittle in the low confinement area and thus will result in more extreme failure zones with associated confining pressure profile and therefore, the depth of yield or extension of damage would be much smaller.

It can be appreciated that with $m_r$=12 the Spalling limit in DISL is at 5MPa of confinement while when it was previously modeled with $m_r$=7 (Figure 3-12a) the spalling limit was at 9 MPa.

In order to get a brittle material with a great depth of yield, the DISL model is selected with a $m_r$ value equal 7.

Besides studying the behaviour of an excavation in different materials the excavations were subjected to different stress states by varying the $k_o$ ratio and by changing the stress state by considering mining-induced vertical loading. Three different situations are analyzed: (a) the excavations are subjected to a uniform stress field with ko = 1; (b) to a non-uniform stress field with ko = 0.5; and (c) to mining-induced stress change, simulated by adding a vertical uniformly distributed vertical stress to a tunnel excavated in ko = 1. For comparison purposes, the initial stress level was set to ko = 1 and the vertical stress was chosen to reach k = 0.6 after the mining imposed load. This simulates the case of a tunnel that is close to a mine, and is experiencing induced stresses. It is important to estimate tunnel convergence when affected by external stress changes. As will be demonstrated, the tunnel convergence is much larger in mining-loading situations than if excavated in a virgin stress field. In fact, it will demonstrate that bulking induced by mining tends to dominate the deformation behaviour of tunnels.

## 3.5 Bulking Estimation for Different Levels of Stress

The second part of the analysis presented in the following section, focuses on the effect of stress state and stress-path on the bulking behaviour. For this purpose, identical tunnels are excavated in different stress states of subjected to a different loading path. This is illustrated by Figure 3-13.

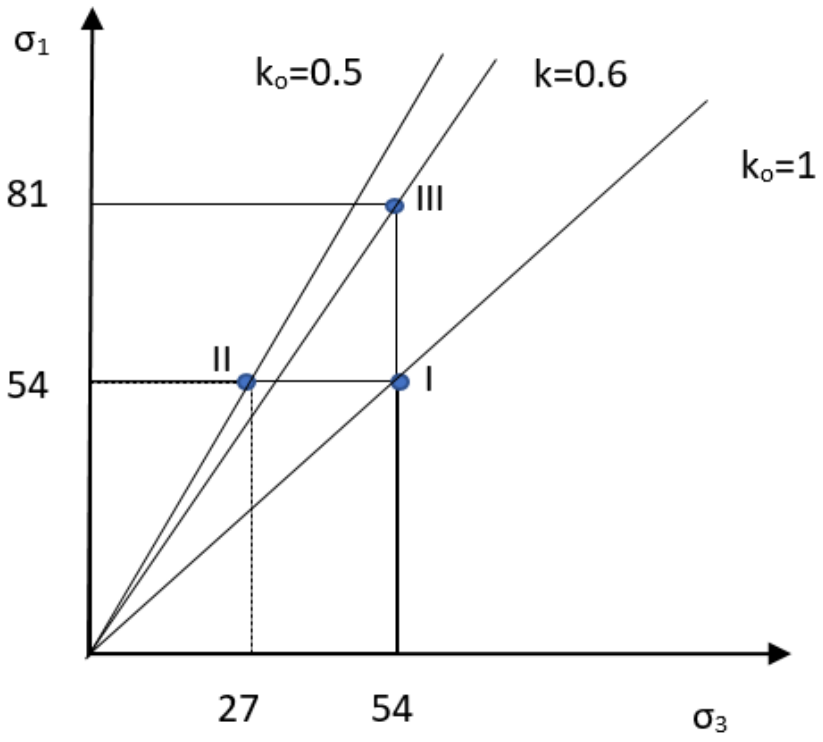


*Figure 3-13: Representation of states of stress used to model the excavations.*

Point I with $k_o = 1$ represents a tunnel excavated in a uniform or hydrostatic field stress. Point II corresponds to a tunnel under a stress ratio ko = 0.5. The third case takes a tunnel from Point I to III with an ultimate stress ratio k = 0.6.

For a circular tunnel at Point I the yield zone shape is circular. For a circular tunnel at Point II it is elliptical with a deeper failure zone in the horizontal direction. For these stress states ko will affect the bulking behaviour.

For the stress path from Point I to III the tunnel is exposed to a stress change leading to a much higher average stress state (even thought the ultimate k is comparable to the second case). As a consequence, the depth of yield is much deeper, and this will lead to much more bulking deformation. The tunnel at Point III will experience two combined mechanisms: high mean stress (states of stress), which gives deeper depth of yield, and additional deformation caused by the additional loading process. In other words, part of the deepening of the yield zone is due to the added stress. The additional deformation is because the tunnel experiences deformation from the excavation process and the loading of the rockmass. It will be shown, in following sections, that brittle rock is most sensitive to stress increases when the stress-fractured rock mass is bulking.

Results are presented for each of the above described material types and stress conditions. What is new in this thesis is that these analyses are performed by accounting for bulking in a semi-empirical manner and by considering the impact of confinement variability on bulking. The analysis will show that the three failure criteria lead to different confining pressure distributions and, as a consequence, to different contributions of bulking to the tunnel convergence.

Furthermore, the influence of bulking in two failure modes, tensile and shear, is explored to distinguish between bulking coming from each mechanism. The goal is to bound estimates between a minimum of tensile bulking only and a maximum of shear and tensile bulking. Of course, many other factors influence the excavation behaviour. This analysis is intended to demonstrate the impact of bulking alone.

The ultimate goal is to provide an approximation of the anticipated deformation behaviour in terms of the final displacement, such that efficient and effective support systems can be selected.

## 3.6 Tunnel Excavated in a Uniform Stress Field ($k_o = 1$)

Three tunnel cases, excavated at 2000 m depth experiencing same horizontal and vertical stress of 54 MPa, are modeled in the three material types described in the introduction. The order of the analysis performed was as follows: (1) the distribution of confinement near the excavation is obtained stage by stage; (2) the state when yielding of the tunnel begins is established as only then bulking can occur; (3) the confining pressure dependent bulking profile is obtained (assuming a logarithmic relationship between a rock mass bulking and confinement); and (4) the displacement distribution is obtained for two contribution failure mechanisms (extension or tensile failure and shear yield). The resulting displacements at the tunnel wall are then incorporated into GRCs that represent not only the displacement of the numerical model but also the convergence contributions from bulking.

### *3.6.1 Tunnel in Elastic-Plastic rock*

Figure 3-14 presents the tunnel failure mode, in tensile or shear (o or x) respectively, and the extent of the damage (radial measurements shown in the image).

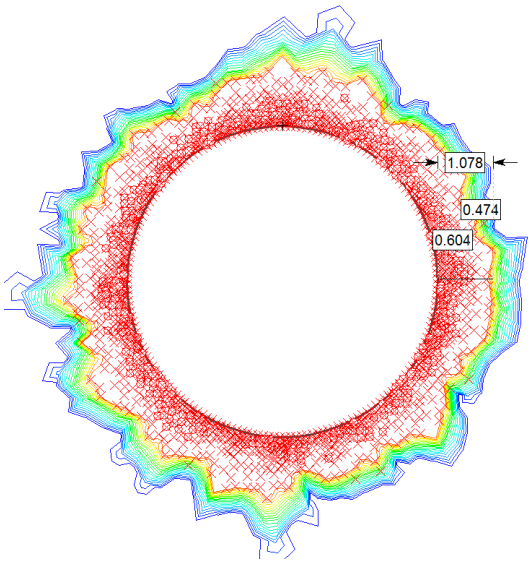

*Figure 3-14 Extent of the damaged zone around tunnel boundary for elastic-perfectly plastic rock excavated at 2000 m depth in a uniform stress field (ko = 1).*

The distribution in confinement is presented in Figure 3-15 for each excavation stage (see legend for confinement pressures). The confining pressure drops below 10 MPa in a very limited zone of ≤1 m from the wall.

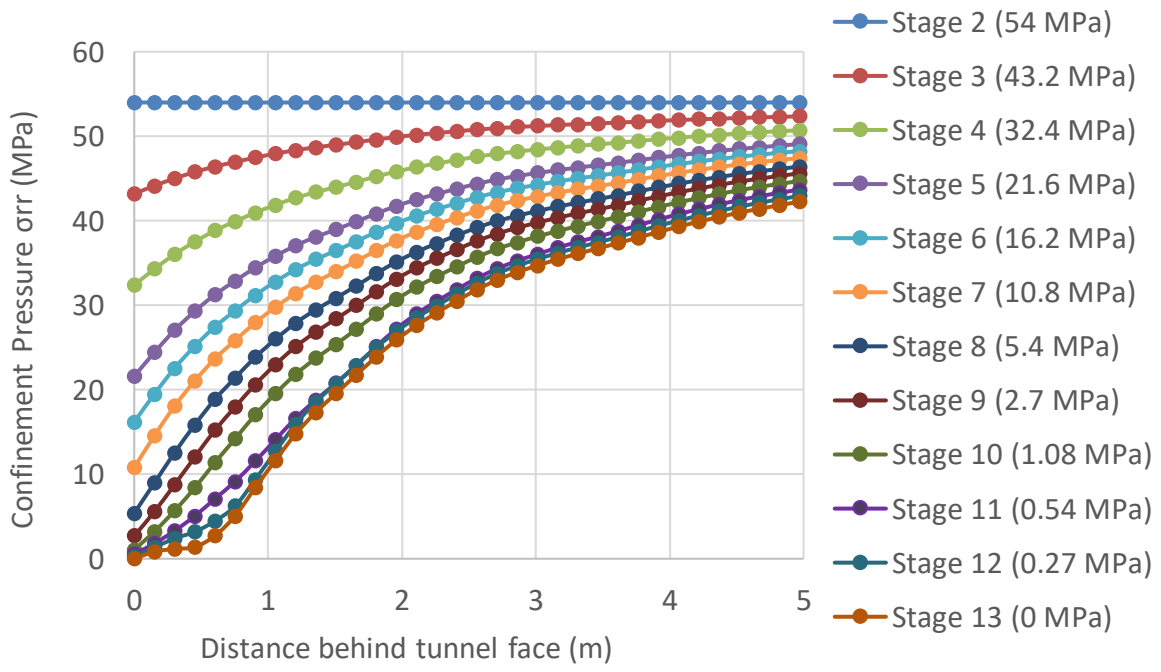


*(a)*

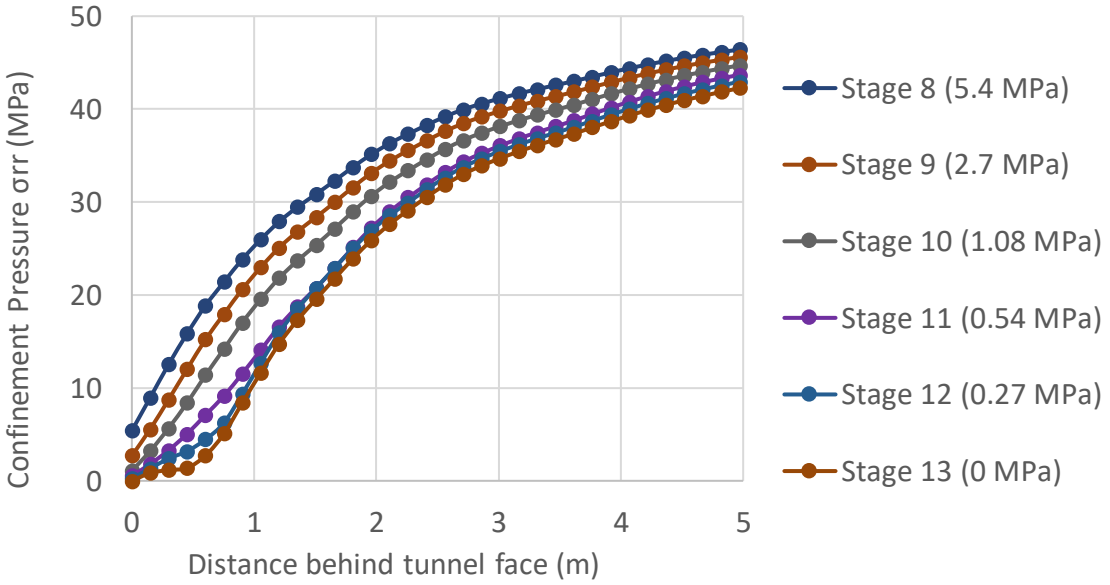


*(b)*

*Figure 3-15 (a) Distribution of confinement in 13 stages of excavation; and (b) close-up for the stages after yielding was initiated.*

The corresponding bulking factor (BF) profiles, resulting from the logarithmic dependence of BF on the confinement (see section 4.1.1; a = b = 1.3), are presented in Figure 3-16.

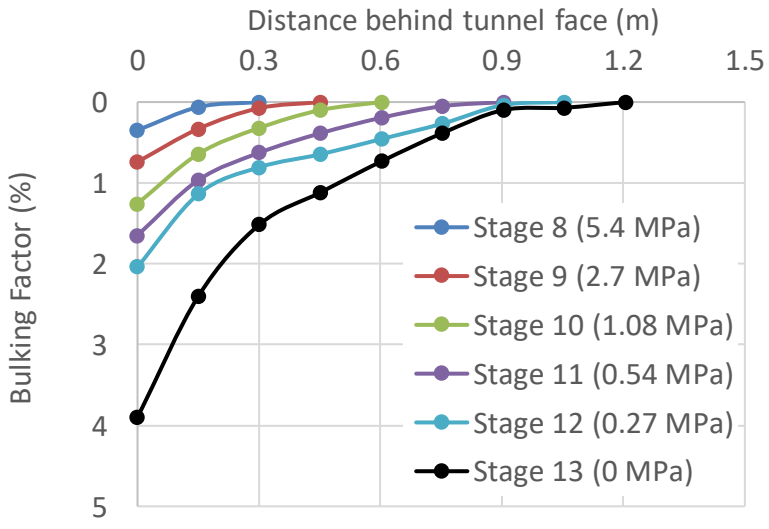


*Figure 3-16 Evolution of total bulking at last 6 excavation stages.*

As mentioned previously, it is important to differentiate between the failure mechanisms that generate bulking. Figure 3-17 shows the distribution of the two failure mechanisms and, Figure 3-18 presents the respective bulking for each of the two failure types.

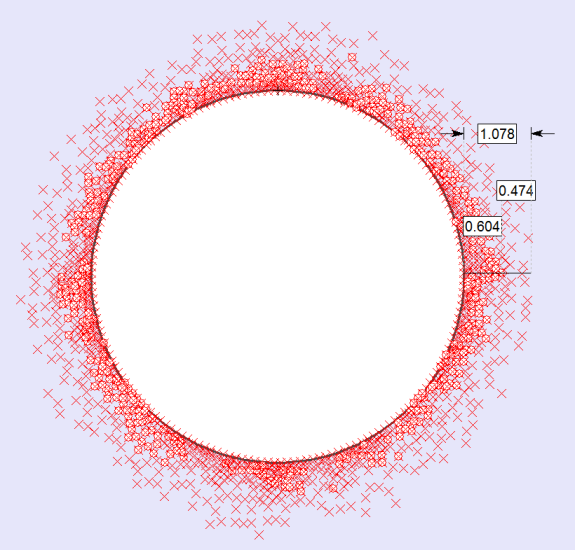


*Figure 3-17 Representation of tensile (o) and the shear (x) failure with their extent for the elastic-perfectly plastic tunnel with ko = 1 (excavated at 2000 m depth).*

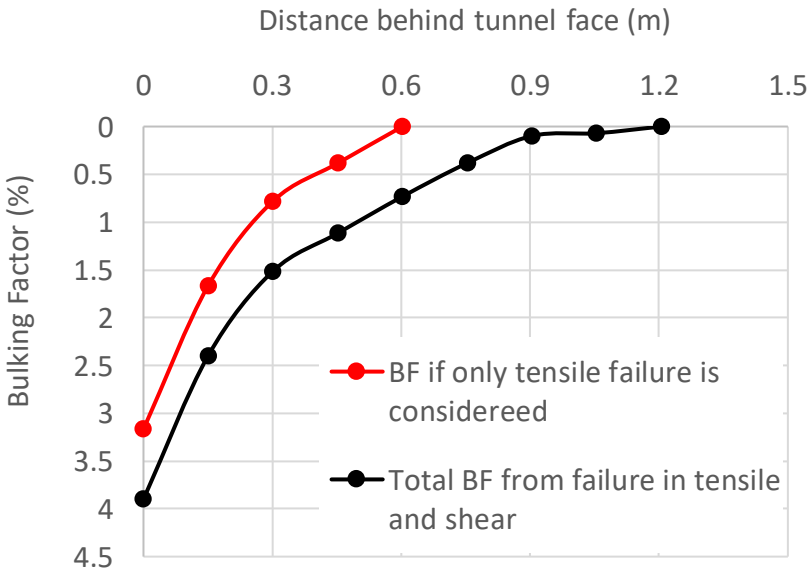


*Figure 3-18 Bulking percentage for each failure mechanism.*

By summation of the extra volume that is created by bulking in the damaged zone the displacement or added convergence is then obtained and plotted in Figure 3-19.

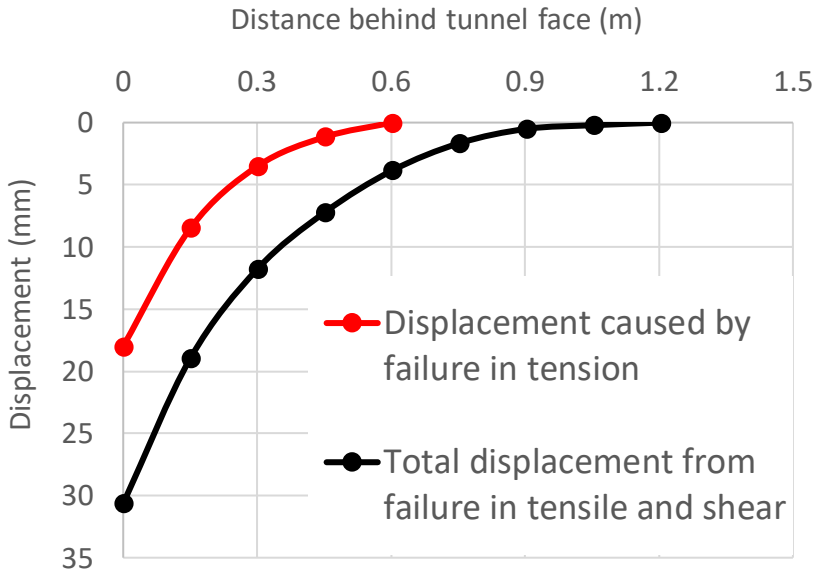


*Figure 3-19 Displacement caused by bulking of the rock mass damaged in tension and tension and shear.*

About half a metre of broken rock mass bulks in tension generating 17 mm of bulking displacement at the walls. If the entire damage zone is considered to be prone to bulking, with the combination of shear and tension, then 1.2 m of broken rock generates an extra bulking displacement of 30 mm. Reality is expected somewhere in between because, as commented earlier, consider only tensile failure as the only factor contributing to bulking ignores the often-observed interaction of shear causing extension failure. However, at some distance from the wall, confinement is high enough to prevent shear induced bulking. Hence, the reality is likely somewhere in between.

In any case, the bulking related displacements have to be added to the displacements obtained from the numerical model. This leads to a translation of the GRC to the right as is shown in Figure 3-20 presenting various combinations of total displacement GRCs.

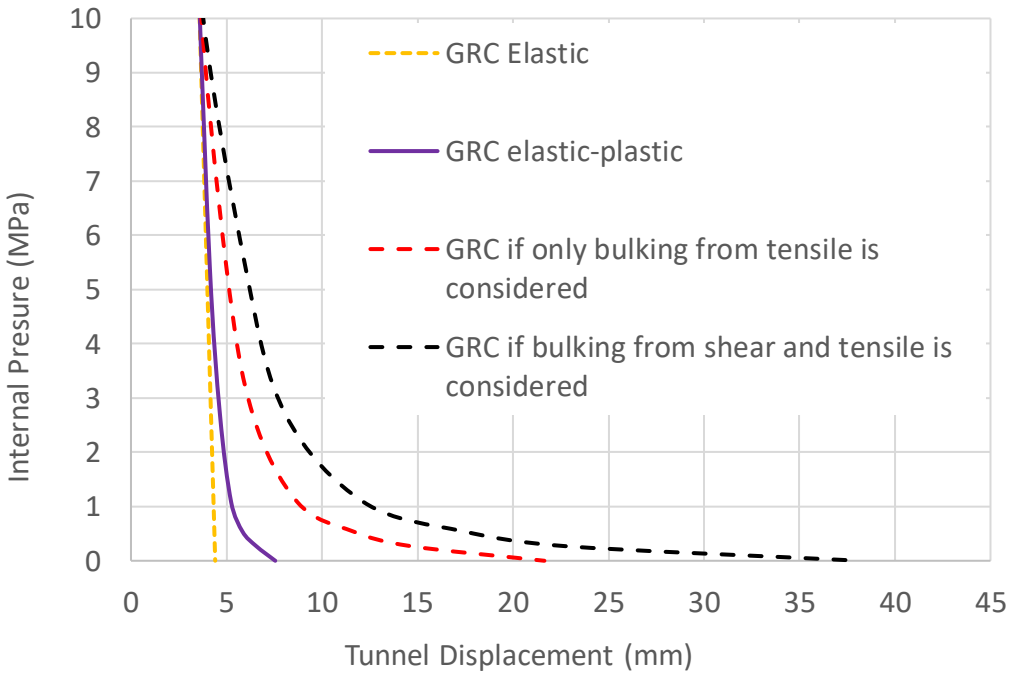


*Figure 3-20 Convergence of an elastic-perfectly plastic tunnel with ko = 1 excavated at 2000 m depth with deformation from bulking.*

The total displacement of the unsupported tunnel increases from 8 mm (numerical model) to 22 mm with bulking from the tensile failure zone and to 37 mm when the bulking is added (conservatively) from shear and extension. This example shows that bulking can dominate over plastic yield with the implication that the deformations from the model alone are not conservative and can lead to an ineffective support system. Even at a support pressure of <0.5 MPa, the support would experience between 10 and 20 mm of convergence rather than the modeled 6 mm. In reality support will experience much more deformation than reflected by the model (Phase2 in this case).

### *3.6.2 Tunnel in Elastic-Brittle rock*

The same work flow was adopted and the corresponding figures summarize the behaviour of a tunnel in the elastic brittle rock model. Figure 3-21 shows the extension of broken zone around the boundary of the excavation.

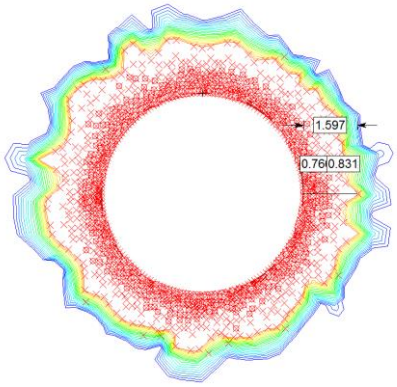


*Figure 3-21 Extent of the damaged for the elastic-brittle model with tunnel excavated at 2000 m depth in a uniform field stress (ko = 1).*

The extent of the damage zone has increased by 0.5 m and this has deepened the distribution of confinement as presented in Figure 3-22Figure 3-22 for each excavation stage.

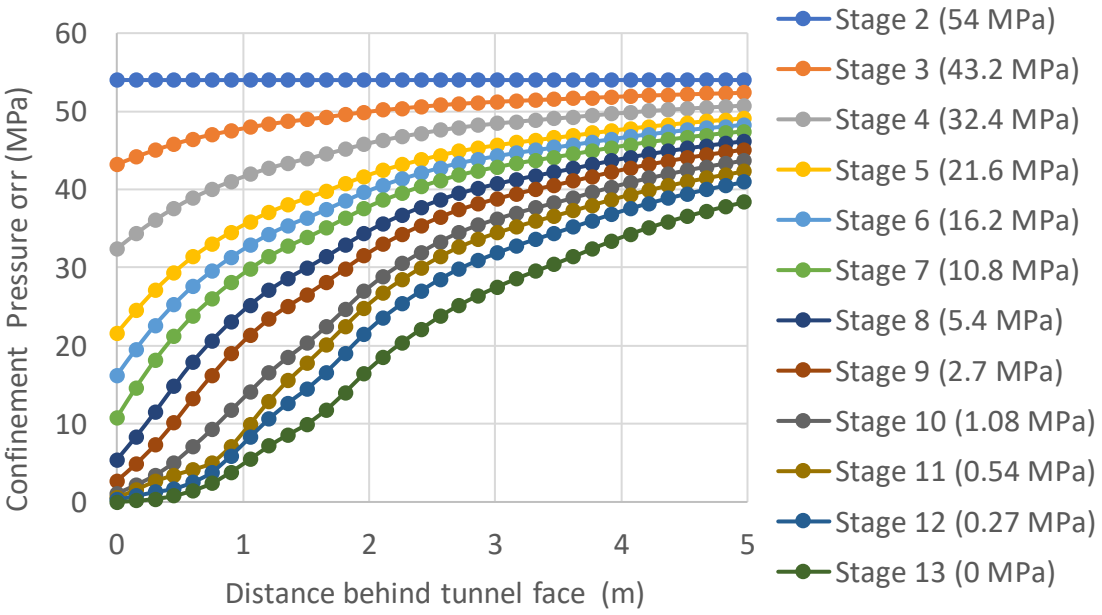


*(a)*

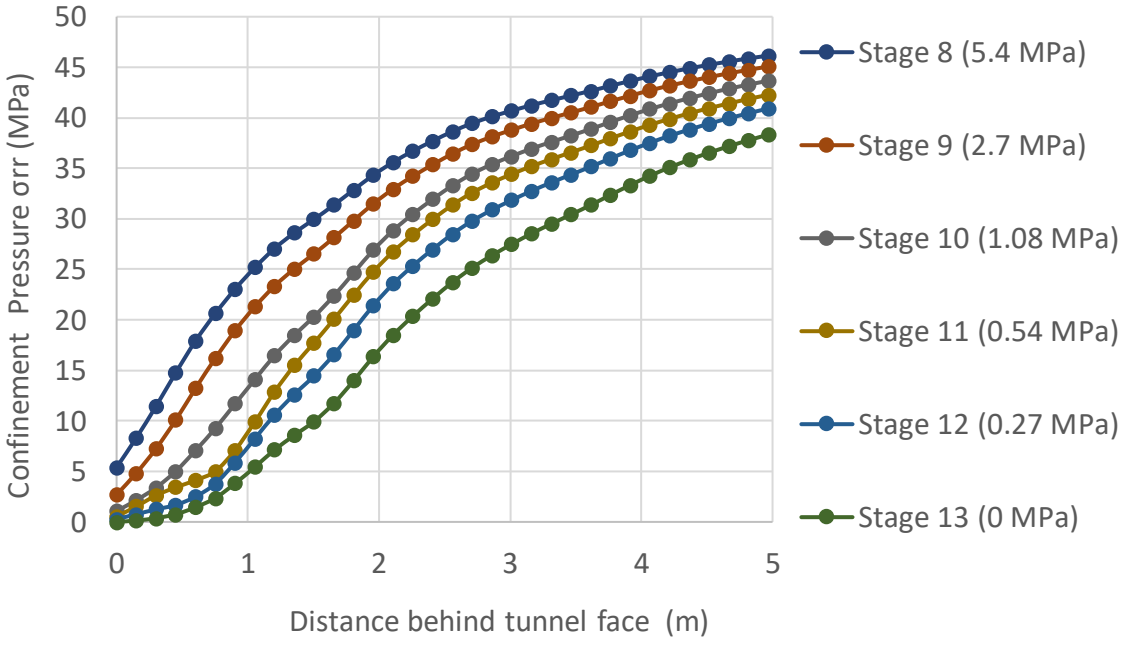


*(b)*

*Figure 3-22 (a) Distribution of confinement in each of 13 excavation stages; and (b) close-up to the stages with plasticity yield.*

The bulking factor distribution for the stages of the excavation that are yielding is represented in Figure 3-23.

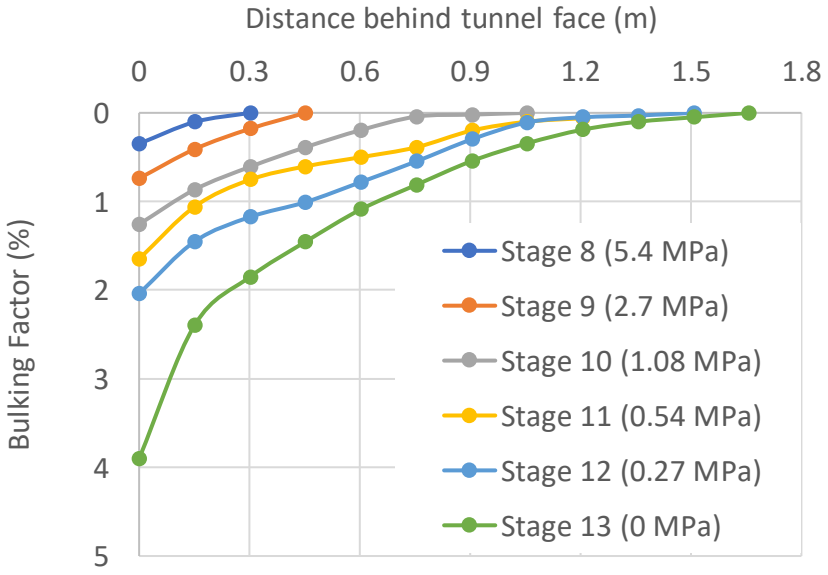

*Figure 3-23 Evolution of bulking at last 6 stages of excavation.*

The bulking now extends over 1.6 m, larger than in previous cases, as was anticipated for this type of material. The failure of the tunnel in tension and shear is shown in Figure 3-24.

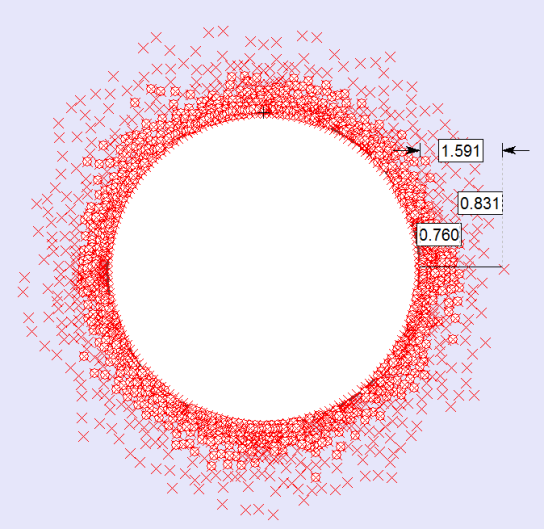


*Figure 3-24 Tensile and shear failure for tunnel in elastic-brittle rock with ko = 1 (at 2000 m depth).*

The bulking profile is presented in Figure 3-25 each failure mechanism.

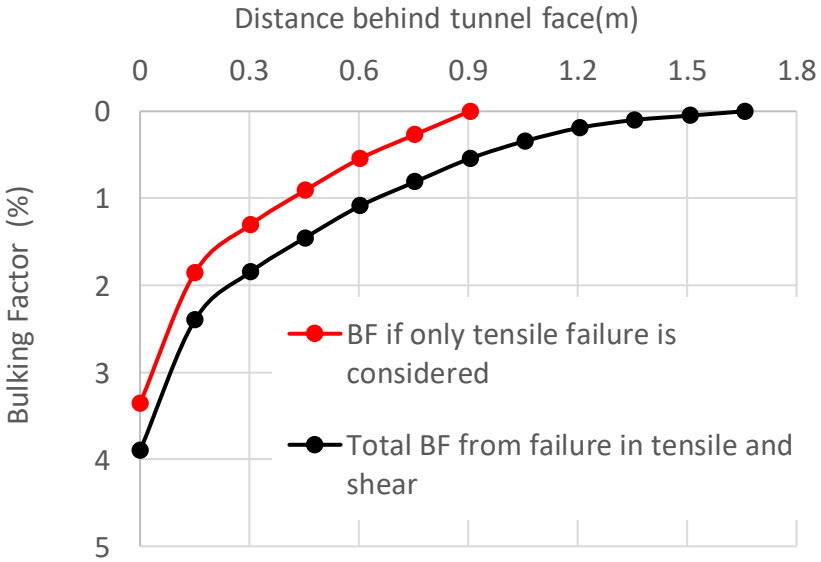

*Figure 3-25 Bulking profile for each failure mechanism.*

About 0.9 m fails in tension and almost double in shear. The resulting displacement profiles are shown in Figure 3-26.

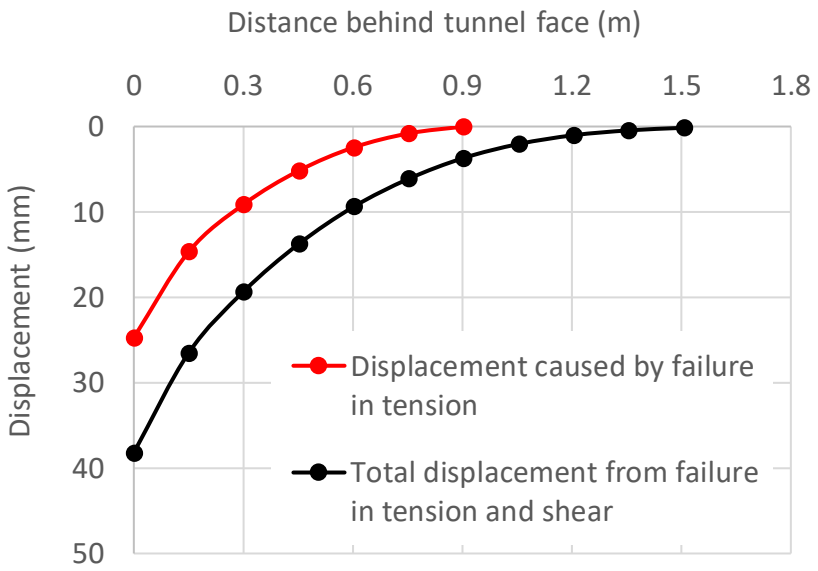


*Figure 3-26 Displacement from bulking of the rock mass when tunnel fails in tension and shear.*

The first metre failing in tension, creates a convergence of 24 mm; bulking in shear could add 15 mm for a total displacement of almost 40mm. Therefore, this range of displacement between 24-40 mm should be added to the displacement obtained from the numerical solution. Figure 3-27 represents the GRCs obtained for the tunnel in elastic-brittle rock. Again, the GRCs demonstrate that bulking deformations dominate over the plastic deformations.

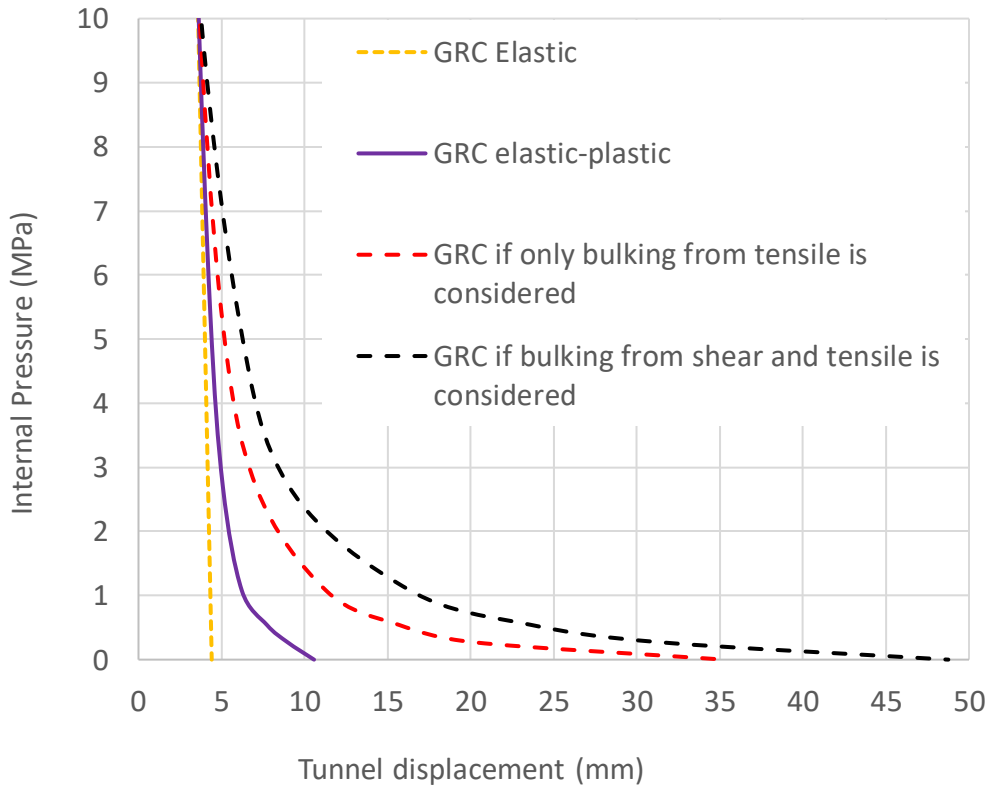


*Figure 3-27 Convergence of an elastic-brittle tunnel with ko = 1 excavated at 2000 m depth with deformation from bulking incorporated.*

### *3.6.3 Tunnel in Brittle Rock (DISL Model)*

The extent of damage obtained from the numerical model are presented in Figure 3-28.

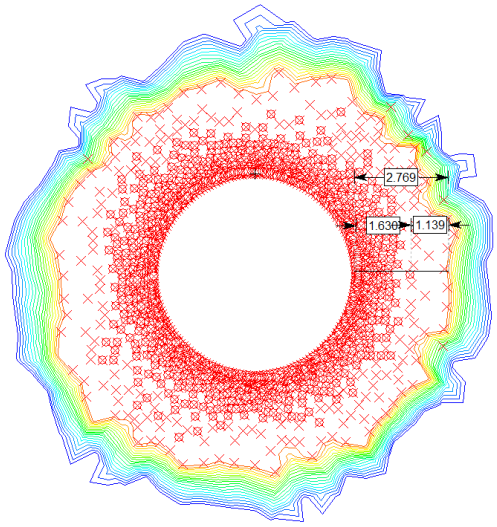


*Figure 3-28 Extent of damaged zone around tunnel boundary for a tunnel excavated in a brittle rock at 2000 m depth in a uniform field stress (ko = 1; DISL model).*

The damage zone extends to 3 m, almost double the damage in the previous models, even though the three tunnels are under the same field stress of 54 MPa.

Figure 3-29 represents the confinement distribution around this excavation in the brittle rock (DISL model). How material properties affect the distribution of the confinement and thus bulking related displacements is explained in Chapter 4 in more detail.

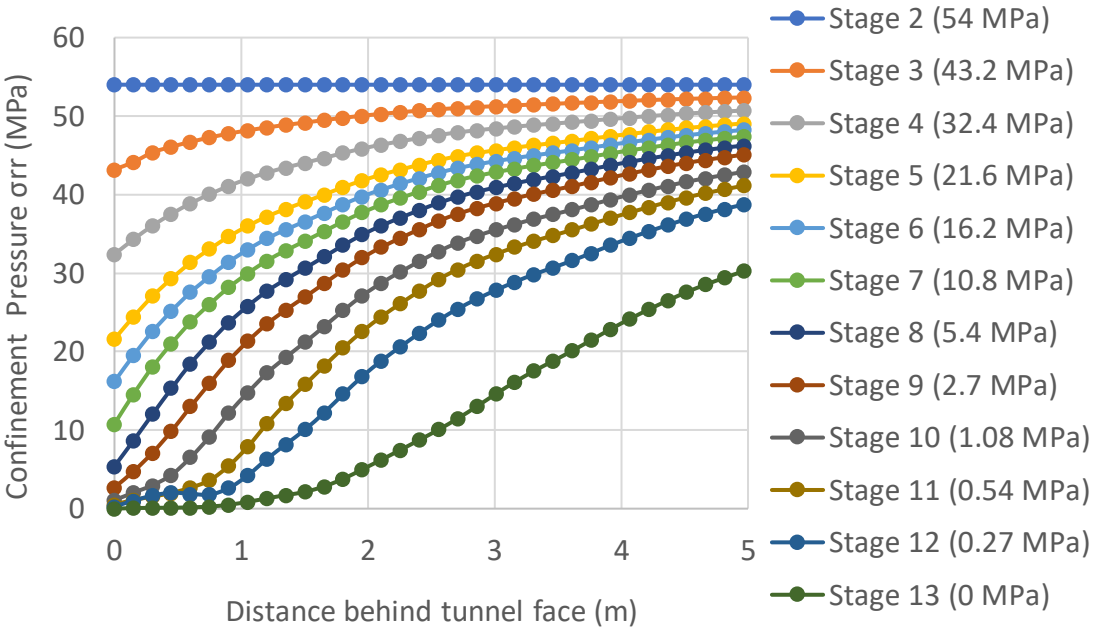


*(a)*

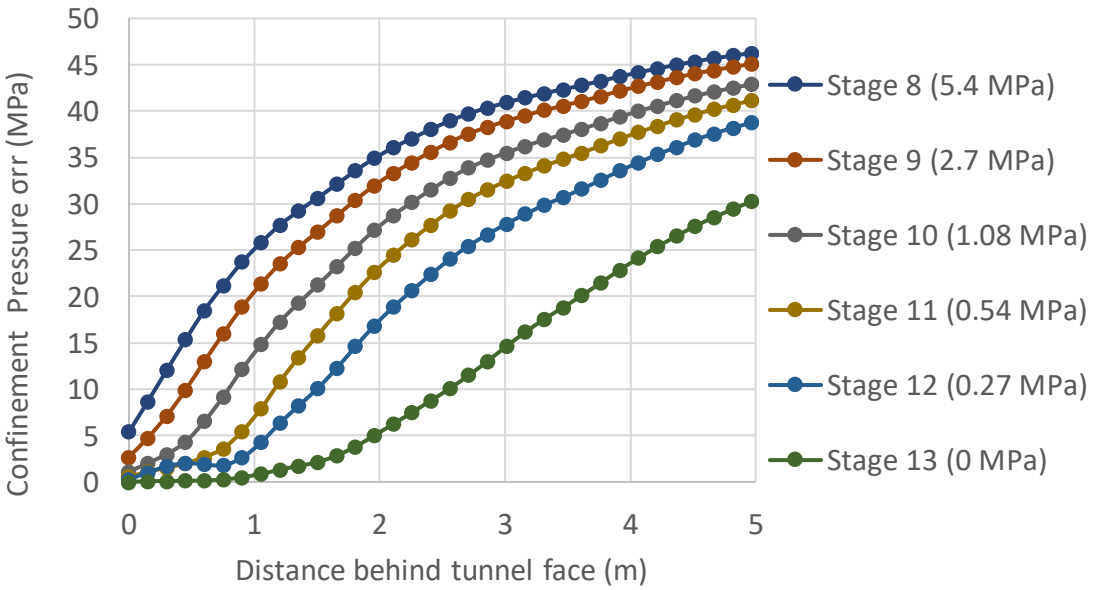


*(b)*

*Figure 3-29 (a) Distribution of confinement in 13 stages of excavation; and (b) close-up for stages with brittle failure.*

From this confinement, the bulking profile is presented in Figure 3-30.

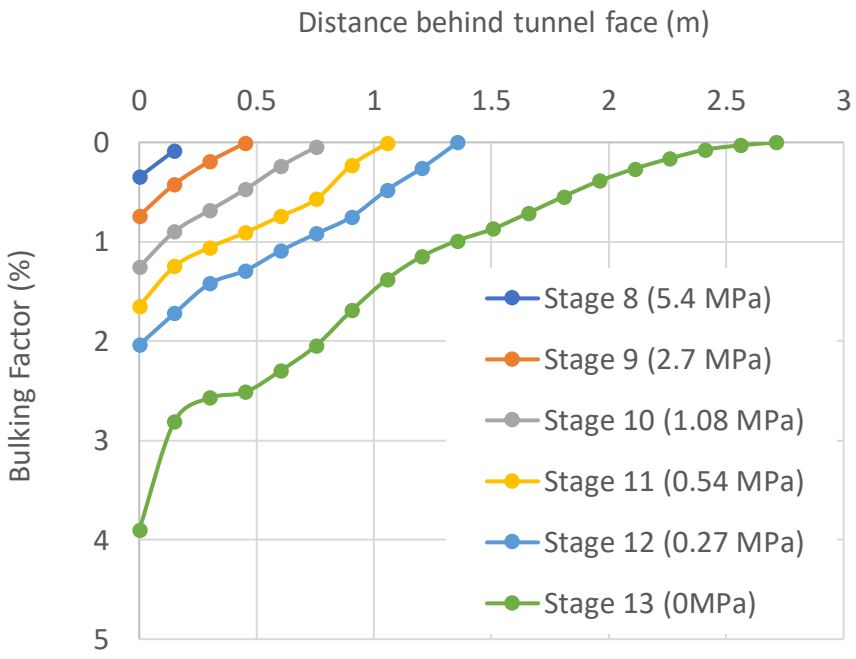


*Figure 3-30 Evolution of bulking at each stage of the excavation sequencing process.*

A slight difference is observed in this evolution of bulking with respect to what was observed in the other two tunnels studied. In the brittle model, the majority of bulking happens in the last stages, i.e., at very low support pressure (under 0.27 MPa). The previous stage experiences almost have as much bulking. So, it is a characteristic of the brittle material in that it doubles the volume of broken rock (bulks) in the final stage of excavation. It is a sudden failure where the progress of the damage is abrupt.

Figure 3-31 shows the final extent of the tensile and shear failures zones.

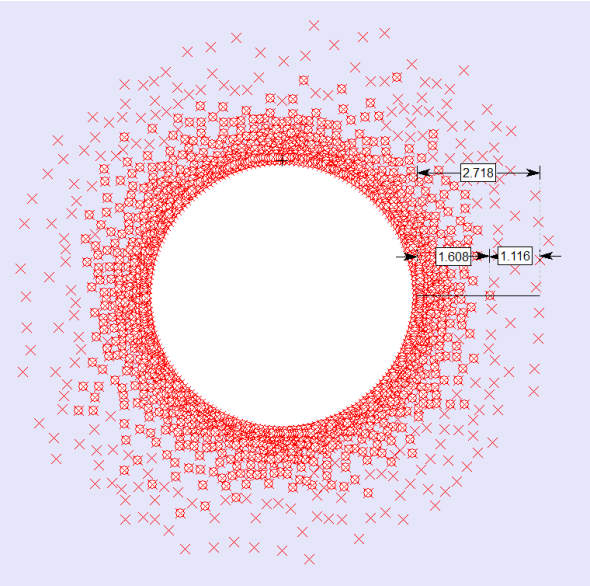


*Figure 3-31 Extent of tensile and shear failure for brittle model with ko = 1 excavated at 2000 m depth.*

The associated bulking profile is presented in Figure 3-32.

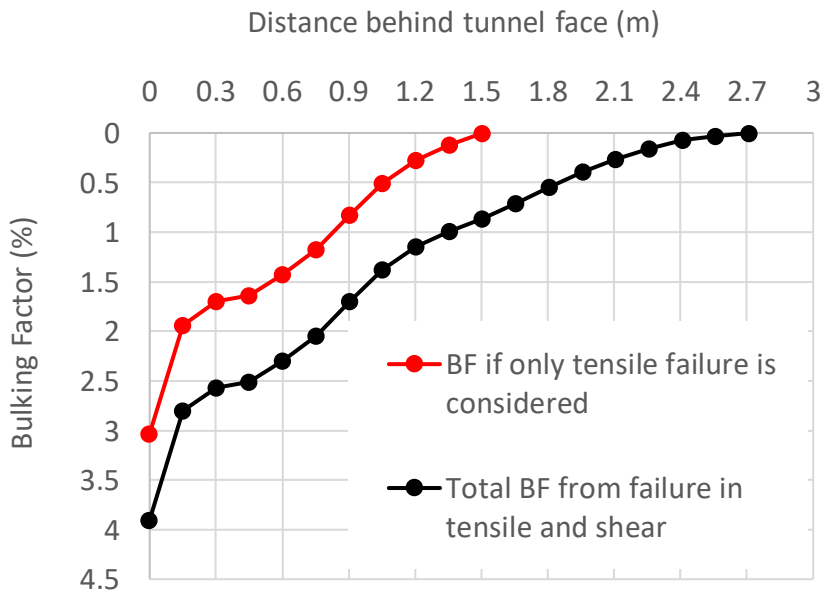


*Figure 3-32 Bulking profile for each failure mechanism.*

Approximately 1.5 m of rock surrounding the tunnel is failing in tension with 3% bulking near the

wall. Shear and tensile together cause 4% bulking at the wall with a damage zone of 2.7 m. This amount of bulking generates the displacements summarized in Figure 3-33.

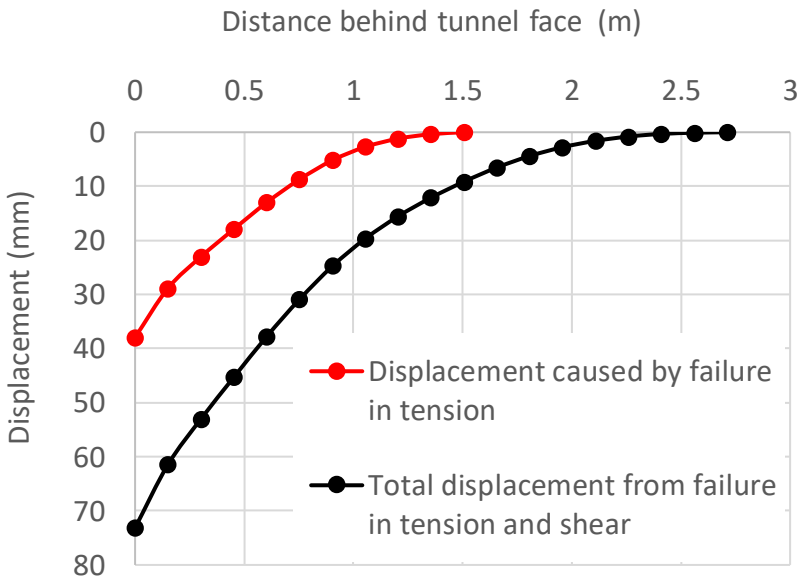


*Figure 3-33 Displacement from bulking for the brittle rock mass when tunnel fails in tension or shear.*

The 1.5 m tensile fractured rock adds 40 mm of extra convergence to the excavation whereas the entire broken rock is creating 73 mm of extra displacement.

Incorporating these results to generate the maximum displacement produces the GRCs in Figure 3-34.

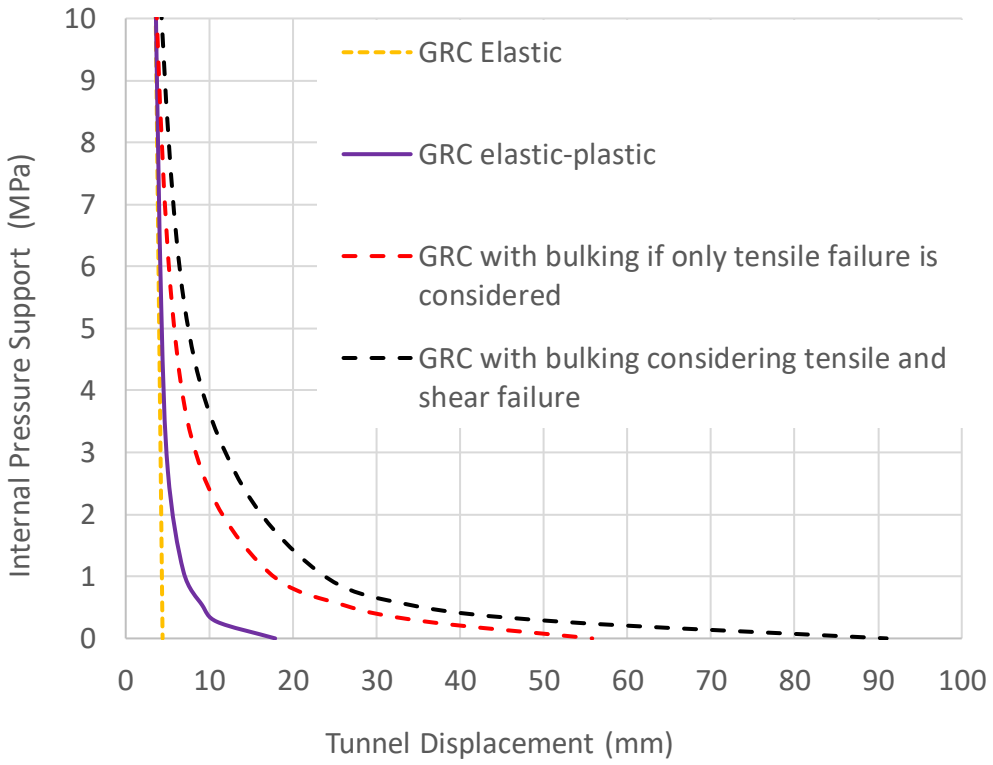


*Figure 3-34 Convergence of a brittle rock model with ko = 1 excavated at 2000 m depth with deformation from bulking incorporated.*

It is evident that the brittle (DISL) model produces the largest displacements. This brittle tunnel has almost double the displacement with respect to the two previous cases for the same level of stress. When considering the effects of differing strength of the materials, the most interesting finding is that the DISL model is showing much deeper rock relaxation and thus a deeper bulking zone.

## 3.7 Tunnel Excavated at $k_o$=0.5 in Three Rock Types

This section presents the equivalent analyses for circular tunnels excavated in the three rock masses (elastic-perfectly plastic material, elastic-brittle-plastic and brittle) subjected to a vertical field stress of 54 MPa and to a horizontal stress of 27 MPa (ko = 0.5. These tunnels will therefore

show a different behaviour at the roof than at the walls as illustrated by damage contours in Figure 3-35.Because of this, these analyses will be performed by separately studying convergence at these two locations.

### *3.7.1 Tunnel in Elastic-Plastic Rock*

For ko = 0.5, the extent of failure is wider in the walls and both shear and tension is concentrated very close to the roof. The application of the bigger tangential stress in the walls will generate high radial deformation at the walls (Figure 3-35).

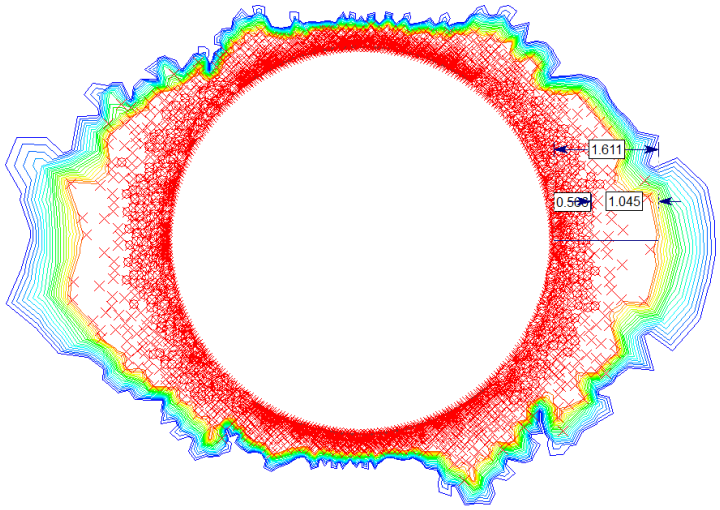


*Figure 3-35 Extent of the damaged zone for tunnel in elastic-perfectly plastic rock at 2000 m depth in a field stress where ko = 0.5.*

The implication of the distribution of the failure for the bulking calculations is that the walls will experience most of the extra deformation. The roof will experience mostly elastic-plastic displacements with some very localized bulking.

The confining pressure distribution for the wall is presented in Figure 3-36.

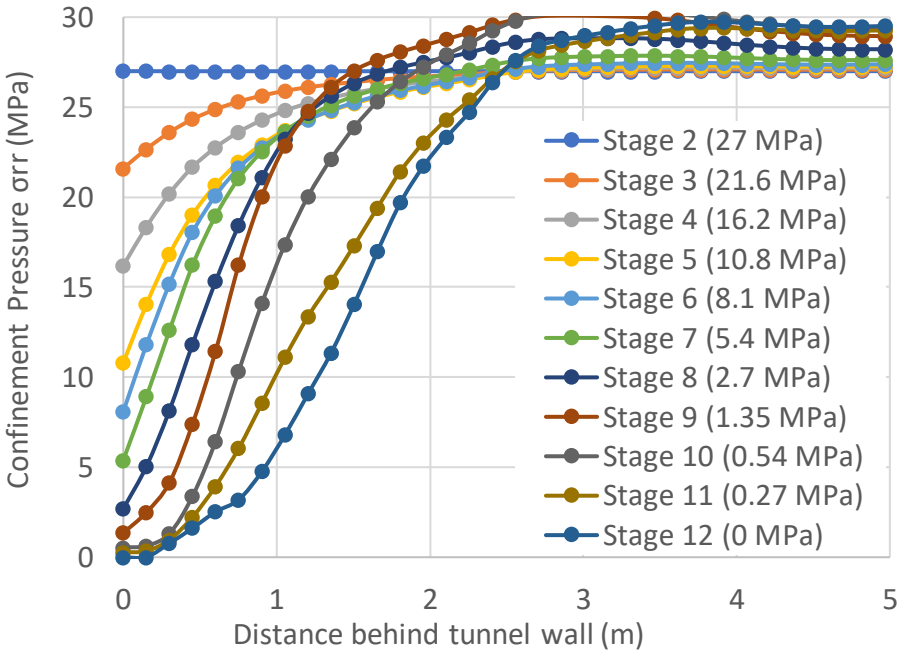


*(a)*

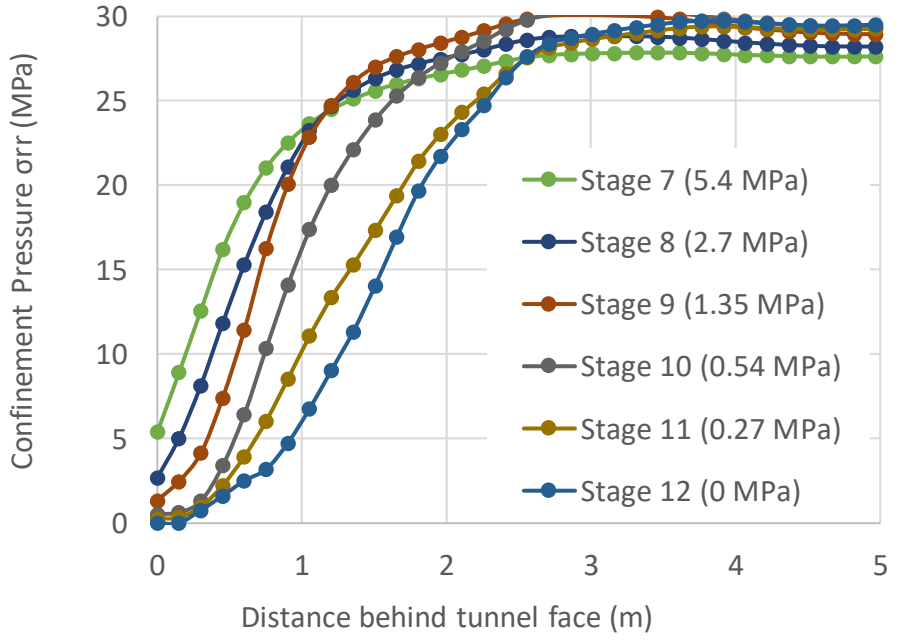


*(b)*

*Figure 3-36 (a) Distribution of confinement in 12 excavation stages; and (b) close -up for stages with plasticity.*

The confinement builds up quickly in the first half metre behind walls which means that there will be relatively shallow bulking, given the logarithmic relationship existing between bulking and confinement. Figure 3-37 presents the evolution of bulking for the stages after yield initiation.

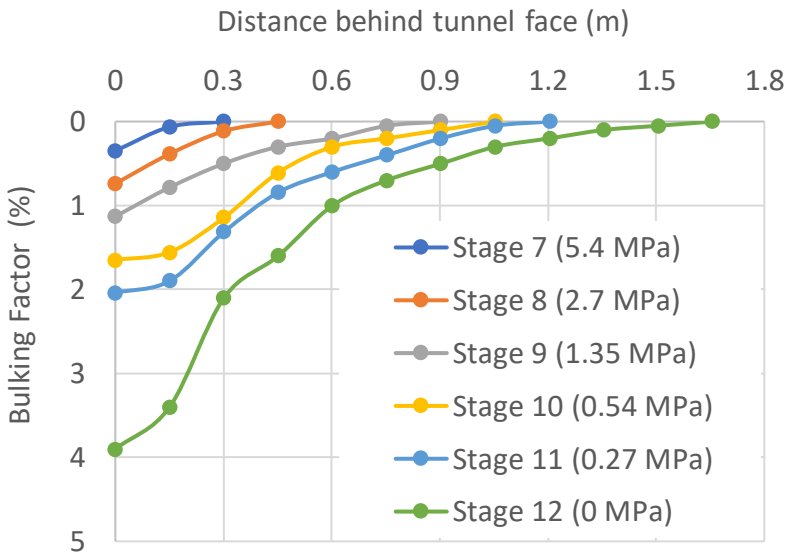


*Figure 3-37 Evolution of Bulking at each stage of the excavation sequencing process.*

The nature of the failure process is highlighted in Figure 3-38, the bulking distribution in Figure 3-39 and the resulting displacement profiles in Figure 3-40.

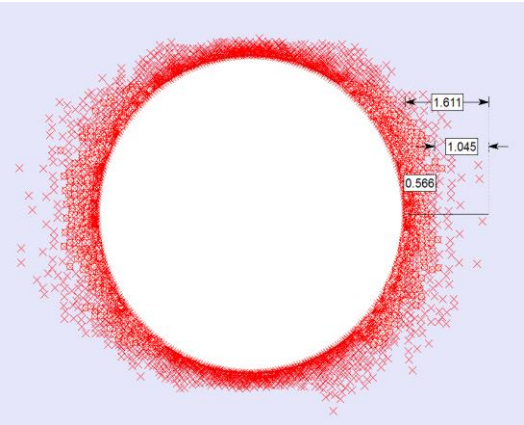


*Figure 3-38 Extent of tensile and shear failure for elastic-plastic rock with ko=0.5 excavated at 2000 m depth.*

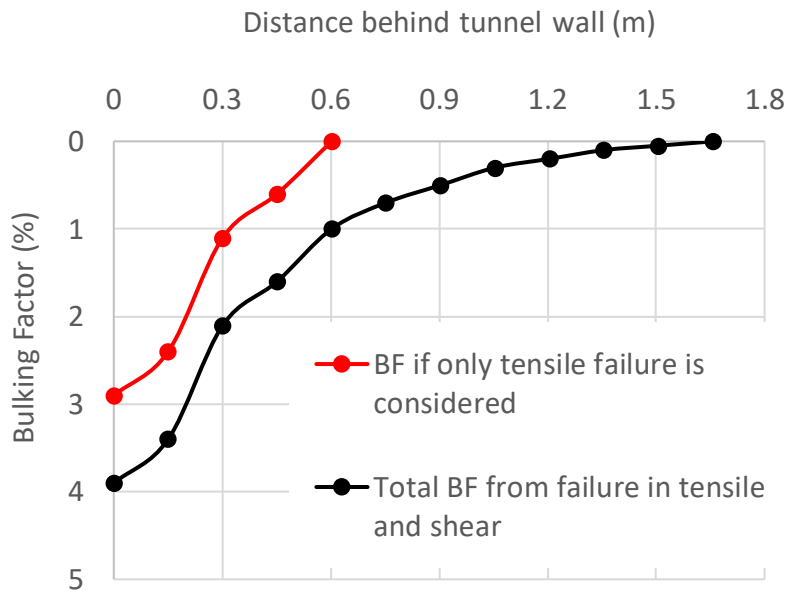


*Figure 3-39 Bulking profile for each failure mechanism.*

This figure illustrates the localized bulking with 3% at the wall from tensile failure and an additional 1% for a total of 4% from shear.

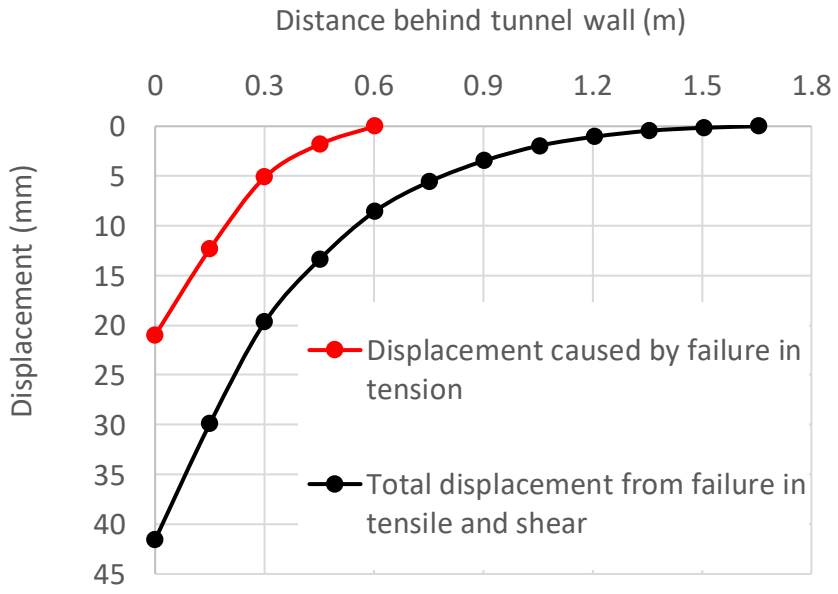


*Figure 3-40 Displacement from bulking of the rock mass when tunnel fails in tension and shear.*

In this case, tensile failure leads to 21 mm of displacement and deeper-seated shear adds another 20 mm for a total of 41 mm.

These deformations once added to the displacements obtained by numerical means are reflected in the GRCs plotted in Figure 3-41.

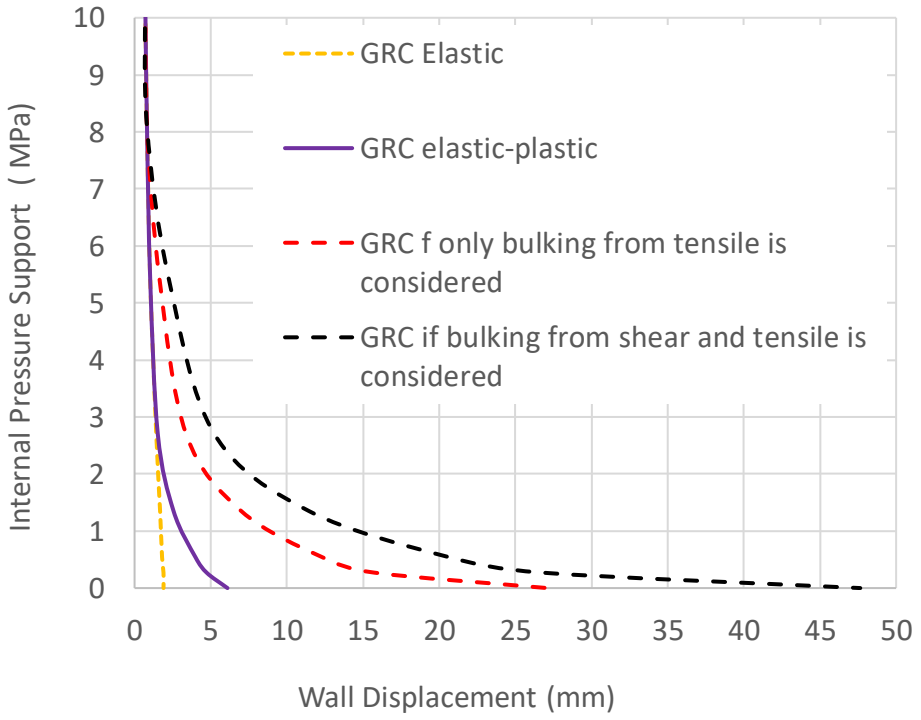


*Figure 3-41 Convergence of an elastic-perfectly plastic tunnel with ko = 0.5 excavated at 2000 m depth, with deformation from bulking incorporated.*

This tunnel with ko = 0.5 experiences more convergence compared to the ko = 1 case. How the stress distribution influences the tunnel behaviour is explained in detail in Section 3.9.

### *3.7.2 Tunnel in Elastic-Brittle Rock*

When studying this case, it was observed that the extent of damage and the distributions of bulking and related displacements were very similar to the elastic-perfectly plastic material case. For this

reason, the results from the elastic-brittle rock model are not presented here.

### *3.7.3 Tunnel in Brittle Rock (DISL Model)*

As Figure 3-42 illustrates, the extent of failure is larger in the walls for the DISL model and the roof is prevented from failing due to stress shedding. Hence, rock mass bulking is only analyzed for the walls.

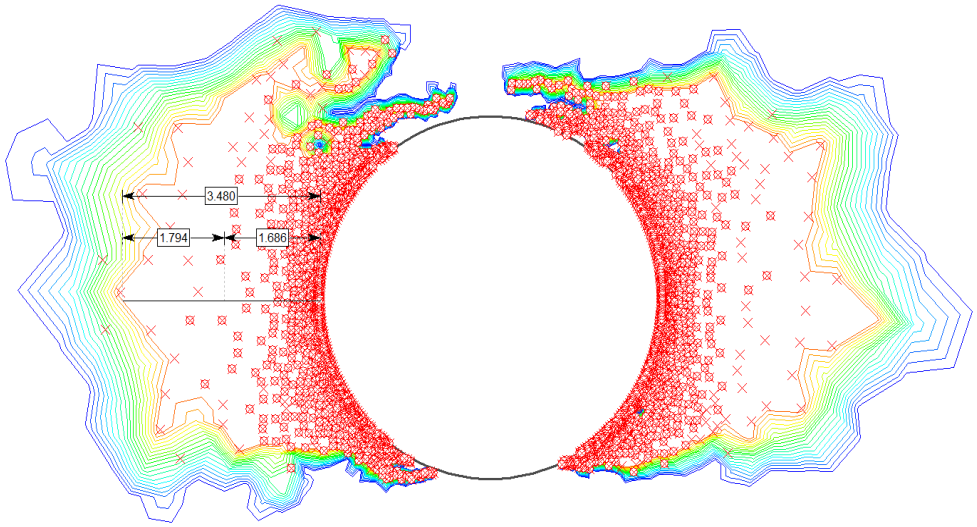


*Figure 3-42 Extent of the damaged around tunnel boundary for tunnel excavated in brittle rock at 2000 m depth with ko = 0.5.*

The confinement distributions presented in Figure 3-43 show a very low rate of confinement gain for internal pressures below 0.54 MPa and particularly for near zero support pressures.

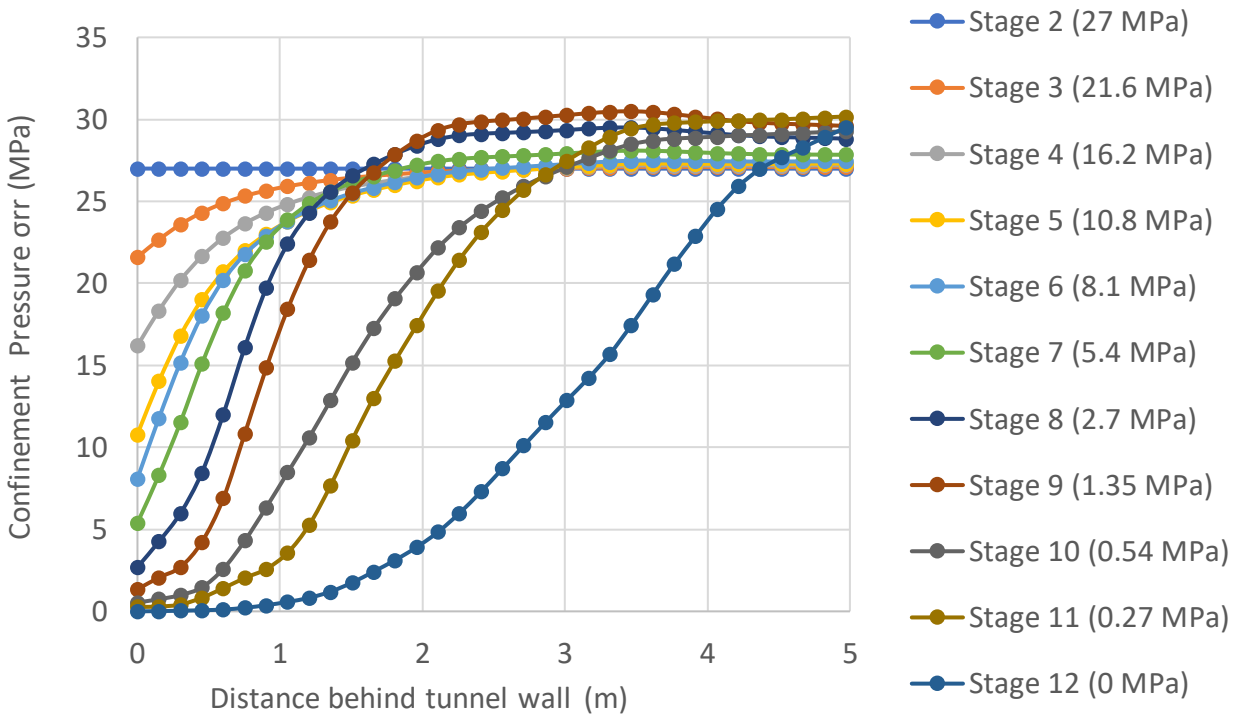


*(a)*

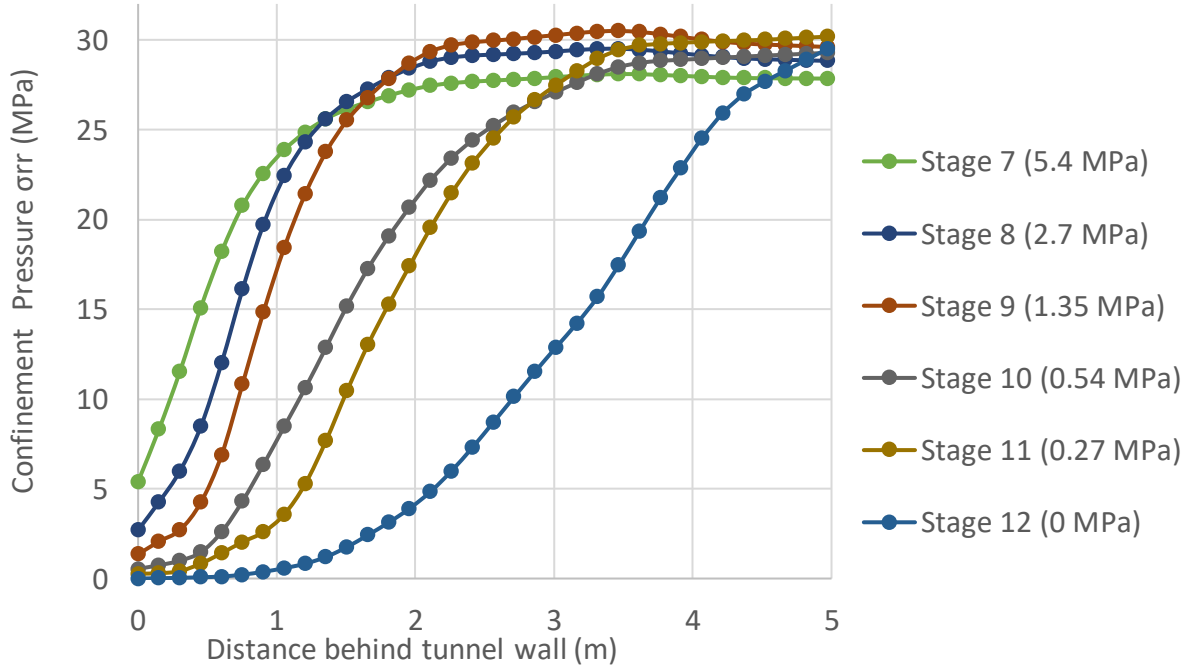


*(b)*

*Figure 3-43 (a) Distribution of confinement in 12 excavation stage; and (b) close-up for stages with plasticity.*

The corresponding bulking profiles are presented in Figure 3-44.

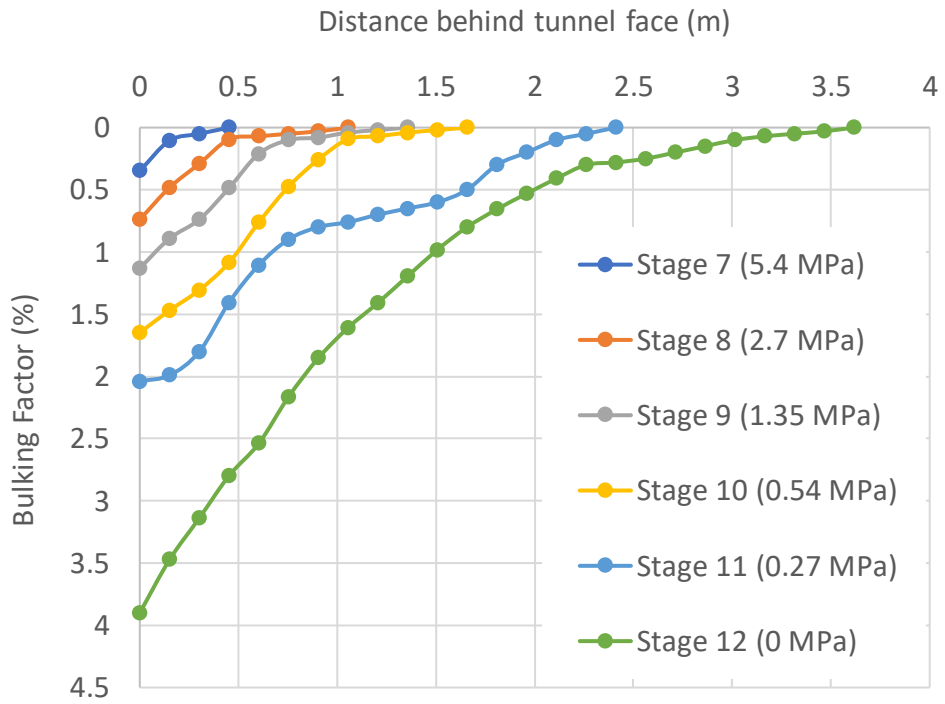


*Figure 3-44 Evolution of bulking at last six stages of excavation.*

In this brittle rock, the majority of bulking is produced at the last stage of excavation. This is because of crack damage propagates in the brittle rock when the confinement approaches very low values. This failure behaviour is characteristic of brittle materials and the resulting bulking behaviour should be representative of brittle rock failure. The extent of each damage type is shown in Figure 3-45 and Figure 3-46 presents the corresponding bulking pattern.

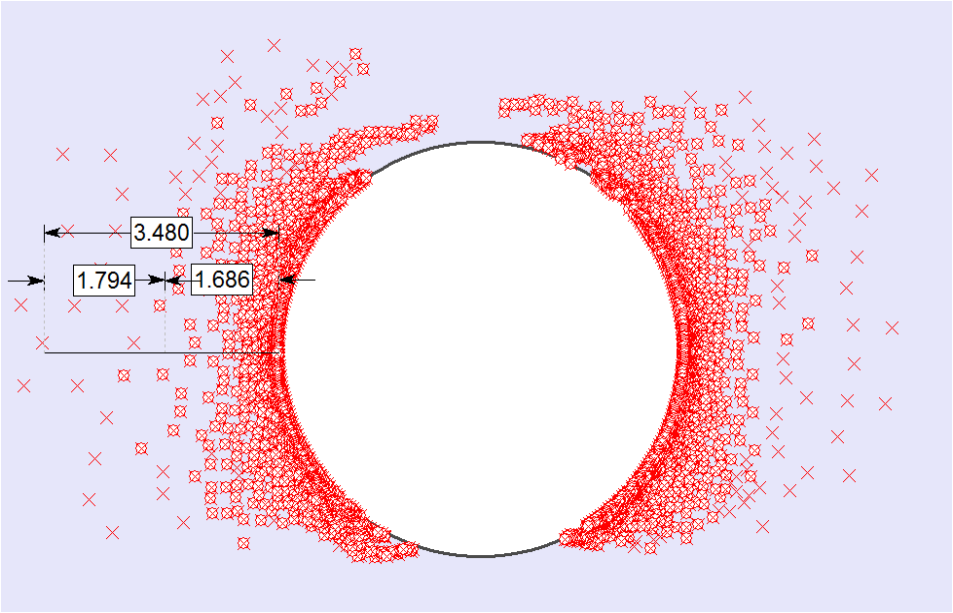


*Figure 3-45 Extent of tensile and the shear failure for tunnel in brittle rock with ko = 0.5 excavated at 2000 m depth*

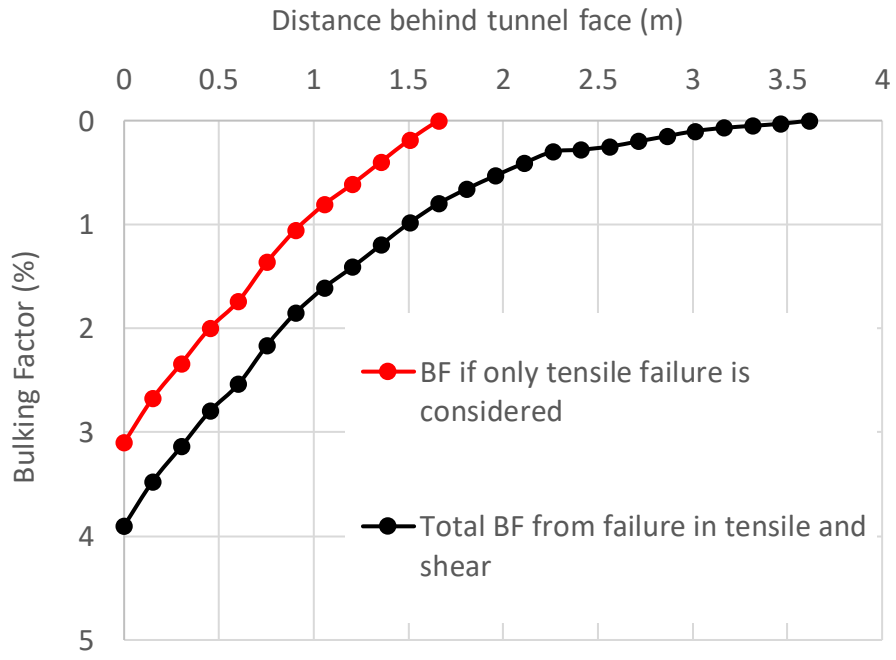


*Figure 3-46 Bulking profiles for each failure mechanism.*

The tensile fracture zone is 1.5 m deep and the tunnel experiences 3% bulking. The shear failure extends to 3.6 m but adds only 1% bulking to produce the displacements plotted in Figure 3-47.

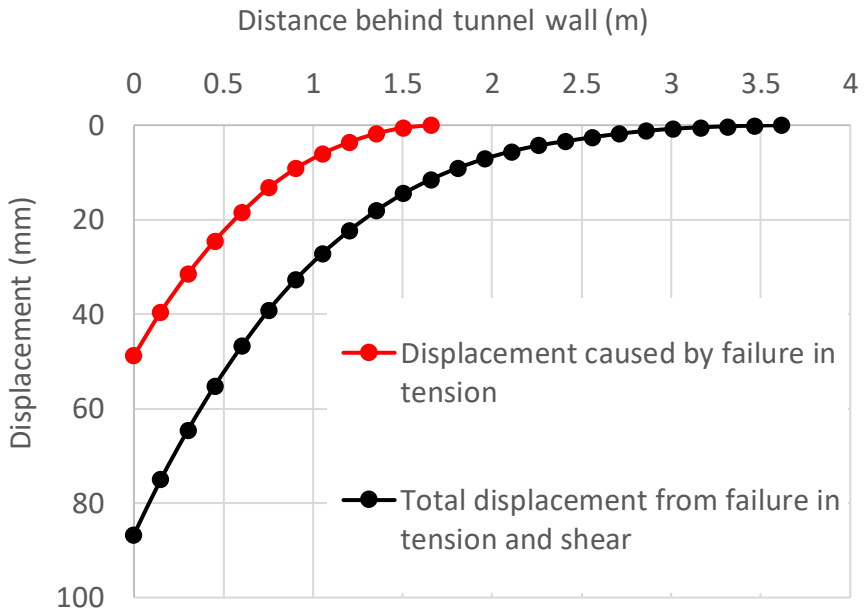


*Figure 3-47 Displacement from bulking when tunnel fails in tension and shear.*

In between 48 and 86 mm of extra displacement are generated by bulking. These displacements are again added to displacements obtained from the numerical model and presented in the GRCs in Figure 3-48.

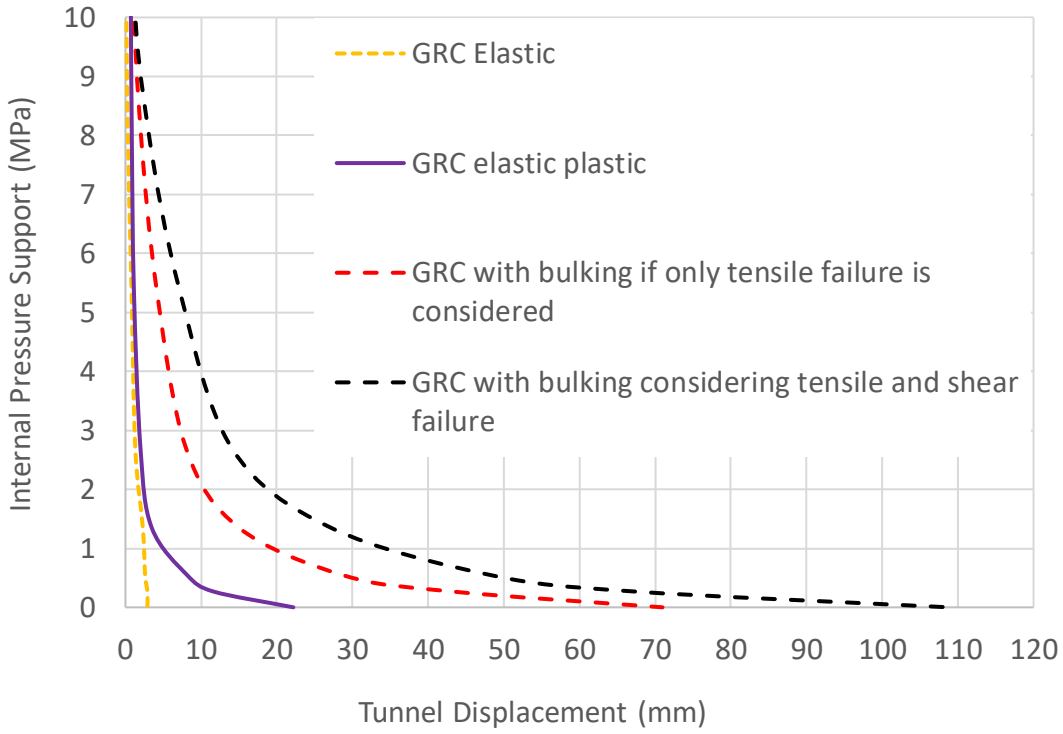


*Figure 3-48 GRCs for brittle rock with ko = 0.5 excavated at 2000 m depth and with deformation from bulking incorporated.*

In between 70 and 108 mm of extra displacement results from bulking. This is the amount of deformation that an installed support system should handle instead of the 22 mm given by the numerical solution. Interestingly, there is a great difference at internal pressures that are representative of typical support systems (e.g., 0.1 to 0.5 MPa). As a consequence, the selection of the retaining and reinforcement system in brittle failing ground must be flexible enough to accommodate such deformations.

## 3.8 Tunnel Affected by Mining-induced Stresses in Three Rock Types

In this section, three tunnels excavated in the same materials are investigated by focusing on mining-induced stress changes, i.e., to understand the implications of a transition from an initial stress level of ko = 1 to a final state at k = 0.6. This change in stress field is again obtained by adding to a fully excavated tunnel a uniformly distributed vertical stress.

### *3.8.1 Tunnel in Elastic-Plastic Rock*

The circular tunnel of 3m radius was excavated in a sequence of 23 stages. Figure 3-49, represents the damage with its measured extension at the wall and at the roof.

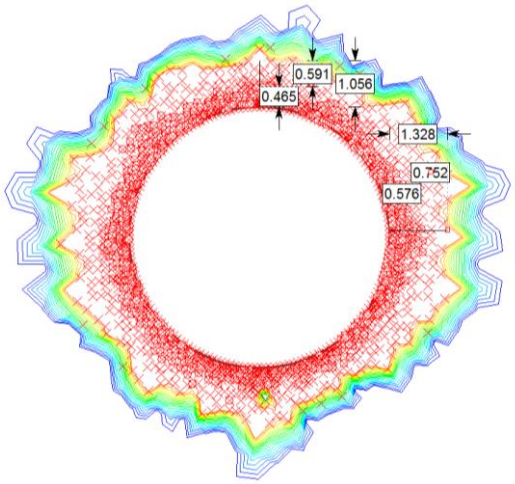


*Figure 3-49 Extent of the damaged zone around tunnel boundary for an elastic-perfectly plastic tunnel excavated at 2000 m depth in a field stress where initially ko=1 and finish with k=0.6.*

The tunnel walls are more highly damaged than the tunnel roof. The distributed load was entirely applied at the roof (tangential loading), and when it redistributes, it imposes a radial deformation, perpendicular to the application point, that is at the wall. Therefore, the wall is the location that will be get the larger displacement, coming from the bulking of the broken rock mass.

#### 3.8.1.1 Analysis of the wall of the excavation

The tunnel was excavated in 12 stages and then loaded incrementally for a total of 23 stages. The sequential loading during stages 13-23 creates what is referred to as the “mining scenario”. The goal is to understand how the excavation is affected by bulking when located close to a mine operation. The loading scenario simulates an extreme condition. In reality, mining-induced effects may be much less severe.

Figure 3-50 shows the distribution of confinement around the tunnel boundary. Relatively little change occurs near the excavation during the loading phase.

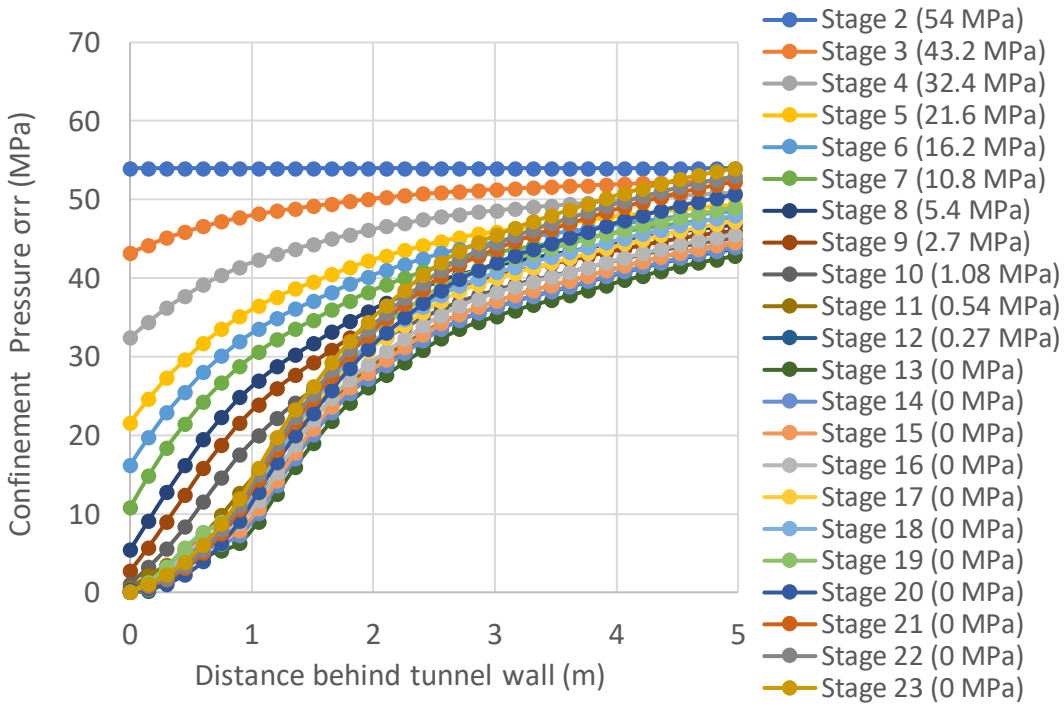


*(a)*

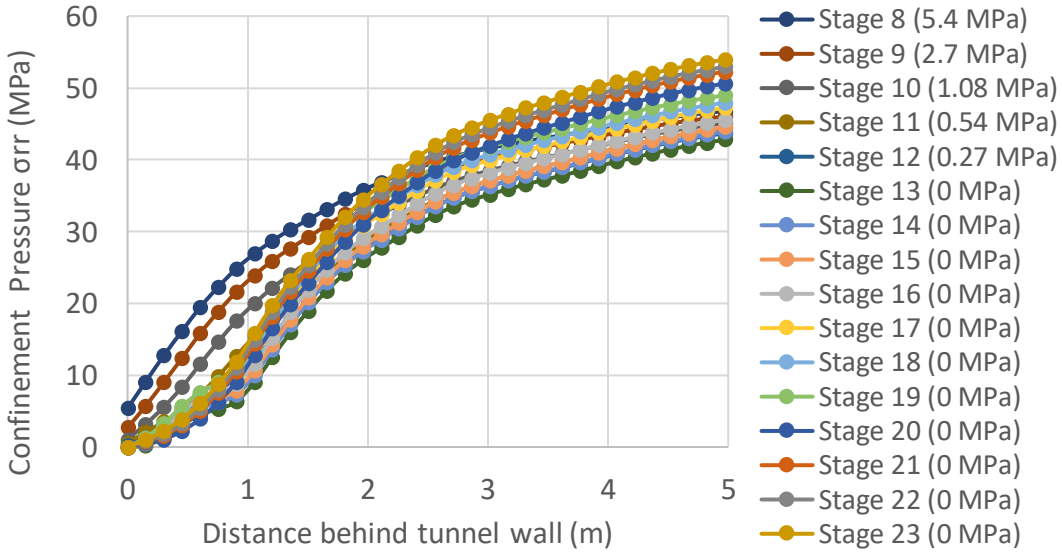


*(b)*

*Figure 3-50 (a) Distribution of confinement in all 23 stages; and (b) close-up for states with plasticity.*

The bulking profile for the excavation phase is presented in Figure 3-51 a (stages 8-13) and for the loading phase in Figure 3-51b (stages 14-23). The loading phase deepens the bulking profiles.

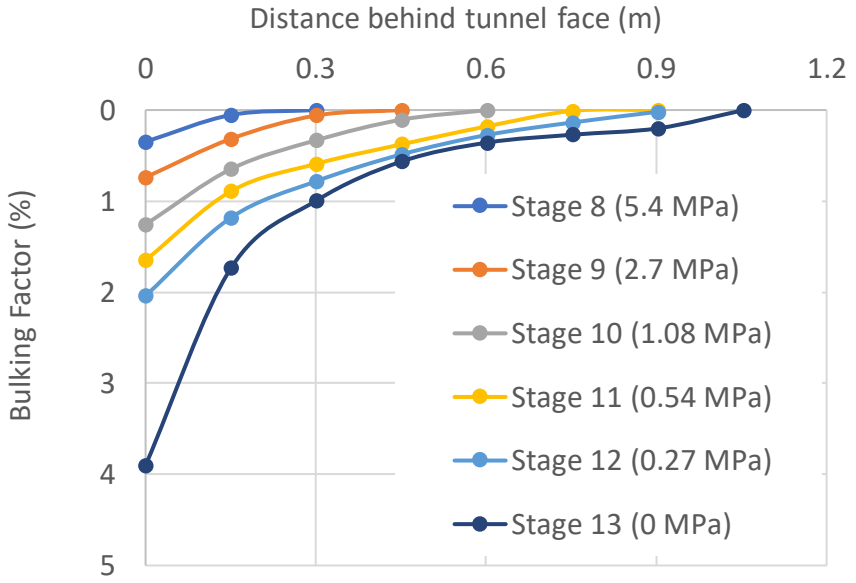


*(a)*

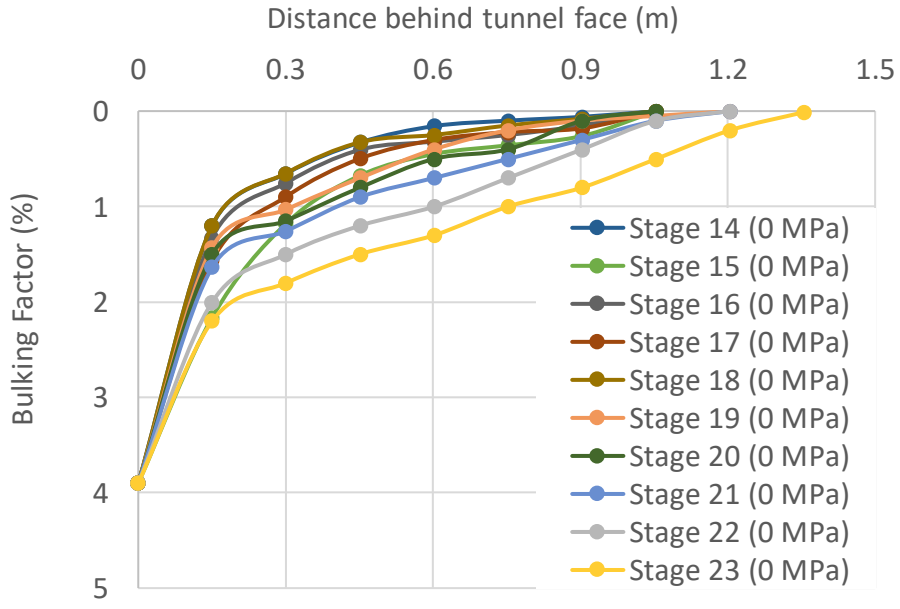


*(b)*

*Figure 3-51 Evolution of bulking percentage for (a) tunnel development state, (b) mining-induced added loading.*

Once the depth of each failure for each failure mechanism is established, the amount of bulking for tensile failure and for the combination of shear and tensile failure can be determined (Figure 3-52) and the corresponding displacement distribution is shown in Figure 3-53.

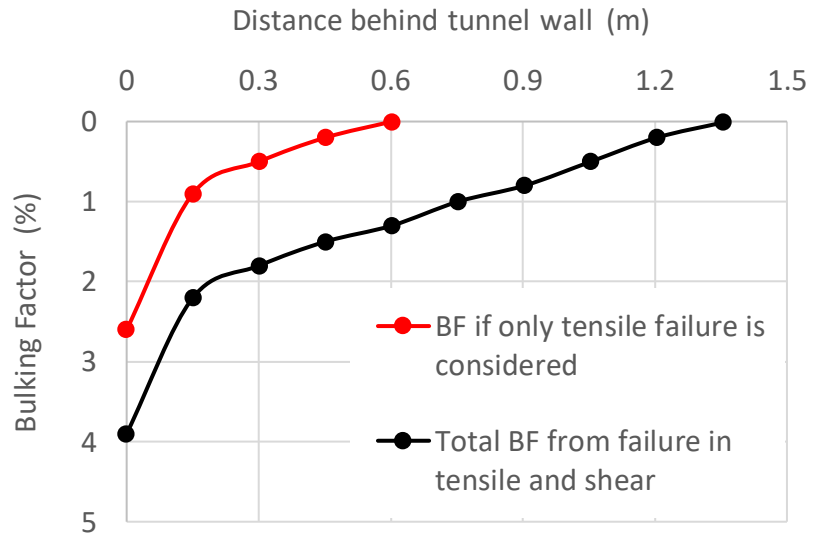


*Figure 3-52 Bulking profile for each failure mechanism at the end of the loading phase.*

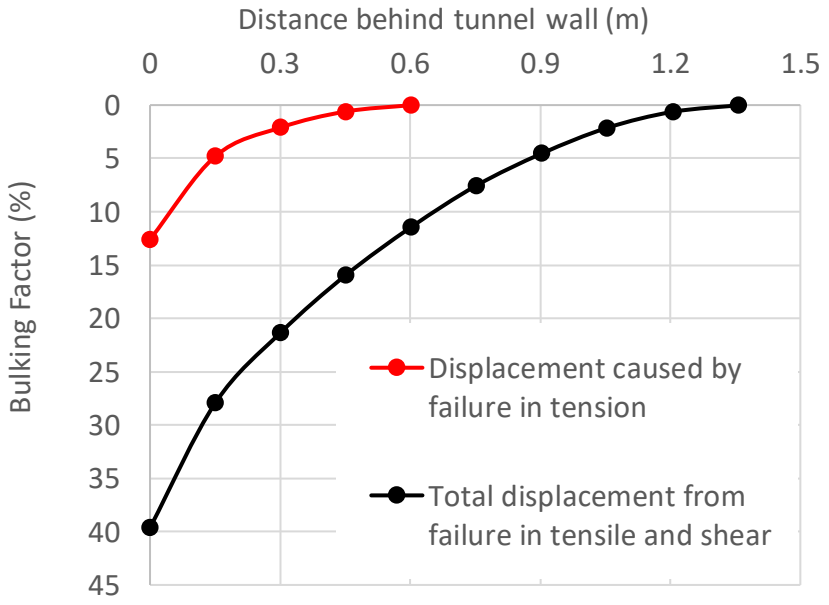


*Figure 3-53 Displacement from bulking of the rock mass fails in tension and shear at end of loading phase.*

An addition displacement between 12 and 40 mm is resulting from bulking and after adding this to the model displacement produced the GRCs in Figure 3-54.

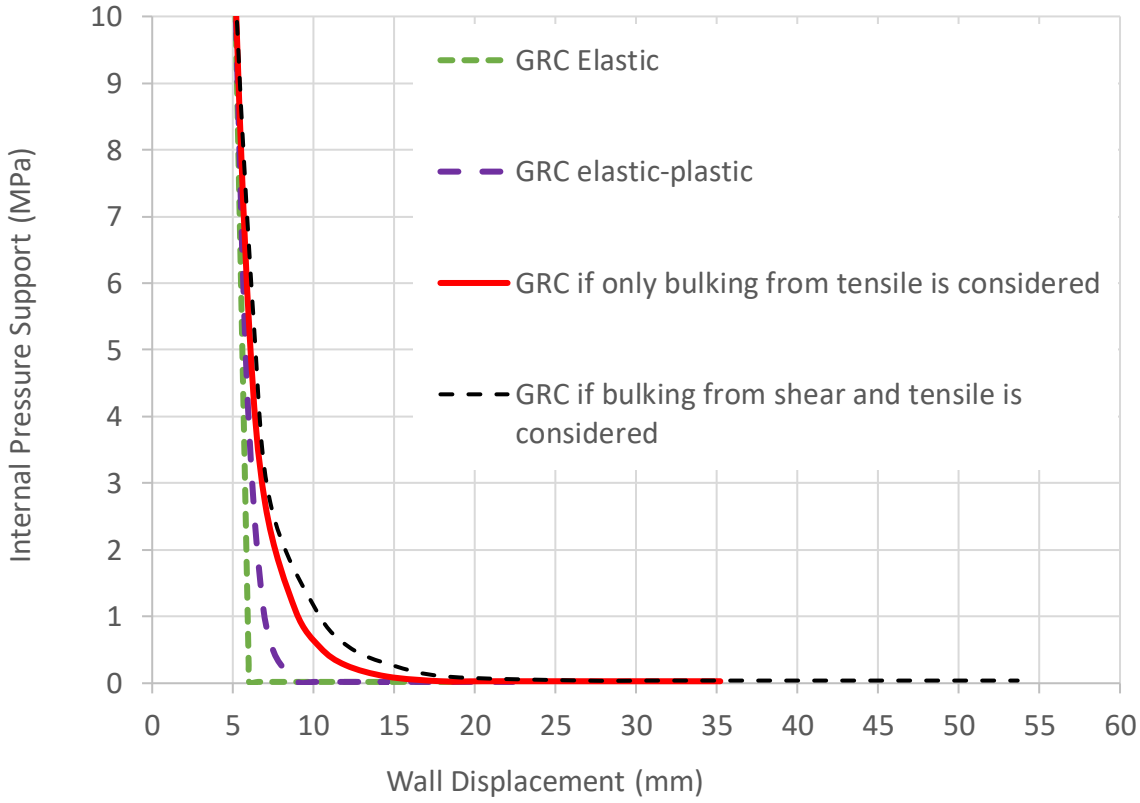


*Figure 3-54 GRCs after mining-induced stress change (from ko = 1 to 0.6) with deformation from bulking incorporated.*

### 3.8.1.2 Analysis of the roof of the excavation

The confinement stress redistribution for the roof is presented in Figure 3-55.

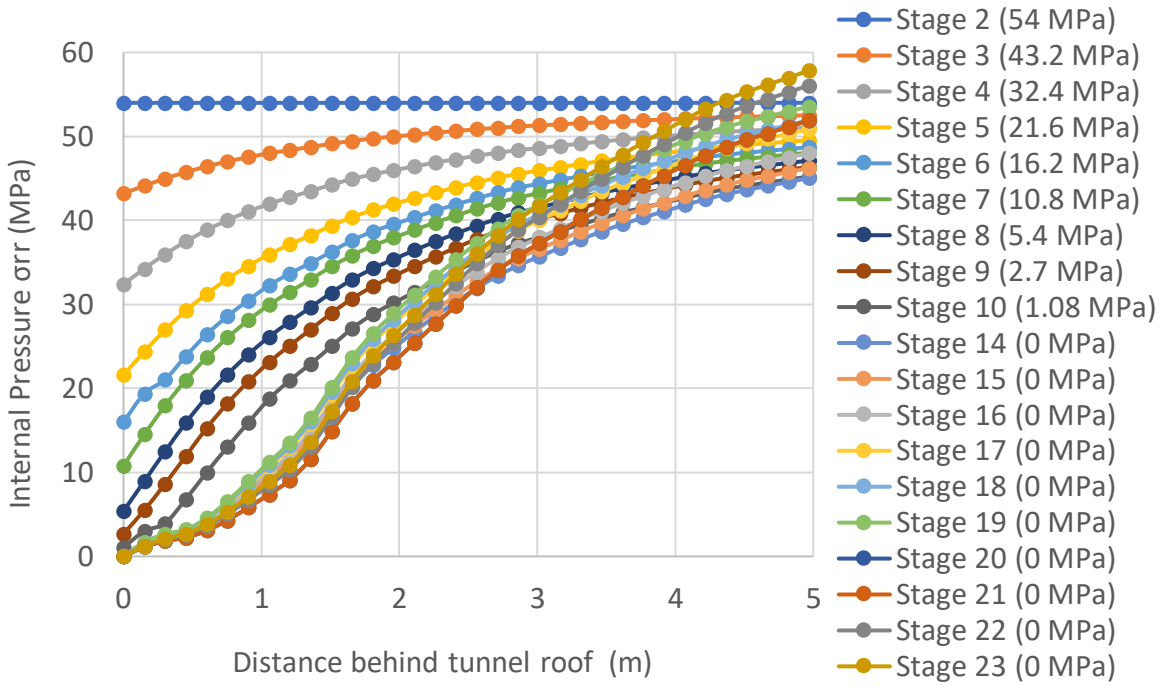


*(a)*

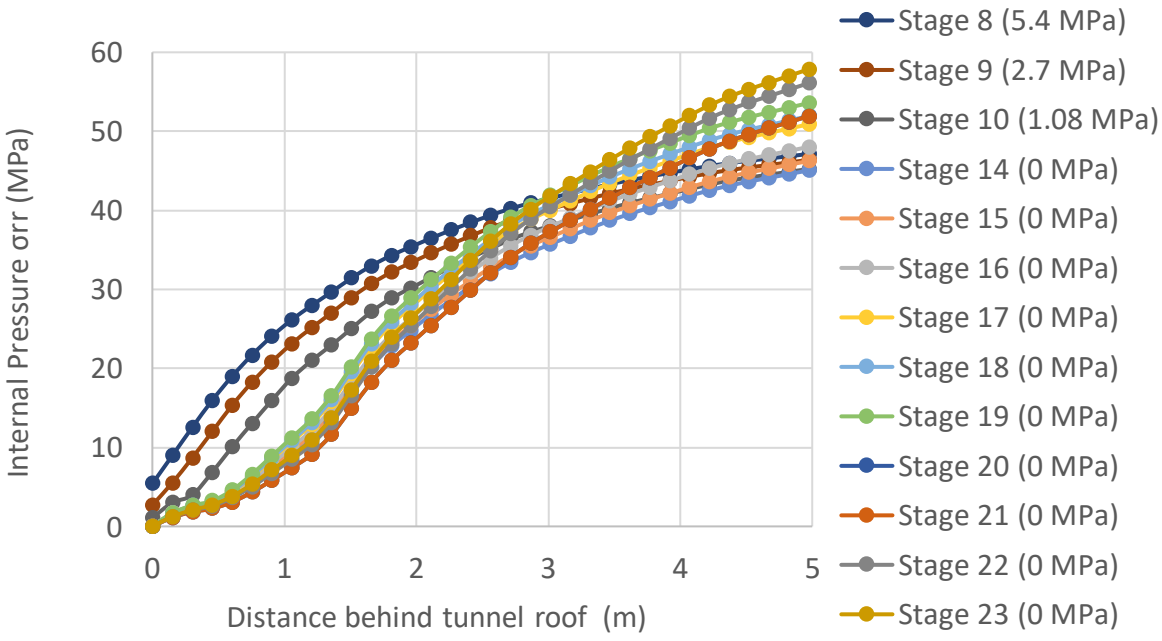


*(b)*

*Figure 3-55 (a) Distribution of confinement 23 stage; and (b) close-up for stages after plasticity began.*

The bulking profiles are presented for Stages 8 to 13 (pre-loading) and for Stages 14 to 22 (during loading) in Figure 3-56.

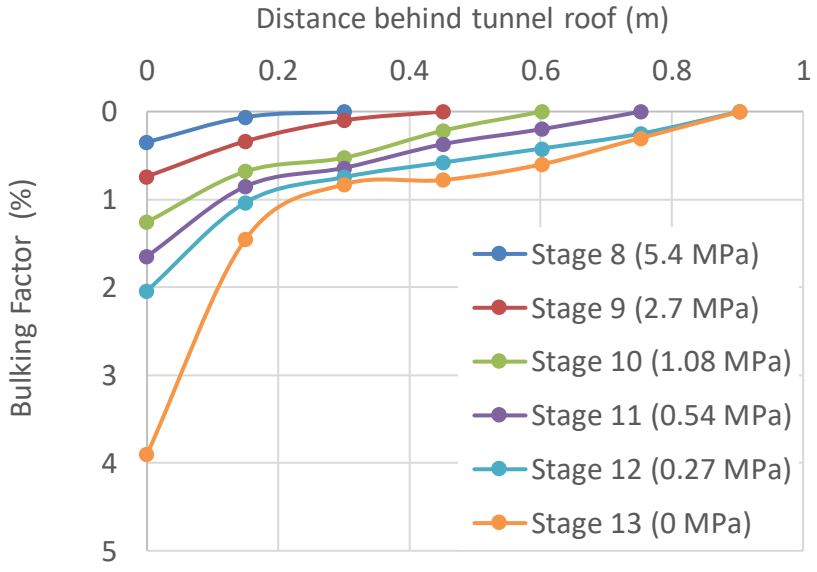


*(a)*

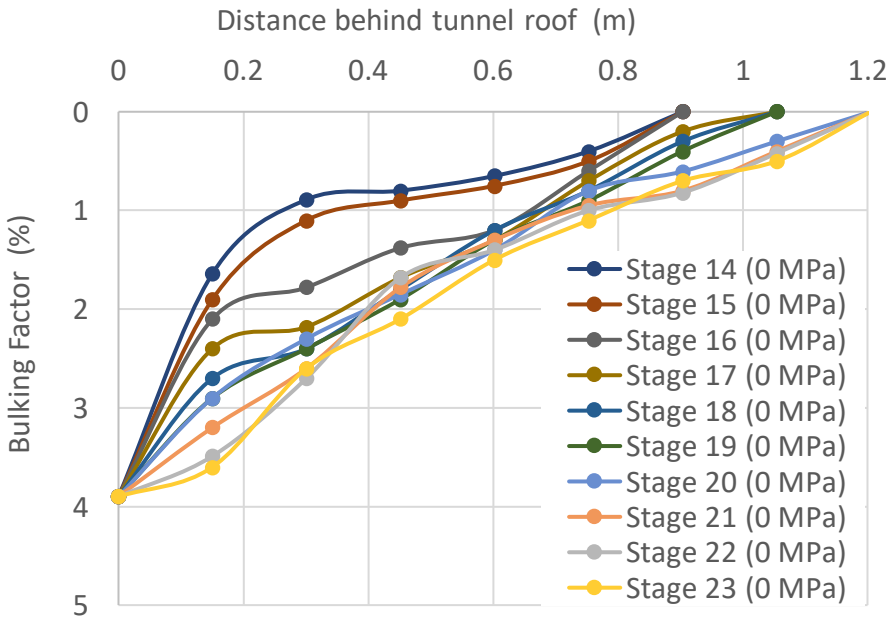


*(b)*

*Figure 3-56 Evolution of bulking (a) during tunnel development and (b) during mining-induced stress change.*

The bulking profiles for the tensile and the combined shear and tensile rupture case are shown in Figure 3-57.

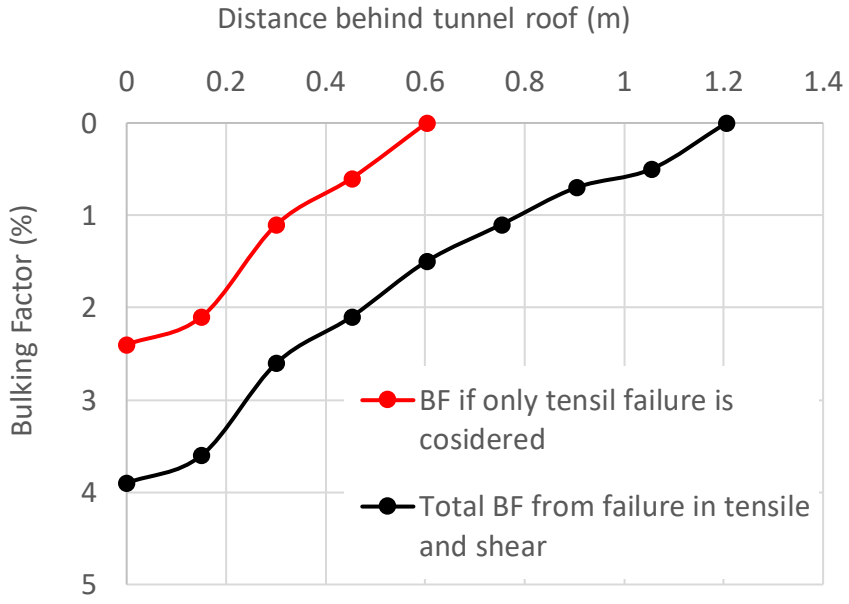


*Figure 3-57 Bulking profiles for each failure mechanism.*

The corresponding displacement graphs are presented in Figure 3-58.

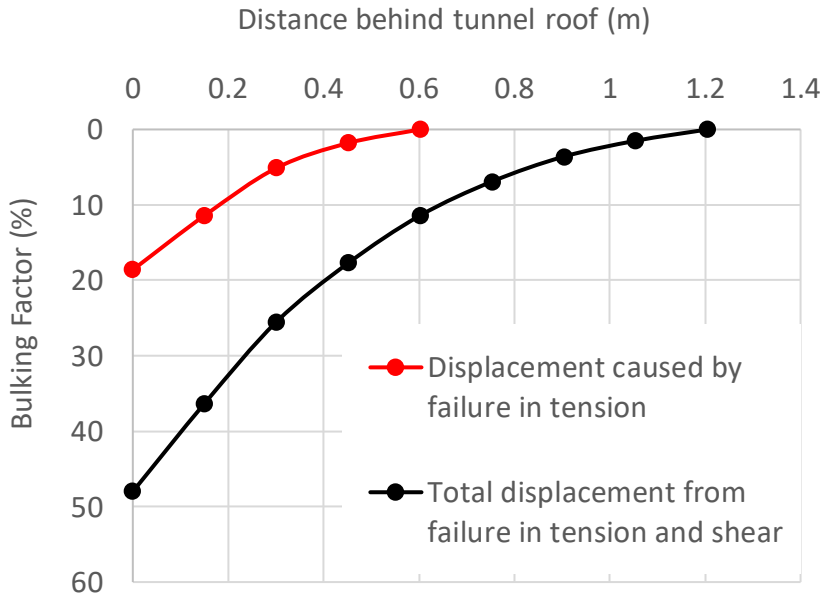


*Figure 3-58 Displacement from bulking of the rock mass when tunnel fails in tension and shear.*

In total, the roof will be experiencing an increment of bulking displacement between 18 and 48 mm and this displacement is superimposed to obtain the GRCs in Figure 3-59.

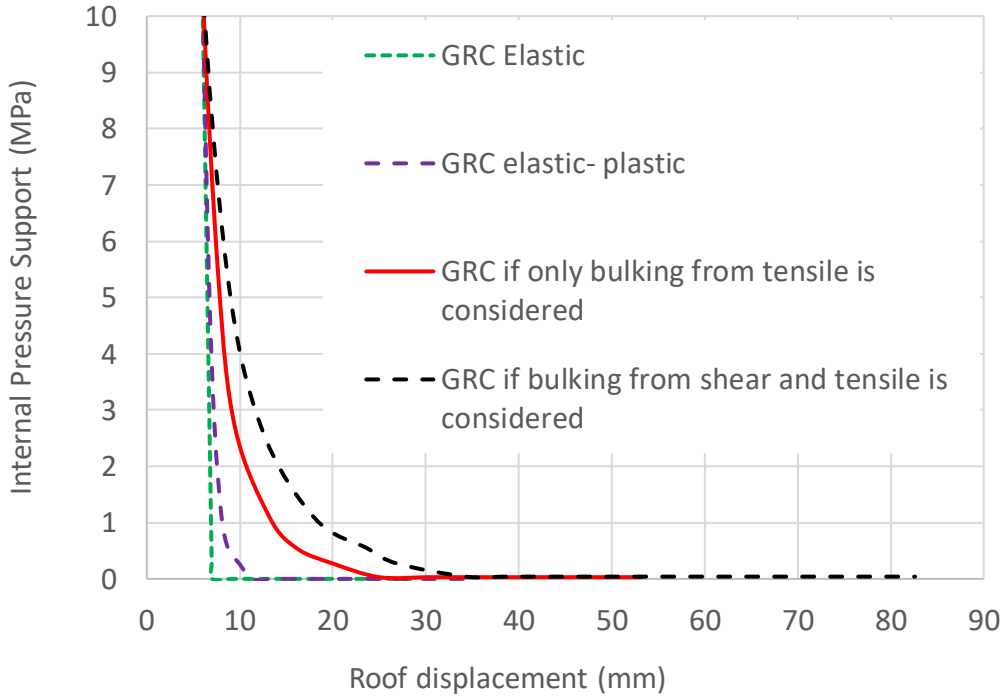


*Figure 3-59 GRCs at roof tunnel with deformation from bulking incorporated after mining-induced stress change from ko=1 to 0.6; tunnel excavated at 2000 m depth.*

The bulking deformation due to loading is reflected in the horizontal leg of the GRC at zero internal pressure.

### *3.8.2 Tunnel in Elastic-Brittle Rock*

For the excavation modeled in this type of rock a slightly greater depth of failure is observed but the overall patterns are similar. Hence, only the resulting displacement profiles and GRCs are presented here.

The displacements are presented in Figure 3-60 and the GRCs in Figure 3-61.

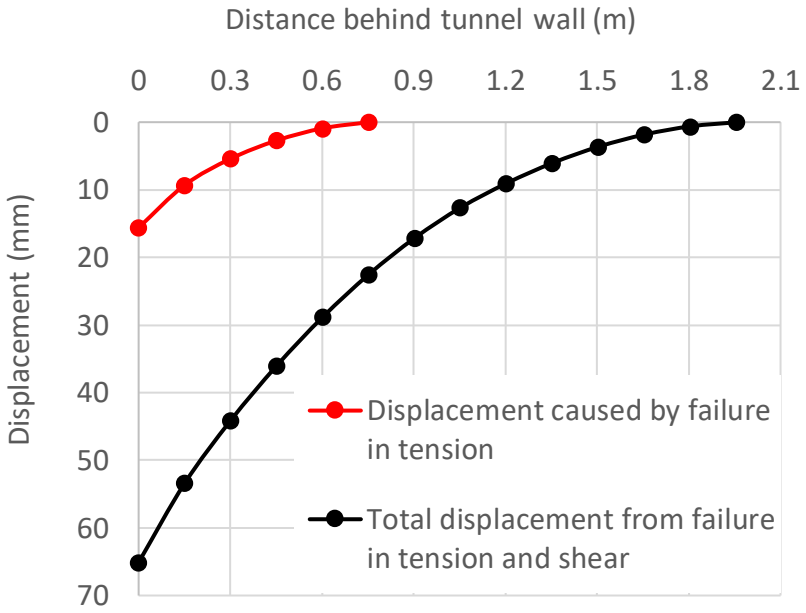


*Figure 3-60 Displacement from bulking of the rock mass when tunnel fails in tension and shear.*

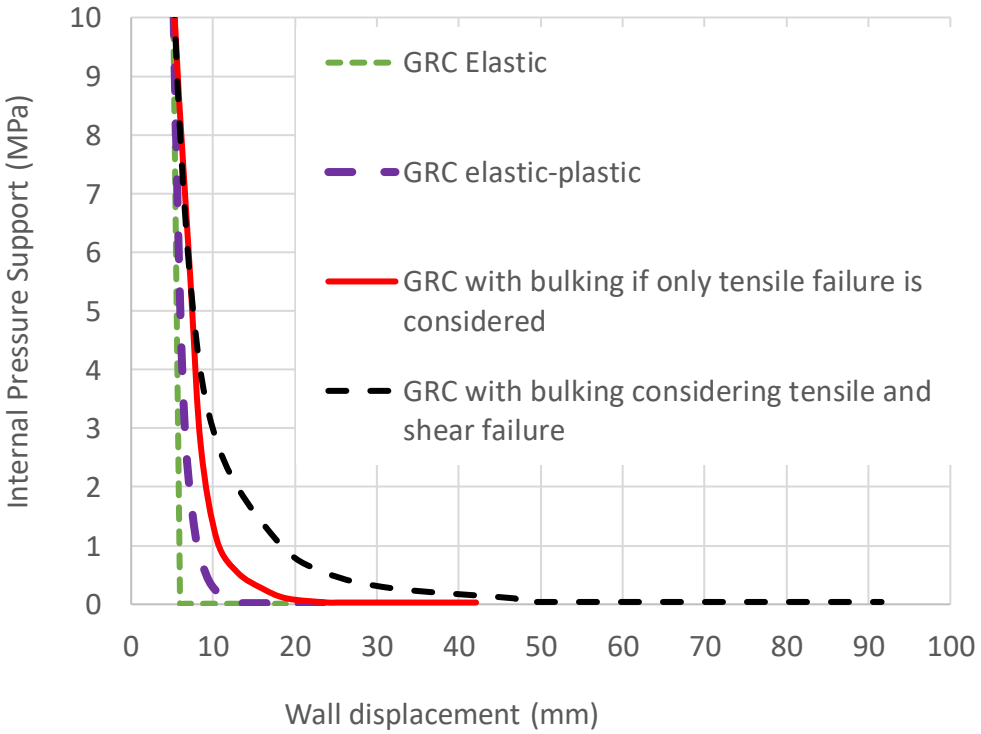


*Figure 3-61 GRCs with mining-induced stress from ko = 1 to 0.6 excavated at 2000 m depth with deformation from bulking incorporated.*

The tensile bulking is less pronounced for this material model, but the mining-induced bulking again causes a large bulking displacement at zero internal pressure. Almost 2 m of broken rock at the wall location produces 46 to 90 mm extra displacement.

For the roof, the displacement profiles are presented in Figure 3-62 and the corresponding GRCs in Figure 3-63.

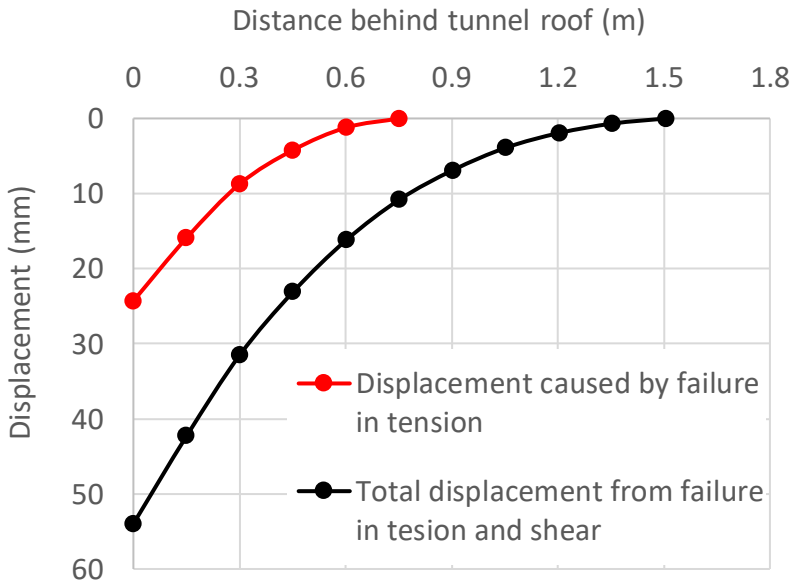


*Figure 3-62 Displacement from bulking for the roof when the tunnel fails in tension and shear.*

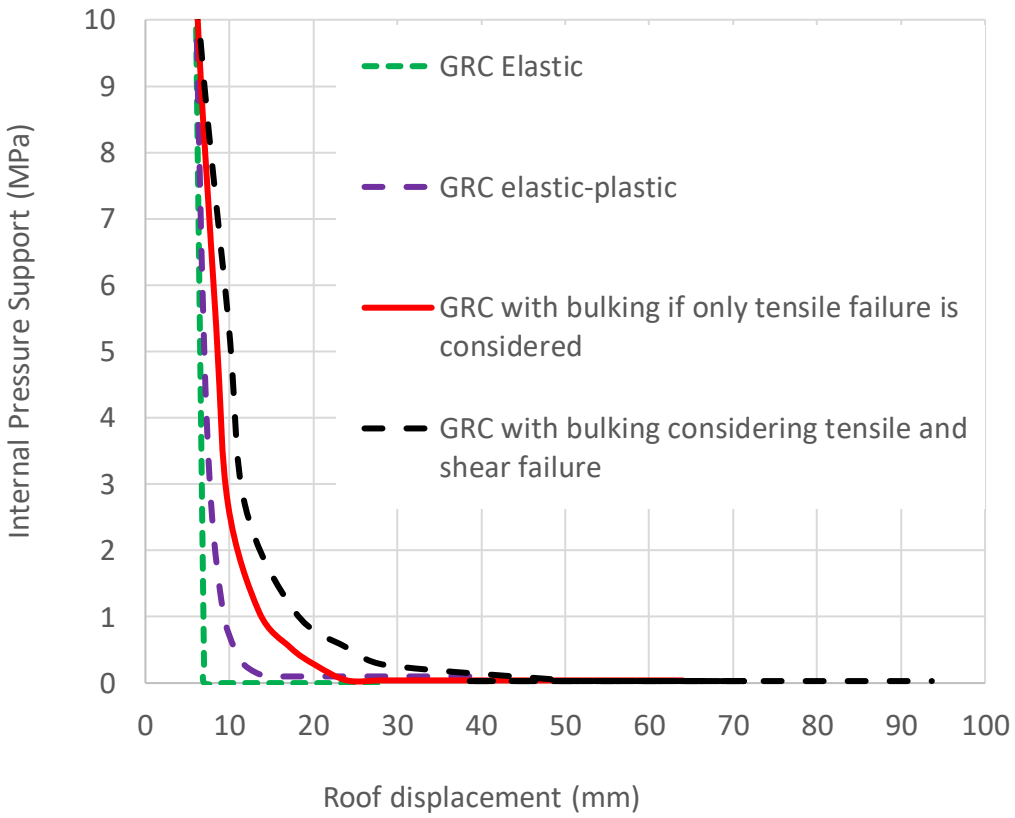


*Figure 3-63 GRCs for the roof due to excavation and mining-induced stress change from ko = 1 to 0.6 with deformation from bulking incorporated.*

The ultimate displacement including bulking are comparable for the roof and the wall due to the impact of bulking.

### *3.8.3 Tunnel in Brittle Rock (DISL Model)*

The DISL approach results in a deep damage zone as reflected in Figure 3-64. The depth of yield reaches almost 5 m at the walls and more than 3.5 m at roof.

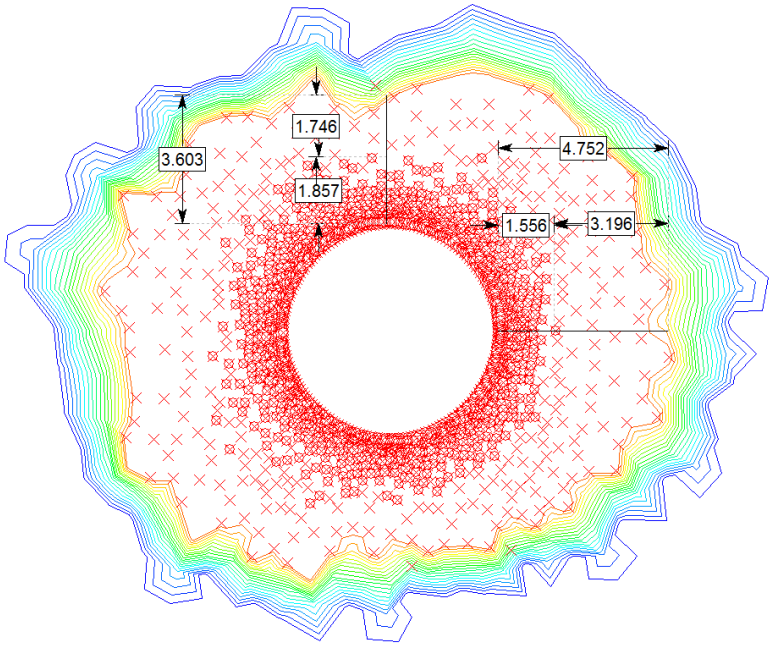


*Figure 3-64 Extent of the damaged zone around tunnel for tunnel in brittle rock (excavated at 2000 m depth with stress change from initial ko = 1 to ko = 0.6.*

### 3.8.3.1 Analysis of the wall of the excavation

Figure 3-65 shows the confinement distribution profile near the boundary of the excavation. The confinement again drops drastically at the last excavation stage and then changes only marginally during loading in the first 2 to 3 m from the walls.

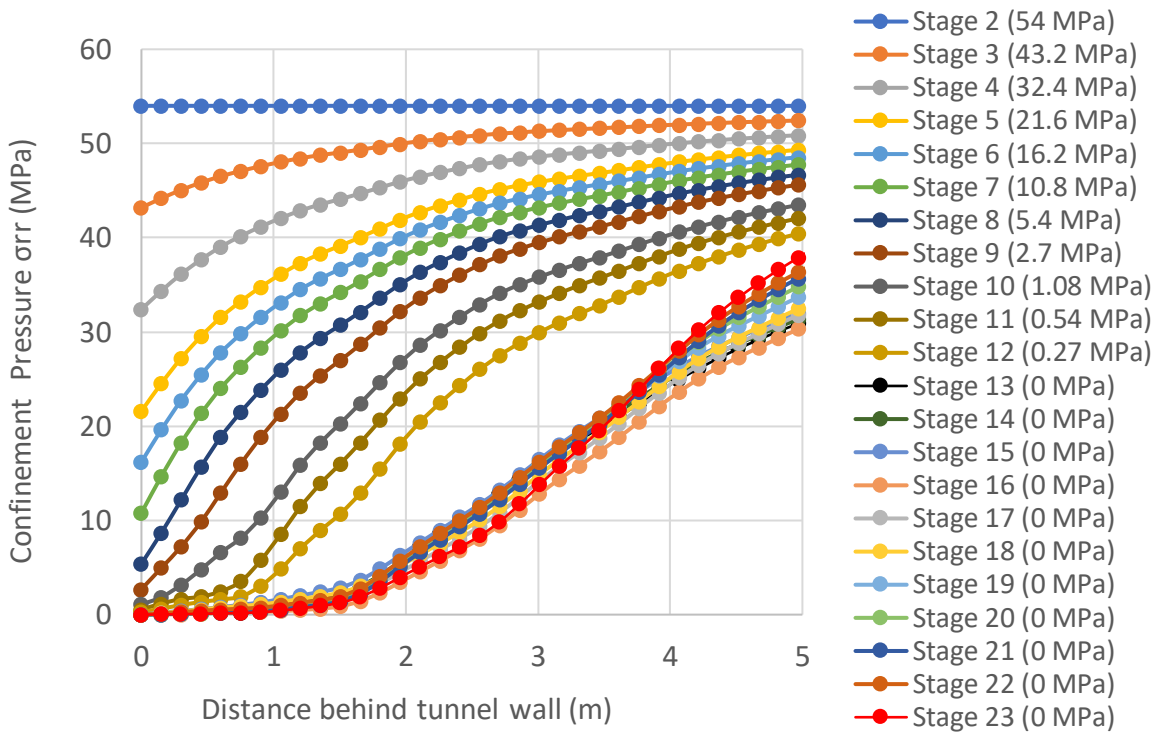


*(a)*

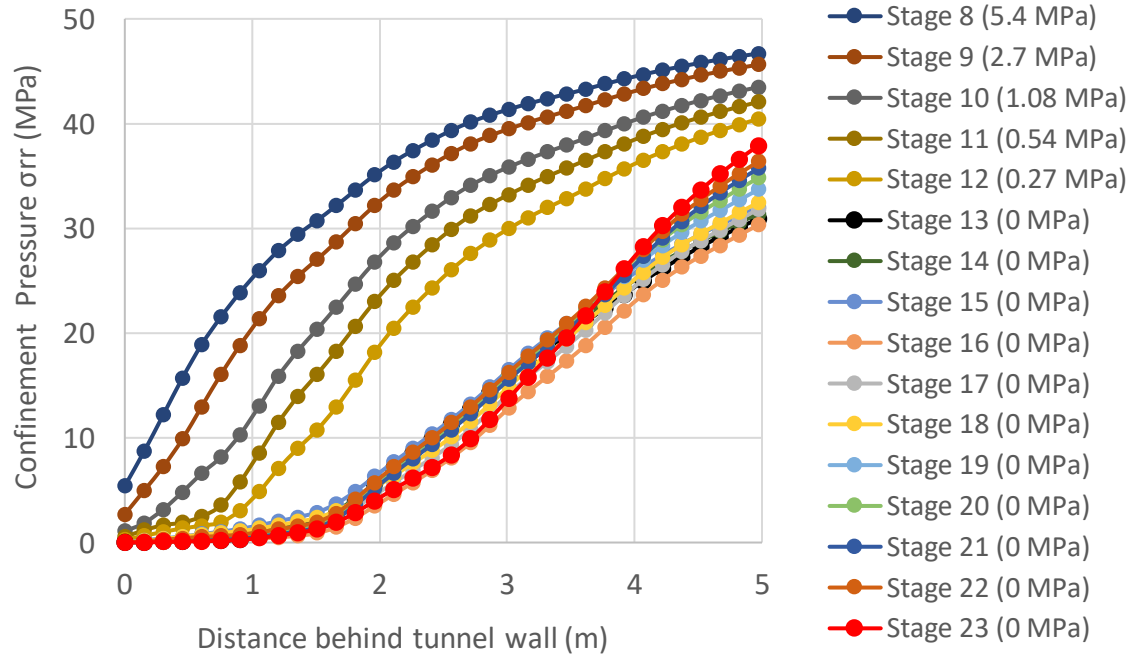


*(b)*

*Figure 3-65 (a) Distribution of confinement at wall in 23 stages; and, (b) close -up for with plasticity.*

The associated bulking patterns for the excavation and loading phase are presented in Figure 3-66 a and Figure 3-66 b.

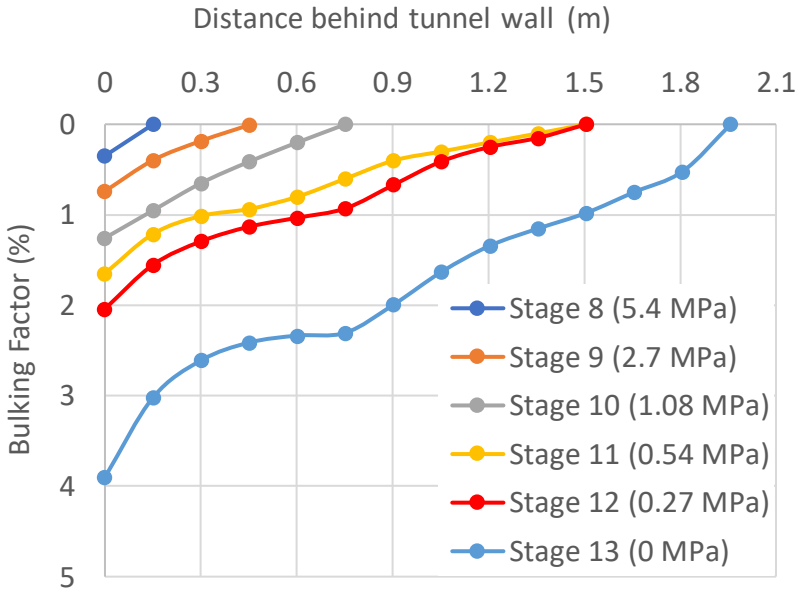


*(a)*

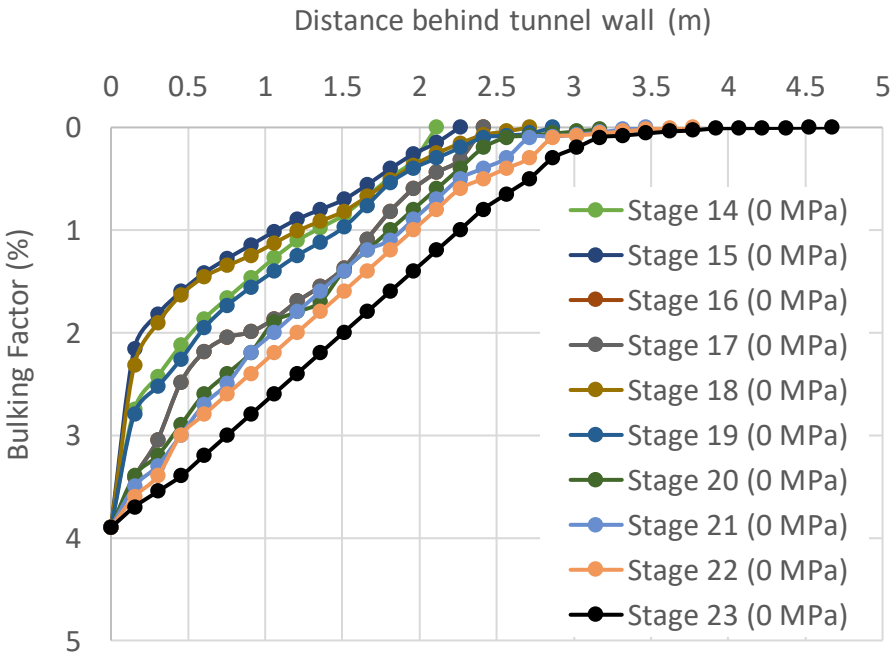


*(b)*

*Figure 3-66 Evolution of bulking for (a) tunnel development phase and (b) mining-induced stress change.*

The bulking profile of Figure 3-67 produces the displacement distributions of Figure 3-68.

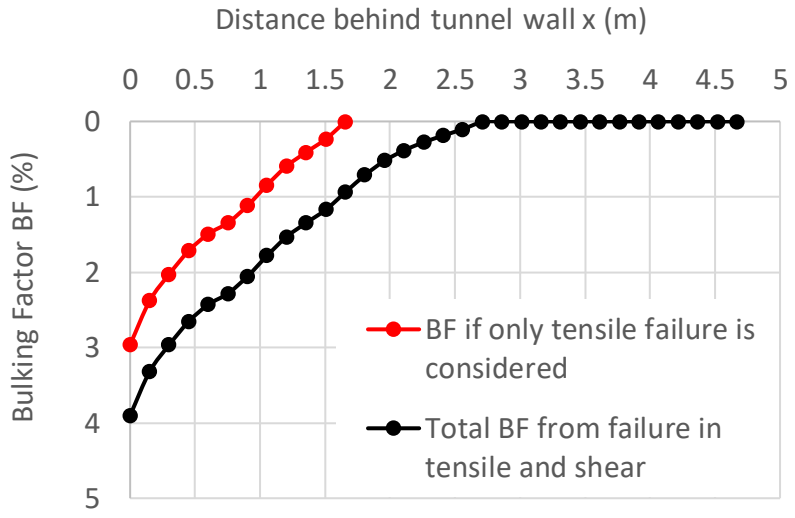


*Figure 3-67 Bulking profile by failure mechanism.*

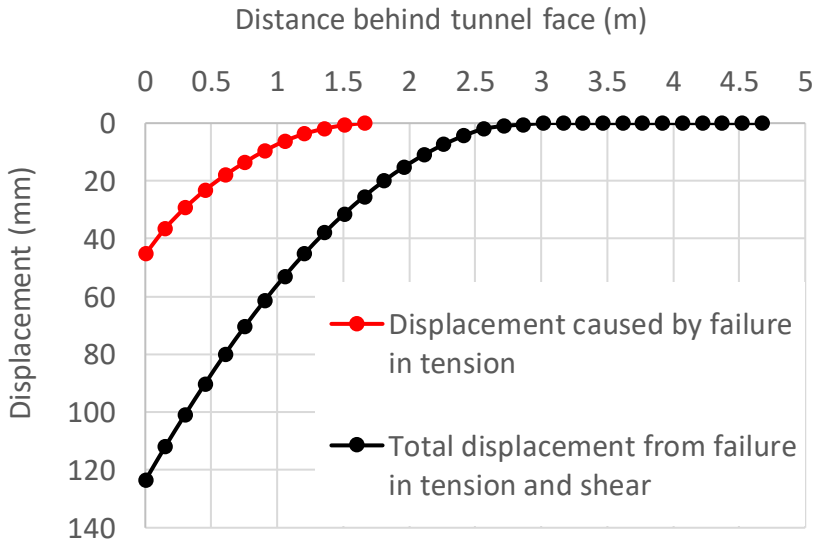


*Figure 3-68 Displacement from bulking of brittle rock mass when tunnel fails in tension and shear.*

It is observed increment of bulking displacement at the wall ranges from 41 and 115 mm. These extra deformations shift the GRC as illustrated by Figure 3-69.Again, the mining-induced loading

causes most of the bulking deformation.

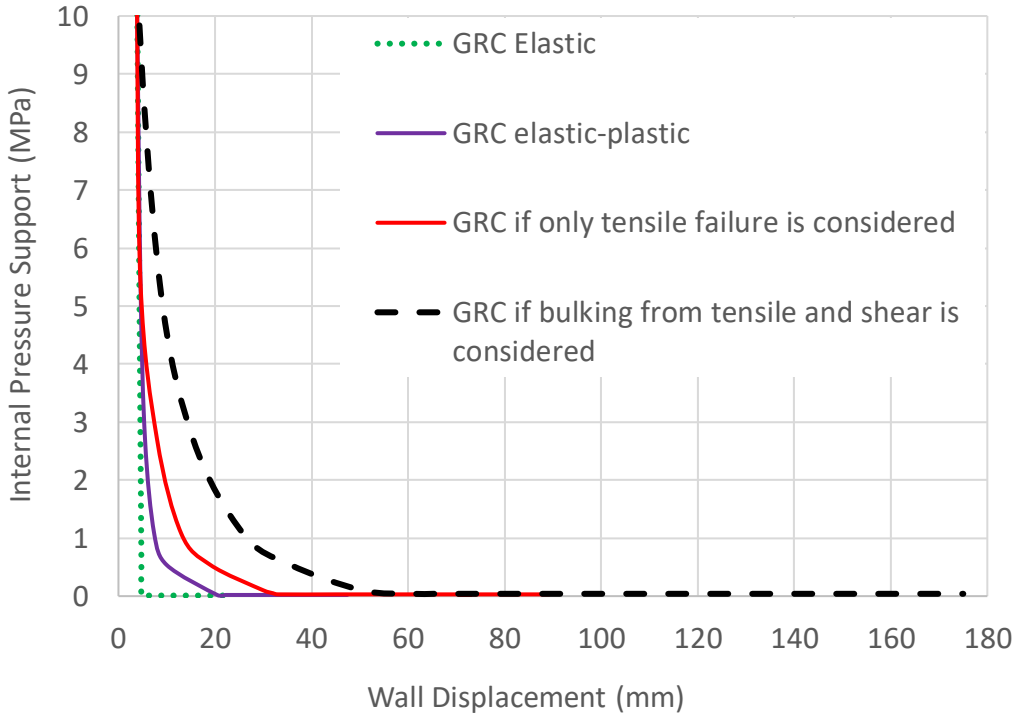


*Figure 3-69 GRCs at the wall of a tunnel in brittle rock with mining-induced stress change from ko = 1 to 0.6 with deformation from bulking incorporated.*

### 3.8.3.2 Analysis of the roof of the excavation

As expected, the analysis of the roof produces similar trends and only the displacement profiles and GRCs are reproduced here. Figure 3-70 presents the displacement profiles and Figure 3-71 the GRCs.

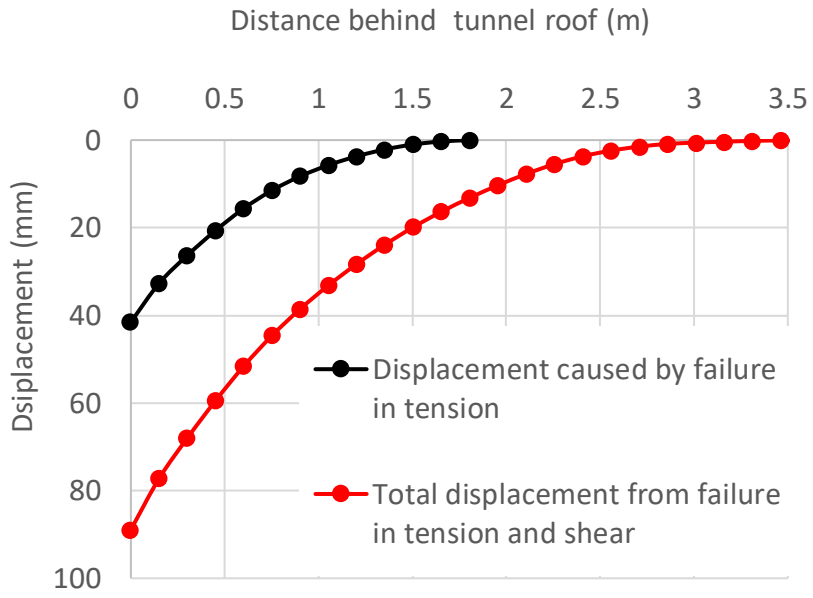


*Figure 3-70 Displacement from bulking of the rock mass tunnel fails in tension and shear.*

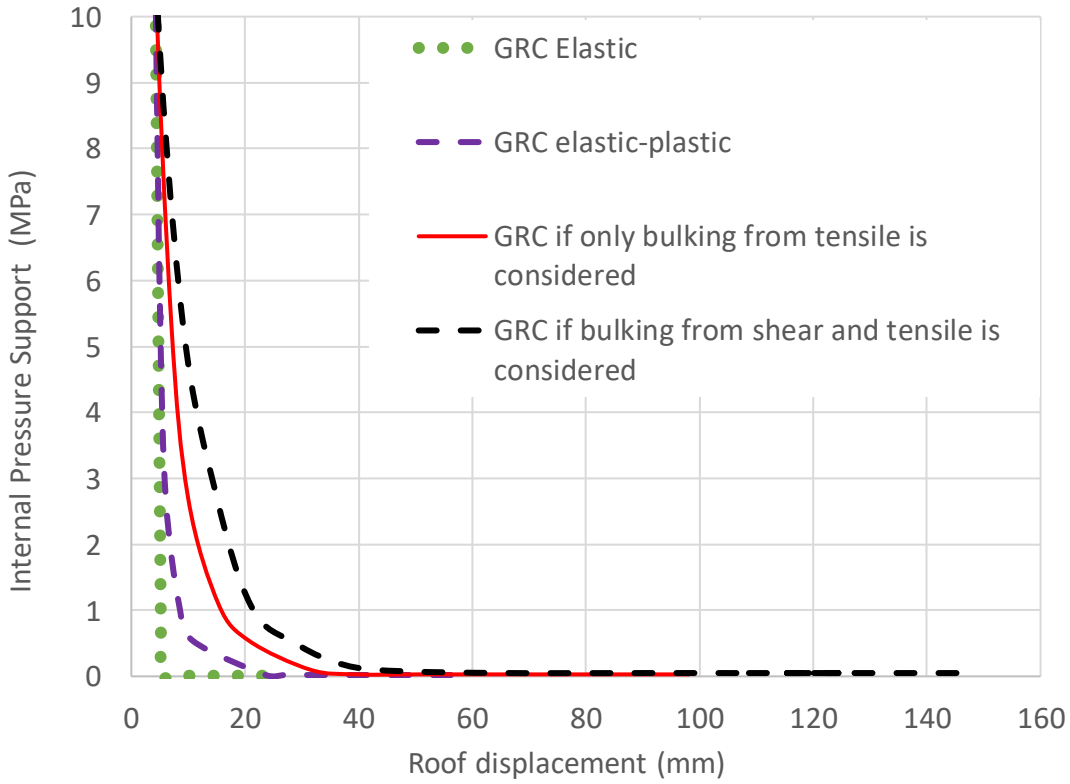


*Figure 3-71 GRCs at roof of tunnel in brittle rock with mining induced stress from ko = 1 to 0.6 excavated at 2000 m depth with deformation from bulking incorporated.*

## 3.9 Interpretation of Model Results

The modelling results presented in the previous section are consolidated here such that it is possible to compare and better understand the impact of rock mass bulking on tunnel displacements and as a consequence on the ground reaction curves.

After the displacement amounts for various tunnels, stress states, and ground conditions presented in previous sections have been calculated, it is now necessary to compare and establish what was the contribution of the rock mass bulking in that displacement.

For this reason, in this current section, the effect of rock mass bulking is analyzed such that when designing or selecting a support system, decisions should be made based on displacement demands. As it has been stated before in this thesis, bulking of a rock mass depends on the confinement level ($\sigma_3$ or $\sigma_{rr}$). This is to say, that for understanding bulking, it is critically important to first understand how $\sigma_3$ is distributed and how this distribution affects the amount of bulking.

Confinement level will depend on: (1) the type of rock mass and (2) the stress path that the excavation experiences. In order to explain the influence that these two characteristics have on the convergence, the same tunnel was modelled in different materials and following different stress path.

These tunnels, analyzed here, are circular with a radius of 3 m and excavated at 2000 m depth. In the first part of the analysis, the tunnel is modelled in three different materials (elastic-plastic, elastic-brittle and brittle material respectively). In the second part, the same tunnel, now excavated, is subjected to different stress path, with the idea to examine which is more or less favorable for the excavation, in terms of convergence magnitude.

The stress states chosen are $k_o = 1$ and $k_o = 0.5$, as well as a stress path with a transition from $k_o = 1$ to $k = 0.6$ (tunnel loaded by vertical mining stresses).

### *3.9.1 Dependence Between Rock Mass Bulking and Material Properties*

In previous section 3.4.2. of this chapter, was commented in more detail how the material properties for each case were chosen. The following Table 3-3 summarizes the three chosen material models and their respective peak (p) and residual (r) material properties.

*Table 3-3 Summary of material properties used to model the tunnel case study*

| **Material modelled Approach** | **(1) Elastic-Plastic $GSI_p = GSI_r = 65$** | **(2) Elastic-Brittle $GSI_p = 65$, $GSI_r = 55$** | **(3) Brittle DISL** |
|---|---|---|---|
| $m_p$ | 5.73 | 5.73 | 1 |
| $s_p$ | 0.02 | 0.02 | 0.0033 |
| $a_p$ | 0.501 | 0.501 | 0.25 |
| $m_r$ | 5.73 | 4.009 | 7 |
| $s_r$ | 0.02 | 0.067 | 0.000001 |
| $a_r$ | 0.501 | 0.504 | 0.75 |

In the next Figure 3-72, it can be appreciated how the depths of failure differ. The brittle material (3) shows the greatest lateral damage extent.

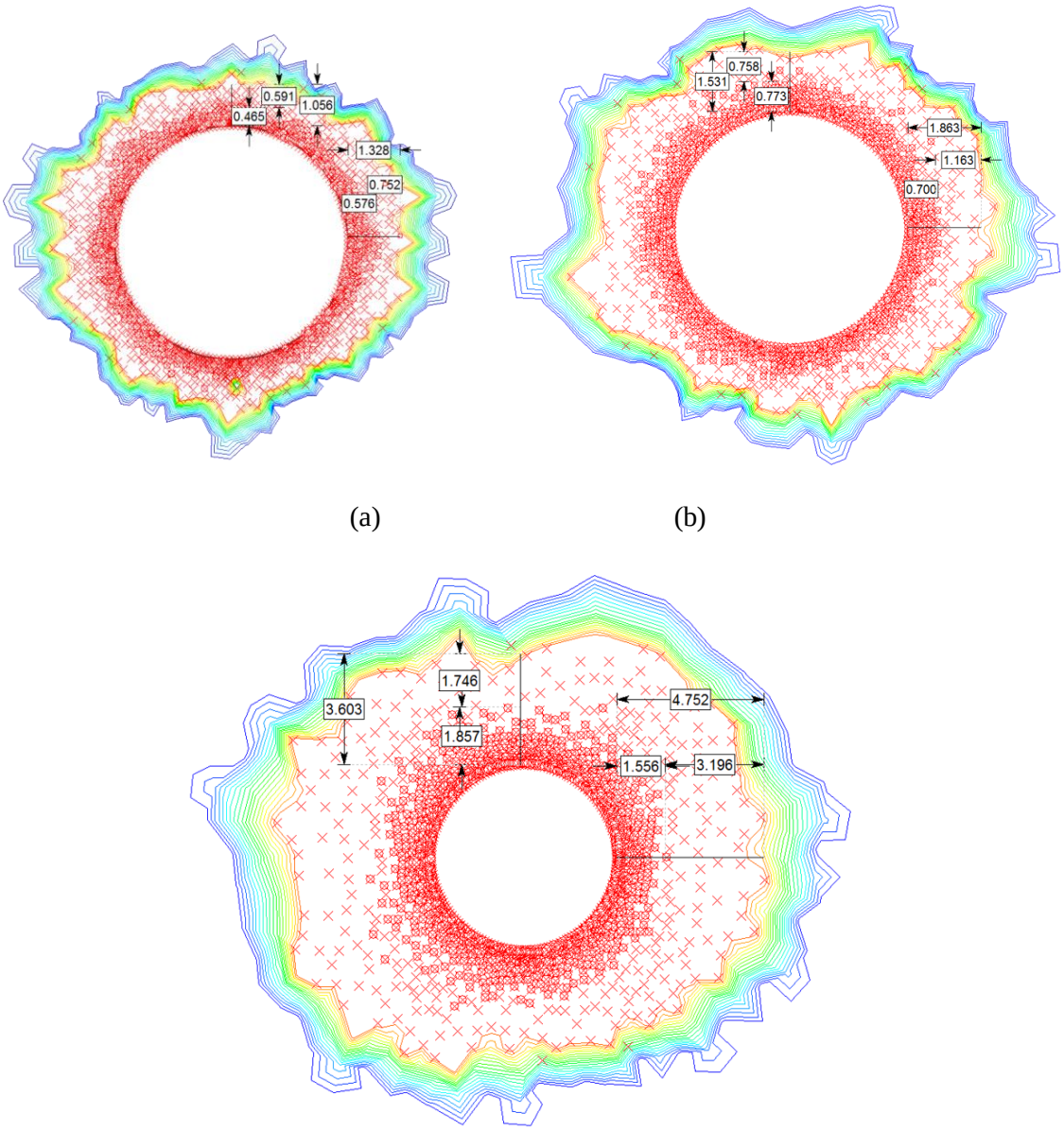


(a) (b)

*(c)*

*Figure 3-72 Extent of the damaged zone for tunnel modeled in three material types: (a) elastic-perfectly plastic, (b) elastic-brittle, and (c) brittle material.*

The reason why the extent of the depth of failure is different in each case is because of how the stress ($\sigma_3$) distributes depending on the material or rock type. To exemplify this, the following Figure 3-73, shows the confinement distribution profile for these three materials:

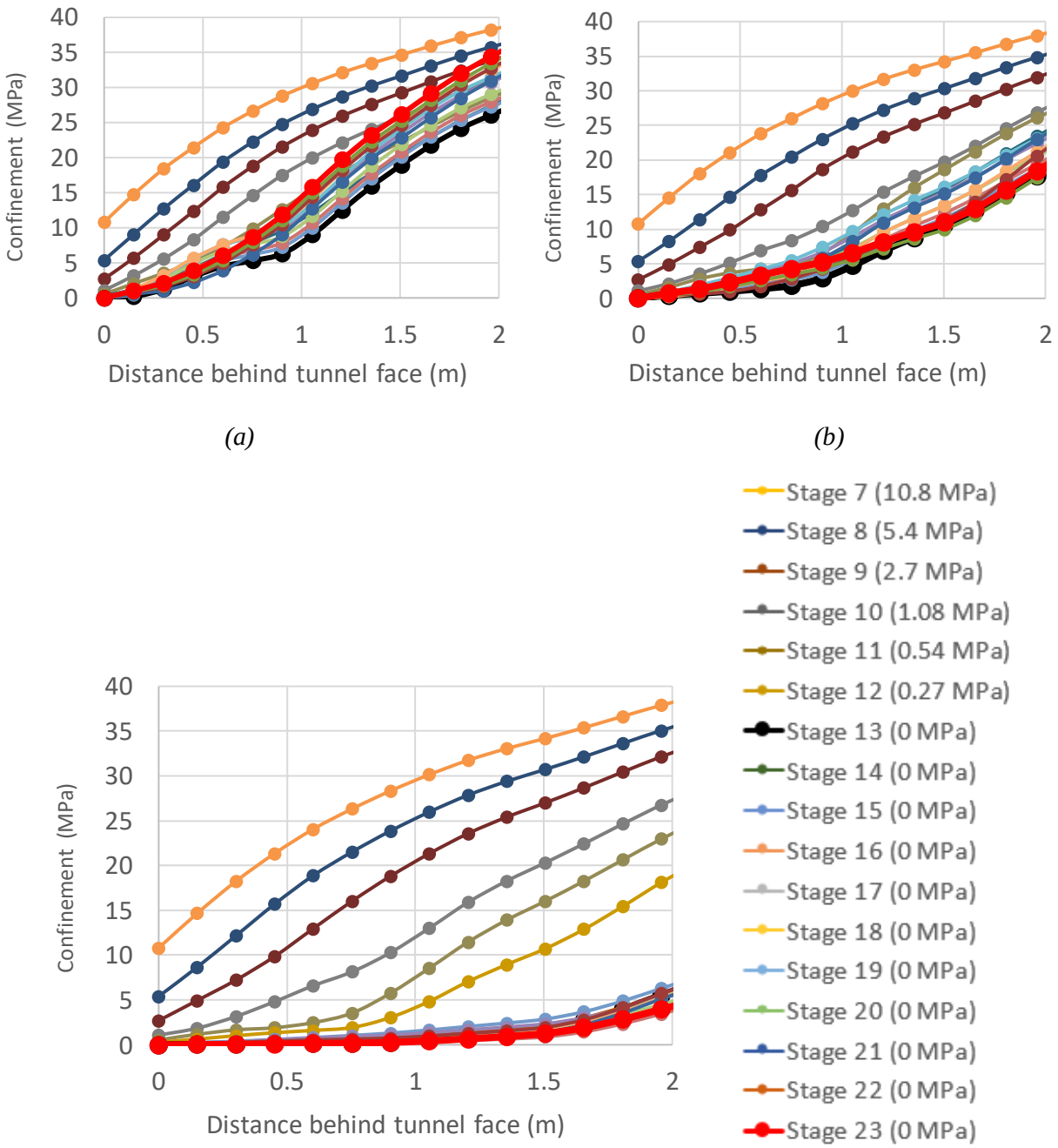


*Figure 3-73 Distribution of confinement near the tunnel face for three material models: (a) elastic-perfectly plastic, (b) elastic-brittle, and (c) brittle material.*

The confinement near boundary rapidly increases (e.g., to 5 MPa at 0.75 m) for the elastic-plastic

material and for the elastic-brittle plastic material (5 MPa at 1 m). For the tunnel in the brittle material the confinement profile is flat and only reaches 5 MPa at 2 m. This means, that when calculating the rock mas bulking as the logarithmic function of confinement (indirect relationship, as shown in Figure 3-74), the material with the lower confinement (brittle) will experience a larger amount of bulking. As it is seen the maximum bulking amount applied to the excavations is 4%, as a result of the parameter a=b=1.3 chosen (characteristic of a single advance tunnel under small strain) and that relate with bulking by BF=a-b*log ($p_s$) as per Kaiser (2016).

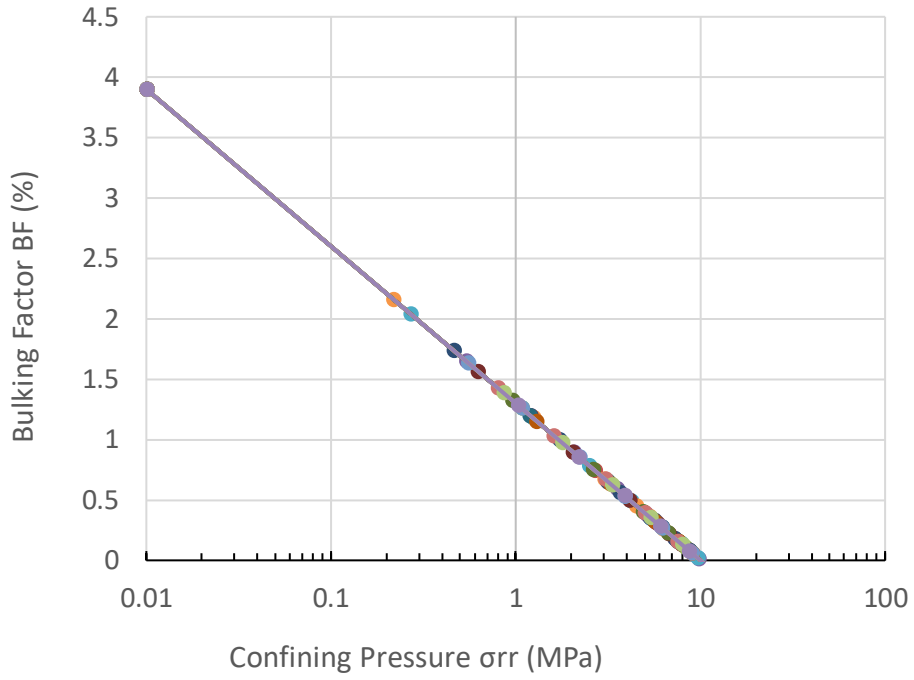


*Figure 3-74 Logarithmic relationship between confinement and bulking factor used for the case studied (with parameter a= 1.3 and b=1.3 applicable for small tangential strains).*

By use of this empirical bulking model the bulking factor distribution and associated displacement for each failure mechanism of the tunnel was calculated and the result are graphically shown in Figure 3-75.

The reasons for providing separated calculations of bulking and displacement for tensile failure and tensile and shear failure were discussed in section 3.3. The bulking distribution for the three different materials with these two differentiate failure mechanisms are plotted in Figure 3-75.

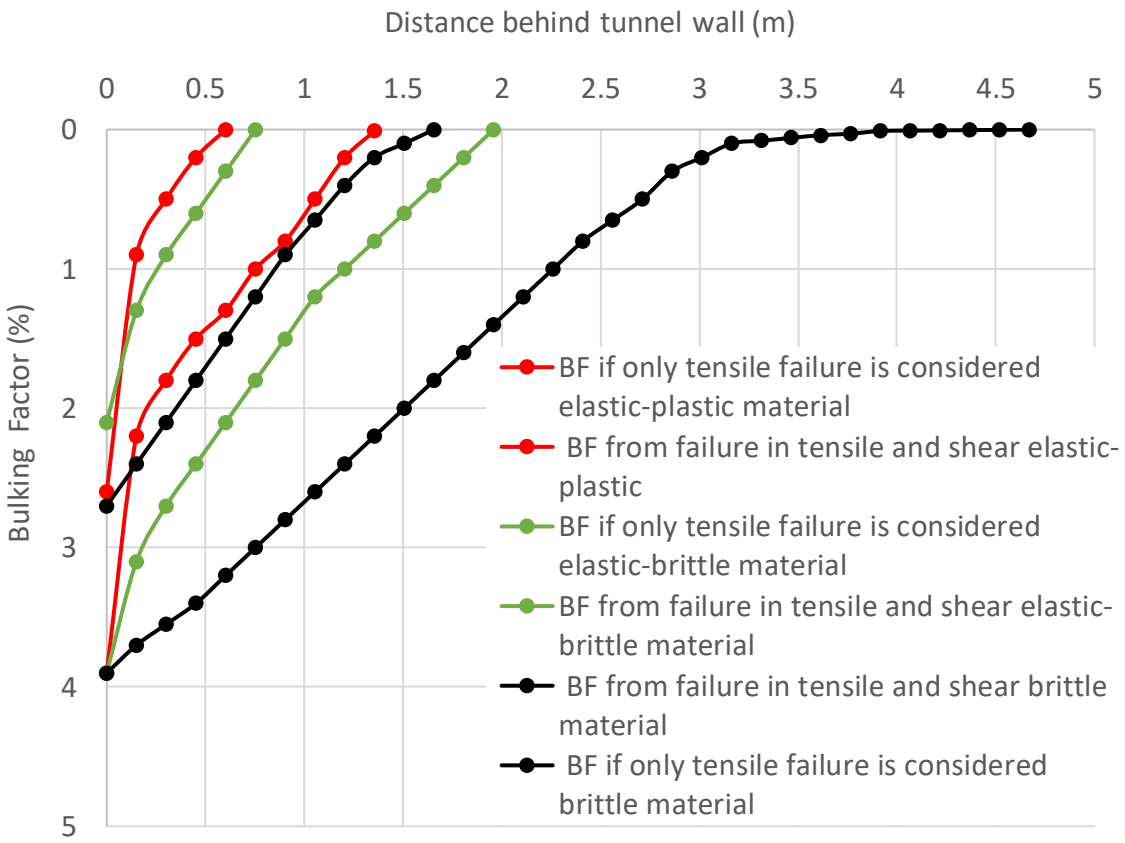


*Figure 3-75 Bulking distribution of three materials for tensile failure only, and for tensile and shear.*

This figure shows that extent of damage as well as the bulking factor increases for the three models. The corresponding displacement from bulking is obtained by incremental summation and is presented in Figure 3-76.

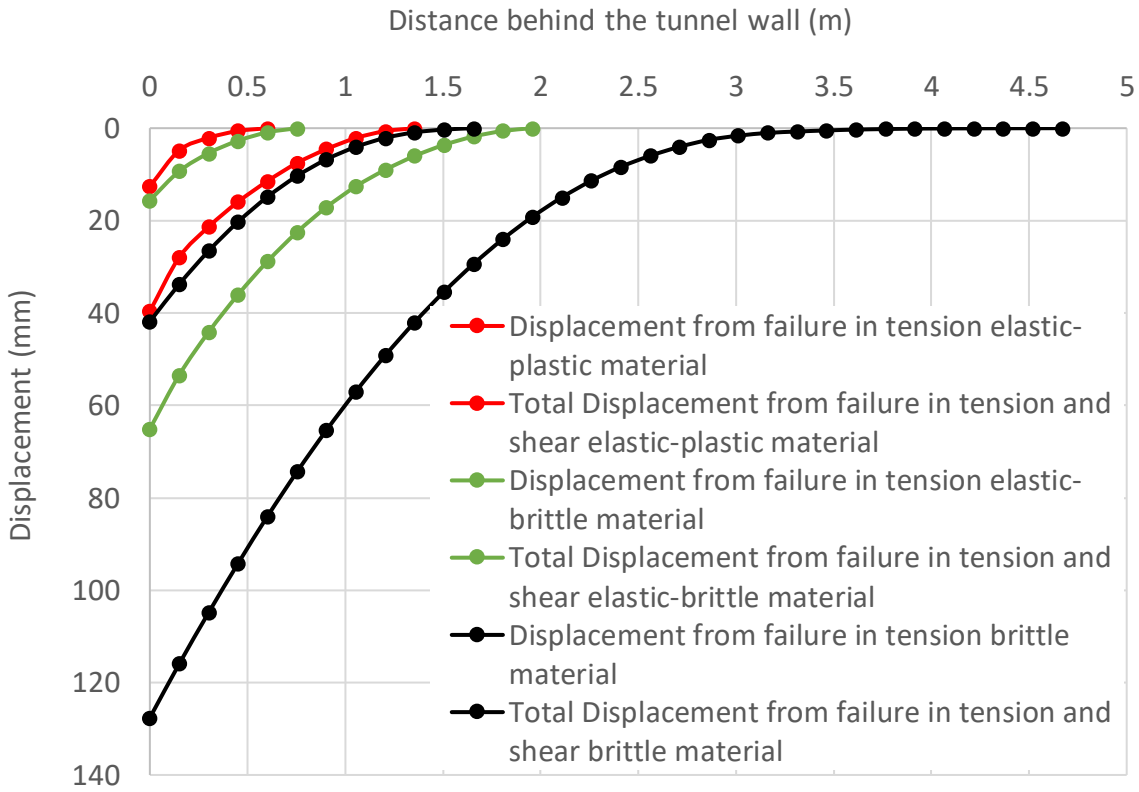


*Figure 3-76 Bulking displacement profiles for tensile only, and tensile and shear for three materials.*

These figures highlight the great difference between bulking displacements generated in the extension zone and in the entire zone experiencing tensile and shear failure. The reality likely falls in between.

In order to provide a better idea of the difference in results obtained from the numerical model (Phase2) and the semi-empirical results here calculated, the following Table 3-4 is provided.

*Table 3-4 Results of displacement from the numerical solution and from calculations for three material types*

| Material | Maximum displacement (mm) without bulking | Bulking displacement (mm) in tensile zone alone | Bulking displacement (mm) in tensile and shear zone |
|---|---|---|---|
| **Elastic plastic** | 22 | 13 | 40 |
| **Elastic Brittle** | 27 | 16 | 65 |
| **Brittle** | 45 | 42 | 128 |

This table highlights the great differences between the two solutions and the three materials. It follows that tunnels excavated in very brittle materials will exhibit much larger convergences than if excavated in the ductile of less brittle materials. The corresponding GRCs for the three excavations, incorporating to the elastic-plastic displacements obtained in the numerical model the displacements from bulking, from the two failure mechanisms, are plotted in Figure 3-77.

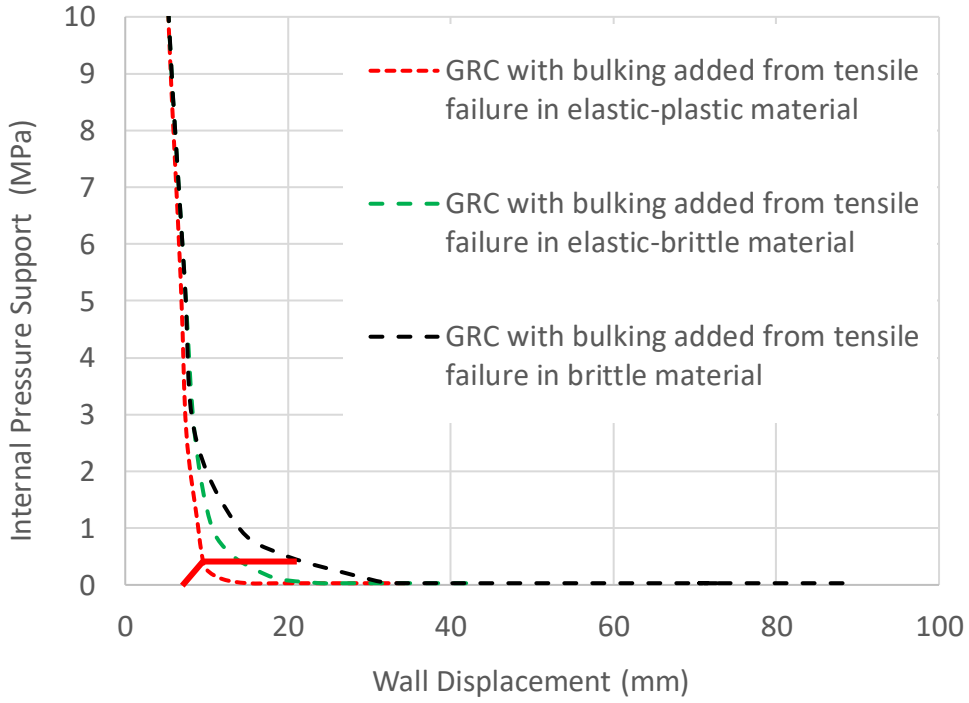


*Figure 3-77 GRC for the three materials, incorporating bulking of the rock mass from failure in tension only.*

The displacements with tensile and shear are plotted in Figure 3-78. It is evident and expected based on the previously listed results that the GRCs for this case is shifted to the right. The reason for presenting both analyses or scenarios is to give a range of what is to be expected.

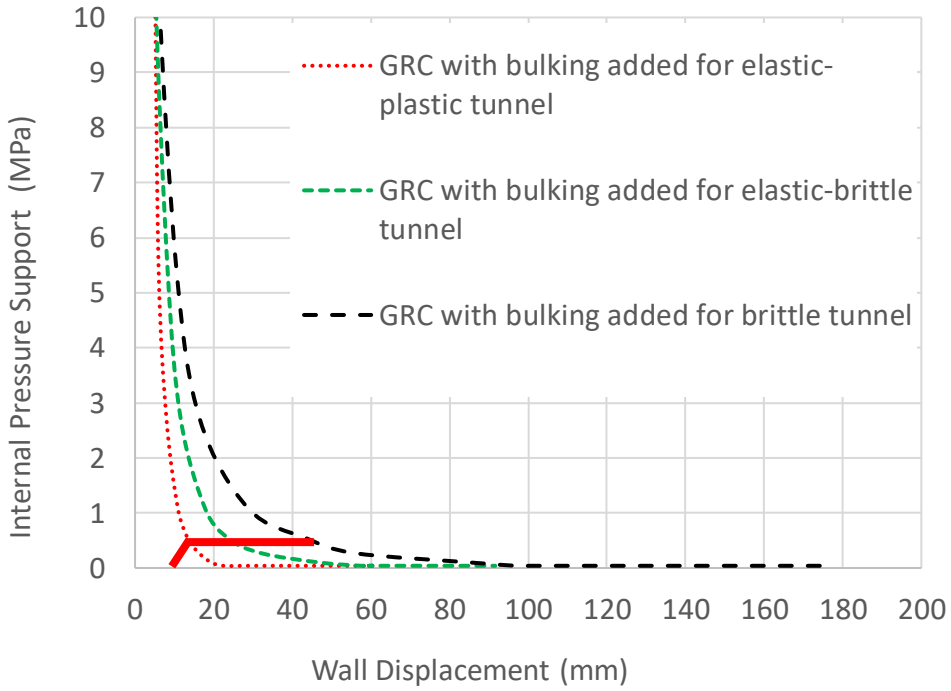


*Figure 3-78 GRCs for three materials with bulking in tension and shear.*

The red line in the graphics represents a fictitious support with a support capacity of 0.5 MPa (see later for comments on support capacities and interactions).

In summary, it is seen how the brittle material offers much more bulking displacements with respect the other two types of materials. The reason for this was demonstrated as being related to the differences in the confinement distributions. Next, the influence of different stress scenarios is analyzed for the brittle material type.

### *3.9.2 Influence of the Stress-Path on Rock Mass Bulking*

Stress path here means, the stress level to which the tunnel is subjected. It is defined by the $k_o$ ratio, the relationship between horizontal stress and vertical stress. It is studied by excavating a tunnel in a brittle material at different stress level (following different stress paths).

First two different stress ratios have been considered: ko = 1 (uniform field stress) and ko = 0.5. The failure zone shapes are shown in Figure 3-79 a, b and c. These cases are then compared with a tunnel that was excavated at ko =1 but then was loaded vertically to simulate a cave mining load scenario. For the assumed stress magnitudes, the stress ratio consequently changed from $k_o = 1$ to k = 0.6. The corresponding failure extent profile is shown in Figure 3-79.

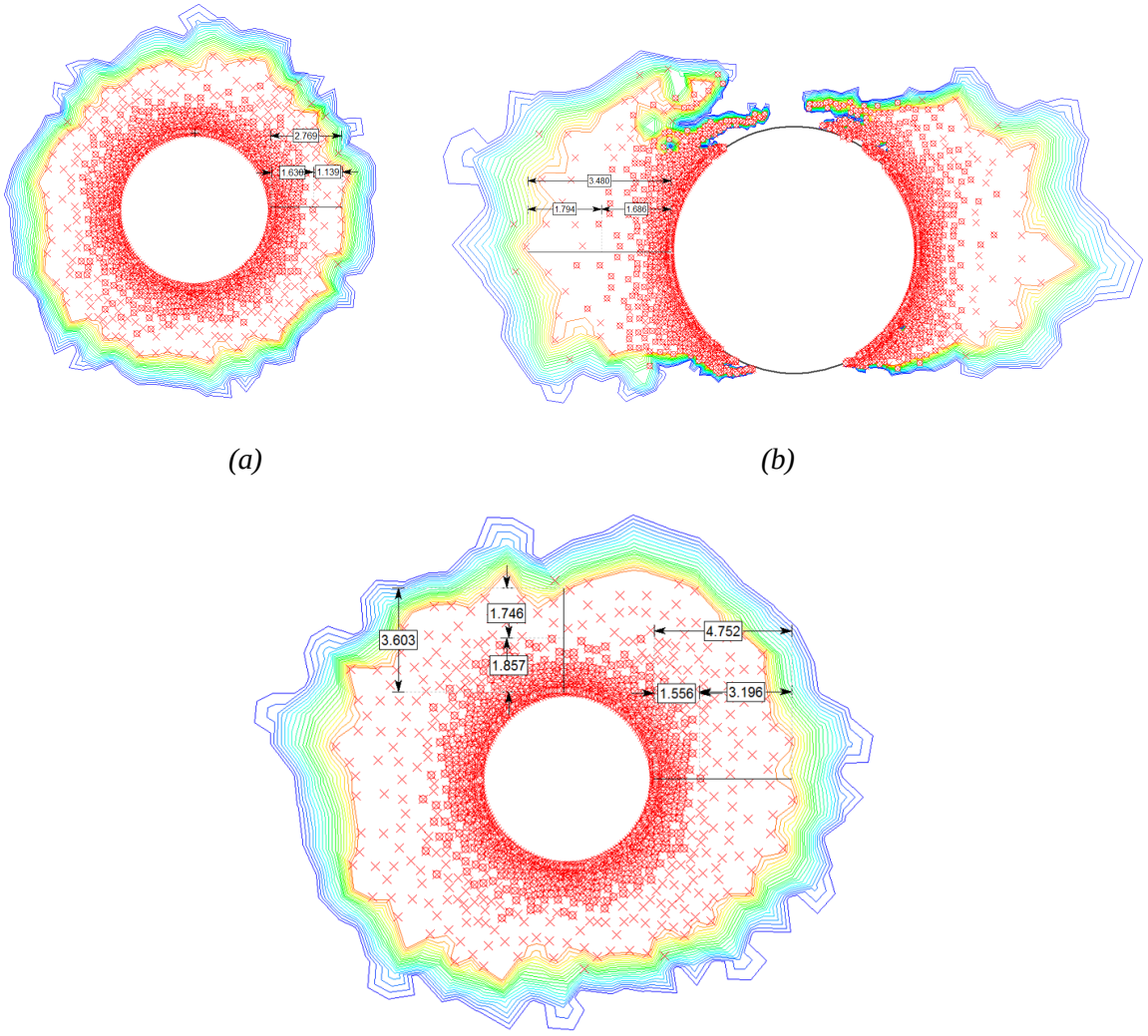


*(a)* *(b)*

*(c)*

*Figure 3-79 Representation of the shear and tensile failure for a tunnel in brittle rock under different stress states: (a): uniform field stress (ko = 1), (b): ko = 0.5, and (c): ko =1 changing to k=0.6 (mining induced stress field scenario).*

The different depth of failure zones causes different confining stress distributions around the excavation as presented in Figure 3-80. The tunnel excavated in the mining scenario presents a distinctly different confinement profile when compared to the other cases with ko = 1 and 0.5.

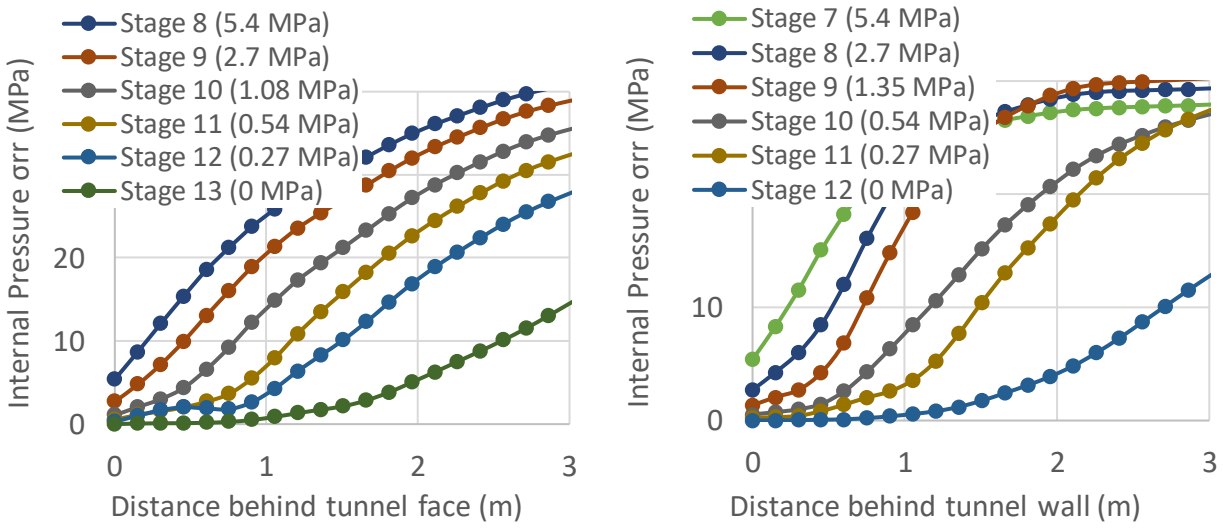


*(a)* *(b)*

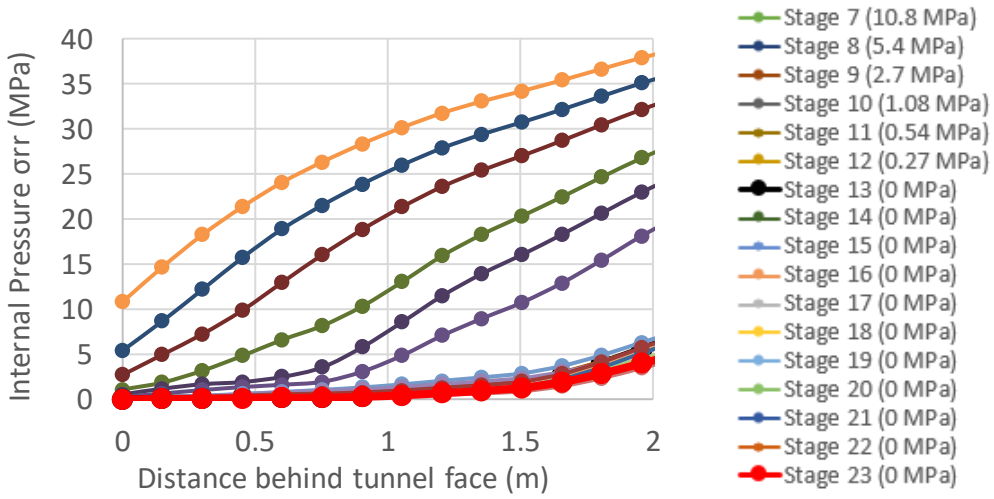


*(c)*

*Figure 3-80 Confinement distribution profiles for tunnel in brittle rock, for different stress scenarios: (a) ko = 1 (uniform field stress), (b) ko = 0.5, and (c) mining induced stress applied, with ko = 1 to k = 0.6.*

For the mining case, Figure 3-80 c, the confinement increases slowly around the excavation boundary which will have a direct impact on the amount of bulking (expected larger bulking).

The bulking amount for each case was calculated and is presented in Figure 3-81a. As indicated earlier, the maximum bulking factor for the models in this thesis, has been set as 4% for small tangential strain scenario (small bulking). Bulking amount from both failure mechanisms (tensile and shear) are represented separately in the following Figure 3-81a (only bulking from tensile) and bulking from shear and tensile Figure 3-81 b.

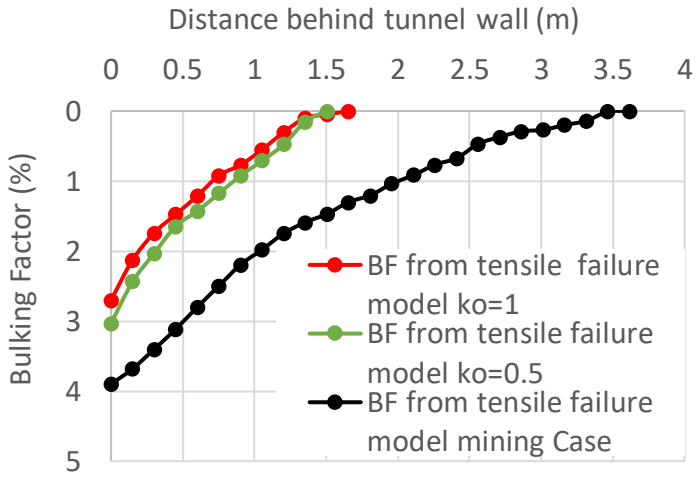


*(a)*

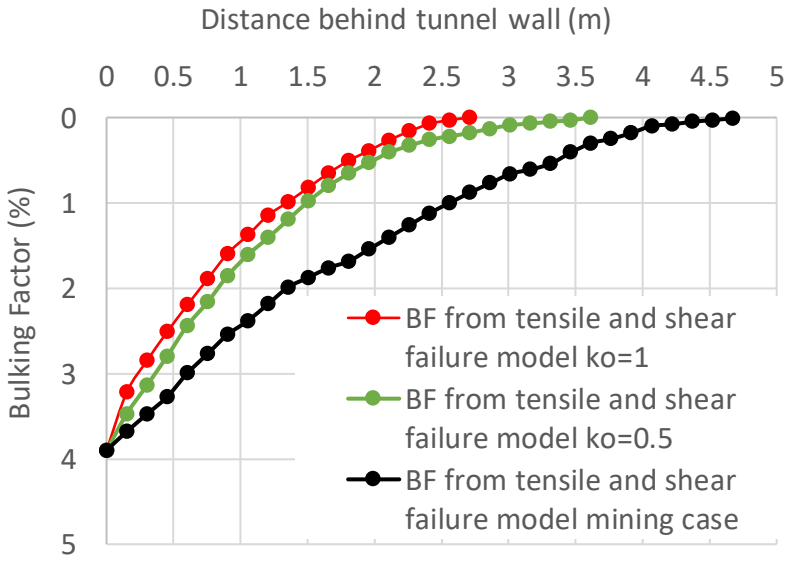


*(b)*

*Figure 3-81 Bulking distributions for (a) failure in tension, and (b) failure in tension and shear.*

Loading of the tunnel by mining-induced stresses increases the extent (depth) of the zone experiencing bulking (over 4.5 m; almost double compared to ko = 1 and 0.5). It can be anticipated that the bulking displacements for the mining scenario will be much larger and dominate the excavation behaviour. This is illustrated by Figure 3-82. The displacement is again categorized according to the failure mechanism that created it. Figure 3-82 a shows the displacement from rock mass bulking for tensile failure only and Figure 3-82b for shear and tensile failure.

(a)

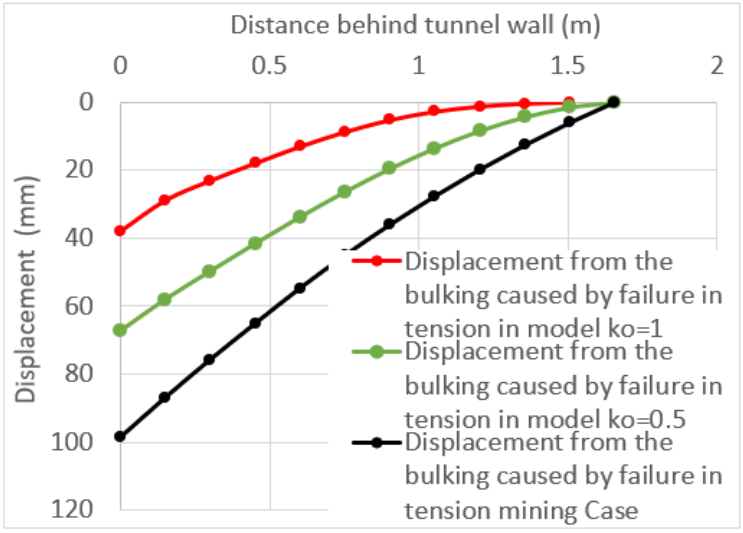


(b)

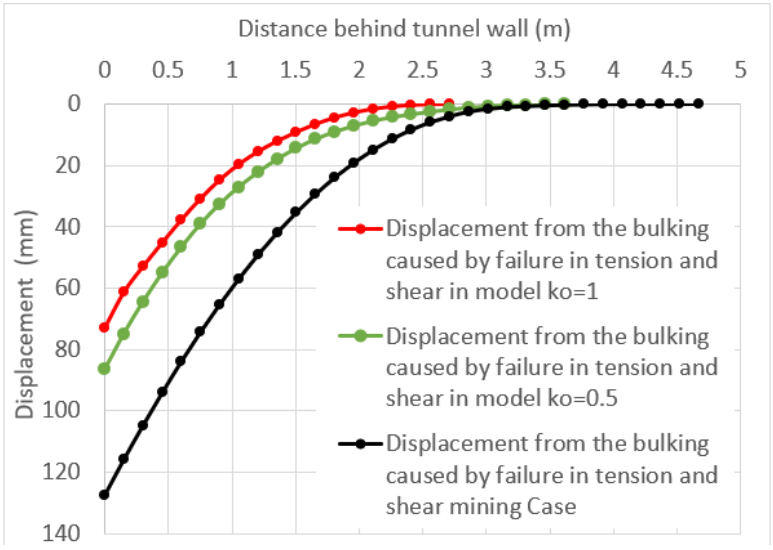


*Figure 3-82 Displacements obtained from the rock mass bulking from: (a) tensile failure mechanism only, and (b) for tensile and shear failure.*

When the bulking displacement is added to the displacements obtained from the numerical model (total elastic-plastic deformation), the total convergence an excavation experiences can be estimated. The Figure 3-83 again summarizes this for two scenarios, i.e., for tensile only (Figure 3-83a) and for both tensile and shear failure (Figure 3-83b).

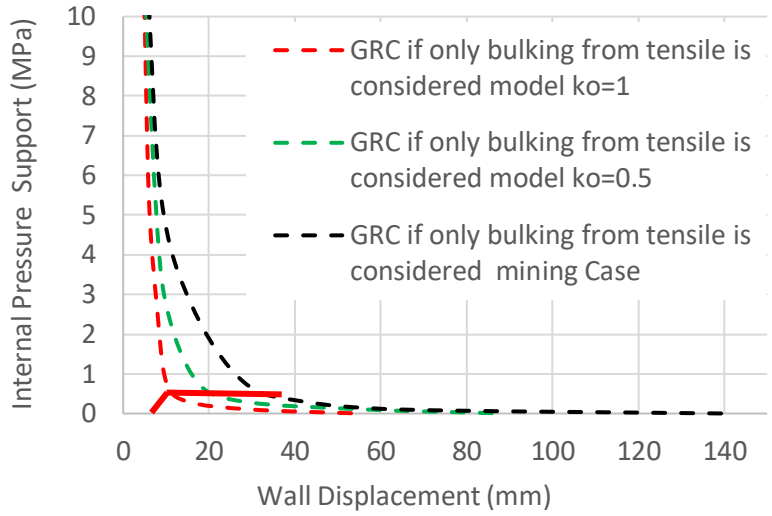


*(a)*

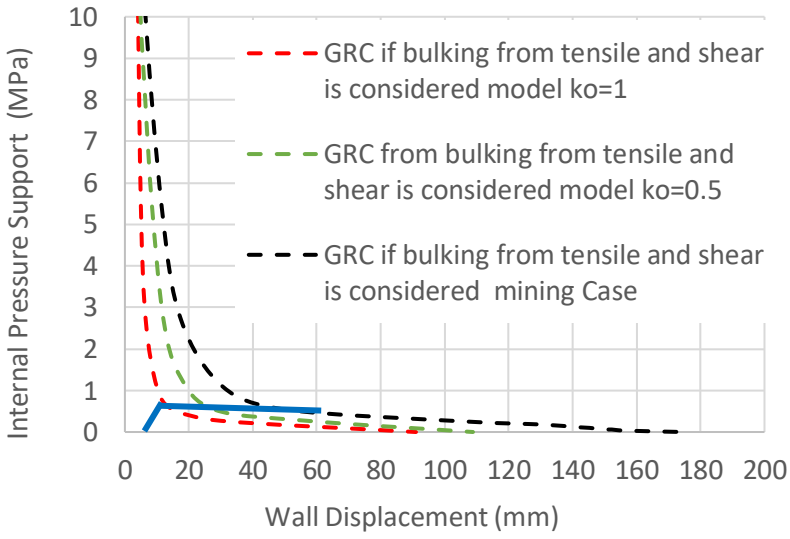


*(b)*

*Figure 3-83 GRCs from a tunnel with (a) bulking from the tensile failure added, and (b) bulking from both, tensile and shear failure added.*

These GRCs illustrate the difference between solutions obtained after adding the empirical bulking to the solutions from numerical models. It is evident again that the wall displacements are dominated by the zone that is bulking, i.e., the tensile and/or shear zone, and the mining-induced deformation. For a better idea of the magnitude of these variations in results, the following Table 3-5 is provided.

*Table 3-5 Results of displacement for the analyses with various stress states*

| Stress State | Maximum displacement (mm) without bulking | Bulking displacement (mm) in tensile zone alone | Bulking displacement (mm) in tensile and shear zone |
|---|---|---|---|
| **ko = 1** | 18 | 55 | 92 |
| **ko = 0.5** | 22 | 89 | 108 |
| **Mining case** | 40 | 141 | 176 |

In summary, this second analysis shows that the different stress states and, in particular, mining-induced stress paths dominate the deformation behaviour. Non-hydrostatic states of stress lead to elevated bulking deformations and the addition of far field deformation during mining-induced loading adds substantial bulking deformations; for the analyzed scenarios, typically more than 60%, It can be inferred that brittle failure near excavations that are influenced by mining-induced stresses will be more challenging.

# Chapter 4

# 4 Summary of research findings, conclusions and recommendations for future research

## 4.1 Summary

Although the Ground Reaction Curve (GRC) constitutes a viable tool to rapidly asses and calculate displacements around an excavation, it presents deficiencies if the under lying model for the displacements does not account.for discontinuum behaviour as encountered in stress-fractured hard rock.

An important deficiency is the lack of the consideration of deformation produced by the geometric bulking of the broken rock mass around the tunnel. In this thesis, a semi-empirical method, whereby the elastic and plastic displacements are obtained from the excavation modelled in Phase2 and the bulking displacements are superimposed, was adopted to overcome this deficiency. Empirical charts developed by Kaiser (2016) were used to estimate the bulking displacement. In this manner, GRCs for tunnels in brittle rock were developed and illustrated for different rock mass types and for three stress states and paths.

## 4.2 Approach

Because the key of the thesis is to correctly estimate displacement from bulking, it was of vital importance to first understand factors that contribute to bulking. It is well known that bulking depends on the level of confinement and several excavations experiencing different confinement distributions were analyzed with the goal of establishing the sensitivity of bulking displacements to

the distribution of the radial confinement around a tunnel.

First, excavations with the same level of stress but in different materials, which gave a different confinement distribution profile, were compared. It was shown how brittle bulking rock experiences much larger displacements than the elastic-plastic or elastic-brittle rock. It was also investigated which failure criteria captures each type of material behaviour best. In this manner, it was established what the applicability of the GSI and DISL approaches is to model the behaviour of excavations.

Second, excavations in brittle rock were subjected to different levels of stress and a mining-induced stress path. In this manner, different amount of bulking was obtained for a given material. The stresses that were induced were states typically encountered in tunnel advancement stages ($k_o = 1$ and $k_o = 0.5$) and induced mining stress, which is a tunnel initially excavated at $k_o = 1$ and then vertically loaded due to mining to final stress ratio of k=0.6. It was clearly shown how this last case imposed larger displacements in the excavation.

## 4.3 Conclusions

Through the thesis development the original hypothesis of the importance of considering the deformations originating from the bulking of stress-fractured ground was reassured with calculations including numerical modelling and empirical bulking relations. The dominance of this deformation on the displacements into excavations was demonstrated.

It is shown that the confinement redistributes near excavations and that this strongly affects the radial displacements and thus the tunnel convergence. The second conclusion obtained was that deformation due to mining loading can dominate the excavation behaviour and the convergence.

The practical implication of these two conclusions is related to the support design and selection.

Since the displacement demand imposed on the support system is be much higher with bulking it becomes evident that continuum numerical models must underestimate the displacement and strain imposed on the support. As a consequence, the support loads and stresses must be underestimated by continuum models that do not account for bulking.

## 4.4 Future research

It would be important to undertake furthers the influence of rock mass strain on the bulking deformation such that the semi-empirical models can be improved and verified. For the thesis published relations between strain and bulking were assumed but not fully investigated. As a matter of fact, it was ignored during the analysis of a tunnel with mining-induced stress and strain. Therefore, a possible research path forward should account for strain sensitivity.

A main logic consequence that follows from the analysis performed during the thesis is to determine which support will meet the estimated displacement demands.

For this reason, it would be useful to study in detail how an efficient support system controls the bulking and therefore diminishes the convergence of the excavation.

The implications for the selection of a support systems becomes evident from the GRCs plotted in Figure 3-77, Figure 3-78 and in Figure 3-83a and b. It can be seen that the equilibrium in a brittle tunnel when a fictitious support with a support capacity of 0.5 MPa is installed would be reached at 20 mm if only tensile failure is considered and at 43 mm if both bulking from tensile and shear are considered. Figure 3-83a, analyzes the case of a brittle tunnel, where only bulking from tensile is considered (as in Figure 3-77) but where mining is inducing the stresses, and when support is installed in the same conditions before mentioned, it is seen that the equilibrium is reached at 43 mm.

In Figure 3-83b, where bulking from shear and tensile are considered, is appreciated that the equilibrium would be reached at, 70 mm over the 175 mm of total convergence for the mining case. In conclusion, when compared the same equally supported brittle tunnel is appreciated that the support where the mining is inducing extra stress will be needing to accommodate much bigger displacements. Or it can be stated that mining inducing stress will dominate the support response.

For support design or selection, it is therefore necessary to check whether a support can provide sufficient support pressure and can handle the related deformations. For example, it needs to be assessed whether a support with a high capacity of 0.5 MPa, as assumed above, can handle up to 70 mm displacement. If not, it can be seen from the above quoted figures that much higher deformations will be imposed on the support; for example, at 0.25 MPa support capacity, >100 mm instead of 70 mm (blue line in Figure 3-83b).

According to Hoek et al. (1995), a support system of bolted shotcrete (a 50 mm thick, 28 old day,) in a 6 m circular tunnel with ko = 1 would surpass a necessary capacity of 0.5 MPa. However, such a shotcrete ring would not be flexible enough to survive 40 to 70 mm radial displacement. It would have to be slotted but then would provide much less than 0.5 MPa support pressure and the eventual displacement would be much greater than 40 to 60 mm. It is for this reason that deformable support systems are required to manage bulking and mining-induced deformations.

These practical implications deserve further investigations.

# References

Alejano, L.R. et al. (2010). Application of the convergence-confinement-method to tunnels in rock masses exhibiting Hoek–Brown strain-softening behaviour. International Journal of Rock Mechanics and Mining Sciences, 47 (1): 150–160.

Amadei, B. and Stephansson, O. (1997). Rock Stress and its Measurement. Chapman and Hall, London.

Arjang, B. (2004). Database on Canadian in situ ground stresses. CANMET Division Report MMSL 01-029.

Barton, N.R. (2002). Some new Q-value correlations to assist in site characterization and tunnel design. International Journal of Rock Mechanics and Mining Science, 39(2): 185-216.

Barton, N.R., Lien, R. and Lunde, J. (1974). Engineering classification of rock masses for the design of tunnel support. Rock Mechanics, (6): 189-239.

Barton, N.R. (2007b). Rockmass Characterization for excavations in mining and civil engineering. In: Proceedings of International Workshop of Rock Mass Classification in Mining, Vancouver.

Bewick, R.P., Amann, F., Martin, C.D. and Kaiser, P.K. (2015a). Interpretation of UCS test results for engineering design. In: Proc. 13th International ISRM Congress, Montreal.

Bieniawski, Z.T. (1973). Engineering classification of jointed rock masses. Trans S. Afr. Inst. Civil. Engineers, (15): 335-344.

Brook, N. and Dharmaratne, P.G.R. (1985). Simplified rock mass rating system for mine tunnel support. Transactions of the Institution of Mining and Metallurgy, Section A, Mining industry, London, (94): 148-154.

Brown, E.T. and Hoek, E. (1978). Trends in relationships between measured rock in situ stresses

and depth. International Journal of Rock Mechanics and Mining Sciences & Geomechanical Abstracts, (15): 211-215.

Cai, M. and Kaiser, P.K. (2014). In-situ rock spalling strength near excavation boundaries. Rock Mechanics and Rock Engineering, 47(2): 659–675. http://doi.org/10.1007/s00603-013-0437-0

Cai, M., Kaiser, P.K., Tasaka, Y. and Minami, M. (2007). Determination of residual strength parameters of jointed rock masses using the GSI system. International Journal of Rock Mechanics and Mining Sciences, 44(2): 247–265. http://doi.org/10.1016/j.ijrmms.2006.07.005

Cai, M., Kaiser, P.K., Uno, H., Tasaka, Y. and Minami, M. (2004). Estimation of rock mass deformation modulus and strength of jointed hard rock masses using the GSI system. International Journal of Rock Mechanics and Mining Sciences, 41(1): 3–19. http://doi.org/10.1016/S1365-1609(03)00025-X.

Cai, M., Morioka, H., Kaiser, P.K., Tasaka, Y., Kurose, H., Minami, M. and Maejima, T. (2007). Back-analysis of rock mass strength parameters using AE monitoring data. International Journal of Rock Mechanics and Mining Sciences, 44(4): 538–549. http://doi.org/10.1016/j.ijrmms.2006.09.012.

Cantieni, L. and Anagnostou, G. (2009). The interaction between yielding supports and squeezing ground. Tunnelling and Underground Space Technology, 24(3): 309–322. http://doi.org/10.1016/j.tust.2008.10.001

Carranza-Torres C. and Fairhurst C. (2000) “Application of the convergence-confinement method of tunnel design to rock-masses that satisfy the Hoek-Brown failure criterion”. Tunnelling and Underground Space Technology, 15(2): 187–213.

Carranza-Torres C. (2004) “Elasto-plastic solution of tunnel problems using the generalized form of the Hoek-Brown failure criterion”. International Journal of Rock Mechanics and Mining Sciences, 41(3): 480–481.

Carranza-Torres C. and Fairhurst, C. (1999) “The elasto-plastic response of underground excavations in rock masses that satisfy the Hoek-Brown failure criterion”. International Journal of Rock Mechanics and Mining Sciences, 36(6) : 777–809.

Carter, T.G., Diederichs, M.S. and Carvalho, J.L. (2008). Application of modified Hoek-Brown transition relationships for assessing strength and post yield behaviour at both ends of the rock competence scale. The Journal of the South African Institute of Mining and Metallurgy, (108): 325-338.

Corkum A., Lorig, L., DeGagné, D. and Jakubec, J. (2011). Guidelines for Mine Tunnel Support Design Revision 1, Itasca Consulting Group, Inc., SRK Consulting Ltd. And BGC Engineering Inc., Report to Mine Tunnel Support Project Sponsors; based on: Hoek, E. (2007). Practical rock engineering, www.Rocscience.com, and Diederichs, M.S. (2007). 2003 Mechanistic interpretation and practical application of damage and spalling prediction criteria for deep tunnelling. Canadian Geotechnical Journal, 44: 1087-1116.

Corkum, A.G., Lorig, L.J. and DeGagné, D.O. (2012). Continuum representation of brittle rock failure bulking-induced displacement around tunnels. In: Proc. of the 46th US Rock Mechanics Symposium, Chicago.

Deere, D.U. and Miller, R.P. (1966). Engineering classification and index properties of rock. Technical Report Air Force Weapons La., New Mexico, 65-116.

Detournay, E. and St. John, C.M. (1988). Design charts for a deep circular tunnel under non-uniform loading. Rock Mechanics and Rock Engineering, (21): 119-137.

Diederichs, M.S., Kaiser, P.K. & Eberhardt, E. (2004). Damage initiation and propagation in hard rock during tunnelling and the influence of near-face stress rotation. International Journal of Rock Mechanics and Mining Sciences, 41(5): 785–812. http://doi.org/10.1016/j.ijrmms.2004.02.003

Diederichs, M.S. and Kaiser, P.K. (1999). Tensile strength and abutment relaxation as failure control mechanisms in underground excavations. International Journal of Rock

Mechanics and Mining Sciences & Geomechanics Abstracts, (36): 69-96.

Diederichs, M.S. (2001). Instability of hard rock masses: The role of tensile damage and relaxation. PhD Thesis. Waterloo, ON, Canada: University of Waterloo.

Diederichs, M.S. and Martin, C.D. (2010). Measurement of spalling parameters from laboratory testing. Rock Mechanics in Civil and Environmental Engineering - Proceedings of the European Rock Mechanics Symposium, EUROCK 2010, 323–326. Retrieved from http://www.scopus.com/inward/record.url?eid=2-s2.0-84860159377&partnerID=tZOtx3y1

Diederichs, M.S. (2003). Manuel Rocha Medal Recipient Rock Fracture and Collapse Under Low Confinement Conditions. Rock Mechanics and Rock Engineering, 36(5): 339–381. http://doi.org/10.1007/s00603-003-0015-y

Diederichs, M.S., Carter, T.G.and Martin, C.D. (2010). Practical rock spall prediction in tunnels. In: Proc. of ITA World Tunnel Congress, Vancouver, 1-8.

Diederichs, M.S. (2007). The 2003 Canadian Geotechnical Colloquium: Mechanistic interpretation and practical application of damage and spalling prediction criteria for deep tunnelling. Canadian Geotechnical Journal, 44(9): 1082–1116. http://doi.org/10.1139/T07-033

Dinis da Gama, C. and Navarro Torres, V. (2002). Prediction of EDZ (Excavation Damaged Zone) from Explosive detonation in Underground Openings.In: ISRM international symposium on rock engineering for mountainous regions-Eurock 2002.Lisboa: Sociedad Portuguesa de Geotecnia.

Eberhardt, E. (2012). The Hoek–Brown Failure Criterion. Rock Mechanics and Rock Engineering, 45(6): 981–988. http://doi.org/10.1007/s00603-012-0276-4

Eberhardt, E. and Diederichs, M.S. (2012). Review of engineering geology and rock engineering aspects of th construction of a KBS-3 repository at the Forsmark site-initial review phase. SSM report 2012:39. Stockholm: Swedish Radiation Safety Authority.

Eberhardt, E., Stead, D., Stimpson, B. and Read, R.S. (1998). Identifying crack initiation and propagation thresholds in brittle rock. Canadian Geotechnical Journal, 35(2): 222–233. http://doi.org/10.1139/t97-091.

Edelbro, C. (2003). Rock mass strength– A review. Technical report Luleå University of Technology. Department of Civil and Mining Engineering, Division of Rock Mechanics.

Fenner, R. (1938). Study of ground pressures, Technical Translation 515, NRC Division of Building Research, Ottawa. pp.691-96; 705-715.

Ghazvinian, E., Perras, M.A., Diederichs, M.S. and Labrie, D. (2012). Formalized approaches to defining damage thresholds in brittle rock : granite and limestone.In: Proceedings of the 46th US Rock Mechanics/Geomechanics Symposium, Chicago, USA. New York: Curran Associates. Inc.; 2012b.

Griffith, A.A. (1920). The Phenomena of rupture and flow in solids. The Philosophical Transactions of the Royal Society, London, (Series A) 1921; (221): 163-98.

Griffith, A.A. (1924). Theory of rupture. In: Proc. 1st International Congress on Applied Mechanics, Delft, 55-63.

Griggs, D.T. and Handin, J. (1960). Observations on fracture and a hypothesis of earthquakes. In Rock Deformation. Geological Society of America Memoirs. 347-73.

Grimstad, E. and Barton, N. (1993). Updating the Q–system for NMT. In: Proc. of the 1st International Symposium on Sprayed concrete, Oslo.

Gschwandtner, G and Galler, R (2012). Input to the application of the convergence confinement method with time-dependent material behaviour of the support.In: Tunnelling and Underground Space Technology 27(1): 13-22.

Hajiabdolmajid, V., Kaiser, P.K. and Martin, C.D. (2002). Modelling brittle failure of rock. International Journal of Rock Mechanics and Mining Sciences, (39): 731–741. http://doi.org/10.1016/S1365-1609(02)00051-5.

He, M.C. (2006). Rock mechanics and hazard control in deep mining engineering in China. Rock Mechanics in Underground Construction, Proceedings ISRM International Symposium 2006 4th Asian Rock Mechanics Symposium, pp. 14-31.

Heard, H.C. (1960). Transition from brittle fracture to ductile flow in Solenhofen limestone as a function of temperature confining pressure and intersticial fluid pressure. Bull. Geol. Soc.Am., (79): 193-226.

Hoek, E. and Bieniawski, Z.T. (1965). Brittle Rock Fracture Propagation In Rock Under Compression Brittle Rock Fracture Propagation in Rock Under Compression. International Journal of Fracture Mechanics, 1(3): 137–155. http://doi.org/10.1007/BF00186851.

Hoek, E. and Bieniawski, Z.T. (1965). Brittle rock fracture propagation in rock under compression. International Journal of Fracture Mechanics, (1): 137-155.

Hoek, E. and Brown, E.T. (1980a). Underground Excavations in Rock. Institution of Mining and Metallurgy, London, 527 p.

Hoek, E. and Brown, E.T. (1997). Practical estimates of rock mass strength. International Journal of Rock Mechanics and Mining Sciences, 34(8): 1165-1186.

Hoek, E. (2010). Rock mass properties. Ch 11 in Practical Rock Engineering. http://download.rocscience.com/hoek/PracticalRockEngineering.asp

Hoek, E. (2001). Rock mass properties for underground mines in Underground Mining Methods: Engineering Fundamentals and International Case Studies (Edited by W.A.Hustrulid and R.L. Bullock), Littleton, Colorado: Society for Mining, Metallurgy and Exploration (SME) 2001.

Hoek, E. & Martin, C.D. (2014). Fracture initiation and propagation in intact rock - A review. Journal of Rock Mechanics and Geotechnical Engineering, 6(4): 287–300. http://doi.org/10.1016/j.jrmge.2014.06.001.

Hoek, E. (1968). Brittle failure of rock. In: Rock Mechanics in Engineering Practice. Wiley, New York.

Hoek, E. (2008). Rock–support interaction analysis for tunnels in weak rock. Available for downloading at Hoek's corner at www.rocscience.com

Hoek, E., Carranza-Torres, C.T. and Corkum, B. (2002). Hoek-Brown failure criterion – 2002 edition. In: Proc. NARMS-TAC Conference, Toronto, (1):267-273.

Hoek, E., Kaiser, P.K. and Bawden, W.F. (1995). Support of Underground Excavations in Hard Rock. Balkema, Rotterdam.

Hoek, E., Wood, D. and Shah, S. (1992). A modified Hoek-Brown criterion for jointed rock masses. In: Proc. of Rock Characterization Symposium, EUROCK 92, London, 209-213.

ISRM 1979.Commission on Standardization of Laboratory and Field Tests. Suggested methods for determining the uniaxial compressive strength and deformation of rock materials. International Journal of Rock Mechanics and Mineral Sciences, (15): 319-368.

Kaiser, P.K. (1993). Keynote address: Support of tunnels in burst-prone ground-toward a rational design methodology. Rockburst and Seismicity in Mines, Balkema, Rotterdam, pp.13-27.

Kaiser, P.K., McCreath, D., and Tannant, D. (1996). Canadian rockburst support handbook. Sudbury, Ontario, Canada: Geomechanics Research Centre and CAMIRO.

Kaiser, P.K., Wiles, T. (1990). In situ stress determination for mine design by stress change monitoring. 92nd CIM Annual General Meeting, Montreal.

Kaiser, P.K. and Kim, B. (2008). Rock mechanics challenges in underground construction and mining. In: Proc. 1st Southern Hemisphere International Rock Mechanics Symposium, (1): 3-38.

Kaiser, P.K. (2006). Rock mechanics considerations for construction of deep tunnels in brittle rock. In: Proc. 4th Asian Rock Mechanics Symposium, Singapore, 47-58.

Kaiser, P.K., Diederichs M.S., Martin C.D., Sharp J. and Steiner W. (2000). Underground works in hard rock tunnelling and mining. In: Proc. of GeoEng 2000, Melbourne, 841-926.

Kaiser, P.K., Maloney, S. and Yong, S. (2016). Role of large scale heterogeneities on in-situ stress and induced stress field. In: Proc. of the 50th US Rock Mechanics Symposium, Houston.

Kaiser, P.K. (2016). Challenges in rock mass strength determination for the design of underground excavations. 13th ISRM Online lecture. Web-cast March 15, 2016; www.isrm.net/gca/?id=1104

Kaiser, P.K. (2016). Ground support for constructability of deep underground excavations: challenge of managing highly stressed ground in civil and mining projects. Muir Wood Lecture of International Tunnelling Association (ITA). San Francisco, United States.

Kaiser, P.K. (2014). Deformation- based support selection for tunnels in strain-burstprone ground. In: 7 th International Conference on Deep and High Stress Mining, Sudbury, Ontario, Canada. ACG, editors Hudyma and Potvin, 227-240.

Kármán, Th. von (1911). Uber die Formänderung dünnwandiger- Röhre, insbesondere federnder Ausgleichröhre. (Strength tests under pressure from all sides). Verein Deutscher Ingenieure (German).

Latjai, E.Z. and Dzik, E.J. (1996). Searching for the damage threshold in intact rock. In NARMS '96, Rotterdam: Balkema. pp. 701-708.

Laubscher, D.H. and Jakubec, J. (2000). The MRMR rock mass classification for jointed rock masses. In: Underground Mining Methods: Engineering Fundamentals and International Case Studies, SMME, 475-481.

Laubscher, D.H. (1977). Geomechanics classification of jointed rock masses – mining applications. Transactions of the Institution of Mining and Metallurgy, Section A, Mining industry, London, (86): A1-8.

Laubscher, D.H. (1984). Design aspects and effectiveness of support systems in different mining conditions. Transactions of the Institution of Mining and Metallurgy, Section A, Mining industry, London, 93(10): 70-81.

Malan, D.F. (1999). Time-dependent behaviour of deep level tabular excavations in hard rock. Rock Mechanics and Rock Engineering. (32):123-155.

Malan, D.F. (2002). Simulation of the time-dependent behaviour of excavations in hard rock. Rock Mechanics and Rock Engineering. 35 (4):225-254.

Maloney, S., Kaiser, P.K. and Vorauer, A. (2006). A Re-Assessment of In Situ Stresses in the Canadian Shield. 41st US Symposium on Rock Mechanics.

Martin, C.D. (1990). Characterizing in situ stress domains at the AECL Underground Research Laboratory. Canadian Geotechnical Journal, 27(5): 631–646. http://doi.org/10.1139/t90-077

Martin, C.D. (1993). The strength of massive Lac du Bonet granite around underground openings. PhD Thesis. Winnipeg, Manitoba, Canda: University of Manitoba

Martin, C.D. (1997). Seventeenth Canadian Geotechnical Colloquium: The effect of cohesion loss and stress path on brittle rock strength. Canadian Geotechnical Journal, 34(5): 698–725. http://doi.org/10.1139/t97-030

Priest, S. D., and Hudson, J. A. (1976). Discontinuity spacings in rock. International Journal of Rock Mechanics and Mining Sciences and, 13(5), 135–148. https://doi.org/10.1016/0148-9062(76)90818-4

Martin, C.D., and Chandler, N.A. (1994). The progressive fracture of Lac du Bonnet granite. International Journal of Rock Mechanics and Mining Science & Geomechanics Abstract, (31): 643-59.

Martin, C.D., Kaiser, P.K., and Christiansson, R. (2003). Stress, instability and design of underground excavations. International Journal of Rock Mechanics and Mining Sciences, 40 (7-8): 1027–1047. http://doi.org/10.1016/S1365-1609(03)00110-2.

Martin, C.D., and Christiansson, R. (2009). Estimating the potential for spalling around a deep nuclear waste repository in crystalline rock. International Journal of Rock Mechanics and Mining Sciences, 46(2): 219-28.

Martin, C.D., Kaiser, P.K. & Christiansson, R. (2003). Stress, instability and design of underground excavations. International Journal of Rock Mechanics and Mining Science, (40):1027-1047.

Martin, C.D., Kaiser, P.K., and McCreath, D.R. (1999). Hoek-Brown parameters for predicting the depth of brittle failure around tunnels. Canadian Geotechnical Journal, 36(1): 136–151. http://doi.org/10.1139/t98-072

McClintock, F.A., and Walsh, J.B. (1962). Friction on Griffith cracks in rock under pressure. In: Proc. of the 4th US National Congress of Applied Mechanics, New York, 1015-1021.

Merrit, A.H. (1972). Geological predictions for underground excavations. In: Proc. of the North American Rapid Excavation and Tunnelling Conference, (1): 115-132.

Milne, D., Germain, P., Grant, D. and Noble, P. (1991). Field observation for the standardization of the NGI classification system for underground mine design. In: Proc. 7th ISRM congress, Balkema, Germany.

Mogi, K. (1965). Deformation and fracture of rocks under confining pressure: elasticity and plasticity of some rocks. Bull. Earthquake Res. Inst. Tokyo University, (43):349-379.

Mogi, K. (1966). Pressure dependence of rock strength and transition from brittle fracture to ductile flow. Bull. Earthquake Res. Inst Tokyo University. (44):215-232.

Mogi, K. (1966). Some precise measurements of fracture strength of rocks under uniform compressive stress. Felsmechanik und Ingenieurgeologie, (4):41-55.

Muir Wood, A.M. (1972). Tunnels for Rods and Motorways. Engineering Geology Journal. (5):111-126

Murrel, S.A.F. (1963). A criterion for brittle fracture of rocks and concrete under triaxial stress and the effect of pore pressure on the criterion. In: Proc. of the 5th US rock Mechanics Symposium, Minneapolis, 14p.

Ortlepp, W.D. and Gay, N.C. (1984). Performance of an experimental tunnel subjected to stresses ranging from 50 MPa to 230 MPa. In: Brown E, Hudson J, editors. Proceedings of ISRM Symposium on Design and Performance of Underground Excavations. London: British Geotechnical Society, 337-346.

Ortlepp, W.D. (1992). The design of support for the containment of rockburst damage in tunnels-and engineering approach. In: Kaiser, P.K. and McCreath, D.R., Eds., Rock Support in Mining and Underground Construction. Balkema, Rotterdam, 593-609.

Pacher, F. (1964). Deformationsmessungen im Versuchsstollen als Mittel zur Erforschung des Gebirgsverhaltens und zur Bemessung des Ausbaues. Felmsmechanik, 149-161.

Palmström, A. (1982). The volumetric joint count – A useful and simple measure of the degree of jointing. In: Proc. of the 4th International Congress IAEG, New Delhi, pp. V.221- V.228.

Palmström, A. (1995). RMi – A rockmass characterization system for rock engineering purposes, PhD thesis, University of Oslo, 400 p.

Paterson, M.S. (1958). Experimental deformation and faulting in Wombeyan marble. Bull. Geol. Soc. Am., (69):465-467.

Paterson, M.S. (1978). Experimental Rock Deformation- the Brittle Field. Springer-Verlag Berlin Heidelberg GmbH.

Perras, M.A., and Diederichs, M.S. (2014). A review of the tensile strength of rock: concepts and testing. Geotechnical ad Geological Engineering, 32(2):525-546.

Perras, M.A., Langford, C., Ghazvinian, E. and Diederichs, M.S. (2012). Numerical delineation of the excavation damage zones: from rock properties to statistical distribution of the dimensions. In: Proceedings of Eurock, Stockholm, Sweden.

Perras, M.A., and Diederichs, M.S. (2016). Predicting excavation damage zone depths in brittle rocks. Journal of Rock Mechanics and Geotechnical Engineering, 8(1): 60–74. http://doi.org/10.1016/j.jrmge.2015.11.004

Pestman, B.J. and Van Munster, J.G. (1996). An acoustic emission study of damage development and stress memory effects in sandstone. International Journal of Rock Mechanics and Mining Sciences, (36): 279-289.

Priest, S. D., and Hudson, J. A. (1976). Discontinuity spacings in rock. International Journal of Rock Mechanics and Mining Sciences 13(5): 135–148. https://doi.org/10.1016/0148-9062(76)90818-4

Radoncic, N., Pilgerstorfer, T. and Schubert, W. (2008) Prediction of displacements in tunnels. In: Proc. 5th Asian Rock Mechanics Symposium, Tehran, Iran.

Read, R.S., Martin, C.D. and Dzik E.J. (1995). Asymmetric Borehole at the URL. In: Proc. of the 35th US Rock Mechanics Symposium, Reno, 6 p.

Riedmüller, G. and Schubert, W. (1999). Critical comments on quantitative rockmass classification. Felsbau, 17(3).

Rocscience Phase2 v.8.0, Finite element analysis for excavations and slopes. www.rocscience.com.

Sheorey, P.R. (1994). A theory for in situ stresses in isotropic and transversely isotropic rock. International Journal of Rock Mechanics and Mining Sciences, 31(1): 23-34.

Singh, J. et al. (1989). Strength of rocks at depth. In: Maury & Fourmaintraux eds. Rock at great

depth. Rotterdam: A.A. Balkema.37-44.

Siren, T., Kantia, P. and Rinne, M. (2015). Considerations and observations of stress-induced and construction-induced excavation damage zone in crystalline rock. International Journal of Rock Mechanics and Mining Sciences, (73): 165-174.

Schmertmann, J.H., and Osterberg, J.H. (1960). An experimental study of the development of cohesion and friction with axial strain in saturated cohesive soil. In: Research Conference on Shear Strength of Cohesive Soil. New York: American Society of Civil Engineers, 643-694.

Tsang, C.F., Bernier, F., and Davies, C. (2005). Geohydromechanical processes in the excavation damage zone in crystalline rock, rock salt, and indurated and plastic clays-in the context of radioactive waste disposal. International Journal of Rock Mechanics and Mining Sciences, 42 (1):109-125.

Vlachopoulous, N. and Diederichs, M.S. (2009). Improved longitudinal displacement profiles for convergence confinement analysis of deep tunnels. Rock Mechanics and Rock Engineering, (42): 131-146.

Vlachopoulous, N. and Diederichs, M.S. (2014). Appropriate uses and practical limitations of 2D numerical analysis of tunnels and tunnel support response. Geotechnical and Geological Engineering Journal, 31(6).

Zuo, J.P., Li, H.T., Xie H.P., Ju, Y., and Peng, S.P. (2008). A nonlinear strength criterion for rock-like materials based on fracture mechanics. International Journal of Rock Mechanics and Mining Sciences, 45(4): 594-9.